

Firefly genomes illuminate parallel origins of bioluminescence in beetles

Authors:

Timothy R. Fallon^{1,2,*}, Sarah E. Lower^{3,*}, Ching-Ho Chang⁴, Manabu Bessho-Uehara^{5,6}, Gavin J. Martin⁷, Adam J. Bewick⁸, Megan Behringer⁹, Humberto J. Debat¹⁰, Isaac Wong⁴, John C. Day¹¹, Anton Suvorov⁷, Christian J. Silva^{4,12}, Kathrin F. Stanger-Hall¹³, David W. Hall⁸, Robert J. Schmitz⁸, David R. Nelson¹⁴, Sara M. Lewis¹⁵, Shuji Shigenobu¹⁶, Seth M. Bybee⁷, Amanda M. Larracuente⁴, Yuichi Oba⁵, Jing-Ke Weng^{1,2,†}

Affiliations:

¹Whitehead Institute for Biomedical Research, Cambridge, Massachusetts 02142, USA.

²Department of Biology, Massachusetts Institute of Technology, Cambridge, Massachusetts 02139, USA.

³Department of Molecular Biology & Genetics, Cornell University, Ithaca, New York 14850, USA.

⁴Department of Biology, University of Rochester, Rochester, New York 14627, USA.

⁵Department of Environmental Biology, Chubu University, Kasugai, Aichi 487-8501, Japan.

⁶Graduate School of Bioagricultural Sciences, Nagoya University, Nagoya, Aichi 464-8601, Japan.

⁷Department of Biology, Brigham Young University, Provo, Utah 84602, USA.

⁸Department of Genetics, University of Georgia, Athens, Georgia 30602, USA.

⁹Biodesign Center for Mechanisms of Evolution, Arizona State University, Tempe, Arizona 85287, USA.

¹⁰Center of Agronomic Research National Institute of Agricultural Technology, Córdoba, Argentina.

¹¹Centre for Ecology and Hydrology (CEH) Wallingford, Wallingford, Oxfordshire, UK.

¹²Department of Plant Sciences, University of California Davis, Davis, California, USA.

¹³Department of Plant Biology, University of Georgia, Athens, Georgia 30602, USA.

¹⁴Department of Microbiology Immunology and Biochemistry, University of Tennessee HSC, Memphis 38163, USA.

¹⁵Department of Biology, Tufts University, Medford, Massachusetts 02155, USA.

¹⁶NIBB Core Research Facilities, National Institute for Basic Biology, Okazaki 444-8585, Japan.

[†]Corresponding author. Email: wengj@wi.mit.edu (J.K.W.)

*These authors contributed equally to this work.

One Sentence Summary:

Comparative analyses of the first linkage-group-resolution genomes of fireflies and related bioluminescent beetles address long-standing questions of the origin and evolution of bioluminescence and its associated traits.

Abstract

Fireflies and their fascinating luminous courtships have inspired centuries of scientific study. Today firefly luciferase is widely used in biotechnology, but the evolutionary origin of their bioluminescence remains unclear. To shed light on this long-standing question, we sequenced the genomes of two firefly species that diverged over 100 million-years-ago: the North American *Photinus pyralis* and Japanese *Aquatica lateralis*. We also sequenced the genome of a related click-beetle, the Caribbean *Ignelater lumenosus*, with bioluminescent biochemistry near-identical to fireflies, but anatomically unique light organs, suggesting the intriguing but contentious hypothesis of parallel gains of bioluminescence. Our analyses support two independent gains of bioluminescence between fireflies and click-beetles, and provide new insights into the genes, chemical defenses, and symbionts that evolved alongside their luminous lifestyle.

Fireflies (Coleoptera: Lampyridae) represent the best-studied case of bioluminescence. The coded language of their luminous courtship displays (Fig. 1A; Video S1) has been long studied for its role in mate recognition (1–3), while non-adult bioluminescence is likely a warning signal of their unpalatable chemical defenses (4), such as the cardiotoxic lucibufagins of *Photinus* fireflies (5). The biochemical understanding of firefly luminescence: an ATP, Mg²⁺, and O₂-dependent luciferase-mediated oxidation of the substrate luciferin (6), along with the cloning of the luciferase gene (7, 8), led to its widespread use of luciferase as a reporter with unique applications in biomedical research and industry (9). With >2000 species globally, fireflies are undoubtedly the most culturally-appreciated bioluminescent group, yet there are at least three other beetle families with bioluminescent species: click beetles (Elateridae), American railroad worms (Phengodidae) and Asian starworms (Rhagophthalmidae) (10). These four closely related families (superfamily Elateroidea) have homologous luciferases and structurally identical luciferins (6), implying a single origin of beetle bioluminescence. However, as Darwin recognized in his “Difficulties on Theory” (11), the light organs of the luminous beetles are clearly distinct (Fig. 1C). Thus, whether beetle bioluminescence is derived from single or multiple origins remains unresolved.

To address this long-standing question, we sequenced and analyzed the genomes of three bioluminescent beetle species. To represent the fireflies, we sequenced the widespread North American “Big Dipper Firefly”, *Photinus pyralis* (Fig. 1A, B) used in classic studies of firefly bioluminescent biochemistry (12) and the cloning of luciferase (7), and the Japanese “Heike-botaru” firefly *Aquatica lateralis* (Fig. 1C), a species with specialized aquatic larvae and one of the few fireflies that can be cultured

in the laboratory (13). These two fireflies represent the two major firefly subfamilies, Lampyrinae and Luciolinae, which diverged from a common ancestor over 100 Mya (Fig. 1C) (14, 15). To facilitate evolutionary comparison, we also sequenced the “Cucubano”, *Ignelater luminosus* (Fig. 1C), a Caribbean bioluminescent click beetle, and one of the “*Pyrophorus*” species used by Raphaël Dubois to first establish the enzymological basis of bioluminescence in the late 1800s (16). Comparative analyses of the genomes of these three species allowed us to reconstruct the origin(s) and evolution of beetle bioluminescence.

Sequencing and assembly yield high-quality genomes

P. pyralis adult males were collected from the Great Smoky Mountains National Park, USA (GSMNP) and Mercer Meadows New Jersey, USA (MMNJ) (Fig. 1B), and sequenced using short-insert, mate-pair, Hi-C, and long-read Pacific Biosciences (PacBio) approaches (table S1). These datasets were combined in a MaSuRCA (17) hybrid genome assembly (Supp. Text 1.5). The *A. lateralis* genome was derived from an ALL-PATHs (18) assembly of short insert and mate-pair reads from a single partially-inbred laboratory-reared adult female, whose lineage was first collected 25 years ago from a now extinct population in Yokohama, Japan (Supp. Text 2.5). A single *Ignelater luminosus* adult male, collected in Mayagüez Puerto Rico, USA, was used to produce a high-coverage Supernova (19) linked-read draft genome (Supp. Text 3.5), which was further scaffolded using low-coverage long-read Oxford Nanopore MinION sequencing (Supp. Text 3.5.5).

The gene completeness and contiguity statistics of our *P. pyralis* (Ppyr1.3) and *A. lateralis* (Alat1.3) genome assemblies are comparable to the genome of the model

beetle *Tribolium castaneum* (Fig. 2F; Supp. Text 4.1), indicating their high quality. The *I. luminosus* genome assembly (Illumi1.2) is less complete, but is comparable to other published insect genomes (Fig. 2F; Supp. Text 4.1). Our coding gene annotation sets for *P. pyralis*, *A. lateralis*, and *I. luminosus* are comprised of 15,770, 14,285, and 27,552 genes containing 94.2%, 90.0%, and 91.8% of the Endopterygota Benchmarking Single Copy Orthologs (BUSCOs), respectively. Protein clustering via predicted orthology (20) indicated a high similarity between the *P. pyralis* and *A. lateralis* genesets, whereas the *I. luminosus* geneset differed (Fig. 2E; fig. S4.2.1.1). This is as expected given the phylogenetic divergence of these species. Remaining redundancy in the *P. pyralis* assembly, as indicated by duplicates of the BUSCOs (21) and the assembly size (Fig 2F; Supp. Text 4.1) is likely due to the heterozygosity of the outbred input libraries (Supp. Text 1).

To characterize long-range evolutionary events in the *P. pyralis* genome, we super-scaffolded the assembly into 11 pseudo-chromosomal linkage groups using a Hi-C proximity-ligation linkage approach (Fig. 2A; Supp. Text 1.5.3). These linkage groups contain 95% of the assembly (448.8 Mbp). Linkage group LG3a corresponds to the X-chromosome based on read coverage and gene content (Supp. Text 1.6.3) and its size (22.2 Mbp) is comparable to the expected X-chromosome size based on sex-specific genome size estimates using flow cytometry (~26 Mbp) (22). Homologs to *T. castaneum* X-chromosome genes were enriched on LG3a, compared to every other linkage group, suggesting that the X-chromosomes of these distantly related beetles are homologous, and that their content has reasonably conserved for >200 MY (Supp. Text 1.6.4) (15). Overall, 42.6% of the *P. pyralis* assembly was found to be repetitive, and 66.7% of

these repeats could not be classified as any known repetitive sequence. Helitrons, DNA transposons that transpose through rolling circle replication (23), are among the most abundant individual repeat elements in the assembly. Via *in situ* hybridization, we were able to identify that *P. pyralis* chromosomes have canonical telomeres with telomeric repeats (TTAGG) (Fig. 2B; Supp. Text 1.13).

DNA methylation is common in eukaryotes, but varies in degree across insects, especially within Coleoptera (24). Furthermore, the functions of DNA methylation across insects remain obscure (24, 25). To examine firefly cytosine methylation, we characterized the methylation status of *P. pyralis* DNA with whole genome bisulfite sequencing (WGBS). Methylation at CpGs (mCG) was unambiguously detected at ~20% within the genic regions of *P. pyralis* and its methylation levels were at least twice of those reported from other holometabolous insects (Fig. 2D; Supp. Text 1.12). Molecular evolution analyses of the DNA methyltransferases (DNMTs) show that orthologs of both DNMT1 and DNMT3 were conserved in *P. pyralis* and *A. lateralis* (fig. S4.2.2; Supp. Text 4.2), implying that most firefly lineages likely possess mCG.

We assembled the complete mitochondrial genomes (mtDNA) of *P. pyralis* (Fig. 2C; Supp. Text 1.8) and *I. luminosus* (Supp. Text 3.10), while the mtDNA sequence of *A. lateralis* was recently published (26). These mtDNA assemblies show high conservation of gene content and synteny, with the exception of the variable ~1 kbp tandem repeat unit (TRU) found in firefly mtDNAs.

The genomic context of firefly luciferase evolution

Two luciferase paralogs have been previously described in fireflies (13, 27). *P. pyralis* *Luc1* was the first firefly luciferase cloned (7), and its orthologs have been widely

identified from other fireflies (28). The luciferase paralog *Luc2* was previously known only from a handful of Asian taxa, including *A. lateralis* (13, 27). Previous investigations of these Asian taxa have shown that *Luc1* is responsible for light production from the lanterns of adults, larvae, prepupae and pupae, whereas *Luc2* is responsible for the dim glow of eggs, ovaries, prepupae and the whole pupal body (27). We unequivocally identified two firefly luciferases, *Luc1* and *Luc2*, in both the *P. pyralis* and *A. lateralis* genomes. Our RNA-Seq data further show that in both *P. pyralis* and *A. lateralis* *Luc1* and *Luc2* display expression patterns consistent with these previous reports (Fig. 3C). *Luc2* is essentially not expressed in the adult male or larval lanterns, while it is more highly expressed in eggs than larvae (Fig. 3C). These results suggest that, since their divergence via gene duplication prior to the divergence of Lampyrinae and Luciolinae, *Luc1* and *Luc2* have established different, but conserved roles in bioluminescence throughout the firefly life cycle.

Firefly luciferase is hypothesized to be derived from an ancestral peroxisomal fatty acyl-CoA synthetase (*PACS*) (Fig. 3A) (29, 30). We found that in both firefly species, *Luc1* is clustered with its closely related homologs, including *PACSs* and non-peroxisomal acyl-CoA synthetases (*ACSs*), which can be identified by their lack of the C-terminal peroxisomal-targeting-signal-1 (PTS1), as well as an orthologous microsomal glutathione S-transferase (MGST) family gene (Fig. 3D). Genome-wide phylogenetic analysis of the luciferases, *PACSs* and *ACSs* indicates that *Luc1* and *Luc2* form two orthologous groups, and that the neighboring *PACS* and *ACS* genes near *Luc1* form three major clades (Fig. 3C): Clade A, whose common ancestor and most extant members are *ACSs*, and Clades B and C whose common ancestors and most

extant members are PACSs. *Luc1* and *Luc2* are highly conserved at the level of gene structure—both are composed of seven exons with completely conserved exon/intron boundaries (fig. S4.3.1.1), and most members of Clades A, B, and C also have 7 exons. The exact syntenic and orthology relationships of the ACS and *PACS* genes adjacent to the *Luc1* locus remains unclear, likely due to subsequent gene divergence and shuffling (Fig. 3, C and D).

Luc2 is located on a different linkage-group from *Luc1* in *P. pyralis* and on a different scaffold from *Luc1* in *A. lateralis*, consistent with the interpretation that *Luc1* and *Luc2* lie on different chromosomes in both firefly species. No *PACS* or *ACS* genes were found in the vicinity of *Luc2* in either species. These data support that tandem gene duplication in a firefly ancestor gave rise to several ancestral *PACS* paralogs, one of which neofunctionalized in place to become the ancestral luciferase (*AncLuc*) (Fig. 3B). Prior to the divergence of the firefly subfamilies Lampyrinae and Luciolinae around 100 Mya (Supp. Text 4.3), this *AncLuc* duplicated and subfunctionalized, possibly via a long-range gene duplication event (e.g. transposon mobilization), to give rise to *Luc2*, while the original *AncLuc* subfunctionalized in place to give rise to *Luc1* (Fig. 3B). From the shared *Luc* gene clustering in both fireflies, we infer the structure of the pre-duplication *AncLuc* locus contained one or more *ACS* genes (Clade A), one or more *PACS* genes (Clade B/C), and one or more MGST family genes (Fig. 3B).

Independent origins of firefly and click beetle luciferase

To resolve the number of origins of luciferase activity, and therefore bioluminescence, between fireflies and click beetles, we first identified the luciferase of *I. luminosus* luciferase (*IlumLuc*), and compared its genomic context to that of *P. pyralis* and *A.*

lateralis (Fig. 3D). We identified a single luciferase in *I. luminosus* genome, *IlumLuc*, on a 366 kbp scaffold containing 18 other genes, including extant *PACS* genes likely descended from genes ancestral to *IlumLuc* (Fig. 3D; Fig. 4). *IlumLuc* is highly expressed in both the prothorax and abdominal lanterns (Fig. 3C). Synthetic analysis shows that the *IlumLuc* locus is not orthologous to the extant firefly *Luc1* locus, as *IlumLuc* is not clustered with Clade A, B or C ACS or *PACS* genes (Fig. 3, C and D). Instead, we identified a different scaffold in *I. luminosus* that is likely orthologous to the firefly *Luc1* locus. This assessment was based on the presence of adjacent Clade A and B ACS and *PACS* genes, as well as orthologous exoribonuclease family (PRNT) and inositol monophosphatase family (IMP) genes, both of which were found adjacent to the *A. lateralis* *Luc1* locus, but not the *P. pyralis* *Luc1* locus (Fig. 3D). These genomic observations therefore support independent origins of firefly and click beetle luciferase.

We then carried out a targeted molecular evolution analysis including the known beetle luciferases and their closely related homologs. Ancestral state reconstruction of luminescent activity on the gene tree recovered two independent gains of luminescence as the most parsimonious and likely scenario: once in click beetles, and once in the common ancestor of firefly, phengodid, and rhagophthalmid beetles (Fig. 4A; Supp. Text 4.3.3). In an independent molecular adaptation analysis, 35% of the sites of the ancestral click beetle luciferase showed a statistically significant signal of episodic positive selection with $d_N/d_S > 1$ (ω or $d_N/d_S = 3.98$) as compared to the evolution of its paralogs using the aBSREL branch-site selection test (31) (Fig. 4B; Supp. Text 4.3.4). This implies that the common ancestor of click beetle luciferases underwent a period of accelerated directional evolution. As the branch under selection in the molecular

adaptation analysis (Fig. 4B) is the same branch of luciferase activity gain via ancestral reconstruction (Fig. 4A), we conclude that the identified selection signal represents the relatively recent neofunctionalization of click beetle luciferase from a non-luminous ancestor, distinct from the more ancient neofunctionalization of firefly luciferase. Based on the constraints from our tree, we determine that this neofunctionalization occurred after the divergence of the subfamily Agrypninae. For fireflies, we cannot determine if the original neofunctionalization of AncLuc occurred in the ancestral firefly, or in an ancestral “cantharoid” beetle, a group of beetles including the luminous Rhagophthalmidae, Phengodidae and Lampyridae, but not Elateridae (32). There is evidence for a subsequent luciferase duplication event in phengodids, but not in rhagophthalmids, independent of the duplication event that gave rise to *Luc1* and *Luc2* in fireflies (Figs. 3C and 4). Altogether, our results strongly support the independent neofunctionalization of luciferase activity in click beetles and fireflies, and therefore at least two independent gains of luciferin-utilizing luminescence in beetles.

Metabolic adaptation of the firefly lantern

Beyond luciferase, we sought to characterize other metabolic traits which might have co-evolved in fireflies to support bioluminescence. Of particular importance, the enzymes of the *de novo* biosynthetic pathway for firefly luciferin remain unknown (33). We hypothesized that bioluminescent accessory enzymes, either specialized enzymes with unique functions in luciferin metabolism or enzymes with primary metabolic functions relevant to bioluminescence, would be highly expressed (HE: 90th percentile; Supp. text 1.9.4) in the adult lantern, and would be differentially expressed (DE) between luminescent and non-luminescent tissues. To determine this, we performed

RNA-Seq and expression analysis of the dissected *P. pyralis* and *A. lateralis* adult male lantern tissue compared with a non-luminescent tissue. We identified a set of enzyme-encoding genes shared between *P. pyralis* and *A. lateralis* that met our HE and DE criteria (Fig. 6). Both luciferase and luciferin sulfotransferase (LST), an specialized enzyme recently implicated in luciferin storage in *P. pyralis* (34), were recovered as candidate genes using these four criteria, indicating the validity of our approach. While LST ortholog is present in *A. lateralis*, it is absent from *I. luminosus*, suggesting that LST, and the presumed luciferin storage it mediates, is an exclusive ancestral firefly trait. This finding is consistent with the hypothesis of independent evolution of bioluminescence in Lampyridae and Elateridae (34).

Moreover, we identified several additional enzyme-encoding HE and DE lantern genes that are likely important in firefly lantern physiology (Fig. 6). For instance, adenylate kinase likely plays a critical role in efficient recycling of AMP post-luminescence, and cystathionine gamma-lyase may support a key role of cysteine in luciferin biosynthesis (33) and recycling (35). We also detected a combined adenylyl-sulfate kinase and sulfate adenylyltransferase enzyme among the lantern-enriched gene list (fig. S4.4.2), implicating active biosynthesis of 3'-phosphoadenosine-5'-phosphosulfate (PAPS), a cofactor of LST, in the lantern. This finding in turn highlights the importance of LST-catalyzed luciferin sulfonation for bioluminescence. Furthermore, the firefly orthologs of LST are the only members among their paralogs to contain a PTS1, suggesting specialized localization to the peroxisome, the location of the luminescence reaction. These findings suggest that the levels of sulfoluciferin and

luciferin may be actively regulated within the peroxisome of lantern cells in response to luminescence.

We also performed a similar expression analysis for genes not annotated as enzymes, yielding several genes with predicted lysosomal function (Supp. Text 4.4.1). This suggests that the abundant and as yet unidentified “differentiated zone granule” organelles of the firefly light organ (36) could be lysosomes. Interestingly, we found a HE and DE opsin, *Rh7*, in the light organ of *A. lateralis*, but not *P. pyralis* (fig. S4.5.1; Supp. Text 4.5), suggesting its potential role in light perception in *A. lateralis* lantern.

Genomic insights into firefly chemical defense

Firefly bioluminescence is postulated to have first evolved as an aposematic warning of larval chemical defenses (32). Lucibufagins are major unpalatable defense steroids found in certain North American firefly species, most notably in the genera *Photinus* (5) and *Ellychnia* (37), and hence are candidates for ancestral firefly defense compounds. To test whether lucibufagins are widespread among bioluminescent beetles, we assessed the presence of lucibufagins in *P. pyralis*, *A. lateralis*, and *I. luminosus* by liquid-chromatography high-resolution accurate-mass mass-spectrometry (LC-HRAM-MS). Whereas lucibufagins were found in high abundance in *P. pyralis* adult hemolymph, they were absent in *A. lateralis* adult hemolymph and *I. luminosus* thorax extract (Fig. 5B; Supp. Text 4.6). Since chemical defense is presumably most critical in the long-lived larval stage, we next tested whether lucibufagins are present in all firefly larvae even if they are not present in the adults of certain species. We found lucibufagins in *P. pyralis* larval extracts, however, they were absent in *A. lateralis* larval extracts (Fig. 5B; Supp. Text 4.6). Together, these results suggest that the lucibufagin

biosynthetic pathway is either a derived trait only found in particular firefly taxa (e.g. subfamily: Lampyrinae), or that alternatively lucibufagin biosynthesis was an ancestral trait that was lost in *A. lateralis*. Supporting the former hypothesis, the presence of lucibufagins in non-North-American Lampyrinae has been previously reported (38), but to date there are no reports of lucibufagins in Luciolinae.

The lucibufagin biosynthetic pathway is currently unknown. However, their chemical structure suggests a biosynthetic origin from cholesterol followed by a series of hydroxylations, -OH acetylations, and the side-chain oxidative pyrone formation (Fig. 5A) (5). We hypothesized that cytochrome P450s, an enzyme family widely involved in metabolic diversification of organic substrates (39), could underlie several oxidative reactions in the proposed lucibufagin biosynthetic pathway. We therefore inferred the P450 phylogeny among our three bioluminescent beetle genomes to identify any lineage-specific genes correlated with lucibufagin presence. Our analysis revealed a unique expansion of one P450 family, the CYP303 family, in *P. pyralis*. While essentially all previously sequenced insect genomes (61 out of 62), as well as the *A. lateralis* and *I. luminosus* genomes, contain only a single CYP303 family gene, the *P. pyralis* genome contains 11 CYP303 genes and 2 pseudogenes (Fig. 5C), which expanded via tandem duplication on the same linkage group (Fig. 5D). The CYP303 ortholog of *D. melanogaster*, CYP303A1, has been shown to play a role in mechanosensory bristle development (40). Although the exact biochemical function and substrate of *D. melanogaster* CYP303A1 is unknown, its closely related P450 families operate on a insect steroid hormone ecdysone (40). As ecdysone and lucibufagins are structurally similar, CYP303 may operate on steroid-like compounds, and therefore the lineage-

specific expansion of the CYP303 family in *P. pyralis* is a compelling candidate in the metabolic evolution of lucibufagins as chemical defenses associated with bioluminescence.

Symbionts of bioluminescent beetles

Given the increasingly recognized contributions of symbionts to host metabolism (41), we characterized the holobiomes of all three beetles as potential contributors to metabolic processes related to bioluminescence. Whole genome sequencing of our wild-caught and laboratory reared fireflies revealed a rich holobiont. Amongst our firefly genomes, we found various bacterial genomes, viral genomes, and the complete mtDNA for a phorid parasitoid fly, *Apocephalus antennatus*, the first mtDNA reported for genus *Apocephalus*. This mtDNA was inadvertently included in the *P. pyralis* PacBio library via undetected parasitization of the initial specimens, and was assembled via a metagenomic approach (Supp. Text 5.2). Independent collection of *A. antennatus* which emerged from field-collected *P. pyralis* adults and targeted COI sequencing later confirmed the taxonomic origin of this mtDNA (Supp. Text 5.3). We also sequenced and metagenomically assembled the complete circular genome (1.29 Mbp, GC: 29.7%; ~50x coverage) for a *P. pyralis*-associated mollicute (Phylum: Tenericutes), *Entomoplasma luminosum* subsp. *pyralis* (Supp. Text 5.1). *Entomoplasma* spp. were first isolated from the guts of North American fireflies (42) and our assembly provides the first complete genomic assembly of an *Entomoplasma* sp. Broad read coverage for the *E. luminosus* subsp. *pyralis* genome was detected in 5/6 of our *P. pyralis* DNA libraries, suggesting that *Entomoplasma* is a highly prevalent symbiont of *P. pyralis*. It has been hypothesized

that these *Entomoplasma* mollicutes could play a role in firefly metabolism, specifically via contributing to cholesterol metabolism and lucibufagin biosynthesis (37).

Within our unfiltered *A. lateralis* genomic assembly (Alat1.2), we also found 43 scaffolds (2.3 Mbp; GC:29.8%, ~64x coverage), whose taxonomic annotation corresponded to the Tenericutes (Supp. Text 2.1.1), suggesting that *A. lateralis* may also harbor a mollicute symbiont. Alat1.2 also contains 2119 scaffolds (13.0 Mbp, GC:63.7%, ~25x coverage) annotated as of Proteobacterial origin. Limited Proteobacterial symbionts were detected in the *I. luminosus* Ilumi1.0 assembly (0.4 Mbp; GC:30-65% ~10x coverage) (Supp. Text 3.5.3), suggesting no stable symbiont is present in *I. luminosus*. Lastly, we detected two species of novel orthomyxoviridae-like ssRNA viruses, which we dub *Photinus pyralis* orthomyxo-like virus 1 and 2 (PpyrOMLV1/2), that were highly prevalent in our *P. pyralis* RNA-Seq dataset, and showed multi-generational transovarial transmission in the laboratory (Supp. Text 5.4). We found several endogenous viral elements (EVEs) for PpyrOMLV1/2 in *P. pyralis* (Supp. Text 5.4.1). These viruses are the first reported in any firefly species, and represent only the second report of transgenerational transfer of any *Orthomyxoviridae* virus (43), and the second report of *Orthomyxoviridae* derived EVEs (44). Together, these genomes from the firefly holobiont provide valuable resources for the continued inquiry of the symbiotic associates of fireflies and their biological and ecological significance.

Discussion

In summary, we generated high-quality genomes of three evolutionarily informative and historically well-studied bioluminescent beetles, and used a series of comparative

analyses to answer long-standing questions on the origins and evolution of beetle bioluminescence. By analyzing the genomic synteny and molecular evolution of the beetle luciferases and their extant and inferred-ancestral homologs, we found strong support for the independent origins of luciferase, and therefore bioluminescence, between fireflies and click beetles. Our approaches and analyses lend molecular evidence to the previous morphology-phylogeny based hypotheses of parallel gain, first proposed by Darwin and others (11, 32, 45–48). Additional genomic information from basal fireflies (e.g. *Pterotus*), other luminous cantharoid beetle taxa (e.g. Phengodidae and Rhagophthalmidae), and non-luminous elateroid taxa (e.g. Cantharidae and Lycidae), will be useful to further develop and test this model of luciferase evolution, including the hypothesis that bioluminescence also originated independently in the Phengodidae and/or Rhagophthalmidae. The independent origins of the firefly and click beetle luciferases provide an exemplary natural system to understand enzyme evolution through parallel mutational trajectories. The abundance of gene duplication events of PACSs and ACSs at the ancestral luciferase locus in both fireflies and *I. lumenosus* indeed suggests ancestral promiscuous enzymatic activities as raw materials for the selection of new adaptive catalytic functions (49).

Although we conclude that parallel evolution of luciferase implies evolutionary independence of bioluminescence, other subtraits related to bioluminescence likely possess yet more complex evolutionary histories among bioluminescent beetles. These subtraits include luciferin *de novo* biosynthesis and recycling, the developmental program and specialized physiology associated with the light producing cells and organs, and the neurobiology that enables control of bioluminescent signals. While

subtraits like specialized tissues and neural control likely arose after luciferase specialization, and are thus likely to have separate origins between fireflies and click beetles. Luciferin, which was presumably a prerequisite to luciferase neofunctionalization, might have been present in the common ancestor. Through tissue-specific transcriptomics, we identified conserved, lantern-enriched firefly genes which encode enzymes likely involved in luciferin metabolism. Alternatively, microbial endosymbionts, such as the tenericutes detected in our *P. pyralis* and *A. lateralis* datasets, may contribute to luciferin metabolism. A recent report has shown that firefly luciferin is readily produced non-enzymatically by mixing benzoquinone and cysteine (50). Benzoquinone is known to be a defense compound of distantly related beetles and other arthropods (e.g. millipedes) Therefore, the evolutionary role of promiscuous luciferin synthesis through spontaneous chemical reactions, either in the ancestral bioluminescent taxa themselves, or in non-bioluminescent taxa, and dietary acquisition by either the ancestral or modern bioluminescent taxa, should be considered.

The chemical analysis of tissues across species and life stages presented in this work provides new insights into the evolutionary occurrence of lucibufagins, the most well-studied defense compounds associated with fireflies. Our results reject lucibufagins as ancestral defense compounds of fireflies, but rather suggest them as a derived metabolic trait associated with Lampyrinae. Our LC-HRAM-MS and MS2 molecular networking-based lucibufagin identification approach is particular well suited to broaden sampling in the future, including those of rare taxa and possibly museum specimens. Combined with genomic data showing a concomitant expansion of the CYP303 gene

family in *P. pyralis*, we present a promising path towards elucidating the biosynthetic mechanism underlying these potent firefly toxins.

The rich genomic and other resources generated in this study will greatly expedite future inquiries into all components contributing to the complex trait of beetle bioluminescence, and further aid the development of effective strategies to monitor and protect wild bioluminescent beetle populations in the face of rapidly changing climate and habitats due to human activities.

References and Notes

1. J. E. Lloyd, Studies on the flash communication system in *Photinus* fireflies (1966) (available at <https://deepblue.lib.umich.edu/bitstream/handle/2027.42/56374/MP130.pdf?sequence=1&isAllowed=y>).
2. S. M. Lewis, C. K. Cratsley, Flash signal evolution, mate choice, and predation in fireflies. *Annu. Rev. Entomol.* **53**, 293–321 (2008).
3. K. F. Stanger-Hall, J. E. Lloyd, Flash signal evolution in *Photinus* fireflies: character displacement and signal exploitation in a visual communication system. *Evolution*. **69**, 666–682 (2015).
4. R. De Cock, E. Matthysen, Aposematism and Bioluminescence: Experimental evidence from Glow-worm Larvae(Coleoptera: Lampyridae). *Evol. Ecol.* **13**, 619–639 (1999).
5. M. A. Goetz, J. Meinwald, T. Eisner, Lucibufagins, IV. New defensive steroids and a pterin from the firefly, *Photinus pyralis* (coleoptera: Lampyridae). *Experientia*. **37**, 679–680 (1981).
6. O. Shimomura, *Bioluminescence: Chemical Principles and Methods* (World Scientific, 2012).
7. J. R. de Wet, K. V. Wood, D. R. Helinski, M. DeLuca, Cloning of firefly luciferase cDNA and the expression of active luciferase in *Escherichia coli*. *Proc. Natl. Acad. Sci. U. S. A.* **82**, 7870–7873 (1985).
8. D. W. Ow *et al.*, Transient and stable expression of the firefly luciferase gene in plant cells and transgenic plants. *Science*. **234**, 856–859 (1986).
9. H. Fraga, Firefly luminescence: a historical perspective and recent developments. *Photochem. Photobiol. Sci.* **7**, 146–158 (2008).
10. G. J. Martin, M. A. Branham, M. F. Whiting, S. M. Bybee, Total evidence phylogeny and the evolution of adult bioluminescence in fireflies (Coleoptera: Lampyridae). *Mol. Phylogenet. Evol.* **107**, 564–575 (2017).
11. Charles Darwin, *The Origin of Species* (PF Collier & Son, New York, ed. 6th, 1872).
12. B. Bitler, W. D. McElroy, The preparation and properties of crystalline firefly luciferin. *Arch. Biochem. Biophys.* **72**, 358–368 (1957).
13. Y. Oba *et al.*, Bioluminescence of a firefly pupa: involvement of a luciferase isotype in the dim glow of pupae and eggs in the Japanese firefly, *Luciola lateralis*. *Photochem. Photobiol. Sci.* **12**, 854–863 (2013).

14. B. Misof *et al.*, Phylogenomics resolves the timing and pattern of insect evolution. *Science*. **346**, 763–767 (2014).
15. D. D. Mckenna *et al.*, The beetle tree of life reveals that Coleoptera survived end-Permian mass extinction to diversify during the Cretaceous terrestrial revolution. *Syst. Entomol.* **40**, 835–880 (2015).
16. R. Dubois, Note sur la physiologie des pyrophores. *CR Soc Biol.* **2**, 559 (1885).
17. A. V. Zimin *et al.*, The MaSuRCA genome assembler. *Bioinformatics*. **29**, 2669–2677 (2013).
18. J. Butler *et al.*, ALLPATHS: de novo assembly of whole-genome shotgun microreads. *Genome Res.* **18**, 810–820 (2008).
19. N. I. Weisenfeld, V. Kumar, P. Shah, D. M. Church, D. B. Jaffe, Direct determination of diploid genome sequences. *Genome Res.* **27**, 757–767 (2017).
20. D. M. Emms, S. Kelly, OrthoFinder: solving fundamental biases in whole genome comparisons dramatically improves orthogroup inference accuracy. *Genome Biol.* **16**, 157 (2015).
21. F. A. Simão, R. M. Waterhouse, P. Ioannidis, E. V. Kriventseva, E. M. Zdobnov, BUSCO: assessing genome assembly and annotation completeness with single-copy orthologs. *Bioinformatics*. **31**, 3210–3212 (2015).
22. S. S. Lower *et al.*, Genome Size in North American Fireflies: Substantial Variation Likely Driven by Neutral Processes. *Genome Biol. Evol.* **9**, 1499–1512 (2017).
23. V. V. Kapitonov, J. Jurka, Rolling-circle transposons in eukaryotes. *Proc. Natl. Acad. Sci. U. S. A.* **98**, 8714–8719 (2001).
24. A. J. Bewick, K. J. Vogel, A. J. Moore, R. J. Schmitz, Evolution of DNA Methylation across Insects. *Mol. Biol. Evol.* **34**, 654–665 (2017).
25. K. M. Glastad *et al.*, Variation in DNA Methylation Is Not Consistently Reflected by Sociality in Hymenoptera. *Genome Biol. Evol.* **9**, 1687–1698 (2017).
26. J. Maeda *et al.*, The complete mitochondrial genome sequence and phylogenetic analysis of Luciola lateralis, one of the most famous firefly in Japan (Coleoptera: Lampyridae). *Mitochondrial DNA Part B*. **2**, 546–547 (2017).
27. M. Bessho-Uehara, K. Konishi, Y. Oba, Biochemical characteristics and gene expression profiles of two paralogous luciferases from the Japanese firefly Pyrocoelia atripennis (Coleoptera, Lampyridae, Lampyrinae): insight into the evolution of firefly luciferase genes. *Photochem. Photobiol. Sci.* **16**, 1301–1310 (2017).

28. Y. Oba, K. H. Hoffmann, Insect Bioluminescence in the Post-Molecular Biology Era. *Insect Molecular Biology and Ecology*, 94–120 (2014).
29. Y. Oba, M. Ojika, S. Inouye, Firefly luciferase is a bifunctional enzyme: ATP-dependent monooxygenase and a long chain fatty acyl-CoA synthetase. *FEBS Lett.* **540**, 251–254 (2003).
30. Y. Oba, M. Sato, Y. Ohta, S. Inouye, Identification of paralogous genes of firefly luciferase in the Japanese firefly, *Luciola cruciata*. *Gene*. **368**, 53–60 (2006).
31. M. D. Smith *et al.*, Less is more: an adaptive branch-site random effects model for efficient detection of episodic diversifying selection. *Mol. Biol. Evol.* **32**, 1342–1353 (2015).
32. M. A. Branham, J. W. Wenzel, The origin of photic behavior and the evolution of sexual communication in fireflies (Coleoptera: Lampyridae). *Cladistics*. **19**, 1–22 (2003).
33. Y. Oba, N. Yoshida, S. Kanie, M. Ojika, S. Inouye, Biosynthesis of Firefly Luciferin in Adult Lantern: Decarboxylation of L-Cysteine is a Key Step for Benzothiazole Ring Formation in Firefly Luciferin Synthesis. *PLoS One*. **8**, e84023 (2013).
34. T. R. Fallon, F.-S. Li, M. A. Vicent, J.-K. Weng, Sulfoluciferin is Biosynthesized by a Specialized Luciferin Sulfotransferase in Fireflies. *Biochemistry*. **55**, 3341–3344 (2016).
35. K. Okada, H. Iio, I. Kubota, T. Goto, Firefly bioluminescence III. Conversion of oxyluciferin to luciferin in firefly. *Tetrahedron Lett.* **15**, 2771–2774 (1974).
36. H. Ghiradella, J. T. Schmidt, Fireflies at one hundred plus: a new look at flash control. *Integr. Comp. Biol.* **44**, 203–212 (2004).
37. S. R. Smedley *et al.*, Bufadienolides (lucibufagins) from an ecologically aberrant firefly (*Ellychnia corrusca*). *Chemoecology*. **27**, 141–153 (2017).
38. J. Tyler, W. Mckinnon, G. A. Lord, P. J. Hilton, A defensive steroidol pyrone in the Glow-worm *Lampyris noctiluca* L.(Coleoptera: Lampyridae). *Physiol. Entomol.* **33**, 167–170 (2008).
39. B. Hamberger, S. Bak, Plant P450s as versatile drivers for evolution of species-specific chemical diversity. *Philos. Trans. R. Soc. Lond. B Biol. Sci.* **368**, 20120426 (2013).
40. A. T. Willingham, T. Keil, A tissue specific cytochrome P450 required for the structure and function of *Drosophila* sensory organs. *Mech. Dev.* **121**, 1289–1297 (2004).
41. D. J. Newman, G. M. Cragg, Endophytic and epiphytic microbes as “sources” of

- bioactive agents. *Front Chem.* **3**, 34 (2015).
42. K. J. Hackett *et al.*, Lampyridae (Coleoptera): A plethora of mollicute associations. *Microb. Ecol.* **23**, 181–193 (1992).
 43. S. H. Marshall, R. Ramírez, A. Labra, M. Carmona, C. Muñoz, Bona fide evidence for natural vertical transmission of infectious salmon anemia virus in freshwater brood stocks of farmed Atlantic salmon (*Salmo salar*) in Southern Chile. *J. Virol.* **88**, 6012–6018 (2014).
 44. A. Katzourakis, R. J. Gifford, Endogenous viral elements in animal genomes. *PLoS Genet.* **6**, e1001191 (2010).
 45. R. Sagegami-Oba, Y. Oba, H. Ohira, Phylogenetic relationships of click beetles (Coleoptera: Elateridae) inferred from 28S ribosomal DNA: insights into the evolution of bioluminescence in Elateridae. *Mol. Phylogenet. Evol.* **42**, 410–421 (2007).
 46. M. Bocakova, L. Bocak, T. Hunt, M. Teraväinen, A. P. Vogler, Molecular phylogenetics of Elateriformia (Coleoptera): evolution of bioluminescence and neoteny. *Cladistics*. **23**, 477–496 (2007).
 47. J. C. Day, The role of gene duplication in the evolution of beetle bioluminescence. *Trends Entomol.* **9**, 55–63 (2013).
 48. Y. Oba, On the origin of beetle luminescence. *Bioluminescence in focus. Res Signpost, India*, 277–290 (2009).
 49. J.-K. Weng, The evolutionary paths towards complexity: a metabolic perspective. *New Phytol.* **201**, 1141–1149 (2014).
 50. S. Kanie, T. Nishikawa, M. Ojika, Y. Oba, One-pot non-enzymatic formation of firefly luciferin in a neutral buffer from p-benzoquinone and cysteine. *Sci. Rep.* **6**, 24794 (2016).
 51. I. Letunic, P. Bork, Interactive tree of life (iTOL) v3: an online tool for the display and annotation of phylogenetic and other trees. *Nucleic Acids Res.* **44**, W242–5 (2016).

Acknowledgments

We thank Fu-Shuang Li, Geoff Liou, Tomáš Pluskal, Aska Pluskal, and Tina Udhwani, for their assistance with collection of *P. pyralis*, and D. Winston Bellot for his advice on genome assembly. Collection permits and permission from the Mercer County Parks Commission, the National Park Service, and the Arlington Virginia Parks and Resources division are gratefully acknowledged. The authors thank the Whitehead Institute Genome Technology Core, Whitehead Institute high-performance-computing support, MIT BioMicroCenter, University of Rochester Center for Integrated Research Computing, and the Georgia Advanced Computing Resource Center (GACRC) for sequencing and computation resources. We thank Nick A. Rohr for MethylC-Seq library preparation and the Georgia Genomics Facility (GGF) for sequencing. We thank Beijing Genomics Institute for library prep and BGISEQ-500 RNA-Seq of *I. lumninosus*. We thank Dr. Katsushi Yamaguchi for *A. lateralis* sequencing and data submission. We thank Mr. Haruyoshi Ikeya (Toin Gakuen High School, Yokohama, Japan) for providing *A. lateralis* specimens and advice on laboratory culture. We thank Dr. Kota Ogawa, Ryosuke Nakai, and Takahiro Bino for determining *A. lateralis* genome size, and R.N. for useful discussions.

Funding

This work was supported by the Beckman Foundation (JKW), the Pew Scholar Program in the Biomedical Sciences (JKW), the Searle Scholars Program (JKW), the National Science Foundation (SES, Graduate Research Fellowship), and the Lars G. Ljungdahl Distinguished Investigator award (RJS), and the Experiment.com crowdfunding

platform. The authors would like to thank crowdfunding contributors (table S6). A part of work was supported by NIBB Cooperative Research Program (No. 12-202).

Author contributions

T.R.F., S.E.S.L. and J.K.W. conceived the project. T.R.F. performed *P. pyralis* PacBio and Hi-C sequencing. S.E.S.L. performed *P. pyralis* Illumina sequencing. C.H.C. performed *P. pyralis* genome assembly. S.S. performed *A. lateralis* genome assembly. T.R.F. performed *I. luminosus*, mitochondrial, and non-viral symbiont genome assemblies. A.M.L. and C.J.S. performed repeat analysis. I.W. performed in situ hybridizations, A.J.B. performed methylation analysis. M.B. performed bacterial symbiont annotation and analysis. H.J.D. performed viral genome assembly and analysis. M.B.-U. performed *A. lateralis* RNA-Seq, luciferase phylogenetic analysis, and Rh7 phylogenetic analysis. D.N. performed P450 manual annotation. T.R.F., S.E.S.L., K.S.H, and J.K.W. wrote the manuscript. All authors reviewed the manuscript and discussed the work.

Competing interests

The authors declare no competing financial interests.

Data and materials availability

Genomic assemblies (Ppyr1.3, Alat1.3, and Ilumi1.2), associated official geneset data, a BLAST server, and a genome browser are available at www.firebaseio.org. Raw genomic and RNA-Seq reads for *P. pyralis*, *A. lateralis*, and *I. luminosus*, are available

under the NCBI/EBI/DDBJ BioProjects PRJNA378805, PRJDB6460, and PRJNA418169 respectively. Mitochondrial genomes for *P. pyralis* and *I. luminosus* and *A. antennatus* are available on NCBI GenBank with accessions KY778696, MG242621, and MG546669. The complete genome of *Entomoplasma luminosum* subsp. *pyralis* is available on NCBI GenBank with accession CP027019. The viral genomes for Photinus *pyralis* orthomyxo-like virus 1 & 2 are available on NCBI Genbank with accessions MG972985-MG972994. LC-MS data is available on MetaboLights (Accession # XXXXXX). Other supporting datasets are available on FigShare (DOI:10.6084).

Figures

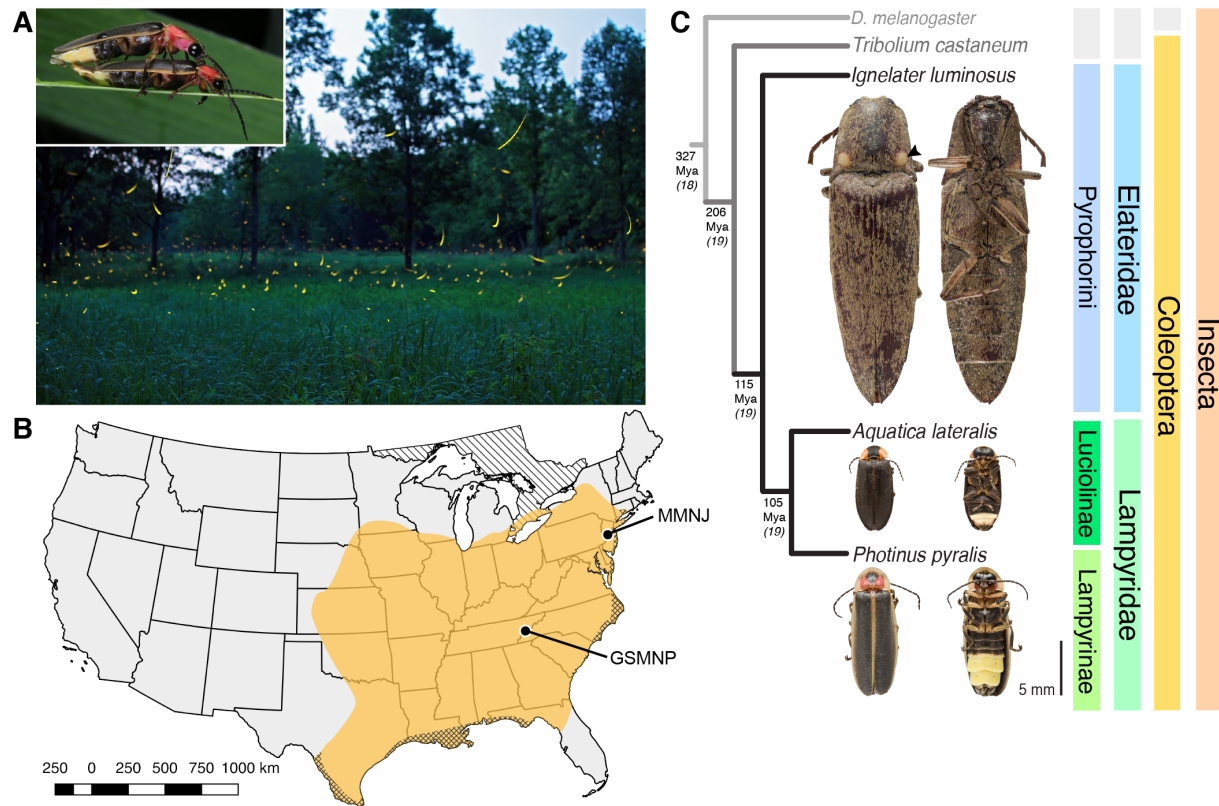


Fig. 1. Geographic and phylogenetic context of the Big Dipper firefly, *Photinus pyralis*.

(A) *P. pyralis* males emitting their characteristic swooping “J” patrol flashes over a field in Homer Lake, Illinois. Females cue in on these species-specific flash patterns and respond with their own species-specific flash (1). Photo credit: Alex Wild. Inset: male and female *P. pyralis* in early stages of mating. Photo credit: Terry Priest. (B) Empirical range of *P. pyralis* in North America, extrapolated from 541 reported sightings (Supp. Text 1.2). Collection sites of individuals used for genome assembly are denoted with circles and location codes. Cross hatches represent areas which likely have *P. pyralis*, but were not sampled. Diagonal hashes represent Ontario, Canada. (C) Cladogram

depicting the hypothetical phylogenetic relationship between *P. pyralis* and related bioluminescent and non-bioluminescent taxa with *Tribolium castaneum* and *Drosophila melanogaster* as outgroups. Numbers at nodes give approximate dates of divergence in millions of years ago (mya) (14, 15). Right: Dorsal and ventral photos of adult male specimens. Note the well-developed ventral light organs on the true abdominal segments 6 & 7 of *P. pyralis* and *A. lateralis*. In contrast, the luminescent click beetle, *I. luminosus*, has paired dorsal light organs at the base of its prothorax (arrowhead) and a lantern on the anterior surface of the ventral abdomen (not visible).

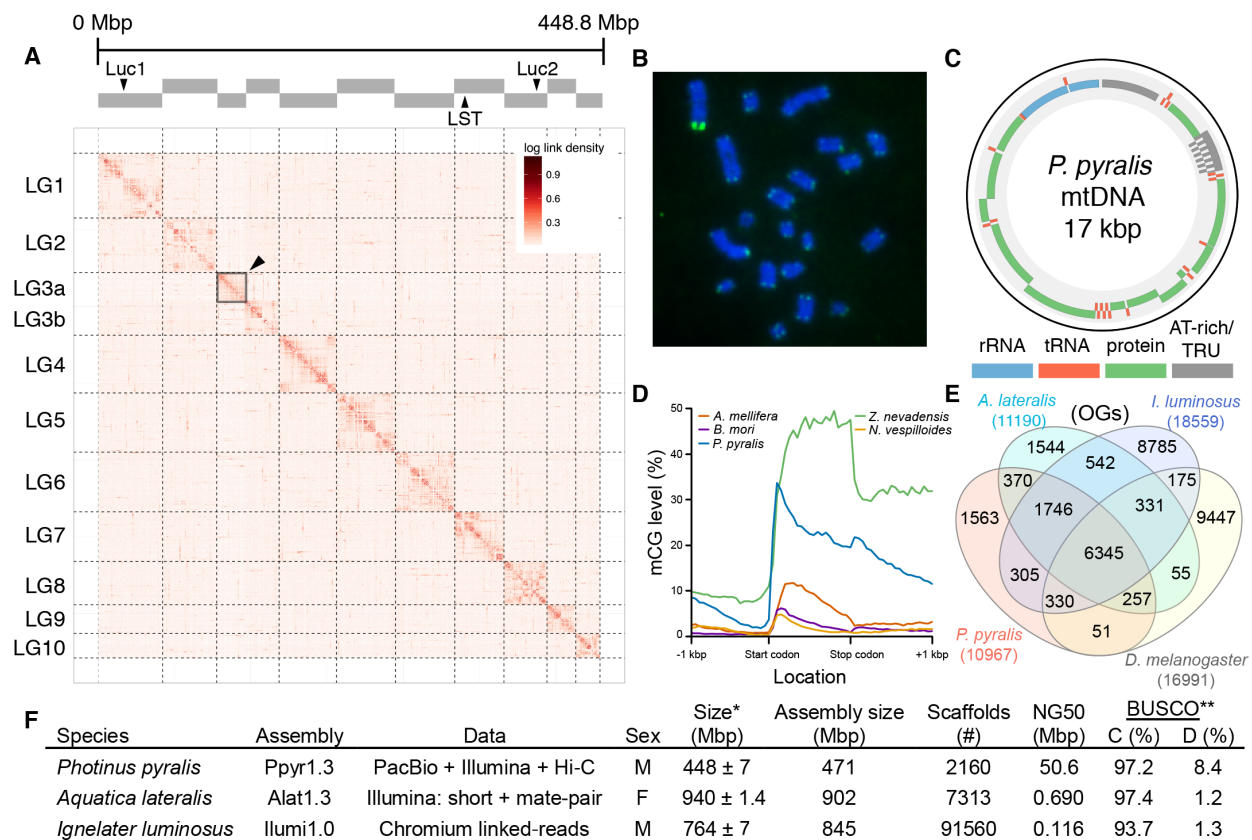


Fig. 2. *Photinus pyralis* genome assembly and analysis.

(A) Assembled Ppyr1.3 linkage groups with annotation of the location of known luminescence related genes, combined with Hi-C linkage density maps. Linkage group 3a (black arrow) corresponds to the X chromosome. **(B)** Fluorescence *in situ* hybridization (FISH) on mitotic chromosomes of a *P. pyralis* larvae. The telomeric repeats TTAGG (green) localize to the ends of chromosomes stained with DAPI (blue). 20 paired chromosomes indicates that this individual was female (Supp. Text 1.13) **(C)** Genome schematic of *P. pyralis* mitochondrial genome (mtDNA). Like other firefly mtDNAs it has a tandem repetitive unit (TRU). **(D)** mCG is enriched across gene bodies of *P. pyralis* and shows methylation levels that are at least twice higher than other holometabolous insects (Supp. Text 1.12) **(E)** Orthogroup (OGs) clustering analysis of

peptides with Orthofinder(20) shows a high degree of overlap of the *P. pyralis*, *A. lateralis*, and *I. luminosus* genesets with the geneset of *D. melanogaster*. **(F)** Assembly statistics for presented genomes. *Genome size estimated by FC: flow cytometry. *P. pyralis* n=5 females (SEM) *I. luminosus* n = 5 males (SEM), *A. lateralis* n = 3 technical-replicates of one female (SD). **Complete (C), and Duplicated (D), percentages for the Endopterygota BUSCO (21) profile.

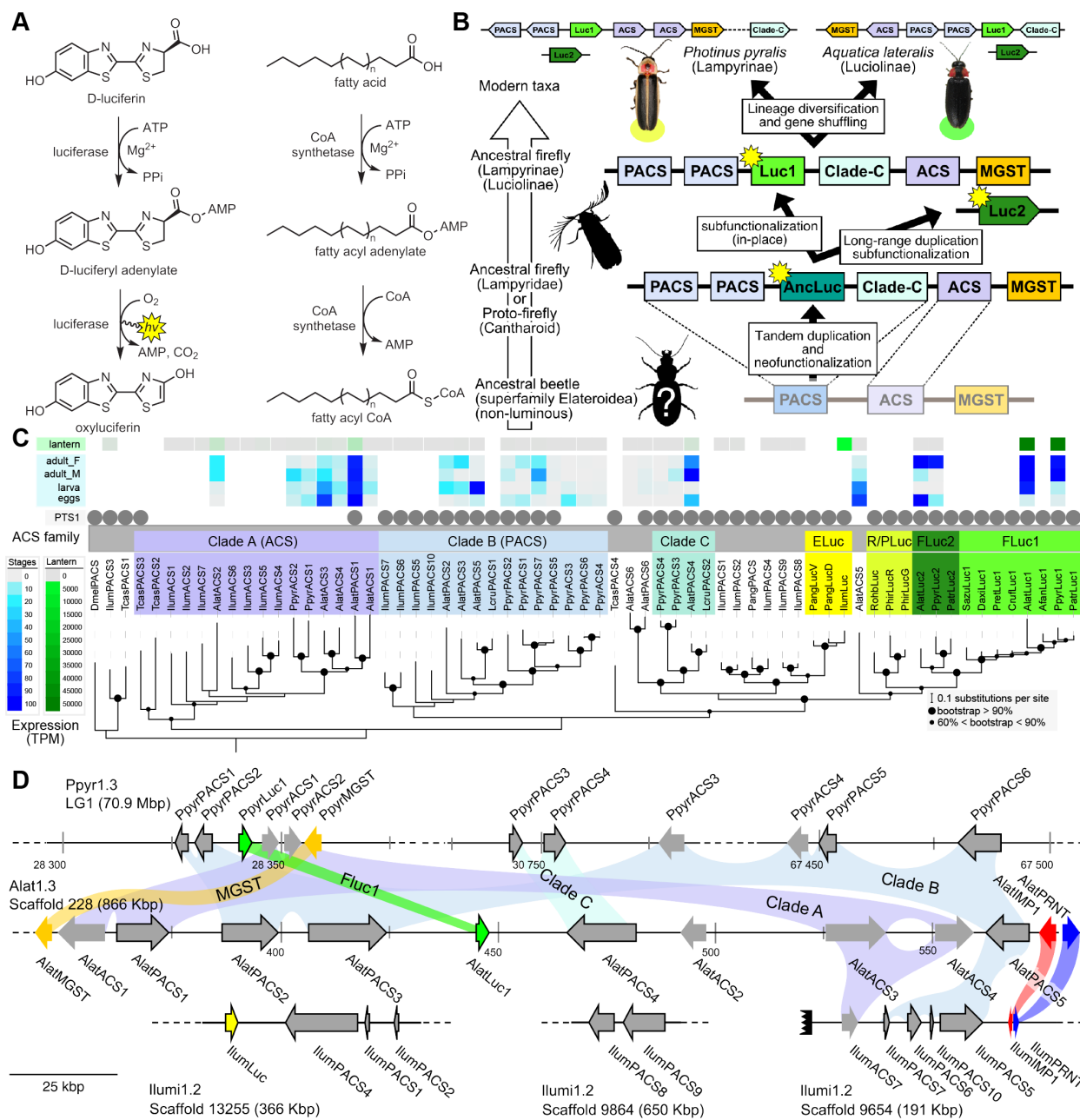


Fig. 3. A genomic view of luciferase evolution

(A) The reaction scheme of firefly luciferase is related to that of fatty acyl-CoA synthetases. **(B)** Model for genomic evolution of firefly luciferases. **(C)** Maximum likelihood tree of luciferase homologs. Grey circles above gene names indicate the presence of peroxisomal targeting signal 1 (PST1). Color gradients indicate the TPM

values of whole body in each sex/stage (grey to blue) and in the lantern (grey to green). Lantern values for *I. luminosus* are from whole prothorax. Tree and annotation visualized using iTOL (51). Fluc=Firefly luciferases, Eluc=Elaterid luciferases, R/PLuc=Rhagophthalmid/Phengodid luciferases. **(D)** Synteny analysis of beetle luciferases. About ten PACS and ACS genes flank the *Luc1* gene in both firefly genomes. Although the *Luc1* loci in *P. pyralis* and *A. lateralis* are apparently derived from a common ancestor, the relative positions of the flanking PACS and ACS genes have diverged between the two species. *IlumiLuc* was captured on a separate scaffold (Ilumi1.2_Scaffold13255) from its most closely related PACSs (*IlumPACS8*, *IlumPACS9*) on Ilumi1.2_Scaffold9864, although one of the 8 other genes on the scaffold is a lowly expressed and partially assembled PACS gene (*IlumiPACS4*). In contrast, a different scaffold (Ilumi1.2_Scaffold9654) shows orthology to the firefly *Luc1* locus. Genes with PTS1 are indicated by a dark outline. Co-orthologous genes are labeled in the same color in the phylogenetic tree and are connected with corresponding color bands in synteny diagram. Scaffold continuation is shown with a dotted line, whereas scaffold ends are shown with rough black bars. MGST: Microsomal glutathione S-transferase, IMP: Inositol monophosphatase, PRNT: Polyribonucleotide nucleotidyltransferase. Gene accession numbers, annotation, and expression values are available on FigShare (DOI: [10.6084/m9.figshare.5725690](https://doi.org/10.6084/m9.figshare.5725690)).

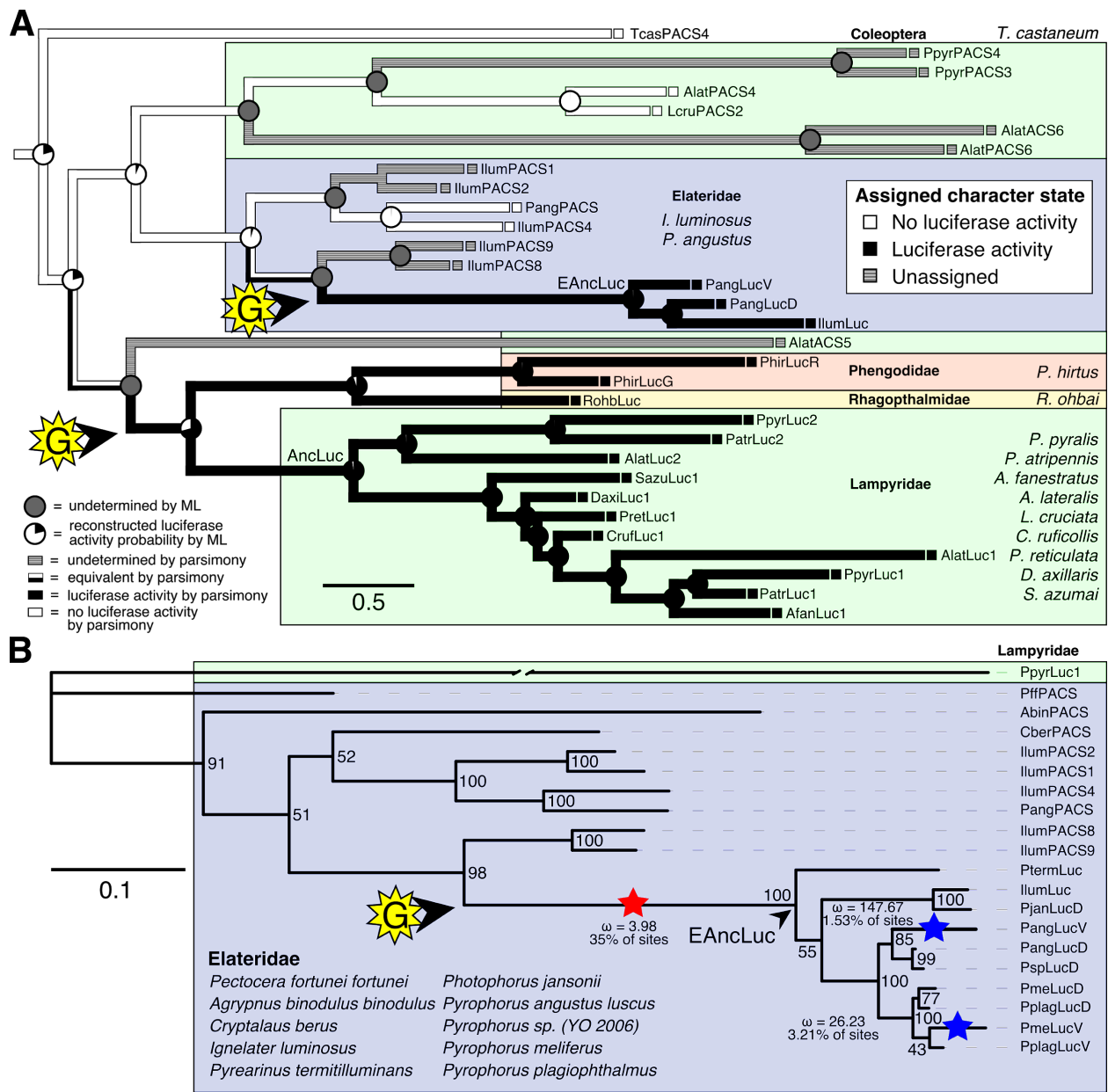


Fig. 4. Parallel evolution of elaterid and firefly luciferase

(A) Ancestral state reconstruction recovers at least two gains of luciferase activity in bioluminescent beetles. Luciferase activity (black: luciferase activity, white: no luciferase activity, shaded: undetermined) was annotated on extant firefly luciferase homologs via literature review or inference via orthology. The ancestral states of luciferase activity within the putative ancestral nodes were then reconstructed with an unordered

parsimony framework and a maximum likelihood (ML) framework (Supp. Text 4.3.3).

Two gains (“G”) of luciferase activity, annotated with black arrows, are hypothesized.

These gains occurred once in a gene within the common ancestor of fireflies, rhagophthalmid, and phengodid beetles, and once in a gene within the common ancestor of bioluminescent elaterid beetles. Scale bar is substitutions per site. (**B**)

Molecular adaptation analysis supports independent neofunctionalization of click beetle luciferase. We tested the molecular adaptation of elaterid luciferase using the adaptive branch-site REL test for episodic diversification (aBSREL) method (31) (Supp. Text 4.3.4). The branch leading to the common ancestor of elaterid luciferases (red star) was one of three branches (red and blue stars) recovered with significant ($p<0.001$) evidence of positive selection, with 35% of sites showing strong directional selection (ω or $d_N/d_S = 3.98$), which we interpret as signal of the initial neofunctionalization of elaterid ancestral luciferase from an ancestor without luciferase activity. The tree and results from the full adaptive model are shown. Branch length, with the exception of the PyrLuc1 branch which was shortened, reflects the number of substitutions per site. Figure was produced with iTOL (51).

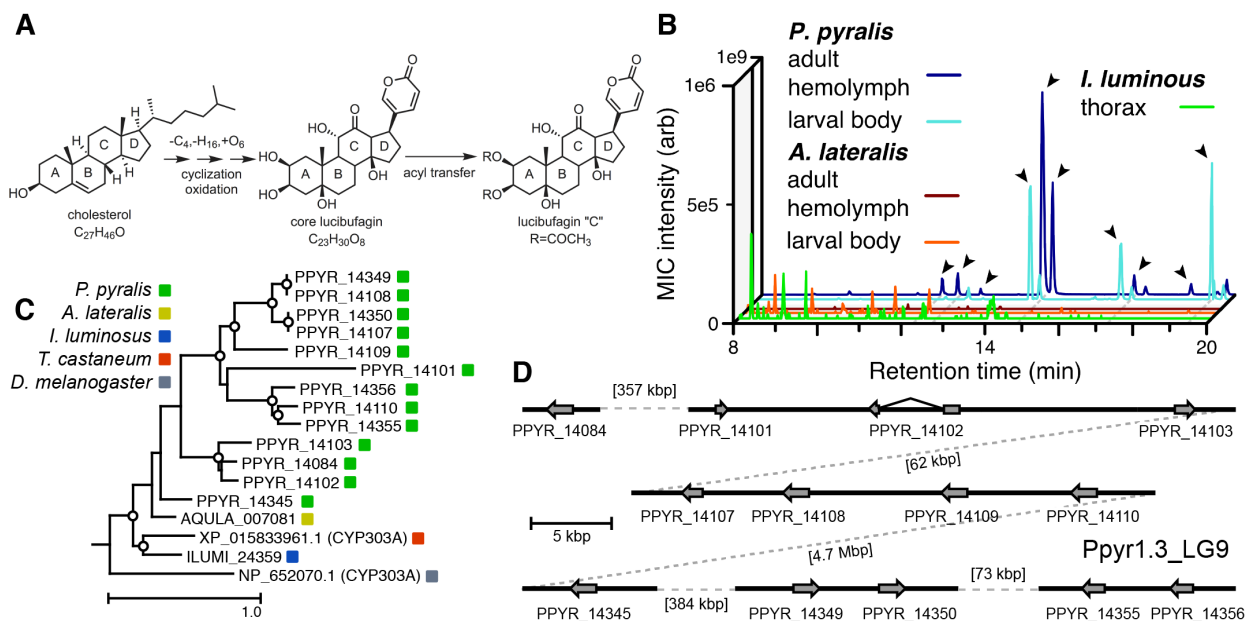


Fig. 5. A expansion in the CYP303-P450 family correlates with lucibufagin content

(A) Hypothesized lucibufagin biosynthetic pathway, starting from cholesterol. **(B)** LC-HRAM-MS multi-ion-chromatograms (MIC) showing the summation of exact mass traces for the $[M+H]$ of 11 lucibufagin chemical formulas \pm 5 ppm, calibrated for run-specific systematic m/z error (table S4.6.5.5). Y-axis upper limit for *P. pyralis* adult hemolymph and larval body extract is 1000x larger than other traces. Arrows indicate features with high MS2 spectral similarity to known lucibufagins. Sporadic peaks in *A. lateralis* body, and *I. luminosus* thorax traces are not abundant, preventing MS2 spectral acquisition and comparison, but do not match the m/z and RT of *P. pyralis* lucibufagins.

(C) Maximum likelihood tree of CYP303 family cytochrome P450 enzymes from *P. pyralis*, *A. lateralis*, *T. castaneum*, and *D. melanogaster*. *P. pyralis* shows a unique CYP303 family expansion, whereas the other species only have a single CYP303. Circles represent node bootstrap support $>60\%$. Branch length measures substitutions per site. **(D)** Genomic loci for *P. pyralis* CYP303 family genes. These genes are found in

multiple gene clusters on LG9, supporting origin via tandem duplication. Introns >4 kbp are shown.

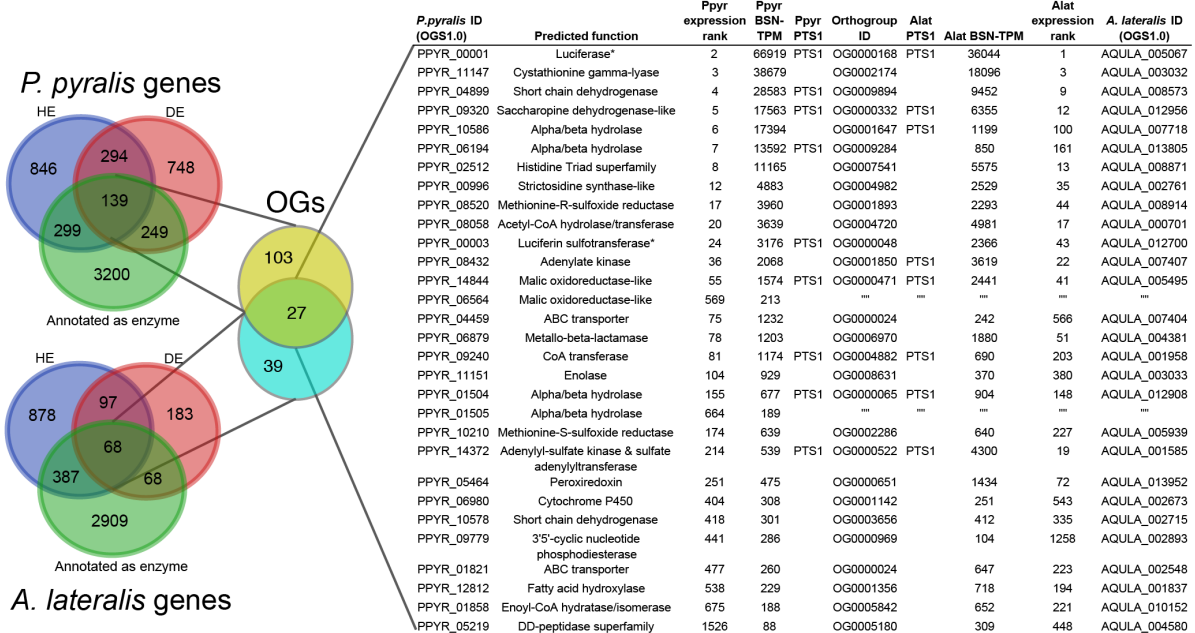


Fig. 6. Comparative analyses of firefly lantern expression highlight likely metabolic adaptations to bioluminescence

Candidate enzymes of bioluminescent accessory metabolism (*= genes of previously described function). Enzymes which are highly expressed (HE), differentially expressed (DE), and annotated as enzymes via InterProScan are shown in the Venn diagrams for their respective species. Those genes in the intersection of the two sets which are within the same orthogroup (OGs) as determined by OrthoFinder are shown in the table. Many-to-one orthology relationships are represented with blank cells.

Supplementary Materials for

Firefly genomes illuminate parallel origins of bioluminescence in beetles

Timothy R. Fallon*, Sarah E. Lower*, Ching-Ho Chang, Manabu Bessho-Uehara, Gavin J. Martin, Adam J. Bewick, Megan Behringer, Humberto J. Debat, Isaac Wong, John C. Day, Anton Suvorov, Christian J. Silva, Kathrin F. Stanger-Hall, David W. Hall, Robert J. Schmitz, David R. Nelson, Sara Lewis, Shuji Shigenobu, Seth M. Bybee, Amanda M. Larracuente, Yuichi Oba & Jing-Ke Weng[†]

*These authors contributed equally to this work.

[†]Corresponding author: wengj@wi.mit.edu

TABLE OF CONTENTS

SUPPLEMENTARY TEXT 1: Photinus pyralis additional information	4
1.1 Taxonomy, biology, and life history	4
Video S1: A <i>Photinus pyralis</i> courtship dialogue	6
1.2 Species distribution	6
Figure S1.2.1: Detailed geographic distribution map for <i>P. pyralis</i>	7
1.3 Specimen collection and identification	8
Figure S1.3.1: <i>P. pyralis</i> aedeagus (male genitalia)	8
1.3.2 Collection and rearing of <i>P. pyralis</i> larvae	9
Figure S1.3.2.1: Luminescence of <i>P. pyralis</i> eggs.	11
Figure S1.3.2.2: Successful gregarios predation of young <i>P. pyralis</i> larvae on live <i>Lumbricus terrestris</i>	12
1.4 Karyotype and genome size	12
1.5 Library preparation and sequencing	12
1.5.1 Illumina	12
1.5.2 PacBio	13
Figure S1.5.2.1: PFGE of <i>P. pyralis</i> HMW DNA used for PacBio sequencing	14
Figure S1.5.2.2: Subread length distribution for <i>P. pyralis</i> PacBio RSII sequencing	15
1.5.3 Hi-C	15
1.6 Genome assembly	16
1.6.2 Ppyr1.1: MaSuRCA hybrid assembly	16
1.6.3 Ppyr1.2: Scaffolding with Hi-C	16
1.6.4 Ppyr1.3: Manual curation and taxonomic annotation filtering	17
1.6.4.1 Defining the X chromosome	17

1.6.4.2 Taxonomic annotation filtering	17
Figure S1.6.4.2.1: Blobplot of Illumina short-insert reads aligned against Ppyr1.2	19
Figure S1.6.4.2.2: Blobplot of <i>P. pyralis</i> PacBio reads aligned against Ppyr1.2	20
Figure S1.6.4.2.3: Venn diagram representation of blobtools taxonomic annotation filtering approach for Ppyr1.2 scaffolds.	21
1.7 Ppyr0.1-PB: PacBio only genome assembly	21
1.8 Mitochondrial genome assembly and annotation	21
Figure S1.8.1: Mitochondrial genome of <i>P. pyralis</i>	23
1.9 Transcriptome analysis	24
1.9.1 RNA-extraction, library preparation and sequencing	24
Table S1.9.1.1: <i>P. pyralis</i> RNA sequencing libraries	25
1.9.2 De novo transcriptome assembly and genome alignment	25
1.9.3 Reference guided transcriptome assembly	26
1.9.4 Transcript expression analysis	27
1.10 Official coding geneset annotation (PPYR_OGS1.0)	27
1.10.1 P450 annotation	28
Figure S1.10.1.1: <i>P. pyralis</i> P450 gene phylogenetic tree	29
1.10.2 Virus annotation and analysis	29
1.11 Repeat annotation	32
Table S1.11.1: Annotated repetitive elements in <i>P. pyralis</i>	32
1.12 Methylation analysis	33
1.13 Telomere FISH analysis	33
SUPPLEMENTARY TEXT 2: <i>Aquatica lateralis</i> additional information	34
2.1 Taxonomy, biology, and life history	34
2.2 Species distribution	34
2.3 Specimen collection	34
2.4 Karyotype and genome size	35
2.5 Genomic sequencing and assembly	35
2.5.1 Taxonomic annotation filtering	36
Figure S2.5.1.1: Blobplot of <i>A. lateralis</i> Illumina reads aligned against Alat1.2	37
2.6 RNA-extraction, library preparation and sequencing	37
Table S2.6.1: <i>Aquatica lateralis</i> RNA sequencing	38
2.7 Transcriptome analysis	39
2.7.1 De novo transcriptome assembly and alignment	39
2.7.2 Reference guided transcriptome alignment and assembly	39
2.7.3 Transcript expression analysis	39
2.8 Official coding geneset annotation (Alat_OGS1.0)	40
2.9 Repeat annotation	40
Table S2.9.1: Annotated repetitive elements in <i>A. lateralis</i>	40
SUPPLEMENTARY TEXT 3: <i>Ignelater luminosus</i> additional information	42

3.1 Taxonomy, biology, and life history	42
3.2 Species distribution	43
3.3 Collection	43
Figure S3.3.1: <i>I. luminosus</i> aedeagus (male genitalia)	44
3.4 Karyotype and genome size	44
3.5 Genomic sequencing and assembly	44
3.5.3 Taxonomic annotation filtering	45
Figure S3.5.3.1: Blobtools plot of Ilumi1.0	46
3.5.4 Ilumi1.1: Indel polishing	47
3.5.5 Ilumi1.2: Manual long-read scaffolding	47
Table S3.5.5.2 Sequence of the <i>I. luminosus</i> luciferase cluster splitting complex tandem repeat	49
Figure S3.5.5.3: Diagram of manual scaffold merges between Ilumi1.1 and Ilumi1.250	50
3.6 RNA extraction, library prep, and sequencing	50
3.6.1 HiSeq2500	50
3.6.2 BGISEQ-500	50
Table S3.6.3: <i>I. luminosus</i> RNA-Seq libraries	51
3.7 Transcriptome analysis	51
3.7.1 De novo transcriptome assembly and alignment	52
3.7.2 Reference guided transcriptome alignment and assembly	52
3.8 Official coding geneset annotation (ILUMI_OGS1.0)	53
3.9 Repeat annotation	53
Figure S3.10.1: Mitochondrial genome of <i>I. luminosus</i>	56
SUPPLEMENTARY TEXT 4: Comparative analyses	57
4.1 Assembly statistics and comparisons	57
Table S4.1.1: Assembly statistics	57
Table S4.1.2: Comparison of BUSCO conserved gene content with other insect genome assemblies	58
4.2 Protein similarity analyses	59
4.2.1 Protein orthogroup clustering	59
Figure S4.2.1.1: Venn diagram of <i>P. pyralis</i> , <i>A. lateralis</i> , <i>I. luminosus</i> , <i>T. castaneum</i> , and <i>D. melanogaster</i> orthogroup relationships.	60
Figure S4.2.2: DNA and tRNA methyltransferase gene phylogeny	61
4.2.3 CYP303 evolutionary analysis	61
4.3 Luciferase evolution analyses	62
4.3.1 Luciferase genetics overview	62
Figure S4.3.1.1: Conserved intron-exon structure of <i>P. pyralis</i> and <i>A. lateralis</i> luciferases	63
4.3.2 Luciferase homolog gene tree	64
Figure S4.3.2.1: Maximum likelihood phylogeny of luciferase homologs	65
4.3.3 Ancestral state reconstruction of luciferase activity (Fig. 4A)	66

4.3.4 Testing for ancestral selection of Elaterid ancestral luciferase (Fig. 4B)	66
4.4 Non-enzyme highly and differentially expressed genes of the firefly lantern	67
Table S4.4.1: Highly expressed (HE), differentially expressed (DE), non-enzyme annotated (NotE), lantern genes whose closest relative in the opposite species is also HE, DE, NotE. BSN-TPM = between sample normalized TPM	68
Figure S4.4.2: Maximum likelihood gene tree of the combined adenylyl-sulfate kinase & sulfate adenylyltransferase orthogroup.	70
4.5 Opsin analysis	70
Figure S4.5.1: ML tree and gene expression levels of opsin genes.	72
4.6 LC-HRAM-MS of lucibufagin content in <i>P. pyralis</i> , <i>A. lateralis</i> , and <i>I. luminosus</i>	73
Figure S4.6.1: Positive mode MS1 total-ion-chromatogram (TIC) of <i>P. pyralis</i> adult hemolymph LC-HRAM-MS data	76
Figure S4.6.2: Negative mode MS1 total-ion-chromatogram (TIC) of <i>P. pyralis</i> adult hemolymph LC-HRAM-MS data	76
Figure S4.6.3: Positive mode MS1 total-ion-chromatogram (TIC) of <i>P. pyralis</i> larval whole body minus 2 posterior segments LC-HRAM-MS data.	77
Figure S4.6.4: Positive mode MS1 total-ion-chromatogram (TIC) of <i>P. pyralis</i> larval whole body minus 2 posterior segments LC-HRAM-MS data.	77
Figure S4.6.5: Positive mode MS1 total-ion-chromatogram (TIC) of <i>A. lateralis</i> adult hemolymph LC-HRAM-MS data.	78
Figure S4.6.6: Negative mode MS1 total-ion-chromatogram (TIC) of <i>A. lateralis</i> adult hemolymph LC-HRAM-MS data.	78
Figure S4.6.7: Positive mode MS1 total-ion-chromatogram (TIC) of <i>A. lateralis</i> larval whole body LC-HRAM-MS data	79
Figure S4.6.8: Negative mode MS1 total-ion-chromatogram (TIC) of <i>A. lateralis</i> larval whole body extract LC-HRAM-MS data	79
Figure S4.6.9: Positive mode MS1 total-ion-chromatogram (TIC) of <i>I. luminosus</i> abdomen extract LC-HRAM-MS data	80
Figure S4.6.10: Negative mode MS1 total-ion-chromatogram (TIC) of <i>I. luminosus</i> abdomen extract LC-HRAM-MS data	80
4.6.5 MS2 similarity search for <i>P. pyralis</i> lucibufagins	81
Figure S4.6.5.2: MS2 spectral similarity network for <i>P. pyralis</i> adult hemolymph lucibufagins	82
Table S4.6.5.3: Putative lucibufagin compounds from LC-HRAM-MS of <i>P. pyralis</i> adult hemolymph.	83
Table S4.6.5.4: Putative lucibufagin compounds from LC-HRAM-MS of <i>P. pyralis</i> larval partial body extracts.	84
Table S4.6.5.5: Putative lucibufagin [M+H] exact masses adjusted for instrument run specific systematic m/z error (Fig. 5B)	84
4.6.7 MS2 similarity search for <i>A. lateralis</i> lucibufagins	85
Table S4.6.7.1: Relative quantification of features identified by lucibufagin MS2 similarity search	86
SUPPLEMENTARY TEXT 5: Holobiont analyses	87

5.1 Assembly and annotation of the complete <i>Entomoplasma luminosum</i> subsp. <i>pyralis</i> genome	87
5.2 Assembly and annotation of Phorid mitochondrial genome	87
Figure S5.2.1: Mitochondrial genome of <i>Apocephalus antennatus</i> .	89
5.3 Taxonomic identification of Phorid mitochondrial genome origin	89
5.4 <i>Photinus pyralis</i> orthomyxo-like viruses	90
Figure S5.4.1: <i>Photinus pyralis</i> viruses and endogenous viral-like elements.	99
Figure S5.4.2: Pairwise identity of OMLV viral proteins amongst identified OMLV viruses.	101
Table S5.4.3: Best hits from BLASTP of PpyrOMLV proteins against the NCBI database	102
Table S5.4.4: InterProScan domain annotation of PpyrOMLV proteins	103
Table S5.4.5: Reads mapped to PpyrOMLV genome segments in available SRA and newly described <i>P. pyralis</i> RNA-Seq datasets	104
Table S5.4.6: Reads mapped to PpyrOMLV genome segments in with FPKM values in available SRA and newly described <i>P. pyralis</i> RNA-Seq datasets	105
5.5 <i>P. pyralis</i> Endogenous virus-like Elements (EVEs)	106
Table S5.5.1: FEVE hits from BLASTX of PpyrOMLV PB1	109
Table S5.5.2: FEVE hits from BLASTX of PpyrOMLV PB2	111
Table S5.5.3: FEVE hits from BLASTX of PpyrOMLV PA	111
Table S5.5.4: FEVE hits from BLASTX of PpyrOMLV HA	111
Table S5.5.5: FEVE hits from BLASTX of PpyrOMLV NP	112
Table S6: Experiment.com donors	113
SUPPLEMENTARY TEXT 7: Data availability	114
Bibliography	115

SUPPLEMENTARY TEXT 1: *Photinus pyralis* additional information

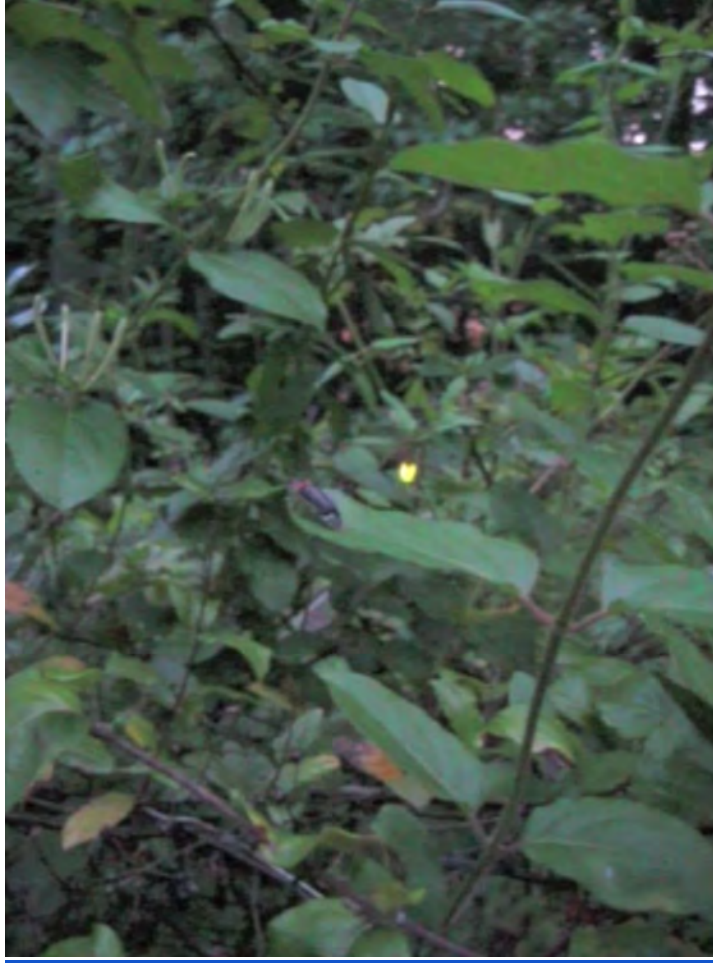
1.1 Taxonomy, biology, and life history

Photinus pyralis (Linnaeus 1767) is amongst the most widespread and abundant of all U.S. fireflies (1, 2). It inspired extensive work on the biochemistry and physiology of firefly bioluminescence in the early 20th century, and the first luciferase gene was cloned from this species (3). A habitat generalist, *P. pyralis* occurs in fields, meadows, suburban lawns, forests, and woodland edges, and even urban environments. For example, the authors have observed *P. pyralis* flashing in urban New York City and Washington D.C. Adults rest on vegetation during the day and signaling begins as early as 20 minutes before sunset (1). Male flashing is cued by ambient light levels, thus shaded or unshaded habitats can show up to a 30 minute difference in the initiation of male flashing (1). Males can be cued to flash outside of true twilight if exposed to light intensities simulating twilight (4). *P. pyralis* were also reported to flash during totality of the total solar eclipse of 2017 (Personal communication: L.F. Faust, M.A. Branham). Courtship activity lasts for 30-45 minutes and both sexes participate in a bioluminescent flash dialog, as is typical for *Photinus* fireflies.

Males initiate courtship by flying low above the ground while repeating a single ~300 ms patrol flash at ~5-10 second intervals (4). Males emit their patrol flash while dipping down and then ascending vertically, creating a distinctive J-shaped flash gesture (1, 4) (Fig. 1A). During courtship, females perch on vegetation and respond to a male patrol flash by twisting their abdomen towards the source of the flash and giving a single response flash given after a 2-3 sec delay ([Video S1](#)). Receptive females will readily respond to simulated male flashes, such as those produced by an investigator's penlight. Females have fully developed wings and are capable of flight. Both sexes are capable of mating several times during their adult lives. During mating, males transfer to females a fitness-enhancing nuptial gift consisting of a spermatophore manufactured by multiple accessory glands (5); the molecular composition of this nuptial gift has recently been elucidated for *P. pyralis* (6). In other *Photinus* species, male gift size decreases across sequential matings (7), and multiple matings are associated with increased female fecundity (8).

Adult *P. pyralis* live 2-3 weeks, and although these adults are typically considered non-feeding, both sexes have been reported drinking nectar from the flowers of the milkweed *Asclepias syriaca* (9). Mated females store sperm and lay ~30-50 eggs over the course of a few days on moss or in moist soil. The eggs take 2-3 weeks to hatch. Larval bioluminescence is thought to be universal for the Lampyridae, where it appears to function as an aposematic warning signal. Like other *Photinus*, *P. pyralis* larvae are predatory, live on and beneath the soil, and appear to be earthworm specialists (10). In the northern parts of its range, slower development likely requires *P. pyralis* to overwinter at least twice, most likely as larvae. Farther south, *P. pyralis* may complete development within several months, achieving two generations per year (11), which may be possibly be observed in the South as a “second wave” of signalling *P. pyralis* in September.

Anti-predator chemical defenses of male *P. pyralis* include several bufadienolides, known as lucibufagins, that circulate in the hemolymph (12). Pterins have also been reported to be abundant in *P. pyralis* (13), however the potential defense role of these compounds has never been tested (Personal communication: J. Meinwald). When attacked, *P. pyralis* males release copious amounts of rapidly coagulating hemolymph and such “reflex-bleeding” may also provide physical protection against small predators (14, 15).



Video S1: A Photinus pyralis courtship dialogue

1.2 Species distribution

Although *Photinus pyralis* is widely distributed in the Eastern United States, published descriptions of its range are limited, with the notable exception of Lloyd's 1966 monograph (1) which addresses the range of many *Photinus* species. We therefore sought to characterize the current distribution of *P. pyralis* in order to produce an updated map to inform our experimental design and enable future population genetic studies. Four sources of data were used to produce the presented range map of *P. pyralis*: (i) Field surveys by the authors (ii) Published (1, 16) and unpublished sightings of *P. pyralis* at county level resolution, provided by Dr. J. Lloyd (University of Florida), (iii) coordinates and dates of *P. pyralis* sightings, obtained by targeted e-mail surveys to firefly field biologists, (iv) citizen scientist reports of *P. pyralis* through the iNaturalist platform (17). iNaturalist sightings were manually curated to only include reports which could be unambiguously identified as *P. pyralis* from the photos, and also that also included GPS geotagging to <100 m accuracy. A spreadsheet of these sightings is available on FigShare (DOI: [10.6084/m9.figshare.5688826](https://doi.org/10.6084/m9.figshare.5688826)).

QGIS (v2.18.9) (18) was used for data viewing and figure creation. A custom Python script (19) within QGIS was used to link *P. pyralis* sightings to counties from the US census shapefile (20). Outlying points that were located in Desert Ecoregions of the World Wildlife Fund (WWF) Terrestrial Ecoregions shapefile (21, 22) or the westernmost edge of the range were manually removed, as they are likely isolated populations not representative of the general range. For Fig. 1B, these points were converted to a polygonal range map using the “Concave hull” QGIS plugin (“nearest neighbors = 19”) followed by smoothing with the Generalizer QGIS plugin with Chaiken’s algorithm (Level=10, and Weight = 3.00). Below (Figure S1.2.1), red circles indicate county-centroided presence records.

In our field surveys, we found that the range of *P. pyralis* was notably extended from the range reported by Lloyd, specifically we found *P. pyralis* in abundance to the west of the Mill river in Connecticut. *P. pyralis* is found with confidence roughly from Connecticut to Texas, and possibly as far south as Guatemala (Personal communication: A. Catalán). These possible southern populations require further study.

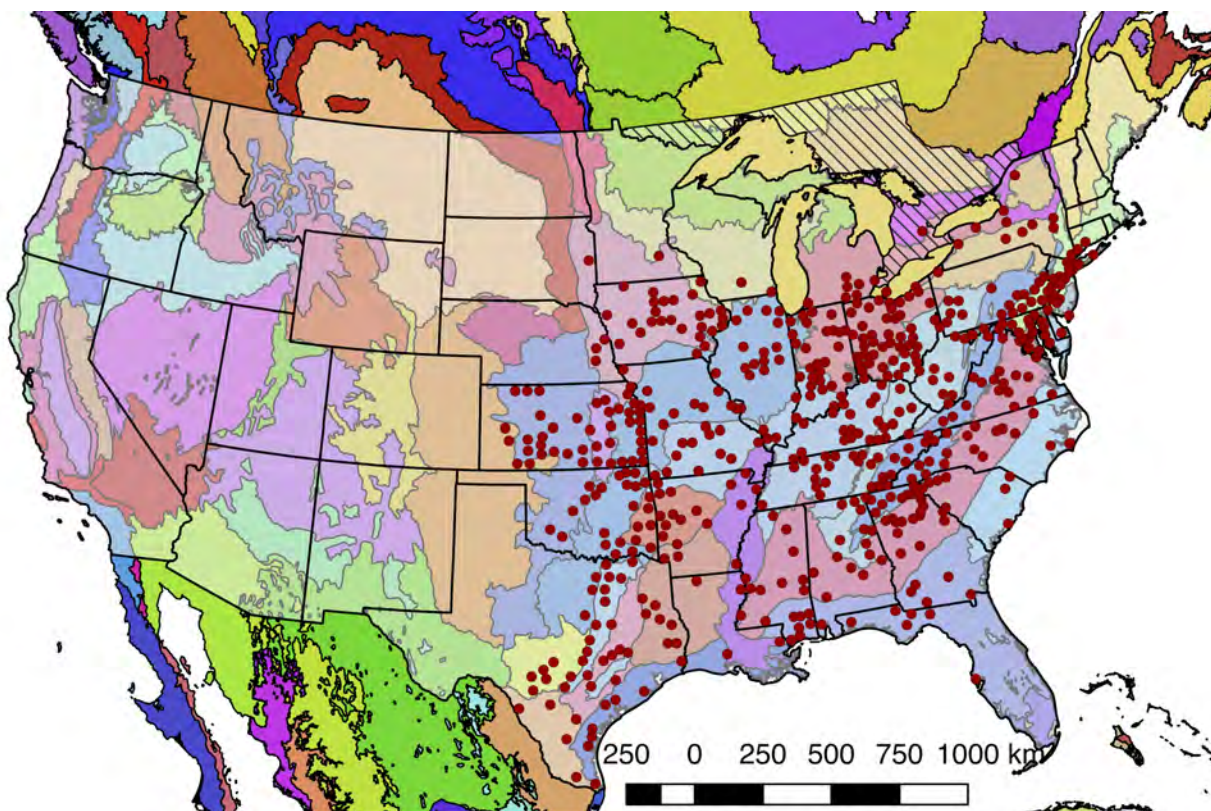


Figure S1.2.1: Detailed geographic distribution map for *P. pyralis*

P. pyralis sightings (red circles show county centroids) in the United States and Ontario, Canada (diagonal hashes). The World Wildlife Fund Terrestrial Ecoregions (21, 22) are also

shown (colored shapes). The *P. pyralis* sighting dataset shown is identical to that used to prepare Fig. 1B.

1.3 Specimen collection and identification

Adult male *P. pyralis* specimens for Illumina short-insert and mate-pair sequencing were collected at sunset on June 13th, 2011 near the Visitor's Center at Great Smoky Mountains National Park (permit to Dr. Kathrin Stanger-Hall). Specimens were identified to species and sex via morphology (23), flash pattern and behavior (1), and *cytochrome-oxidase I* (*COI*) similarity (partial sequence: primers HCO, LCO (24)) when blasted against an in-house database of firefly *COI* nucleotide sequences. Collected fireflies were stored in 95% ethanol at -80°C until DNA extraction.

Adult male *P. pyralis* specimens for Pacific Biosciences (PacBio) RSII sequencing were captured during flight at sunset on June 9th, 2016, from Mercer Meadows in Lawrenceville, NJ (40.3065 N 74.74831 W), on the basis of the characteristic "rising J" flash pattern of *P. pyralis* (permit to TRF via Mercer County Parks Commission). Collected fireflies were sorted, briefly checked to be likely *P. pyralis* by the presence of the margin of ventral unpigmented abdominal tissue anterior to the lanterns, flash frozen with liquid N₂, lyophilized, and stored at -80°C until DNA extraction. A single aedeagus (male genitalia) was dissected from the stored specimens and confirmed to match the *P. pyralis* taxonomic key (23) (Fig. S1.3.1).

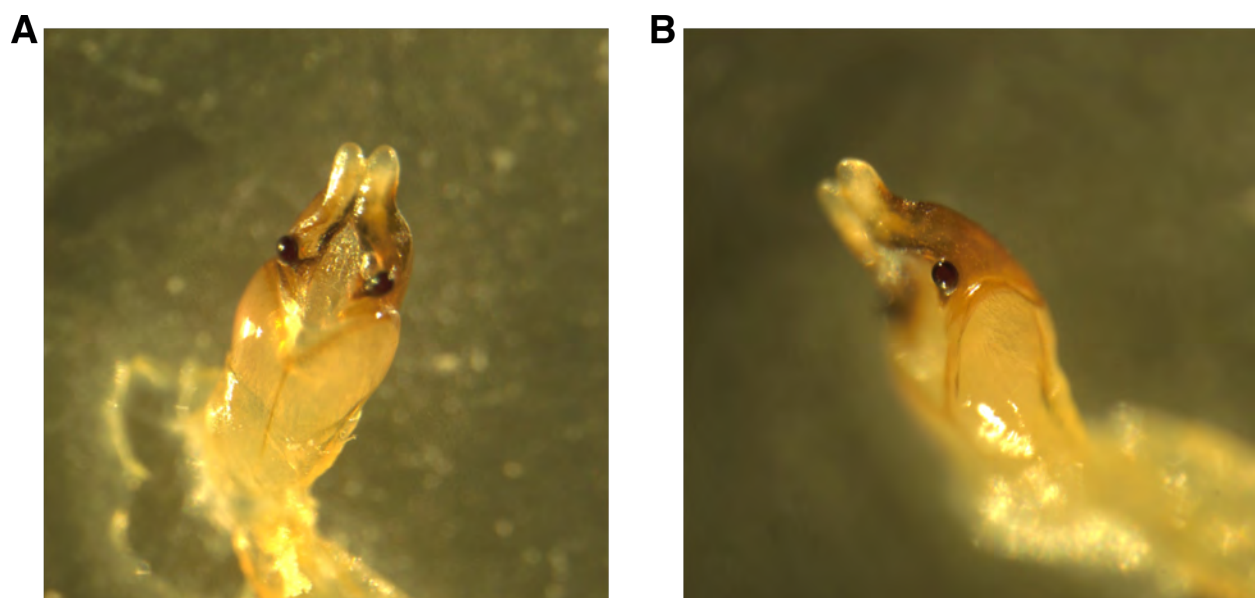


Figure S1.3.1: *P. pyralis* aedeagus (male genitalia)

(A) Ventral and (B) side view of a *P. pyralis* aedeagus dissected from specimens collected on the same date and locality as those used for PacBio sequencing. Note the strongly sclerotized paired ventro-basal processes ("mickey mouse ears") emerging from the median process, characteristic of *P. pyralis* (23).

1.3.2 Collection and rearing of *P. pyralis* larvae

We intended to survey the lucibufagin content of *P. pyralis* larvae (Fig 4B; Supplementary Text 4.6), as well as the transovarial transmission of *P. pyralis* orthomyxo-like viruses from parent to larvae (Supplementary Text 5.4;5.5), but as *P. pyralis* larvae are subterranean and extremely difficult to collect from the wild, we reared *P. pyralis* larvae from eggs laid from mated pairs. It is important to note that these *P. pyralis* larval rearing experiments were unexpectedly successful. Although there has been some success in laboratory rearing and domestication of Asian *Aquatica* spp. (25), including the *A. lateralis* Ikeya-Y90 strain described in this manuscript, rearing of North American fireflies is considered extremely difficult with numerous unpublished failures for unclear reasons (26), and limited reports of successful rearing of mostly non-*Photinus* genera, including *Photuris* sp. (27), *Pyractomena angulata* (28), and *Pyractomena borealis* (Personal communication: Scott Smedley). The below protocol for *Photinus pyralis* larval rearing is presented in the context of disclosure of the methods of this manuscript, and should be considered a preliminary unoptimized rearing protocol. A full description of the *P. pyralis* larvae and its life history and behavior will be presented in a separate manuscript.

Four adult female *P. pyralis* were collected from the Bluemont Junction Trail in Arlington, VA from June 12th through June 18th 2017 (collection permission obtained by TRF from Arlington County Parks and Recreation department). The females were mated to *P. pyralis* males collected either from the same locality and date, or to males collected from elsewhere in late June. Mating was performed by housing 1-2 males and 1 female in small plastic containers for ~1-3 days with a wet kimwipe to maintain humidity. Mating pairs were periodically checked for active mating, which in *Photinus* fireflies takes several hours. Successfully mated females were transferred to Magenta GA-7 plastic boxes (Sigma-Aldrich, USA), and provided a ~4 cm x 4 cm piece of locally collected moss (species diverse and unknown) as egg deposition substrate, and allowed to deposit eggs until their death in ~1-4 days. Deceased females were removed, artificial freshwater (AFW; 1:1000 diluted 32 PSU artificial seawater) was sprayed into the box to maintain high humidity, and eggs were kept for 2-3 weeks at room temperature and periodically checked until hatching. Like other firefly eggs, the eggs of *P. pyralis* were observed to be faintly luminescent imaging using a cooled CCD camera (Figure S.1.3.2.1), however this luminescence was not visible to the dark-adapted eye, indicating that this luminescence is less intense than other firefly species such as *Luciola cruciata* (29).

Upon hatching, 1st instar larvae were mainly fed ~1 cm cut pieces of Canadian Nightcrawler earthworms (*Lumbricus terrestris*; Windsor Wholesale Bait, Ontario, Canada), and occasional live White Worms (*Enchytraeus albidusare*; Angels Plus, Olean, NY). Although *P. pyralis* larvae were observed to attack live *Enchytraeus albidusare*, an experiment to determine if this would be suitable as a single food source was not performed. Uneaten and putrefying earthworm pieces were removed after 1 day, and the container cleaned. Once the larvae had been manually fed for ~2 weeks and deemed sufficiently strong, they were transferred to plastic shoeboxes (P/N: S-15402, ULINE, USA) which were intended to mimic a soil ecosystem. In personal discussions of unpublished firefly rearing attempts by various firefly researchers, we noted that a common theme was the difficulty of preventing the uneaten prey of these predatory larvae from putrifying. Therefore, we sought to create ecologically inspired “eco-shoeboxes”, where fireflies would prey on live organisms, and other organisms would assist in cleanup of

uneaten or partially eaten prey that had been fed to the firefly larvae, to prevent the growth of pathogenic microorganisms on uneaten prey.

First, these shoeboxes were filled with 1L of mixed 50% (v/v) potting soil, and 50% coarse sand (Quikrete, USA) that had been washed several times with distilled water to remove silt and dust. The soil-sand mix was wet well with AFW, and live *Enchytraeus albidusare* (50+), temperate springtails (50+; *Folsomia candida*; Ready Reptile Feeders, USA), and dwarf isopods (50+; *Trichorina tomentosa*; Ready Reptile Feeders, USA) were added to the box, and several types of moss, coconut husk, and decaying leaves were sparingly added to the corners of the box. The non-firefly organisms were included to mimic a primitive detritivore (*Enchytraeus albidusare* & *Trichorina tomentosa*) and fungivore (*Folsomia candida*) system. About 50 firefly larvae were included per box. No interactions between the *P. pyralis* larvae and the additional organisms were observed. Predation on *Enchytraeus albidusare* seems likely, but careful observations were not made. Distilled water was sprayed into the box every ~2 days to maintain a high humidity. Throughout this period, live *Lumbricus terrestris* (~10-15 cm) were added to the box every 2-3 days as food. These earthworms were first prepared by washing with distilled water several times to remove attached soil, weakened and stimulated to secrete coelomic fluid and gut contents by spraying with 95% ethanol, washed several times in distilled water, and left overnight in ~2 cm depth distilled water at 4°C. Anecdotally this cleaning and preparation process reduced the rate and degree that dead earthworms putrefied. Young *P. pyralis* larvae were observed to successfully kill and gregariously feed on these live earthworms (Figure S1.3.2.2). The possibility that firefly larvae possess a paralytic venom used to stun or kill prey has been noted by other researchers (10, 30). In our observations, an earthworm would immediately react to the bite from a single *P. pyralis* larvae, thrashing about for several minutes, but would then become seemingly paralyzed over time, supporting the role of a potent, possibly neurotoxic, firefly venom. The *P. pyralis* larvae would then begin extra-oral digestion and feeding on the liquified earthworm. Once the earthworm had been killed and broken apart by firefly larvae, *Enchytraeus albidusare* would enter through gaps in the cuticle and begin to feed in large numbers throughout the interior of the earthworm. The other detritivores were observed at later stages of feeding. Between the combined action of the *P. pyralis* larvae, and the other detritivores, the live earthworm was completely consumed within 1-2 days, and no manual cleanup was required.

Compared to the initial manual feeding and cleaning protocol for *P. pyralis* 1st instar larvae, the “eco-shoebox” rearing method was low-input and convenient for large numbers of larvae. The feeding and cleanup process was efficient for ~2 months (July -> September), leading to a large number of healthy 3-4th instar larvae. However after that point, *P. pyralis* larvae, possibly in preparation for a winter hibernation, seemingly became quiescent, and were less frequently seen patrolling throughout the box. At the same time, the *Enchytraeus albidusare* earthworms were observed to become less abundant, either due to continual predation by *P. pyralis*, or due to population collapse from insufficient fulfillment of nutritional requirements from feeding of *Enchytraeus albidusare* on *Lumbricus terrestris* alone.

At this point, earthworms were not consumed within 1-2 days, and became putrid, and *P. pyralis* which had been feeding on these earthworms were frequently found dead nearby, and themselves quickly putrefied. Generally after this point *P. pyralis* larvae were more frequently found dead and partially decayed, indicating the possibility of pathogenesis from

microorganisms from putrefying earthworms. At this stage it was observed that mites (Acari), probably from the soil contained in the guts of fed earthworms, became abundant, and were observed to act as ectoparasitic on *P. pyralis* larvae. An attempt to simulate hibernation of *P. pyralis* larvae was made by storing them at 4°C for ~3 weeks, however a large proportion (~30%) of larvae died during this hibernation to a seeming fungal infection. Other larvae revived quickly when returned to room temperature, but all *Trichorina tomentosa* were killed by even transient exposure to 4°C. To date, a smaller number of 5th and 6th instar *P. larva*e have been obtained, but pupation in the laboratory has not occurred. The lack of pupation is unsurprising as it is likely occurs in the wild after 1-2 years of growth, is likely under temperature and photoperiodic control, and may require a licensing stage of cold temperature hibernation for several weeks. Overall, manual feeding of 1st instar larvae followed by the “eco-shoebox” method was unexpectedly successful approach for the maintenance and growth of *P. pyralis* larvae.

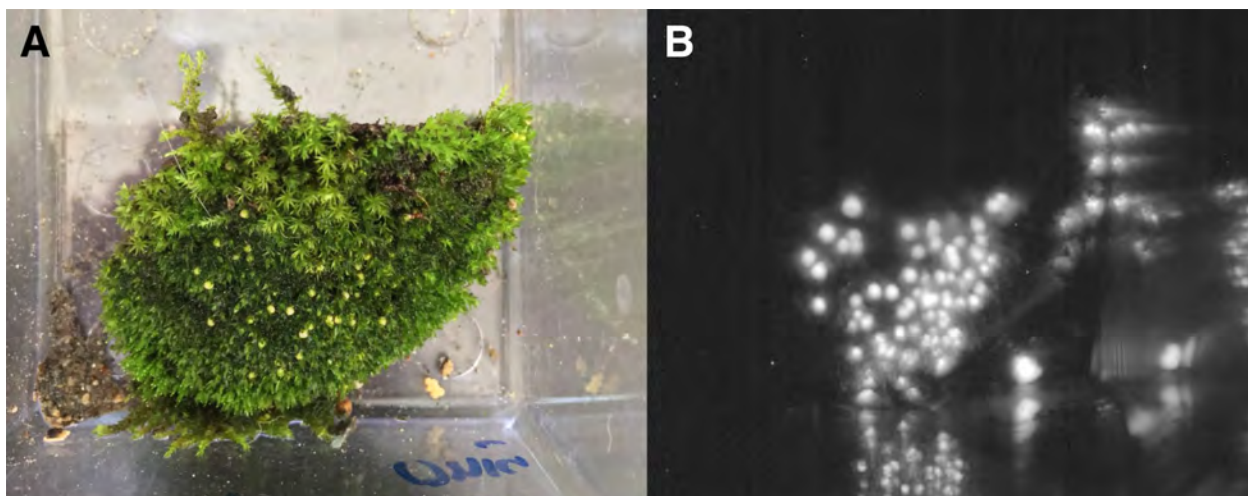


Figure S1.3.2.1: Luminescence of *P. pyralis* eggs.

(A) Photograph under ambient light of ~1 day post deposition *P. pyralis* eggs. **(B)** Photograph of self-luminescence of ~1 day post deposition *P. pyralis* eggs. Both photographs taken with a NightOwl LB98 cooled CCD luminescence imager (Berthold Technologies, USA). Luminescence was not visible to the dark-adapted eye.



Figure S1.3.2.2: Successful gregarious predation of young *P. pyralis* larvae on live *Lumbricus terrestris*

Both *P. pyralis* larvae (red arrows), and *Enchytraeus albidus* (yellow arrow), were observed to feed on the paralyzed earthworms.

1.4 Karyotype and genome size

The karyotype of *P. pyralis* was previously reported to be 2n=20 with XO sex determination (male, 18A+XO; female, 18A+XX) (31). The genome sizes of four *P. pyralis* adult males were previously determined to be 422 ± 9 Mbp (SEM, n=4), whereas the genome sizes of five *P. pyralis* adult females were determined to be 448 ± 7 (SEM, n=5) by nuclear flow cytometry analysis (32). From these analyses, the size of the X-chromosome is inferred to be ~26 Mbp.

1.5 Library preparation and sequencing

1.5.1 Illumina

DNA was extracted from sterile-water-washed thorax using phenol-chloroform extraction with RNase digestion, checked for quality via gel electrophoresis, and quantified by Nanodrop

or Qubit (Thermo Scientific, USA). To obtain sufficient DNA for both short insert and mate-pair library construction, libraries were constructed separately from DNA from each of two individual males and pooled DNA of three males, all from the same population. Males were selected for sequencing as they are more easily found in the field than females. In addition, as *P. pyralis* males are XO (33), differences in sequencing coverage could inform localization of scaffolds to the X chromosome. Illumina TruSeq short insert (average insert size: 300 bp) and Nextera mate-pair libraries (insert size: 3 Kbp, 6 Kbp) were constructed at the Georgia Genomics Facility (Athens, GA) and subsequently sequenced on two lanes of Illumina HiSeq2000 100x100 bp PE reads (University of Texas; [Table S1](#)).

1.5.2 PacBio

High-molecular-weight DNA (HMW DNA) was extracted from lyophilized adult male *P. pyralis* (dry mass 90.8 mg), which were first washed using 95% ethanol, using a 100/G Genomic Tip plus Genomic Buffers kit (Qiagen, USA). DNA extraction followed the manufacturer's protocol, with the exception of the final precipitation step, where HMW DNA was pelleted with 40 µg RNA grade glycogen (Thermo Scientific, USA) and centrifugation (3000 x g, 30 min, 4°C) instead of spooling on a glass rod. Although increased genomic heterozygosity from 4 pooled males and a resulting more complicated genome assembly was a concern for a wild population like *P. pyralis*, four males were used in order to extract enough DNA for workable coverage using 15 Kbp+ size-selected PacBio RSII sequencing. All extracted DNA was used for library preparation, and all of the final library was used for sequencing. Adult males, being XO, were chosen over the preferable XX females, as adult males are much more easily captured because they signal during flight, whereas females are typically found in the brush below and generally only flash in response to authentic male signals.

Precipitated HMW DNA was redissolved in 80 µL Qiagen QLE buffer (10 mM Tris-Cl, 0.1 mM EDTA, pH 8.5) yielding 17.1 µg of DNA (214 ng/µL) and glycogen (500 ng/µL). Final DNA concentration was measured with a Qubit fluorometer (Thermo Scientific) using the Qubit Broad Range kit. Manipulations hereafter, including HMW DNA size QC, fragmentation, size selection, library construction, and PacBio RSII sequencing, were performed by the Broad Technology Labs of the Broad Institute (Cambridge, MA, USA).

First, the size distribution of the HMW DNA was confirmed by pulsed-field-gel-electrophoresis (PFGE). In brief, 100 ng of HMW DNA was run on a 1% agarose gel (in 0.5x TBE) with the BioRad CHEF DRIII system. The sample was run out for 16 hours at 6 volts/cm with an angle of 120 degrees with a running temperature of 14°C. The gel was stained with SYBRgreen dye (Thermo Scientific - Part No. S75683). 1 µg of 5 Kbp ladder (BioRad, part no 170-3624) was used as a standard. These results demonstrated the HMW DNA had a mean size of >48 Kbp (Fig. S1.5.2.1). This pool of HMW DNA is designated 1611_PpyrPB1 (NCBI BioSample SAMN08132578).

Next, HMW DNA (17.1 µg) was sheared to a targeted average size of 20-30 Kbp by centrifugation in a Covaris g-Tube (part no. 520079) at 2500 x g for 2 minutes. SMRTbell

libraries for sequencing on the PacBio platform were constructed according to the manufacturer's recommended protocol for 20 Kbp inserts, which includes size selection of library constructs larger than 15 Kbp using the BluePippin system (Sage Science, Beverly MA, USA). Two separate cassettes were run. In each cassette, 2 lanes were used in which there was 1362 ng/lane (PAC20kb kit). Constructs 15 Kbp and above were eluted over a period of four hours. An additional damage repair step was carried out post size-selection. Insert size range for the final library was determined using the Fragment Analyzer System (Advanced Analytical, Ankeney IA, USA). The size-selected SMRTbell library was then sequenced over 61 SMRT cells on a PacBio RSII instrument of the Broad Technology Labs (Cambridge, MA), using the P6 v.2 polymerase and the v.4 DNA Sequencing Reagent (P6-C4 chemistry; part numbers 100-372-700, 100-612-400). PacBio sequencing data is available on the NCBI Sequence Read Archive (Bioproject PRJNA378805).

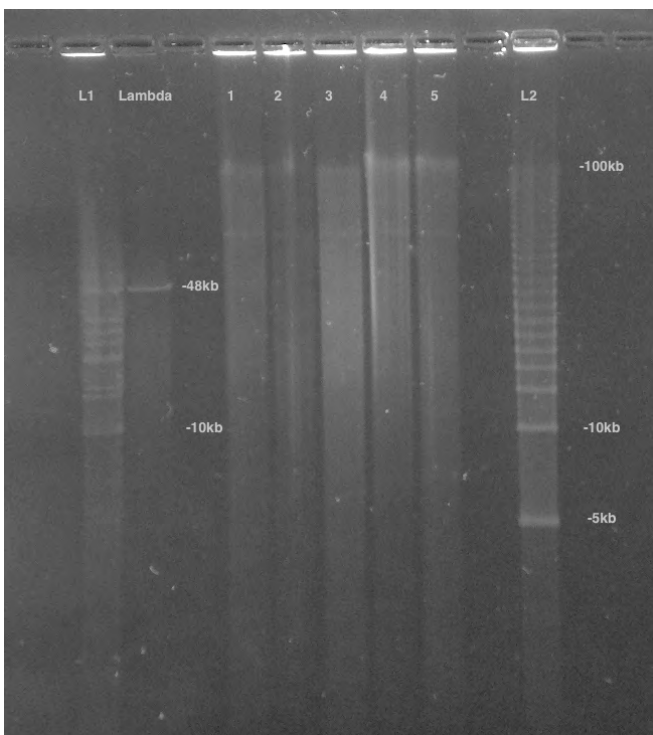


Figure S1.5.2.1: PFGE of *P. pyralis* HMW DNA used for PacBio sequencing

Lane 1 was used for further library prep and sequencing, Lanes 2-5 represent separate batches of *P. pyralis* HMW DNA that was not used for PacBio sequencing. Lane 1 was used as it had the highest DNA yield, and an equivalent DNA size distribution to the other samples.

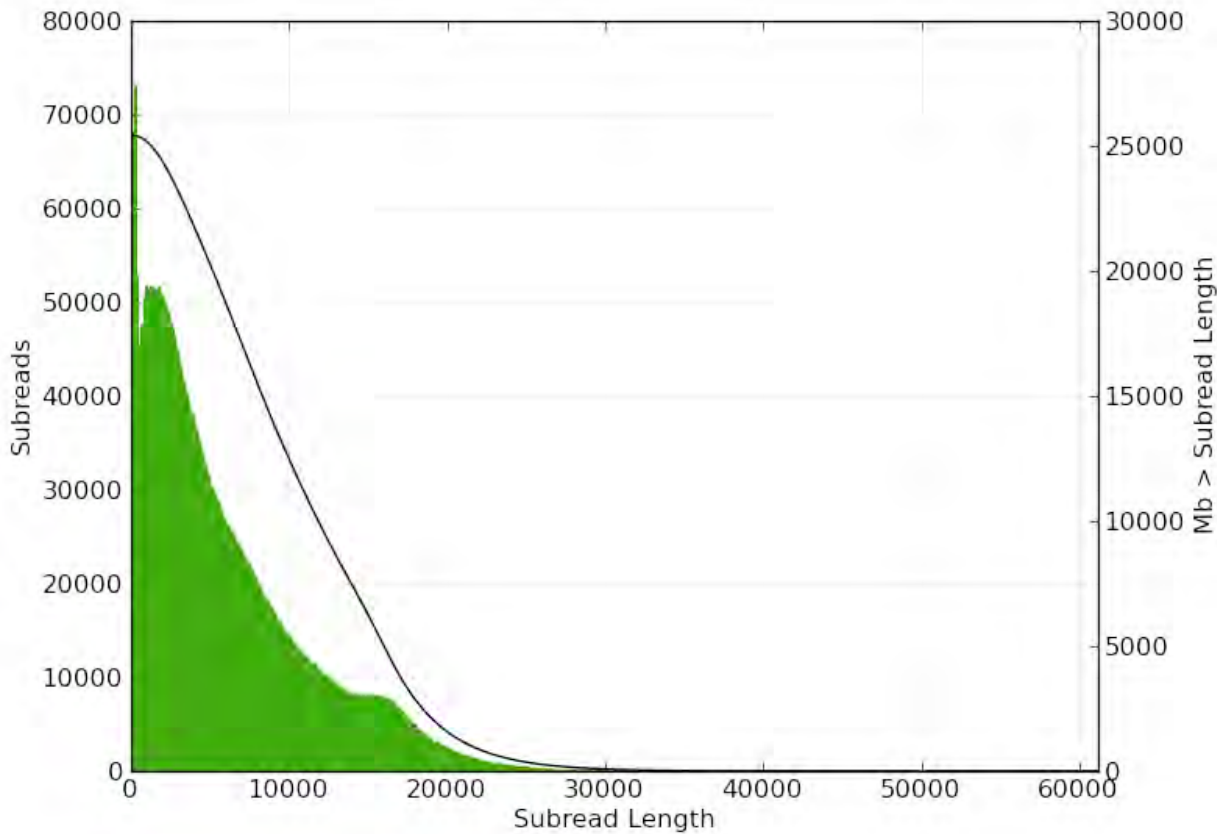


Figure S1.5.2.2: Subread length distribution for *P. pyralis* PacBio RSII sequencing.

Figure produced with SMRTPortal (v2.3.0.140936) (34) by aligning all PacBio reads from data from the 61 SMRT cells against Ppyr1.3 using the RS_Resequencing.1 protocol with default parameters.

1.5.3 Hi-C

Two adult *P. pyralis* MMNJ males were flash frozen in liquid nitrogen, stored at -80°C, and shipped on dry-ice to Phase Genomics (Seattle, WA). Manipulations hereafter occurred at Phase Genomics, following previously published protocols(35–37). Briefly, a streamlined version of the standard Hi-C protocol (35) was used to perform a series of steps resulting in proximity-ligated DNA fragments, in which physically proximate sequence fragments are joined into linear chimeric molecules. First, *in vivo* chromatin was cross-linked with formaldehyde, fixing physically proximate loci to each other. Chromatin was then extracted from cellular material and digested with the Sau3AI restriction enzyme, which cuts at the GATC motif. The resulting fragments were proximity ligated with biotinylated nucleotides and pulled down with streptavidin beads. These chimeric sequences were then sequenced with 80 bp PE sequencing on the Illumina NextSeq platform, resulting in Hi-C read pairs.

1.6 Genome assembly

The *P. pyralis* genome assembly followed three stages: first, a hybrid assembly using Illumina and PacBio reads, producing assembly Ppyr1.1 (Supplementary Text 1.6.2); second, Ppyr1.1 scaffolded using Hi-C data, producing assembly Ppyr1.2 (Supplementary Text 1.6.3), and third, Ppyr1.2 manually curated for proper X-chromosome assembly and removal of putative non-firefly sequences, producing Ppyr1.3 (Supplementary Text 1.6.4).

1.6.2 Ppyr1.1: MaSuRCA hybrid assembly

Several genome assembly approaches were evaluated with the general goal of maximizing conserved gene content and contiguity. The highest quality *P. pyralis* assembly was generated by a hybrid assembly approach using a customized MaSuRCA (v3.2.1_01032017) (38, 39) pipeline that combined both Illumina-corrected PacBio reads (Mega-reads) and synthetic long reads constructed from short-insert reads alone (Super-reads) using a custom small overlap length (59 bp).

We first applied MaSuRCA (v3.2.1_01032017) (40, 41) to correct our long reads (38x coverage; Library ID 1611_PpyrPB1; [Table S1](#)) using our short-insert and mate-pair reads (Libraries: 8369, 375_3K, 8375_6K, 83_3K, 83_6K; [Table S1](#)). No pre-filtering of reads was performed, as Illumina adaptors are automatically removed within the MaSuRCA pipeline. We modified the pipeline to assemble the genome using both corrected long reads (Mega-reads) and synthetic long reads (Super-reads) with a custom smaller overlap length (59 bp). All reads (short-insert, mate-pair and PacBio) were then used within the MaSuRCA pipeline to call a genomic consensus.

To scaffold the contigs, we first filtered Illumina short-reads from the mate-pair libraries (Libraries 8375_3K, 8375_6K, 83_3K, 83_6K) with Nxtrim (v0.4.1) (42) with parameters "--separate --rf --justmp". We then manually integrated the MaSuRCA assembly by replacing the incomplete mitochondrial contigs with complete mitochondrial assemblies from *P. pyralis* and *Apocephalus antennatus* (Supplementary Text 5.2). We scaffolded and gap-filled the assembly using the Illumina short-insert and filtered mate-pair reads (Libraries: 8369, 8375_3K, 8375_6K, 83_3K, 83_6K) via Redundans (v0.13a) (43) with default settings. After scaffolding with our Illumina data, redundant sequences were removed by the MaSuRCA "deduplicate_contigs.sh" script. We then applied PBjelly (v15.8.24) (44) and PacBio reads to scaffold and gap-fill the assembly, and redundancy reduction with "deduplicate_contigs.sh" script was run again. Finally, we replaced mitochondrial sequences which had been artificially extended by the scaffolding, gap-filling and sequence extension process with the proper sequences. This assembly yielding from this process was dubbed Ppyr1.1.

1.6.3 Ppyr1.2: Scaffolding with Hi-C

The Hi-C read pairs were applied in a manner similar to that originally described here (36) and later expanded upon (37). Briefly, Hi-C reads were mapped to Ppyr1.1 with BWA (v1.7.13) (45), requiring perfect, unique mapping locations for a read pair to be considered

usable. The number of read pairs joining a given pair of contigs is referred to as the “link frequency” between those contigs, and when normalized by the number of restriction sites in the pair of contigs, is referred to as the “link density” between those contigs.

A three-stage scaffolding process was used to create the final scaffolds, with each stage based upon previously described analysis of link density (36, 37). First, contigs were placed into chromosomal groups. Second, contigs within each chromosomal group were placed into a linear order. Third, the orientation of each contig is determined. Each scaffolding stage was performed many times in order to optimize the scaffolds relative to expected Hi-C linkage characteristics.

In keeping with previously described methods (36, 37), the number of chromosomal scaffolds to create—10—was an *a priori* input to the scaffolding process derived from the previously published chromosome count of *P. pyralis* (31). However, to verify the correctness of this assumption, scaffolds were created for haploid chromosome numbers ranging from 5 to 15. A scaffold number of 10 was found to be optimal for containing the largest proportion of Hi-C linkages within scaffolds, which is an expected characteristic of actual Hi-C data.

1.6.4 Ppyr1.3: Manual curation and taxonomic annotation filtering

1.6.4.1 Defining the X chromosome

Hi-C data was mapped and converted to .hic format with the juicer pipeline (v1.5.6)(46), and then visualized using juicebox (v1.5.2) (47). This visualization revealed a clear breakpoint in Hi-C linkage density on LG3 at ~22,220,000 bp. Mapping of Illumina short-insert and PacBio reads with Bowtie2 (v2.3.1) (48) and SMRTPortal (v2.3.0.140893) with the “RS_Resequencing.1” protocol, followed by visualization with Qualimap (v2.2.1) (49), revealed that the first section of LG3 (1-22,220,000 bp), here termed LG3a, was present at roughly half the coverage of LG3b (22,220,001-50,884,892 bp) in both the Illumina and PacBio libraries. Mapping of *Tribolium castaneum* X chromosome proteins (NCBI Tcas 5.2) to the Ppyr1.2 assembly using both tblastn (v2.6.0) (50) and Exonerate (v2.2.0) (51) based “protein2genome” alignment through the MAKER pipeline revealed a relative enrichment on LG3a only. Taken together, this data suggested that the half-coverage section of LG3 (LG3a) corresponded to the X-chromosome of *P. pyralis*, and that it was misassembled onto an autosome. Therefore, we manually split LG3 into LG3a and LG3b in the final assembly.

1.6.4.2 Taxonomic annotation filtering

Given the recognized importance of filtering genome assemblies to avoid misinterpretation of the data (52), we sought to systematically remove assembled non-firefly contaminant sequence from Ppyr1.2. Using the blobtools toolset (v1.0.1) (53), we taxonomically annotated our scaffolds by performing a blastn (v2.6.0+) nucleotide sequence similarity search against the NCBI nt database, and a diamond (v0.9.10.111)(54) translated nucleotide sequence similarity search against the of Uniprot reference proteomes (July 2017). Using this similarity information, we taxonomically annotated the scaffolds with blobtools using parameters “-x

bestsumorder --rank phylum". A tab delimited text file containing the results of this blobtools annotation are available on FigShare (DOI: [10.6084/m9.figshare.5688982](https://doi.org/10.6084/m9.figshare.5688982)). We then generated the final genome assembly by retaining scaffolds that either contained annotated features (genes or non-simple/low-complexity repeats), had coverage > 10.0 in both the Illumina (Fig. S1.6.3.2.1) and PacBio libraries (Fig. S1.6.3.2.2), and if the taxonomic phylum was annotated as "Arthropod" or "no-hit" by the blobtools pipeline. This approach removed 374 scaffolds (2.1 Mbp), representing 15% of the scaffold number and 0.4% of the nucleotides of Ppyr1.2. Notably, four tenericute scaffolds, likely corresponding to a partially assembled *Entomoplasma* sp. genome, distinct from the *Entomoplasma luminosus* var. *pyralis* assembled from the PacBio library (Supplementary Text 5) were removed. Furthermore we removed two contigs representing the mitochondrial genome of *P. pyralis* (complete mtDNA available via Genbank: KY778696). The final filtered assembly, Ppyr1.3, is available at www.firebaseio.org.

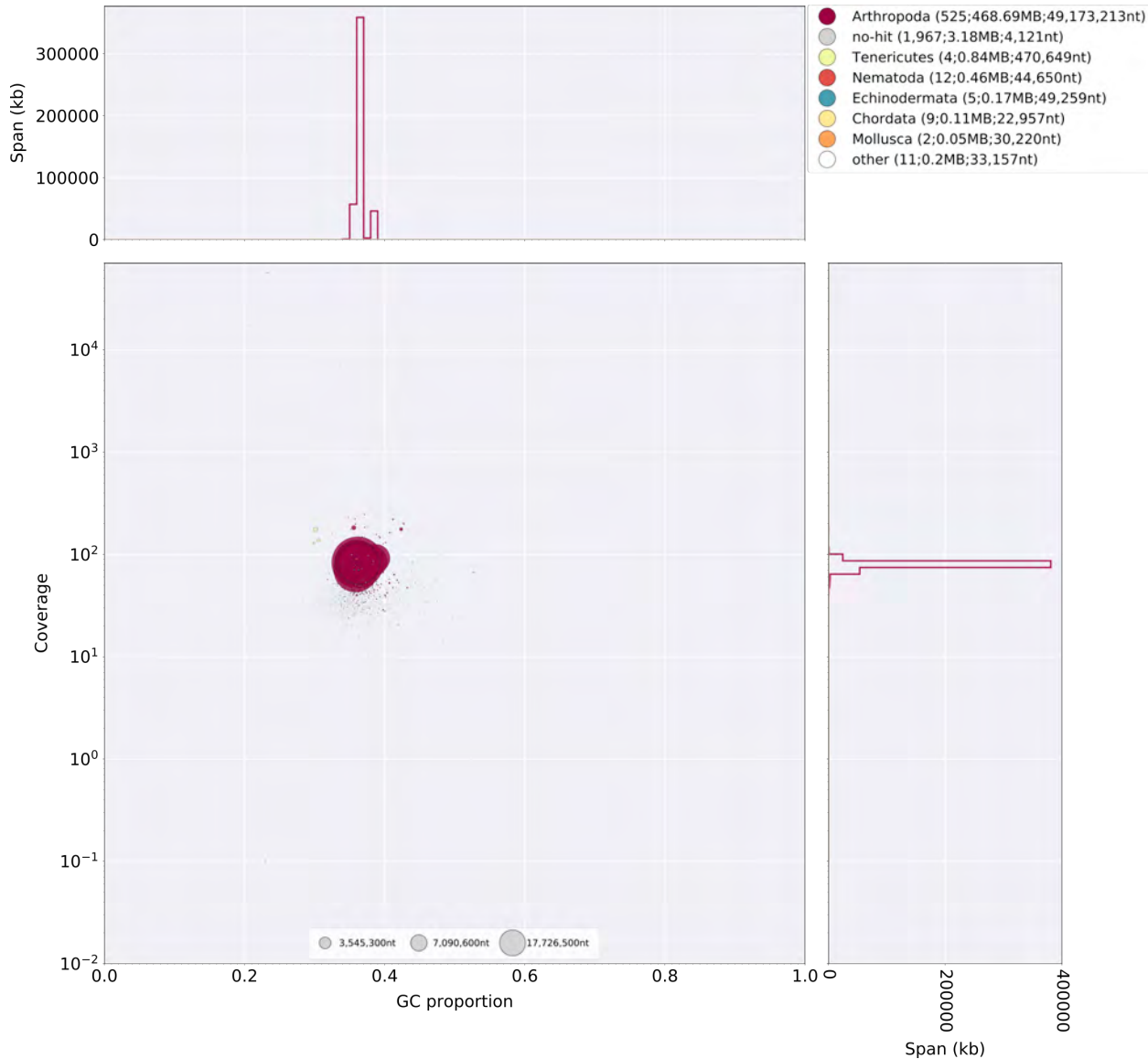


Figure S1.6.4.2.1: Blobplot of Illumina short-insert reads aligned against Ppyr1.2

Coverage shown represents mean coverage of reads from the Illumina short-insert library (Sample name 8369; [Table S1](#)), aligned against Ppyr1.2 using Bowtie2 with parameters (`--local`). Scaffolds were taxonomically annotated as described in Supplementary Text 1.6.3.2.

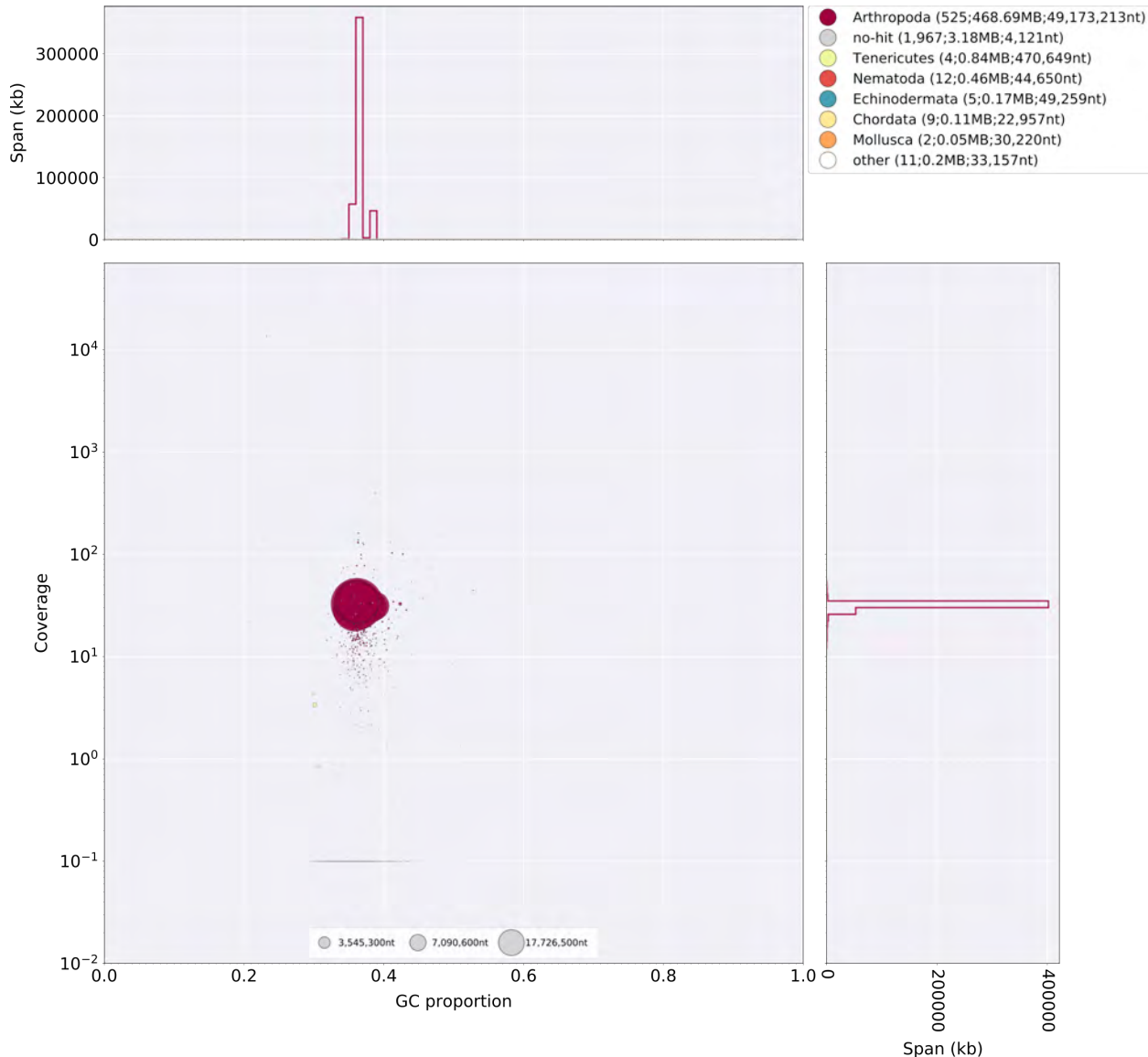


Figure S1.6.4.2.2: Blobplot of *P. pyralis* PacBio reads aligned against Ppyr1.2

Coverage shows represents mean coverage of reads from the PacBio library (Sample name 1611; [Data Table S1](#)). The reads were aligned using SMRTPortal v2.3.0.140893 with the “RS_Resequencing.1” protocol with default parameters. Scaffolds were taxonomically annotated as described in Supplementary Text 1.6.3.2.

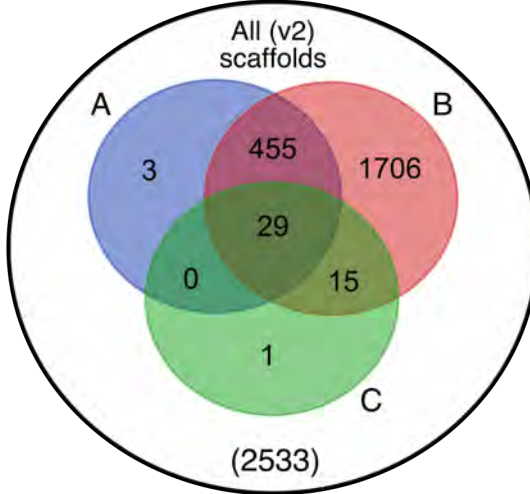


Figure S1.6.4.2.3: Venn diagram representation of blobtools taxonomic annotation filtering approach for Ppyr1.2 scaffolds.

(A) The blue set represents scaffolds which have >10.0 coverage in both Illumina and PacBio libraries, **(B)** The red set represents scaffolds which had either genes or repeats (non simple or low-complexity) annotated, **(C)** The green set represents scaffolds with suspicious taxonomic assignment (Non ‘Arthropod’ or ‘no-hit’). Outside A, B, and C, represents low-coverage, unannotated scaffolds. Ppyr1.3 consists of the intersection of A and B, minus the intersection of C. All linkage groups (LG1-LG10) were annotated as ‘Arthropod’ by blobtools, and captured in the intersection between A and B but not set C.

1.7 Ppyr0.1-PB: PacBio only genome assembly

In addition to our finalized genome assembly (Ppyr1.3), we sought to better understand the symbiont composition that varied between our *P. pyralis* PacBio and Illumina libraries. Therefore we produced a long-read only assembly of our PacBio data to assemble the sequence that might be unique to this library. To achieve this, we first filtered the HDF5 data from the 61 sequence SMRT cells to .FASTQ format subreads using SMRTPortal (v2.3.0.140893) (34) with the “RS_Subreads.1” protocol with default parameters. These subreads were then input into Canu (Github commit 28ecea5 / v1.6) (55) with parameters “genomeSize=450m corOutCoverage=200 ovlErrorRate=0.15 obtErrorRate=0.15 -pacbio-raw”. The unpolished contigs from this produced genome assembly are dubbed Ppyr0.1-PB.

1.8 Mitochondrial genome assembly and annotation

To achieve a full length mitochondrial genome (mtDNA) assembly of *P. pyralis*, sequences were assembled separately from the nuclear genome. Short insert Illumina reads from a single GSMNP individual (Sample 8369; [Data Table S1](#)) were mapped to the known mtDNA of the closest available relative, *Pyrocoelia rufa* (NC_003970.1 (56)) using bowtie2 v2.3.1 (parameters: --very-sensitive-local). All concordant read pairs were input to SPAdes

(v3.8.0) (57) (parameters: --plasmid --only-assembler -k35,55,77,90) for assembly. The resulting contigs were then combined with the *P. rufa* mitochondrial reference genome for a second round of read mapping and assembly. The longest resulting contig aligned well to the *P. rufa* mitochondrial genome, however it was ~1 Kbp shorter than expected, with the unresolved region appearing to be the tandem repetitive region (TRU) (56), previously described in the *P. rufa* mitochondrial genome. To resolve this, all PacBio reads were mapped to the draft mitochondrial genome, and a single high-quality PacBio circular-consensus-sequencing (CCS) read that spanned the unresolved region was selected using manual inspection and manually assembled with the contiguous sequence from the Illumina sequencing to produce a complete circular assembly. The full assembly was confirmed by re-mapping the Illumina short-read data using bowtie2 followed by consensus calling with Pilon v1.21 (58). Re-mapped PacBio long-read data also confirmed the structure of the mtDNA, and indicated variability in the repeat unit copy number of the TRU amongst the four sequenced *P. pyralis* individuals (Sample 1611_PpyrPB1; [Table S1](#)). The *P. pyralis* mtDNA was then “restarted” using seqkit (59), such that the FASTA record break occurred in the AT-rich region, and annotated using the MITOS2 annotation server (60). Low confidence and duplicate gene predictions were manually removed from the MITOS2 annotation. The final *P. pyralis* mtDNA plus annotations is available on GenBank (KY778696).

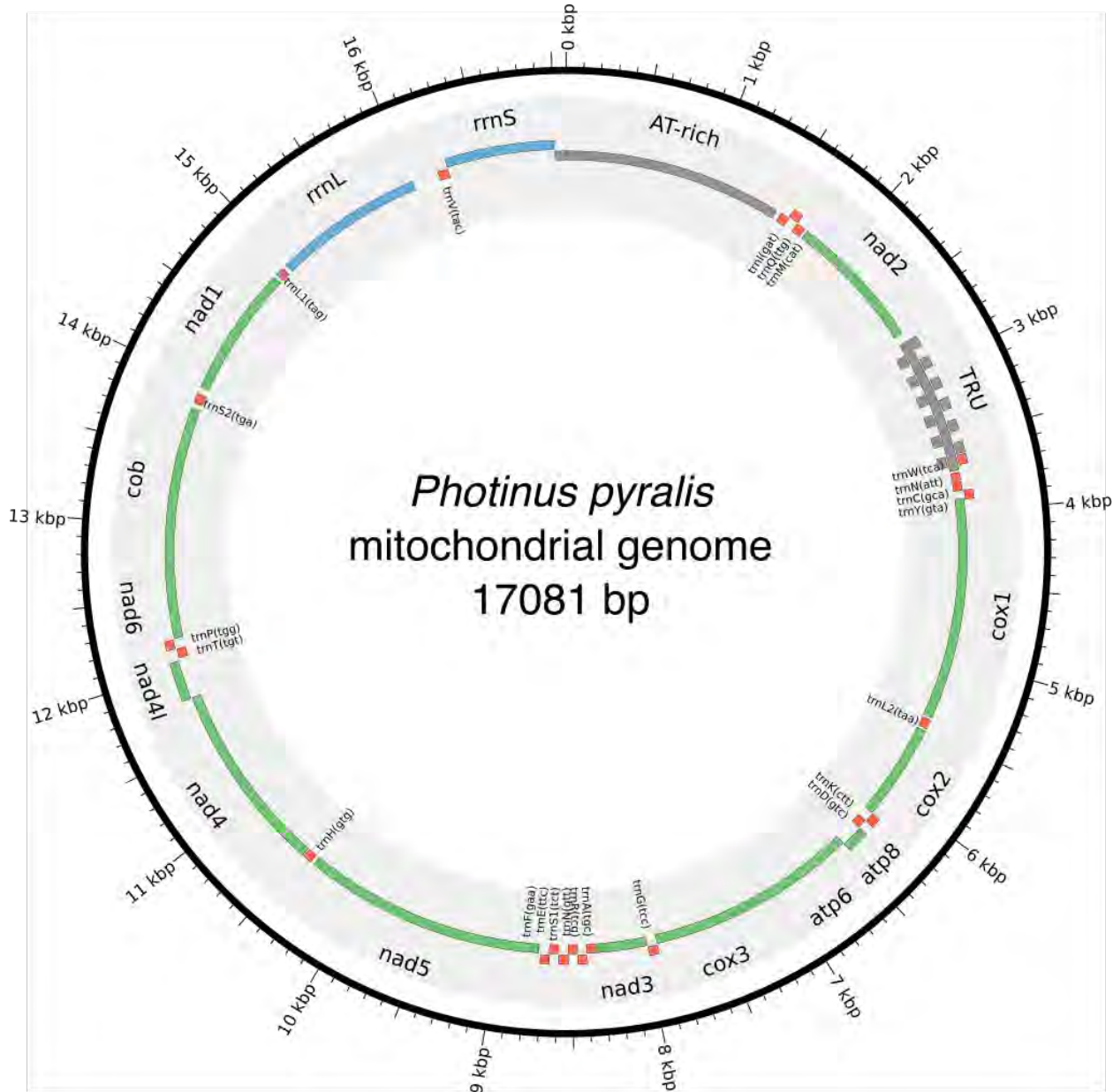


Figure S1.8.1: Mitochondrial genome of *P. pyralis*

The mitochondrial genome of *P. pyralis* was assembled and annotated as described. Note the firefly specific tandem-repeat-unit (TRU) region. Figure produced with Circos (61).

1.9 Transcriptome analysis

1.9.1 RNA-extraction, library preparation and sequencing

In order to capture expression from diverse life stages, stranded RNA-Seq libraries were prepared from whole bodies of four life stages/sexes (eggs, 1st instar larvae, adult male, and adult female; Table S1.9.1.1). Eggs and larvae were derived from a laboratory mating of *P. pyralis* (Collected MMNJ, July 2016). Briefly, live adult *P. pyralis* were transported to the lab and allowed to mate in a plastic container over several days. The female, later sequenced, was observed mating with two independent males on two separate nights. The female was then transferred to a plastic container with moss, and allowed to oviposit over several days. Once no more oviposition was observed, the female was removed, flash frozen with liquid N₂, and stored at -80°C for RNA extraction. Resulting eggs were washed 3x with dilute bleach/ H₂O and reared in aggregate in plastic containers on moist Whatman paper. ~13 days after the start of egg oviposition, a subset of eggs were flash frozen for RNA extraction. The remaining eggs were allowed to hatch and larvae were flash frozen the day after emergence (1st instar). Total RNA was extracted from a single stored adult male (non-paternal to eggs/larvae), the adult female (maternal to eggs/larvae), seven pooled eggs, and four pooled larvae using the RNeasy Lipid Tissue Mini Kit (QIAGEN) with the optional on-column DNase treatment. Illumina sequencing libraries were prepared by the Whitehead Genome Technology Core (WI-GTC) using the TruSeq Stranded mRNA library prep kit (Illumina) and following the manufacturer's instructions with modification to select for larger insert sizes (~300-350 bp). These samples were multiplexed with unrelated plant RNA-Seq samples and sequenced 150x150 nt on one rapid mode flowcell (2 lanes) of a HiSeq2500 (WI-GTC), to a depth of ~30M paired reads per library.

To examine gene expression in adult light organs, we generated non-strand specific sequencing of polyA pulldown enriched mRNA from dissected photophore tissue (Table S1.9.1.1). Photophores were dissected from the abdomens of adult *P. pyralis* males (Collected MMNJ, July 2015) by Dr. Adam South (Harvard School of Public Health), using 3 individuals per biological replicate. These tissues and libraries were co-prepared and sequenced with other libraries (full library preparation and sequencing details here (6)) at a depth of ~10M paired reads per library.

All of these data were combined with previously published tissue, sex, and stage-specific libraries (Table S1.9.1.1) for reference-guided transcriptome assembly. Strand-specific data was used for *de novo* transcriptome assembly.

Table S1.9.1.1: *P. pyralis* RNA sequencing libraries

N: number of individuals pooled for sequencing; **Sex/stage:** M = male, F = female, A = adult, L = larva, L1= larva 1st instar, E13=13 days post fertilization eggs; **Tissue:** H = head, PA = lantern abdominal segments, FB = abdominal fat body, T = thorax, AG = accessory glands, SD = spermatophore digesting gland/bursa, SG = spiral gland, SC = spermatheca, P = dissected photophore, E = egg, WB = whole body

Library name	Source ^a	N	Sex/stage	Tissue	Library type
8175 Photinus pyralis male head (adult) transcriptome	SRA1	1	M/A	H	
8176 Photinus pyralis male light organ (adult) transcriptome	SRA1	1	M/A	PA	
8819 Photinus pyralis light organ (larval) transcriptome	SRA1	1	L	PA	
9_Photinus_sp_1_lantern	SRA2	1	M/A	PA	Strand-specific. Ribo-zero
Ppyr_FatBody_1	SRA3	6	M/A	FB	
Ppyr_FatBody_2	SRA3	6	M/A	FB	
Ppyr_FatBody_3	SRA3	6	M/A	FB	
Ppyr_FatBody_Mated	SRA3	4	M/A	FB	
Ppyr_FThorax	SRA3	3	F/A	T	
Ppyr_MThorax_1	SRA3	6	M/A	T	
Ppyr_MThorax_2	SRA3	6	M/A	T	
Ppyr_MThorax_3	SRA3	6	M/A	T	
Ppyr_OAG_1A	SRA3	6	M/A	AG	
Ppyr_OAG_1B	SRA3	6	M/A	AG	
Ppyr_OAG_2	SRA3	6	M/A	AG	
Ppyr_OAG_Mated	SRA3	4	M/A	AG	
Ppyr_SDGBursa	SRA3	3	F/A	SD	
Ppyr_SG_Mated	SRA3	4	M/A	SG	
Ppyr_Spermatheca	SRA3	3	F/A	SC	
Ppyr_SpiralGland_1	SRA3	6	M/A	SG	
Ppyr_SpiralGland_2	SRA3	6	M/A	SG	
Ppyr_SpiralGland_3	SRA3	6	M/A	SG	
Ppyr_Lantern_1A	**	6	M/A	P	
Ppyr_Lantern_2	**	6	M/A	P	
Ppyr_Lantern_3	**	6	M/A	P	
Ppyr_Eggs	**	7	E13	E	Strand-specific
Ppyr_Larvae	**	4	L1	WB	Strand-specific
Ppyr_wholeFemale*	**	1	F/A	WB	Strand-specific
Ppyr_wholeMale	**	1	M/A	WB	Strand-specific

^aSRA1= NCBI BioProject PRJNA289908; SRA2= NCBI BioProject PRJNA321737; SRA3= NCBI BioProject PRJNA328865

* Parent of eggs and larvae with data from this study

** This study

1.9.2 De novo transcriptome assembly and genome alignment

One strand-specific de novo transcriptome was produced from all available MMNJ strand-specific reads (WholeMale, WholeFemale, eggs, larvae) and strand-specific reads from SRA (SRR3521424). Reads from these 5 libraries were pooled (158.6M paired-reads) as input for de novo transcriptome assembly. Transcripts were assembled using Trinity (v2.4.0) (62) with default parameters except the following: (--SS_lib_type RF --trimmomatic --min_glue 2 --min_kmer_cov 2 --jaccard_clip --no_normalize_reads). Gene structures were then predicted from alignment of the de novo transcripts to the Ppyr1.3 genome using the PASA pipeline (v2.1.0) (63) with the following steps: first, poly-A tails were trimmed from transcripts using the

internal seqclean component; next, transcript accessions were extracted using the accession_extractor.pl component; finally, the trimmed transcripts were aligned to the genome with modified parameters (--aligners blat,gmap --ALT_SPLICE --transcribed_is_aligned_orient --tdn tdn.accs). Using both the blat (v. 36x2) (64) and gmap (v2017-09-11) (65) aligners was required, as an appropriate gene model for *Luc2* was not correctly produced using only a single aligner. Importantly, it was also necessary to set (--NUM_BP_PERFECT_SPLICER_BOUNDARY=0) for the validate_alignments_in_db.dbi step, to ensure transcripts with natural variation near the splice sites were not discarded. Post alignment, potentially spurious transcripts were filtered out using a custom script (66) that removed extremely lowly-expressed transcripts (<1% of the expression of a given PASA assembly cluster). Expression values used for filtering were calculated from the WholeMale library reads using the Trinity align_and_estimate_abundance.pl utility script. The WholeMale library was selected because it was the highest quality library - strand-specific, low contamination, and many reads - thereby increasing the reliability of the transcript quantification. Finally, the PASA pipeline was run again with this filtered transcript set to generate reliable transcript structures. Peptides were predicted from the final transcript structures using Transdecoder (v.5.0.2) (67) with default parameters. Direct coding gene models (DCGMs) were then produced with the Transdecoder “cdna_alignment_orf_to_genome_orf.pl” utility script with the PASA assembly GFF and transdecoder predicted peptide GFF as input. The unaligned *de novo* transcriptome assembly is dubbed “PPYR_Trinity_stranded”, whereas the aligned direct coding gene models are dubbed “Ppyr1.3_Trinity_stranded-DCGM”.

1.9.3 Reference guided transcriptome assembly

Two reference guided transcriptomes, one strand-specific and one non-strand-specific, were produced from all available *P. pyralis* RNA-Seq reads (Table S1.9.1.1) using HISAT2 (v2.0.5)(68) and StringTie (v1.3.3b)(69). For each library, reads were first mapped to the Ppyr1.3 genome assembly with HISAT2 (parameters: -X 2000 --dta --fr) and then assembled using StringTie with default parameters except use of “--rf” for the strand-specific libraries. The resulting library-specific assemblies were then merged into a final assembly using StringTie (--merge), one for the strand-specific and one for the non-strand specific libraries, producing For each final assembly, a transcript fasta file was produced and peptides predicted using Transdecoder with default parameters. Then, the StringTie .GTFs were converted to GFF format with the Transdecoder “gtf_to_alignment_gff3.pl” utility script and direct coding gene models (DCGMs) were produced with the Transdecoder “cdna_alignment_orf_to_genome_orf.pl” utility script, with the Stringtie GFF and transdecoder predicted peptide GFF as input. The aligned direct coding gene models for the stranded and unstranded reference guided transcriptomes are dubbed “Ppyr1.3_Stringtie_stranded-DCGM” and “Ppyr1.3_Stringtie_unstranded-DCGM”.

1.9.4 Transcript expression analysis

P. pyralis RNA-Seq reads were pseudoaligned to the PPYR_OGS1.0 geneset mRNAs using Kallisto (v0.43.1) (70) with 100 bootstraps (-b 100), producing transcripts-per-million reads (TPM). Kallisto expression quantification analysis results are available on FigShare ([10.6084/m9.figshare.5715139](https://doi.org/10.6084/m9.figshare.5715139)).

For differential expression testing, Kallisto results were between sample normalized using Sleuth (v0.29.0) (71) with default parameters producing between-sample-normalized transcripts-per-million reads (BSN-TPM). Differential expression (DE) tests for *P. pyralis* (adult male dissected fatbody vs. adult male dissected lantern) were performed using the Wald test within Sleuth. Genes whose mean BSN-TPM across bioreplicates was above the 90th percentile were annotated as “highly expressed” (HE). Genes with a Sleuth DE q-value < 0.05 were annotated as “differentially expressed.” (DE). Enzyme encoding (E/NotE) genes were predicted from the InterProScan functional annotations using a custom script (72) and GOAtools (73), with the modification that the enzymatic activity GO term was manually added to select InterPro annotations: IPR029058, IPR036291, and IPR001279. HE/DE/E+NotE gene filtering and overlaps (Fig 4e) were performed using custom scripts. These custom scripts and results of the differential expression testing are available on FigShare ([10.6084/m9.figshare.5715151](https://doi.org/10.6084/m9.figshare.5715151)).

1.10 Official coding geneset annotation (PPYR_OGS1.0)

We annotated the coding gene structure of *P. pyralis* by integrating direct coding gene models produced from the *de novo* transcriptome (Supplementary Text 1.9.2) and reference guided transcriptome (Supplementary Node 1.9.3), with a lower weighted contribution of *ab initio* gene predictions, using the Evidence Modeler (EVM) algorithm (v1.1.1) (63). First, Augustus (v3.2.2) (74) was trained against Ppyr1.2 with BUSCO (parameters: -l endopterygota_odb9 --long --species tribolium2012). Next, preliminary gene models for prediction training were produced by the alignment of the *P. pyralis de novo* transcriptome to Ppyr1.2 with the MAKER pipeline (v3.0.0β) (75) in “est2genome” mode. Preliminary gene models were used to train SNAP (v2006-07-28) (76) following the MAKER instructions (77). Augustus and SNAP gene predictions of Ppyr1.3 were then produced through the MAKER pipeline, with hints derived from MAKER blastx/exonerate mediated protein alignments of peptides from *Drosophila melanogaster* (NCBI GCF_000001215.4_Release_6_plus_ISO1_MT_protein.faa), *Tribolium castaneum* (NCBI GCF_000002335.3_Tcas5.2_protein), and *Aquatica lateralis* (AlatOGS1.0; this report), and MAKER blastn/exonerate transcript alignments of the *P. pyralis de novo* transcriptome.

We then integrated the *ab initio* predictions with our *de novo* and reference guided direct coding gene models, using EVM. A variety of evidence sources, and EVM evidence weights were empirically tested and evaluated using a combination of inspection of known gene models (e.g. *Luc1/Luc2*), and the BUSCO score of the geneset. In the final version, 6 sources of evidence were used for EVM: *de novo* transcriptome direct coding gene models (Ppyr1.3_Trinity_stranded-DCGM; weight=11), protein alignments (*D. melanogaster*, *T. castaneum*, *A. lateralis*; weight = 8), GMAP and BLAT alignments of *de novo* transcriptome (via

PASA; weight = 5), reference guided transcriptome direct coding gene models (Ppyr1.3_Stringtie_stranded-DCGM; weight = 3), Augustus and SNAP *ab initio* gene models (via MAKER; weight = 2). A custom script (78) was necessary to convert MAKER GFF format to an EVM compatible GFF format. Lastly, gene models for luciferase homologs which were fragmented or were incorrectly assembled (e.g. adjacent gene fusions) were manually corrected based on the evidence of the *de novo* and reference guided direct coding gene models.

1.10.1 P450 annotation

Translated *de novo* transcripts were formatted to be BLAST searchable with NCBI's standalone software. The peptides were searched with 58 representative insect P450s in a batch BLAST (evalue = 10). The query set was chosen to cover the diversity of insect P450s. The top 100 hits from each search were retained. The resulting 5,837 hit IDs were filtered to remove duplicates, leaving 472 unique hits. To reduce redundancy due to different isoforms, the Trinity transcript IDs (style DNXXX_cX_gX_iX) were filtered down to the "DN" level, resulting in 136 unique IDs. All peptides with these IDs were retrieved and clustered with CD-Hit (v4.5.4) (79) to 99% percent identity to remove short overlapping peptides. These 535 protein sequences were batch BLAST compared to a database of all named insect P450s to identify best hits. False positives were removed and about 30 fungal sequences were removed. These fungal sequences could potentially be from endosymbiotic fungi in the gut. Overlapping sequences were combined and the transcriptome sequences were BLAST searched against the *P. pyralis* genome assembly to fill gaps and extend the sequences to the ends of the genes were possible. This approach was very helpful with the CYP4G gene cluster, allowing fragments to be assembled into whole sequences. When a new genome assembly and geneset became available, the P450s were compared to the integrated gene models in PPYR_OGS1.0. Some hybrid sequences were corrected. The final set contains 170 named cytochrome P450 sequences (166 genes, 4 pseudogenes).

The cytochrome P450s in insects belong to four established clans CYP2, CYP3, CYP4 and Mito (Fig. S1.10.1.1). *P. pyralis* has about twice as many P450s as *Drosophila melanogaster* (86 genes, 4 pseudogenes) and slightly more than the red flour beetle *Tribolium castaneum* (137 genes, 10 pseudogenes). The CYP3 clan is the largest, mostly due to three families: CYP9 (40 sequences), CYP6 (36 sequences) and CYP345 (18 sequences). Insects have few conserved sequences across species. These include the halloween genes for 20-hydroxyecdysone synthesis and metabolism CYP302A1, CYP306A1, CYP307A2, CYP314A1 and CYP315A1 (80) in the CYP2 and Mito clans. The CYP4G subfamily makes a hydrocarbon waterproof coating for the exoskeleton (81). Additional conserved P450s are CYP15A1 (juvenile hormone (81)) and CYP18A1 (20-hydroxyecdysone degradation (82)) in the CYP2 clan. Most of the other P450s are limited to a narrower phylogenetic range. Many are unique to a single genus, though this may change as more sampling is done. It is common for P450s to expand into gene blooms (83).

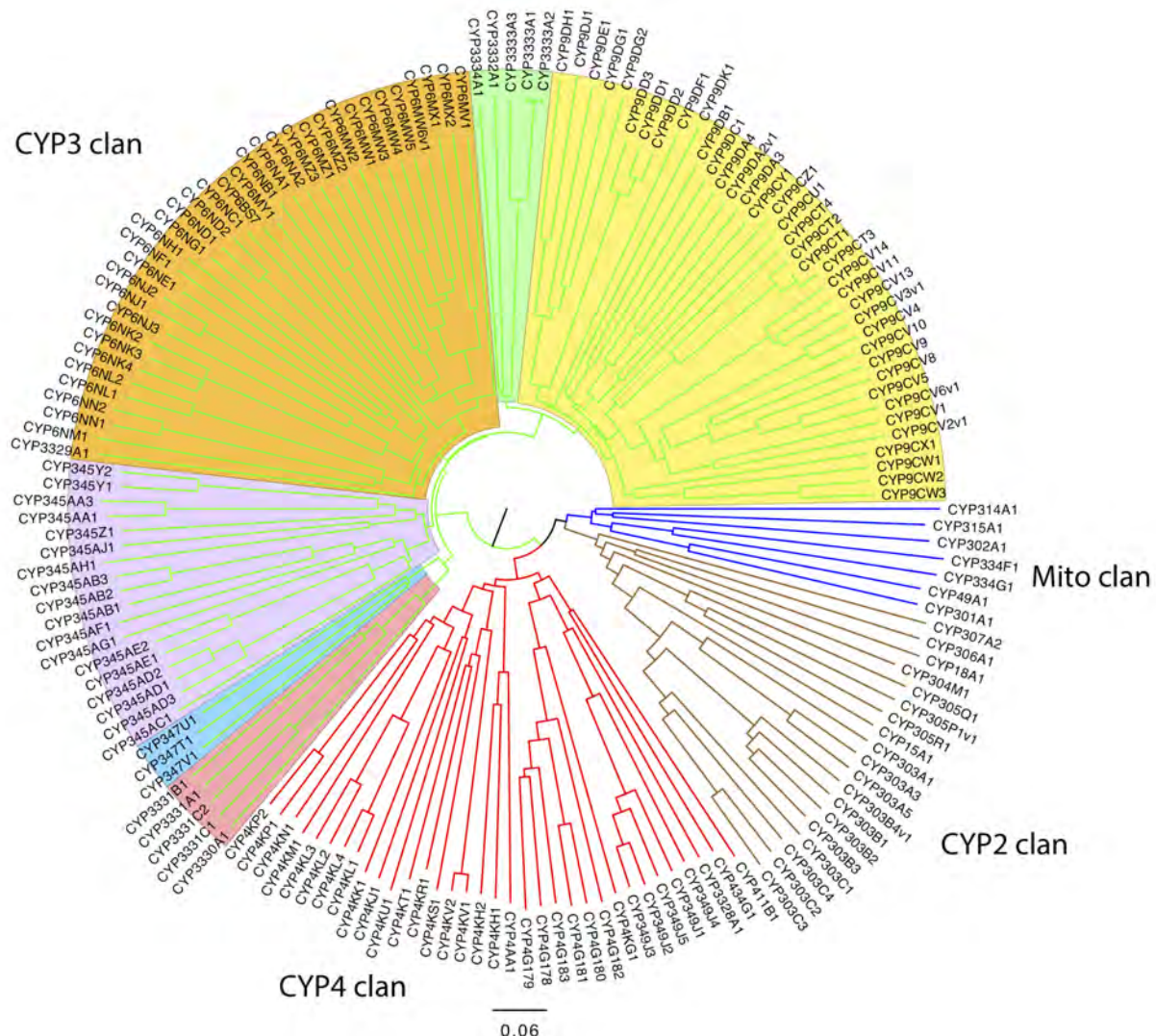


Figure S1.10.1.1: *P. pyralis* P450 gene phylogenetic tree

Neighbour-joining phylogenetic tree of 165 cytochrome P450s from *P. pyralis*. Four pseudogenes and one short sequence were removed. The P450 clans have colored spokes (CYP2 clan brown, CYP3 clan green, CYP4 clan red, Mito clan blue). Shading highlights different families and family clusters within the CYP3 clan. The tree was made using Clustal Omega at EBI (84) with default settings. The resulting multiple sequence alignment is available on FigShare (DOI: [10.6084/m9.figshare.5697643](https://doi.org/10.6084/m9.figshare.5697643)). The tree was drawn with FigTree v1.3.1 using midpoint rooting.

1.10.2 Virus annotation and analysis

Viruses were discovered from analysis of published *P. pyralis* RNA sequencing libraries (NCBI TSA: GEZM00000000.1) and the Ppyr1.2 genome assembly. 24 *P. pyralis* RNA

sequencing libraries were downloaded from SRA (taxid: 7054, date accessed: 15th June 2017). RNA sequence reads were first *de novo* assembled using Trinity v2.4.0 (62) with default parameters. Resulting transcriptomes were assessed for similarity to known viral sequences by TBLASTN searches (max e-value = 1×10^{-5}) using as probe the complete predicted non redundant viral Refseq proteins retrieved from NCBI (date accessed: 15th June 2017). Significant hits were explored manually and redundant contigs discarded. False-positives were eliminated by comparing candidate viral contigs to the entire non-redundant nucleotide (nt) and protein (nr) database to remove false-positives.

Candidate virus genome segment sequences were curated by iterative mapping of reads using Bowtie 2 (v2.3.2) (48). Special attention was taken with the segments terminis -- an arbitrary cut off of 10x coverage was used as threshold to support terminal base calls. The complementarity and folded structure of untranslated ends, as would be expected for members of the Orthomyxoviridae, was assessed by Mfold 2.3 (85). Further, conserved UTR sequences were identified using ClustalW2 (86) (support of >65% required to call a base). To identify/rule out additional segments of no homology to the closely associated viruses we used diverse *in silico* approaches based on RNA levels including: the sequencing depth of the transcript, predicted gene product structure, or conserved genome termini, and significant co-expression with the remaining viral segments.

After these filtering steps, putative viral sequences were annotated manually. First, potential open reading frames (ORF) were predicted by ORFfinder (87) and manually inspected by comparing predicted ORFs to those from the closest-related reference virus genome sequence. Then, translated ORFs were blasted against the non-redundant protein sequences NR database and best hits were retrieved. Predicted ORF protein sequences were also subjected to a domain-based Blast search against the Conserved Domain Database (CDD) (v3.16)(88) and integrated with SMART (89), Pfam (90), and PROSITE (91) results to characterize the functional domains. Secondary structure was predicted with Garnier as implemented in EMBOSS (v6.6) (92), signal and membrane cues were assessed with SignalP (v4.1) (93), and transmembrane topology and signal peptides were predicted by Phobius(94). Finally, the potential functions of predicted ORF products were explored using these annotations as well as similarity to viral proteins of known function.

To characterize *Orthomyxoviridae* viral diversity in *P. pyralis* in relation to known viruses, predicted *P. pyralis* viral proteins were used as probes in TBLASTN (max e-value = 1×10^{-5}) searches of the complete 2,754 Transcriptome Shotgun Assembly (TSA) projects on NCBI (date accessed: 15th June 2017). Significant hits were retrieved and the target TSA projects further explored with the complete *Orthomyxoviridae* refseq collection to assess the presence of additional similar viral segments. Obtained transcripts were extended/curated using the SRA associated libraries for each TSA hit and then the curated virus sequences were characterized and annotated as described above.

To identify *P. pyralis* viruses to family/genus/species, amino acid sequences of the predicted viral polymerases, specifically the PB1 subunit, were used for phylogenetic analyses with viruses of known taxonomy. To do this, multiple sequence alignment were generated using

MAFFT (v7.310) (95) and unrooted maximum-likelihood phylogenetic trees were constructed using FastTree (96) with standard parameters. FastTree accounted for variable rates of evolution across sites by assigning each site to one of 20 categories, with the rates geometrically spaced from 0.05 to 20, and set each site to its most likely rate category using a Bayesian approach with a gamma prior. Support for individual nodes was assessed using an approximate likelihood ratio test with the Shimodaira-Hasegawa-like procedure. Tree topology, support values and substitutions per site were based on 1,000 tree resamples.

To facilitate taxonomic identification we complemented BLASTP data with 2 levels of phylogenetic insights: (i) Trees based on the complete refseq collection of ssRNA (-) viruses which permitted a conclusive assignment at the virus family level. (ii) Phylogenetic trees based on reported, proposed, and discovered *Orthomyxoviridae* viruses that allowed tentative species demarcation and genera postulation. PB1-based trees were complemented independently with phylogenetic studies derived from amino acids of predicted nucleoproteins, hemagglutinin protein, PB2 protein, and PA protein which supported species, genera and family demarcation based on solely on PB1, the standard in *Orthomyxoviridae*. In addition, sequence similarity of concatenated gene products of International Committee on Taxonomy of Viruses (ICTV) allowed demarcation to species and firefly viruses were assessed by Circoletto diagrams (97) (e-value = 1e10-2). Where definitive identification was not easily assessed, protein Motif signatures were determined by identification of region of high identity between divergent virus species, visualized by Sequence Logo (98), and contrasted with related literature. Heterotrimeric viral polymerase 3D structure prediction was generated with the SWISS-MODEL automated protein structure homology-modelling server (99) with the best fit template 4WSB: the crystal structure of Influenza A virus 4WSB. Predicted structures were visualized in UCSF Chimera(100) and Needleman-Wunsch sequence alignments from structural superposition of proteins were generated by MatchMaker and the Match->Align Chimera tool. Alternatively, 3D structures were visualized in PyMOL (v1.8.6.0; Schrodinger).

Viral RNA levels in the transcriptome sequences were also examined. Virus transcripts RNA levels were obtained by mapping the corresponding raw SRA FASTQ read pairs using either Bowtie2 (48) or the reference mapping tool of the Geneious 8.1.9 suite (Biomatters, Ltd.) with standard parameters. Using the mapping results and retrieving library data, absolute levels, TPMs and FPKM were calculated for each virus RNA segment. Curated genome segments and coding annotation of the identified PpyrOMLV1 and 2 are available on FigShare at (DOI [10.6084/m9.figshare.5714806](https://doi.org/10.6084/m9.figshare.5714806)) and (DOI [10.6084/m9.figshare.5714812](https://doi.org/10.6084/m9.figshare.5714812)) respectively, and NCBI Genbank (accessions MG972985 through MG972994)

All curation, phylogeny construction, and visualization were conducted in Geneious 8.1.9 (Biomatters, Ltd.). Animal silhouettes in Fig. S5.4.1 were developed based on non-copyrighted public domain images. Figure compositions were assembled using Photoshop CS5 (Adobe). Bar graphs were generated with Excel 2007 software (Microsoft). RNA levels normalized as mapped transcripts per million per library were visualized using Shinyheatmap (101).

Finally, to identify endogenous viral-like elements, tentative virus detections and the viral refseq collection were contrasted to the *P. pyralis* genome assembly Ppyr1.2 by BLASTX

searches (e-value = 1e-6) and inspected by hand. Then 15 Kbp genome flanking regions were retrieved and annotated. Lastly, transposable elements (TEs) were determined by the presence of characteristic conserved domains (e.g. RNASE_H, RETROTRANSPOSON, INTEGRASE) on predicted gene products and/or significant best BLASTP hits to reported TEs (e-value <1e-10).

1.11 Repeat annotation

Repeat prediction for *P. pyralis* was performed *de novo* using RepeatModeler (v1.0.9) (102) and MITE-Hunter (v11-2011) (103). RepeatModeler uses RECON (104) and RepeatScout (105) to predict interspersed repeats, and then refines and classifies the consensus repeat models to build a repeat library. MITE-Hunter detects candidate MITEs (miniature inverted-repeat transposable elements) by scanning the assembly for terminal inverted repeats and target site duplications <2 kb apart. The RepeatModeler and MITE-Hunter libraries were combined and classified using RepeatClassifier (RepeatModeler 1.0.9 distribution (102)) to create the final repeat library of 3047 interspersed repeats.

Table S1.11.1: Annotated repetitive elements in *P. pyralis*

Repeat class	family	counts	bases	% of assembly
DNA	All	122906	38594900	8.15
	Helitrons	35239	9331558	2
LTR	All	29122	11474038	2.4
Non-LTR	All	52362	17812861	3.8
	LINE	49269	16827648	3.55
	SINE	1245	139910	0.03
Unknown interspersed		702480	143061276	30.2
Satellite		1655	635009	0.13
Simple repeat		48795	2423209	0.5
low complexity		7801	398212	0.09
rRNA		449	161379	0.034

1.12 Methylation analysis

MethylC-seq libraries were prepared from HMW DNA prepared from four *P. pyralis* MMNJ males using a previously published protocol (106), and sequenced to ~36x expected depth on an Illumina NextSeq500. Methylation analysis was performed using methylpy (107) Methylpy calls programs for read processing and aligning: (i) reads were trimmed of sequencing adapters using Cutadapt(108), (ii) processed reads were mapped to both a converted forward strand (cytosines to thymines) and converted reverse strand (guanines to adenines) using bowtie (flags: -S, -k 1, -m 1, --chunkmbs 3072, --best, --strata, -o 4, -e 80, -l 20, -n 0 (109)), and (iii) PCR duplicates were removed using Picard (110). In total, 49.4M reads were mapped corresponding to an actual sequencing depth of ~16x. A sodium bisulfite non-conversion rate of 0.17% was estimated from Lambda phage genomic DNA. Raw WGBS data can be found on the NCBI Gene Expression Omnibus (GSE107177). Previously published Whole Genome Bisulfite Sequencing (WGBS)/MethylC-seq libraries for *Apis mellifera* (111), *Bombyx mori* (112), *Nicrophorus vespilloides* (113), and *Zootermopsis nevadensis* (114) were downloaded from the Short Read Archive (SRA) using accessions SRR445803–4, SRR027157–9, SRR2017555, and SRR3139749, respectively. Libraries were subjected to identical methylation analysis as *P. pyralis*.

Weighted DNA methylation was calculated for CG sites by dividing the total number of aligned methylated reads by the total number of methylated plus un-methylated reads (115). For genic metaplots, the gene body (start to stop codon), 1000 base pairs (bp) upstream, and 1000 bp downstream was divided into 20 windows proportional windows based on sequence length (bp). Weighted DNA methylation was calculated for each window and then plotted in R (v3.2.4) (116).

1.13 Telomere FISH analysis

We synthesized a 5' fluorescein-tagged (TTAGG)₅ oligo probe (FAM; Integrated DNA Technologies) for fluorescence *in situ* hybridization (FISH). We conducted FISH on squashed larval tissues according to previously published methods (117), with some modification. Briefly, we dissected larvae in 1X PBS and treated tissues with a hypotonic solution (0.5% Sodium citrate) for 7 minutes. We transferred treated larval tissues to 45% acetic acid for 30 seconds, fixed in 2.5% paraformaldehyde in 45% acetic acid for 10 minutes, squashed, and dehydrated in 100% ethanol. We treated dehydrated slides with detergent (1% SDS), dehydrated again in ethanol, and then stored until hybridization. We hybridized slides with probe overnight at 30°C, washed in 4X SSCT and 0.1X SSC at 30°C for 15 minutes per wash. Slides were mounted in VectaShield with DAPI (Vector Laboratories), visualized on a Leica DM5500 upright fluorescence microscope at 100X, imaged with a Hamamatsu Orca R2 CCD camera. Images were captured and analyzed using Leica's LAX software.

SUPPLEMENTARY TEXT 2: *Aquatica lateralis* additional information

2.1 Taxonomy, biology, and life history

Aquatica lateralis (Motschulsky, 1860) (Japanese name, Heike-botaru) is one of the most common and popular luminous insects in mainland Japan. This species is a member of the subfamily Luciolinae and had long belonged in the genus *Luciola*, but was recently moved to the new genus *Aquatica* with some other Asian aquatic fireflies (118).

The life cycle of *A. lateralis* is usually one year. Aquatic larva possesses a pair of outer gills on each abdominal segment and live in still or slow streams near rice paddies, wetlands and ponds. Larvae mainly feed on freshwater snails. They pupate in a mud cocoon under the soil near the water. Adults emerge in early to end of summer. While both males and females are full-winged and can fly, there is sexual dimorphism in adult size: the body length is about 9 mm in males and 12 mm in females (119).

Like other firefly larvae, *A. lateralis* larvae are bioluminescent. Larvae possess a pair of lanterns at the dorsal margin of the abdominal segment 8. Adults are also luminescent and possess lanterns at true abdominal segments 6 and 7 in males and at segment 6 in females (119–121). The adult is dusk active. Male adults flash yellow-green for about 1.0 second in duration every 0.5–1.0 seconds while flying ~1 m above the ground. Female adults, located on low grass, respond to the male signal with flashes of 1–2 seconds in duration every 3–6 sec. Males immediately approach females and copulate on the grass (119, 122). Like many other fireflies, *A. lateralis* is likely toxic: both adults and larvae emit an unpleasant smell when disturbed and both invertebrate (dragonfly) and vertebrate (goby) predators vomit up the larva after biting (123). *A. lateralis* larvae have eversible glands on each of the 8 abdominal segments (118). The contents of the eversible glands is perhaps similar to that reported for *A. leii* (124).

2.2 Species distribution

The geographical range of *A. lateralis* includes Siberia, Northeast China, Kuril Isls, Korea, and Japan (Hokkaido, Honshu, Shikoku, Kyushu, Tsushima Isls.) (125). Natural habitats of these Japanese fireflies have been gradually destroyed through human activity, and currently these species can be regarded as ‘flagship species’ for conservation (126). For example, in 2017, Japanese Ministry of Environment began efforts to protect the population of *A. lateralis* in the Imperial Palace, Tokyo, where 3,000 larvae cultured in an aquarium were released in the pond beside the Palace (127).

2.3 Specimen collection

Individuals used for genome sequencing, RNA sequencing, and LC-HRAM-MS were derived from a small population of laboratory-reared fireflies. This population was established from a few individuals collected from rice paddy in Kanagawa Prefecture of Japan in 1989 and 1990 (128) by Mr. Haruyoshi Ikeya, a highschool teacher in Yokohama, Japan. Mr. Ikeya

collected adult *A. lateralis* specimens from their natural habitat in Yokohama and propagated them for over 25 years (~25 generations) in a laboratory aquarium without any addition of wild individuals. This population has since been propagated in the laboratory of YO, and is dubbed the “Ikeya-Y90” cultivar. Because of the small number of individuals used to establish the population and the number of generations of propagation, this population likely represents a partially inbred strain. Larvae were kept in aquarium at 19–21°C and fed using freshwater snails (*Physella acuta* and *Indoplanorbis exustus*). Under laboratory rearing conditions, the life cycle is reduced to 7–8 months. The original habitat of this strain has been destroyed and the wild population which led to the laboratory strain is now extinct.

2.4 Karyotype and genome size

Unlike *P. pyralis*, the karyotype of *A. lateralis* is reported to be 2n=16 with XY sex determination (male, 14A+XY; female, 14A+XX) (129). The Y chromosome is much smaller than X chromosome, and the typical behaviors of XY chromosomes, such as partial conjugation of X/Y at first meiotic metaphase and separation delay of X/Y at first meiotic anaphase, were observed in testis cells (129).

We determined the genome size of *A. lateralis* using flow cytometry-mediated calibrated-fluorimetry of DNA content with propidium iodide stained nuclei. First, the head + prothorax of a single pupal female (gender identified by morphological differences in abdominal segment VIII) was homogenized in 100 µL PBS. These tissues were chosen to avoid the ovary tissue. Once homogenized, 900 µL PBS, 1 µL Triton X-100 (Sigma-Aldrich), and 4 µL 100 mg/mL RNase A (QIAGEN) were added. The homogenate was incubated at 4°C for 15 min, filtered with a 30 µm Cell Tries filter (Sysmex), and further diluted with 1 mL PBS. 20 µL of 0.5 mg/mL propidium iodide was added to the mixture and then average fluorescence of the 2C nuclei determined with a SH-800 flow cytometer (Sony, Japan). Three technical replicates of this sample were performed. Independent runs for extracted Aphid nuclei (*Acyrthosiphon pisum*; 517 Mbp), and fruit fly nuclei (*Drosophila melanogaster*; 175 Mbp) were performed as calibration standards. Genome size was estimated at 940 Mbp ± 1.4 (S.D.; technical replicates = 3).

2.5 Genomic sequencing and assembly

Genomic DNA was extracted from the whole body of a single laboratory-reared *A. lateralis* adult female (c.v. Ikeya-Y90) using the QIAamp Kit (Qiagen). Purified DNA was fragmented with a Covaris S2 sonicator (Covaris, Woburn, MA, USA), size-selected with a Pippin Prep (Sage Science, Beverly, MA, USA), and then used to create two paired-end libraries using the TruSeq Nano Sample Preparation Kit (Illumina) with insert sizes of ~200 and ~800 bp. These libraries were sequenced on an Illumina HiSeq1500 using a 125x125 paired-end sequencing protocol. Mate-pair libraries of 2–20 Kb with a peak at ~5 Kb were created from the same genomic DNA using the Nextera Mate Pair Sample Preparation Kit (FC-132-1001,

Illumina), and sequenced on HiSeq 1500 using a 100x100 paired-end sequencing protocol at the NIBB Functional Genomics Facility (Aichi, Japan). In total, 133.3 Gb of sequence (159x) was generated.

Reads were assembled using ALLPATHS-LG (build# 48546) (130), with default parameters and the “HAPLOIDIFY = True” option. Scaffolds were filtered to remove non-firefly contaminant sequences using blobtools(53), resulting in the final assembly (Alat1.3). The final assembly (Alat1.3) consists of 5,388 scaffolds totaling 908.5 Gbp with an N50 length of 693.0 Kbp, corresponding to 96.6% of the predicted genome size of 940 Mbp based on flow cytometry. Genome sequencing library statistics are available in [Table S1](#).

2.5.1 Taxonomic annotation filtering

Potential contaminants in Alat1.2 were identified using the blobtools toolset (v1.0) (53). First, scaffolds were compared to known sequences by performing a blastn (v2.5.0+) nucleotide sequence similarity search against the NCBI nt database and a diamond (v0.9.10) (54) translated nucleotide sequence similarity search against the of Uniprot reference proteomes (July 2017). Using this similarity information, scaffolds were annotated with blobtools (parameters “-x bestsumorder”). We also inspected the read coverage by mapping the paired-end reads (FFGPE_PE200) on the genome using bowtie2. A tab delimited text file containing the results of this blobtools annotation are available on FigShare (DOI: [10.6084/m9.figshare.5688928](https://doi.org/10.6084/m9.figshare.5688928)). The contigs derived from potential contaminants and/or poor quality contigs were then removed: contigs with higher %GC (>50%) with bacterial hits or no database hits and showing low read coverage (<30x) (see Fig. S2.5.1.1). This process removed 1925 scaffolds (1.17 Mbp), representing 26.3% of the scaffold number and 1.3% of the nucleotides of Alat1.2, producing the final filtered assembly, dubbed Alat1.3.

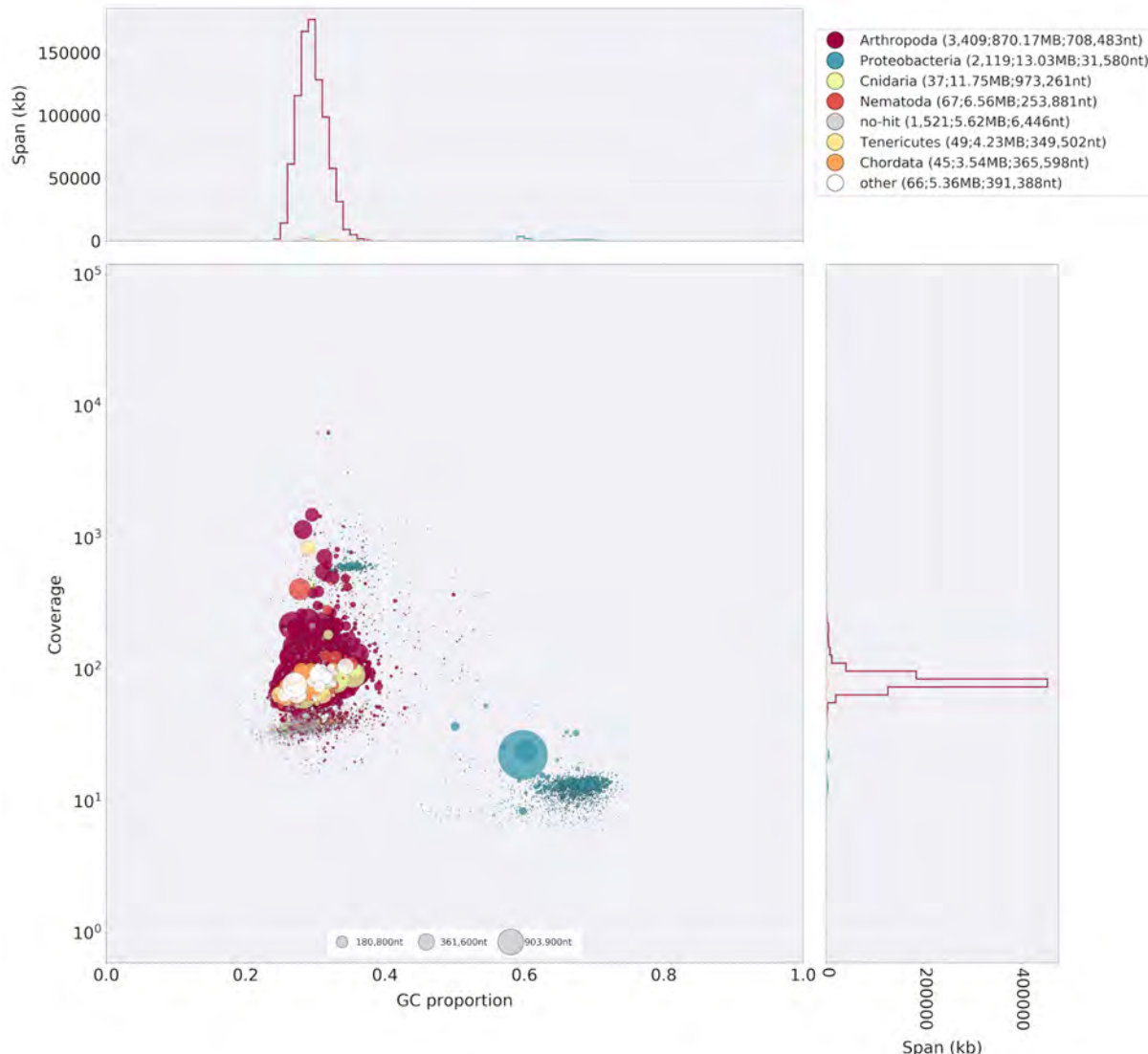


Figure S2.5.1.1: Blobplot of *A. lateralis* Illumina reads aligned against Alat1.2

Coverage shown represents mean coverage of reads from the Illumina short-insert library (Sample name FFGPE_PE200; [Data Table S1](#)), aligned against Alat1.2 using Bowtie2. Scaffolds were taxonomically annotated as described in Supplementary Text 2.5.1.

2.6 RNA-extraction, library preparation and sequencing

In order to capture transcripts from diverse life-stages and tissues, non-stranded RNA-Seq libraries were prepared from fresh specimens of nine life stages/sexes/tissues (eggs, 5th (the last) instar larvae, both sex of pupae, adult male head, male abdomen (prothorax-to-fifth segment), male lantern, adult female head, and female lantern (Table S2.6.1). Live specimens were anesthetized on ice and dissected during the day. The lantern tissue was dissected from the abdomen and contains the cuticle, photocyte layer and reflector layer. For eggs, larvae, and pupae, total RNA was extracted using the RNeasy Mini Kit (QIAGEN) with the optional on-

column DNase treatment. For adult specimens, total RNA was extracted using TRIzol reagent (Invitrogen) to avoid contamination of pigments and uric acid. These were then treated with DNase in solution and then cleaned using a RNeasy Mini kit.

cDNA libraries were generated from purified Total RNA (500 ng from each sample) using a TruSeq RNA Sample Preparation Kit v2 (Illumina) according to the manufacturer's protocol (Low Throughput Protocol), except that all reactions were carried out at half scale. The fragmentation of mRNA was performed for 4 min. The enrichment PCR was done using 6 cycles. A subset of nine libraries (BdM1, HeF1, HeM1, LtF1, LtM1, Egg1, Lrv1, PpEF, PpLM; Table S2.6.1) were multiplexed and sequenced in a single lane of Hiseq1500 101x101 bp paired-end reads. The remaining 23 libraries (BdM2, BdM3, HeF2, HeF3, HeM2, HeM3, LtF2, LtF3, LtM2, LtM3, WAF1, WAF2, WAF3, WAM1, WAM2, WAM3, Egg2, Lrv2, Lrv3, PpEM, PpLF, PpMF, PpMM) were multiplexed and sequenced in two lanes of Hiseq1500 66 bp single-end reads. Sequence quality was inspected with FastQC (131).

Table S2.6.1: *Aquatica lateralis* RNA sequencing

N: number of individuals pooled for sequencing; **Sex/stage:** M = male, F = female, A = adult, L = larva, L = larvae, E = Eggs, P = Pupae, P-E = Pupae early, P-M = Pupae middle, P-L = Pupae late; **Tissue:** H = head, La = lantern containing cuticle, photocyte layer and reflector layer, H = head, B = Thorax, plus abdomen excluding lantern containing segments. W = whole specimen. AEL = After egg laying

Library name	Label	Biosample ID	N	Sex/ Stage	Tissue	Library type
R102L6_idx13	BdM1	SAMD00106518	1	M/A	B	Illumina paired-end, non-stranded specific, PolyA
R128L1_idx25	BdM2	SAMD00106519	1	M/A	B	Illumina single-end, non-stranded specific, PolyA
R128L2_idx27	BdM3	SAMD00106520	1	M/A	B	Illumina single-end, non-stranded specific, PolyA
R102L6_idx15	HeF1	SAMD00106521	3	F/A	H	Illumina paired-end, non-stranded specific, PolyA
R128L1_idx22	HeF2	SAMD00106522	3	F/A	H	Illumina single-end, non-stranded specific, PolyA
R128L2_idx23	HeF3	SAMD00106523	3	F/A	H	Illumina single-end, non-stranded specific, PolyA
R102L6_idx12	HeM1	SAMD00106524	2	M/A	H	Illumina paired-end, non-stranded specific, PolyA
R128L1_idx20	HeM2	SAMD00106525	2	M/A	H	Illumina single-end, non-stranded specific, PolyA
R128L2_idx21	HeM3	SAMD00106526	2	M/A	H	Illumina single-end, non-stranded specific, PolyA
R102L6_idx16	LtF1	SAMD00106527	5	F/A	La	Illumina paired-end, non-stranded specific, PolyA
R128L1_idx06	LtF2	SAMD00106528	5	F/A	La	Illumina single-end, non-stranded specific, PolyA
R128L2_idx12	LtF3	SAMD00106529	5	F/A	La	Illumina single-end, non-stranded specific, PolyA
R102L6_idx14	LtM1	SAMD00106530	5	M/A	La	Illumina paired-end, non-stranded specific, PolyA
R128L1_idx05	LtM2	SAMD00106531	5	M/A	La	Illumina single-end, non-stranded specific, PolyA
R128L2_idx19	LtM3	SAMD00106532	5	M/A	La	Illumina single-end, non-stranded specific, PolyA
R128L2_idx15	WAF1	SAMD00106533"	1	F/A	W	Illumina single-end, non-stranded specific, PolyA
R128L1_idx16	WAF2	SAMD00106534	1	F/A	W	Illumina single-end, non-stranded specific, PolyA
R128L2_idx18	WAF3	SAMD00106535	1	F/A	W	Illumina single-end, non-stranded specific, PolyA
R128L1_idx11	WAM1	SAMD00106536	1	M/A	W	Illumina single-end, non-stranded specific, PolyA
R128L2_idx13	WAM2	SAMD00106537	1	M/A	W	Illumina single-end, non-stranded specific, PolyA
R128L1_idx14	WAM3	SAMD00106538	1	M/A	W	Illumina single-end, non-stranded specific, PolyA
R102L6_idx4	Egg1	SAMD00106539	19.6 mg (~30-50)	E ~6h AEL	W	Illumina paired-end, non-stranded specific, PolyA
R128L1_idx01	Egg2	SAMD00106540	21.6 mg (~30-50)	E ~7d AEL	W	Illumina single-end, non-stranded specific, PolyA
R102L6_idx5	Lrv1	SAMD00106541	1	L	W	Illumina paired-end, non-stranded specific, PolyA

R128L1_idx03	Lrv2	SAMD00106542	1	L	W	Illumina single-end, non-stranded specific, PolyA
R128L2_idx04	Lrv3	SAMD00106543	1	L	W	Illumina single-end, non-stranded specific, PolyA
R128L1_idx07	PpEM	SAMD00106544	1	M/P-E	W	Illumina single-end, non-stranded specific, PolyA
R128L2_idx10	PpLF	SAMD00106545	1	F/P-L	W	Illumina single-end, non-stranded specific, PolyA
R128L1_idx09	PpMF	SAMD00106546	1	F/P-M	W	Illumina single-end, non-stranded specific, PolyA
R128L2_idx08	PpMM	SAMD00106547	1	M/P-M	W	Illumina single-end, non-stranded specific, PolyA
R102L6_idx7	PpEF	SAMD00106548	1	F/P-E	W	Illumina paired-end, non-stranded specific, PolyA
R102L6_idx6	PpLM	SAMD00106549	1	M/P-L	W	Illumina paired-end, non-stranded specific, PolyA

2.7 Transcriptome analysis

2.7.1 *De novo* transcriptome assembly and alignment

To build a comprehensive set of reference transcript sequences, reads derived from the pool of nine libraries (BdM1, HeF1, HeM1, LtF1, LtM1, Egg1, Lrv1, PpEF, PpLM; Table S2.6.1) were pooled. These represent RNA prepared from various tissues (head, thorax+abdomen, lantern) and stages (egg, pupae, adult) of both sexes. The reads were cleaned with Cutadapt (108): Low-quality ends (<QV30) and adapter sequences were trimmed, while reads shorter than 50 bp were discarded. The cleaned reads were assembled *de novo* with Trinity (r20140413p1) (62) in the paired-end mode (parameters: --min_kmer_cov 2, --normalize_max_read_cov 160). This *de novo* transcriptome assembly is dubbed “AQUA_Trinity_unstranded”

2.7.2 Reference guided transcriptome alignment and assembly

The same set of the RNA-Seq reads used in the *de novo* transcriptome assembly (Supplementary Text 2.7.1) were mapped to the genome with TopHat (132) using default parameters except adding an option “--min-intron-length 30” to allow short introns, because our preliminary analysis showed that the *A. lateralis* genome contains a substantial number of genes with short introns, including luciferase. In addition, TopHat with default parameters produced incorrect alignments of the reads spanning short introns. The mapped reads were assembled into transcripts with Cufflinks (133) (parameters: --min-intron-length 30). This reference guided assembly is dubbed “Alat1.3_Cufflinks_unstranded”

2.7.3 Transcript expression analysis

A. lateralis RNA-Seq reads were pseudoaligned to the Alat_OGS1.0 geneset mRNAs using Kallisto (v0.43.1)(70) with 100 bootstraps (-b 100), producing transcripts-per-million reads (TPM). Kallisto expression quantification analysis results are available on FigShare ([10.6084/m9.figshare.5715142](https://doi.org/10.6084/m9.figshare.5715142)).

For differential expression testing, Kallisto results were between sample normalized using Sleuth (v0.29.0) (71) with default parameters producing between-sample-normalized transcripts-per-million reads (BSN-TPM). Differential expression (DE) tests for *A. lateralis* (adult male thorax + abdominal segments 1-5 vs. adult male dissected lantern) were performed using the Wald test within Sleuth. Genes whose mean BSN-TPM across bioreplicates was above the

90th percentile were annotated as “highly expressed” (HE). Genes with a Sleuth DE q-value < 0.05 were annotated as “differentially expressed.” (DE). Enzyme encoding (E/NotE) genes were predicted from the InterProScan functional annotations using a custom script (72) and GOAtools (73), with the modification that the enzymatic activity GO term was manually added to select InterPro annotations: IPR029058, IPR036291, and IPR001279. HE/DE/E+NotE gene filtering and overlaps (Fig 4e) were performed using custom scripts. These custom scripts and results of the differential expression testing are available on FigShare ([10.6084/m9.figshare.5715154](https://doi.org/10.6084/m9.figshare.5715154)).

2.8 Official coding geneset annotation (Alat_OGS1.0)

A protein-coding gene reference set for *A. lateralis* was generated by Evidence Modeler (v1.1.1) using both aligned transcripts and aligned proteins. For transcripts, we combined reference-guided (Supplementary Text 2.7.1) and de-novo transcriptome (Supplementary Text 2.7.2) approaches. In the reference-guided approach, RNA-Seq reads were mapped to the genome assembly with TopHat and assembled into transcripts with Cufflinks. The Cufflinks transcripts were subjected to the TransDecoder program to extract ORFs. In the *de novo* transcriptome approach, RNA-seq reads were assembled *de novo* by Trinity and ORFs were predicted using TransDecoder. We used CD-HIT-EST (79) to reduce the redundancy of the predicted ORFs. The ORF sequences were mapped to the genome using Exonerate in est2genome mode for splice-aware alignment. We processed homology evidence at the protein level using the reference proteomes of *D. melanogaster* and *T. castaneum*. These reference proteins were split-mapped to the *A. lateralis* genome in two steps: first with BLASTX to find approximate loci, and then with Exonerate in protein2genome mode to obtain more refined alignments. These gene models derived from multiple evidence were merged by the EVM program to obtain the reference annotation for the genomes. We also predicted *ab initio* gene models using Augustus, but we didn’t include Augustus models for the EVM integration because our preliminary analysis showed the *ab initio* gene models had no positive impact on gene prediction.

2.9 Repeat annotation

A *de novo* species-specific repeat library for *A. lateralis* was constructed using RepeatModeler (v1.0.9), yielding a final library of 2952 interspersed repeats. We used this library and RepeatMasker (v4.0.5)(134) via the MAKER pipeline (v3.0.0β) (135) to identify and mask interspersed and tandem repeats in the genome assembly.

Table S2.9.1: Annotated repetitive elements in *A. lateralis*

Repeat class	family	counts	bases	% of assembly
DNA	All	229064	73263593	8.06

	Helitrons	930	466679	0.05
LTR	All	59499	23391956	2.6
Non-LTR	All	151797	50395435	5.5
	LINE	151797	50395435	5.5
	SINE	0	0	0
Unknown interspersed		450934	99998958	11.1
Satellite		0	0	0
Simple repeat		155271	6656944	0.73
low complexity		0	0	0
rRNA		0	0	0

SUPPLEMENTARY TEXT 3: *Ignelater luminosus* additional information

3.1 Taxonomy, biology, and life history

Ignelater luminosus is a member of the beetle family Elateridae (“click beetles”), related to Lampyridae, that includes about 10,000 species (136) (17 subfamilies) (137) which are widespread throughout the globe. Unlike in fireflies, where bioluminescence is universal, only ~200 described elaterid species are luminous. These luminous species are recorded only from tropical and subtropical regions of Americas and some small Melanesian islands (137, 138). For instance, the tropical American *Pyrophorus noctilucus* is considered the largest (~30 mm) and brightest insect (139, 140). All luminous species are closely related - luminous click beetles belong to the tribes Pyrophorini and Euplinthini (138, 141) of the subfamily Agrypninae, with the single exception of *Campyloxenus pyrothorax* (Chili) in the related subfamily Campyloxeninae (142). The luminescence of a pair of pronotal ‘light organs’ of the adult *Balgus schnusei* (143), a species that has now been assigned to the Thylacosterninae of the Elateridae (137), has not been confirmed by later observation. This near-monophyly of bioluminescent elaterid taxa is supported by both morphological (144) and molecular phylogenetic analysis (145–147), though early morphological phylogenies were inconsistent (142, 148–151). This suggests a single origin of bioluminescence in this family.

The genus *Ignelater* was established by Costa in 1975 and *I. luminosus* was included in this genus (138). Often this species is called *Pyrophorus luminosus* as an ‘auctorum’, a name used to describe a variety of taxa (152). This use of “*Pyrophorus*” as an auctorum may be due to the heightened difficulty of classifying Elateridae (138). The genus *Ignelater* is characterized by the presence of both dorsal and ventral photophores (138, 153). An unreviewed report suggested that the adult *I. luminosus* has a ventral light organ only in males (154). Phylogenetic analyses based on the morphological characters suggested that the genera *Ignelater* and *Photophorus* (which contain only two species from Fiji and Vanuatu) are the most closely related genera in the tribe Pyrophorini (153). The earliest fossil of an Elateridae species was recorded from the Middle Jurassic of Inner Mongolia, China (155). McKenna and Farrell suggested that, based on molecular analyses, the family Elateridae originated in the Early Cretaceous (130 Mya) (156). It is expected that many recent genera in Elateroidea were established by the Early Tertiary (157).

The exact function of bioluminescence across different life stages remains unknown for many luminous elaterid species. Bioluminescent elaterid beetles typically have 2 paired lanterns on the dorsal surface of the prothorax, and a single lantern on the ventral abdomen which is only exposed during flight. Several bioluminescent elateridae produce different colored luminescence from their prothorax and abdominal lanterns (158, 159). Harvey reported that there was not a marked difference in the luminescence color of the dorsal and ventral lanterns of Puerto Rican *I. luminosus* (29). Like fireflies, elaterid larvae often produce light, with the glowing termite mounds of Brazil that contain the predatory larvae of *Pyrearinus termitilluminans* being a striking example (160). A description of the anatomy of the larval light organ of

Pyrophorus is provided by Harvey (29). *I. luminosus* larvae likely also produce light, though it has not been specifically reported in the literature. Adult *I. luminosus* are luminescent and bioluminescent courtship behavior was described in an unreviewed study (161). Reportedly, males search during flight with their prothorax lanterns illuminated steadily, while females stay on the ground modulating the intensity of their prothorax lanterns in ~2 second intervals. Once a female is observed, the prothorax lanterns of the male go dark, the ventral lantern becomes illuminated, and the male approaches the female via a circular search pattern. Mating is brief, reportedly taking only 5 seconds. It is unclear if the male ventral lantern response represents a direct control of light production from the ventral lantern, or simply the beetle exposing a constitutively luminescent ventral lantern which is normally obscured from view.

Unlike fireflies, bioluminescent elaterid species are not known to have potent chemical defenses. For example, the Jamaican bioluminescent elaterid beetle *Pyrophorus plagiophthalmus*, does not appear to be strongly unpalatable, as bats were observed to regularly capture the beetles during their flying bioluminescent displays (162). A defense role for *I. luminosus* luminescence to startle predators is possible.

3.2 Species distribution

I. luminosus is often considered to be endemic to Puerto Rico (163), however the genus *Ignelater* is reported in Florida (USA), Vera Cruz (Mexico), the Bahamas, Cuba, Isla de la Juventud, Hispaniola (Haiti+Dominican Republic), Puerto Rico, and the Lesser Antilles (138). Similarly, *I. luminosus* itself has been reported on the island of Hispaniola (161, 164), indicating *I. luminosus* is not restricted to Puerto Rico. This geographic distribution of *Ignelater* suggests that Puerto Rico likely contains multiple *Ignelater* species and, given the difficulty of distinguishing different species of bioluminescent elateridae by morphological characters, a definitive species distribution for *I. luminosus* cannot be stated, other than this species is seemingly not endemic to Puerto Rico.

3.3 Collection

I. luminosus (Illiger, 1807) adult specimens were collected from private land in Mayagüez, Puerto Rico ($18^{\circ} 13' 12.1974''$ N, $67^{\circ} 6' 31.6866''$ W) with permission of the landowner by Dr. David Jenkins (USDA-ARS). Individuals were captured at night on April 20th and April 28th 2015 during flight on the basis of light production. The *I. luminosus* specimens were frozen in a -80°C freezer, lyophilized, shipped to the laboratory on dry ice, and stored at -80°C . Full collection metadata is available from the NCBI BioSample records of these specimens (NCBI Bioproject PRJNA418169). Identification to species was performed by comparing antenna and dissected genitalia morphology to published keys (138, 153, 165) (Fig. S3.3.1). All inspected specimens were male (3/3). Separate specimens were used for sequencing. Although the genitalia morphology of the sequenced specimens was not inspected to confirm their sex, sequenced specimens were inferred to be male, based on the fact that female bioluminescent elaterid beetles are rarely seen in flight (Personal communication: S.

Velez) and the dissected specimens collected in the same batch as the sequenced specimens were confirmed to be male.



Figure S3.3.1: *I. luminosus* aedeagus (male genitalia)

(A) dorsal and (B) ventral view of an *Ignelater luminosus* aedeagus, dissected from the same batch of specimens used for linked-read sequencing and genome assembly. The species identity of this specimen was confirmed as *I. luminosus* by comparison of the aedeagus to the keys of Costa and Rosa (138, 153, 165).

3.4 Karyotype and genome size

The karyotype of Puerto Rican *I. luminosus* (as *Pyrophorus luminosus*) was reported as $2n=14A + X_1X_2Y$ (163). The genome sizes of 5 male *I. luminosus* were determined by flow cytometry-mediated calibrated-fluorimetry of DNA content with propidium iodide stained nuclei by Dr. J. Spencer Johnston (Texas A&M University). The frozen head of each individual was placed into 1 mL of cold Galbraith buffer in a 1 mL Kontes Dounce Tissue Grinder along with the head of a female *Drosophila virilis* standard (1C = 328 Mbp). The nuclei from the sample and standard were released with 15 strokes of the "B" (loose) pestle, filtered through 40 μm Nylon mesh, and stained with 25 mg/mL Propidium Iodide (PI). After a minimum of 30 min staining in the dark and cold, the average fluorescence channel number for the PI (red) fluorescence of the 2C (diploid) nuclei of the sample and standard were determined using a CytoFlex Flow Cytometer (Beckman-Coulter). The 1C amount of DNA in each sample was determined as the ratio of the 2C channel number of the sample and standard times 328 Mbp. The genome size of these *I. luminosus* males was determined to be 764 ± 7 Mbp (SEM, n=5).

3.5 Genomic sequencing and assembly

HMW DNA (25 μg) was extracted from a single male specimen of *I. luminosus* using a 100/G Genomic Tip with the Genomic buffers kit (Qiagen, USA). The *I. luminosus* specimen was first washed with 95% ethanol, and DNA was extracted following the manufacturer's protocol, with the exception of the final precipitation step, where HMW DNA was pelleted with 40 μg RNA grade glycogen (Thermo Scientific, USA) and centrifugation (3000 x g, 30 min, 4°C)

instead of spooling on a glass rod. HMW DNA was sent on dry-ice to the Hudson Alpha Institute of Biotechnology Genomic Services Lab (HAIB-GSL), where pulsed-field-gel-electrophoresis (PFGE) quality control and 10x Genomics Chromium Genome v1 library construction was performed. PFGE quality control indicated the mean size of the input DNA was >35 kbp+. The resulting library was then sequenced on one HiSeqX lane. 408,838,927 paired reads (150x150 PE) were produced, corresponding to a genomic coverage of 153x. To evaluate the effect of different Illumina instruments on data and assembly quality, the library was also sequenced on one HiSeq2500 lane, where 145,250,480 reads (150x150 PE) were produced, corresponding to a genomic coverage of 54x. A summary of the library statistics for the genomic sequencing is available in [Data Table S1](#). The draft genome of *I. lumenosus* (Ilumi1.0) was assembled from the obtained HiSeqX genomic sequencing reads using the Supernova assembler (v1.1.1) (166), on a 40 core 1 TB RAM server at the Whitehead Institute for Biomedical Research. The reported mean molecule size was 12.23 kbp. The assembly was exported to FASTA format using Supernova mkoutput (parameters: --style=pseudohap), and modified by taxonomic annotation filtering (Supplementary Text 3.5.3) and polishing (Supplementary Text 3.5.4) to form Ilumi1.1. A Supernova (v2.0.0) assembly was also produced from combined HiSeqX and HiSeq2500 reads, but on a brief inspection the quality was equivalent to Ilumi1.1, so the new assembly was not used for further analyses. Manual long-read based scaffolding was then applied to produce a final assembly Ilumi1.2 (Supplementary Text 3.5.5).

3.5.3 Taxonomic annotation filtering

We sought to systematically remove assembled non-elaterid contaminant sequence from Ilumi1.0. Using the blobtools toolset (v1.0.1),(53) we taxonomically annotated our scaffolds by performing a blastn (v2.6.0+) nucleotide sequence similarity search against the NCBI nt database, and a diamond (v0.9.10.111) (54) translated nucleotide sequence similarity search against the of Uniprot reference proteomes (July 2017). Using this similarity information, we taxonomically annotated the scaffolds with blobtools using parameters “-x bestsumorder --rank phylum” (Fig. S3.5.3.1). A tab delimited text file containing the results of this blobtools annotation are available on FigShare (DOI: [10.6084/m9.figshare.5688952](https://doi.org/10.6084/m9.figshare.5688952)). We then generated the final genome assembly by retaining scaffolds that had coverage > 10.0 in the 1610_IlumiHiSeqX library, and did not have a high scoring (score > 5000) taxonomic assignment for “Proteobacteria”, and polishing indels and gap-filling with Pilon (Supplementary Text 3.5.4). This approach removed 235 scaffolds (330 Kbp), representing 0.2% of the scaffold number and 0.03% of the nucleotides of Ilumi1.0. While filtering the Ilumi1.0 assembly, we noted a large contribution of scaffolds taxonomically annotated as Platyhelminthes (1740 scaffolds; 119.56 Mbp). Upon closer inspection, we found conflicting information as to the most likely taxonomic source of these scaffolds. Diamond searches of these scaffolds had hits in Coleoptera, whereas blastn searches showed these scaffold had confident hits (nucleotide identity >90%, evalue = 0) against the Rat Tapeworm *Hymenolepis diminuta* genome (NCBI BioProject PRJEB507). Removal of these scaffolds decreased the endopterygota BUSCO

score, from C:97% D:1.3% to C:76.0% D:1.1%. This loss of the endopterygota BUSCOs led us to conclude that the Platyhelminthes annotated scaffolds were authentic scaffolds of *I. luminosus*, but sequences of *Hymenolepis* sp. may have been transferred into the *I. luminosus* genome via horizontal-gene-transfer (HGT). Although *Hymenolepis diminuta* infects mammals, it also spends a period of its life cycle in intermediate insect hosts, including beetles, as cysticercoids (167, 168). For a beetle like *I. luminosus*, which has a extended predatory larval stage, the accidental ingestion and harboring of a *Hymenolepis* sp. is plausible, potentially enabling HGT between *Hymenolepis* sp. and *I. luminosus* over evolutionary timescales.

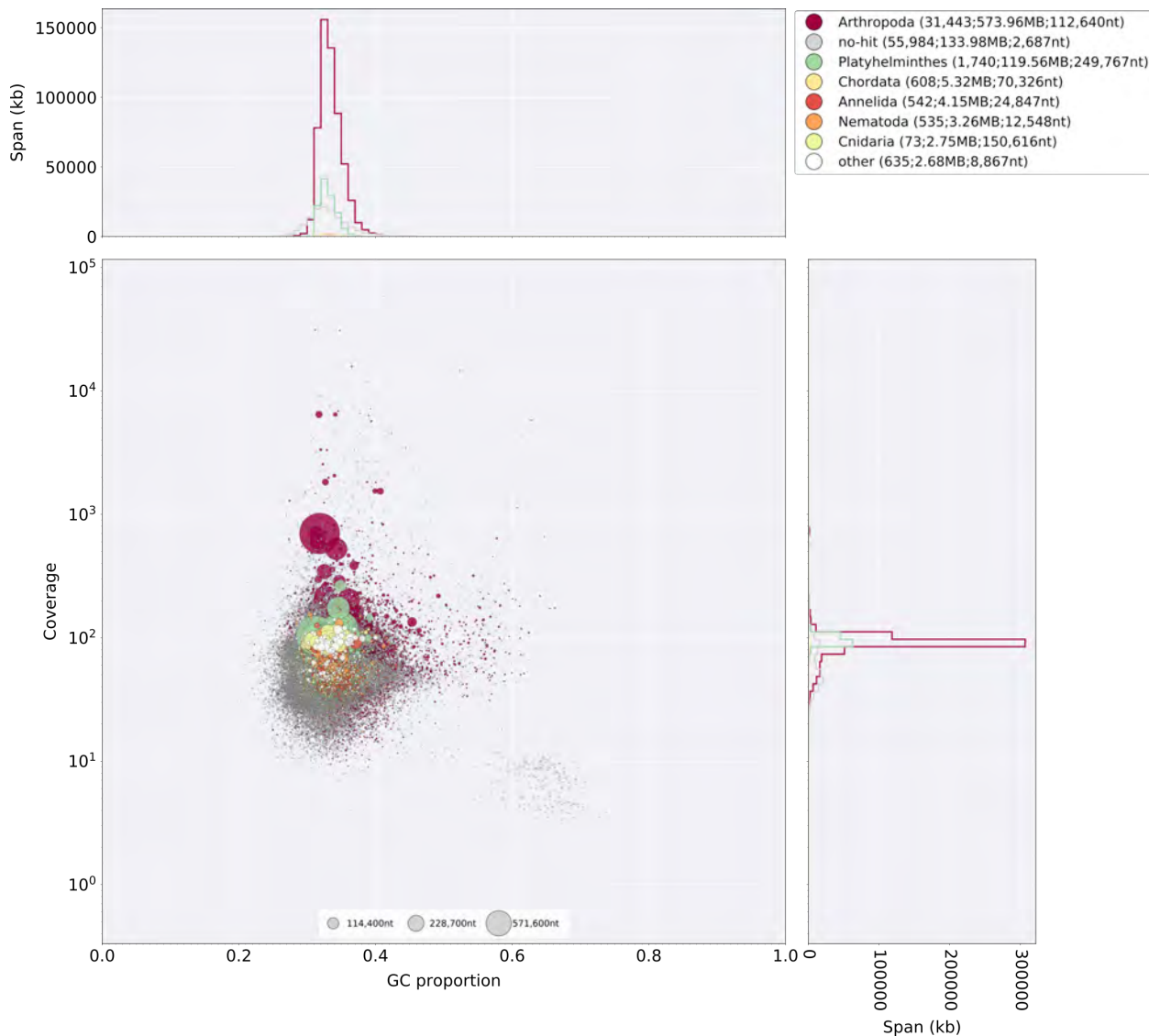


Figure S3.5.3.1: Blobtools plot of Ilumi1.0

Coverage shown represents mean coverage of reads from the HiSeqX Chromium library sequencing (Sample name 1610_IlumiHiSeqX; Table S3.5.1, S3.5.2), aligned against Ilumi1.0 using Bowtie2 with parameters (--local). Scaffolds were taxonomically annotated as described in Supplementary Text 3.5.3.

3.5.4 Ilumi1.1: Indel polishing

Manual inspection of the initial gene-models for Ilumi1.0 revealed a key luciferase homolog had an unlikely frameshift occurring after a polynucleotide run. Mapping of the 1610_IlumiHiSeqX and 1706_IlumiHiSeq2500 reads (Table S3.5.1, S3.5.2) with Bowtie2 using parameters (--local), revealed that this indel was not supported by the majority of the data, and that indels were present at a notable frequency after polynucleotide runs. As a greatly increased indel rate after polynucleotide runs (~10% error) is a known systematic error of Illumina sequencing, and has been noted as the major error type in Supernova assemblies (166), we therefore sought to correct these errors globally through the use of Pilon (v1.2.2) (58). In order to run Pilon efficiently, we split the taxonomically filtered Ilumi1.0 reference (Ilumi1.0b; Supplementary Text 3.5.3) using Kirill Kryukov's `fasta_splitter.pl` script (v0.2.6) (169), partitioned the previously mapped 1610_IlumiHiSeqX paired-end reads to these references using samtools, and ran Pilon in parallel on the partitioned reads and records with parameters (`--fix gaps,indels --changes --vcf --diploid`). The final consensus FASTAs produced by Pilon were merged to produce the polished assembly (Ilumi1.1). Ilumi1.1 (842,900,589 nt; 91,325 scaffolds) was slightly smaller than Ilumi1.0b (845,332,796 nt; 91,325 scaffolds), indicating the gaps filled by Pilon were smaller than their predicted size. The BUSCO score increased modestly after polishing (C:93.3% to C:94.8%), suggesting that indel polishing and gap filling had a net positive effect.

3.5.5 Ilumi1.2: Manual long-read scaffolding

We determined via manual gene-model annotation of Ilumi1.1 (Supplementary Text 3.8), that the 2nd through 7th exon of IlumPACS4 (ILUMI_06433-PA) were present on Ilumi1.1_Scaffold13255, but that the 1st exon was missing from this scaffold. Targeted tblastn using PangPACS (AB479114.1)(158), the most closely related gene sequence to IlumPACS4, indicated that the most similar region in the *I. luminosus* genome to the predicted PanPACS 1st exon was a right-pointing region on Ilumi1.1_Scaffold11560, not captured in any gene model, but downstream of the existing luciferase homolog genes IlumPACS1 and IlumPACS2. We surmised that this region was the correct 1st exon for IlumPACS4, and that the IlumPACS4 gene model spanned Ilumi1.1_Scaffold13255 and Ilumi1.1_Scaffold11560, and thus that the right edge of Ilumi1.1_Scaffold13255 and the left edge of the reverse complement of Ilumi1.1_Scaffold11560 should be joined. To substantiate this, we performed long-read Oxford Nanopore MinION sequencing at the MIT BioMicroCenter. The HMW DNA used was the same DNA used for Chromium library prep, and had been stored at -80°C since extraction. Thawing of DNA and size distribution QC on a Femto Pulse (Advanced Analytical Technologies Inc, USA) indicated the DNA had a mean size distribution peak of ~17 kbp. A 1D Nanopore library was prepared from this DNA using the standard kit and protocol (Part #: SQK-LSK108). The resulting library was sequenced for 48 hours on a MinION sequencer using a R9.4 flow cell (Part #:FLO-MIN106). Raw trace data was basecalled live within the MinKNOW software (v18.01.6). 824,248 reads (2.4 Gbp; ~1-2x of the *I. luminosus* genome) were obtained. Reads

were mapped to Ilumi1.1 with minimap2 (v2.8-r686-dirty)(170) using parameters (-ax map-ont). Inspection of mapped reads with Integrated Genomics Viewer revealed a 17.6 kbp anti-parallel with 7kbp anti-parellel alignment to the right edge of Scaffold13255. Inspection of the extension of this read off Scaffold13255 revealed it contained 10 kbp+ of a non-palindromic complex tandem repeat DNA with an ~100 bp repeat unit (Figure S3.5.5.1). The repeat unit of this complex tandem repeat DNA (Table S3.5.5.2) was not captured in our de novo repeat library construction (Supplementary Text 3.9), but via blastn was clearly interspersed throughout the Ilumi1.1 genome assembly. Notably, this repeat unit was present the right edge of Ilumi1.1_Scaffold13255, while the reverse complement of this repeat unit was present on the right edge of Ilumi1.1_Scaffold11560, supporting that these scaffolds were adjacent to one another, but the assembly had been broken by this large stretch of tandem repetitive DNA. Although our Nanopore sequencing did not unambiguously span this repetitive element and bridge the two scaffolds, we surmised that this information was sufficient to manually merge these scaffolds (Figure S.3.5.5.3). The long Ilumi1.1_Scaffold13255 extending read was adaptor trimmed with porechop (v0.2.3) (171), removing 35 bp from the start of the read. Next, the 3' end which aligned up to the last nucleotide of Ilumi1.1_Scaffold13255 was trimmed. Finally, the remaining read was reverse complemented, and concatenated to the right edge of Ilumi1.1_Scaffold13255. 1337 Ns were concatenated to the right edge of the extended Ilumi1.1_Scaffold13255 to indicate an uncertainty in the repeat copy number, and Ilumi1.1_Scaffold11560 was reverse complemented and concatenated to Ilumi1.1_Scaffold13255 to produce the final version of Ilumi1.2_Scaffold13255 (Figure S3.5.5.3). Whole genome scaffolding using this Nanopore data and the LINKS pipeline (v1.8.5) (172) with parameters (-d 4000,8000,10000,14000,16000,20000 -t 2,3,5,9 -l 2 -a 0.75) was attempted, but only a single pair of scaffolds was merged, so this whole-genome scaffolding was not used further.

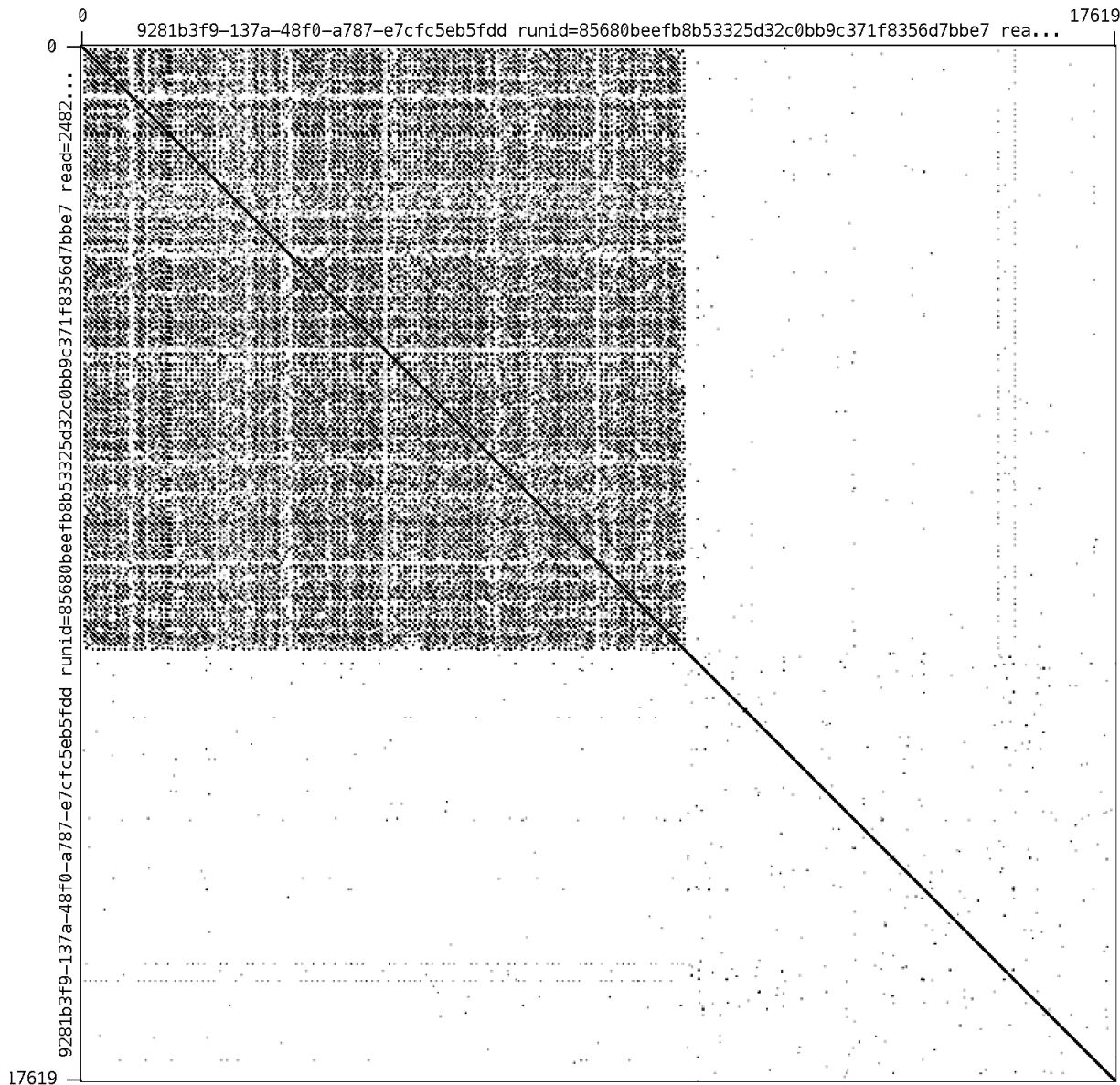


Figure S3.5.5.1 Self alignment in Gepard of the Illumi1.1_Scaffold13255 right-edge extending long MinION read. Note the large (10 kbp+) tandem repetitive region.

Table S3.5.5.2 Sequence of the *I. luminosus* luciferase cluster splitting complex tandem repeat

Repeat name	Repeat unit length	Repeat unit sequence
<i>I. luminosus</i> luciferase cluster splitting complex tandem repeat	~ 100 bp	TGGTACGAAC TATA CACGTATA CTAACTCAAATCTA ATTGTGATA CAGCAAAG TAATAATGCAGCATTGTTGCCGCTCTACTGCGATT TATA GTGGT

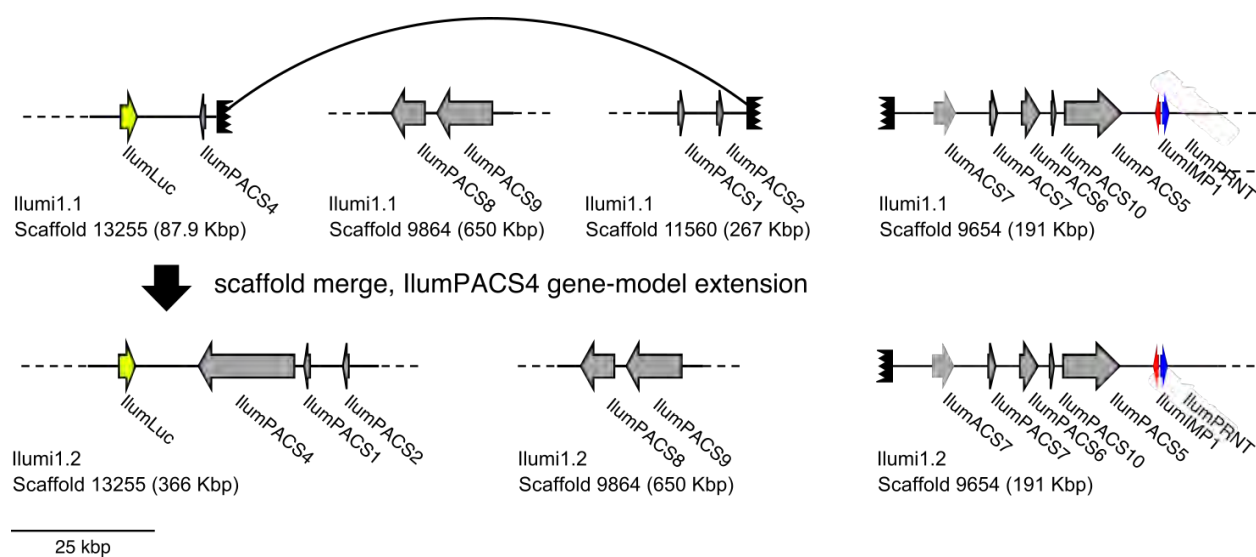


Figure S3.5.5.3: Diagram of manual scaffold merges between Ilumi1.1 and Ilumi1.2

Diagram of the manual merge of Ilumi1.1_Scaffold13255 with Ilumi1.1_Scaffold11560 between *I. luminosus* genome assembly versions Ilumi1.1 and Ilumi1.2. This merge was supported by:
(1) The putative missing 1st exon of IlumPACS4 being present on the right edge of Ilumi1.2_Scaffold11560 (2) The right edge of Ilumi1.1_Scaffold13255, and the right edge of Ilumi1.1_Scaffold11560, having anti-parallel versions of a homologous complex tandem repeat. See Figure 3 in the maintext for explanation of presented genes.

3.6 RNA extraction, library prep, and sequencing

3.6.1 HiSeq2500

Total RNA was extracted from the head + prothorax of an *I. luminosus* presumed male using the RNeasy Lipid Tissue Mini Kit (Qiagen, USA). Illumina sequencing libraries were prepared from total RNA enriched to mRNA with a polyA pulldown using the TruSeq RNA Library Prep Kit v2 (Illumina, San Diego, CA). The library was sequenced at the Whitehead Institute Genome Technology Core (Cambridge, MA) on two lanes of an Illumina HiSeq 2500 using rapid mode 100x100 bp PE. This library was multiplexed with the *P. pyralis* RNA-Seq libraries of Al-Wathiqui and colleagues (6), and thus, *P. pyralis* reads arising from index misassignment were present in this library which necessitated downstream filtering to avoid misinterpretation.

3.6.2 BGISEQ-500

Total RNA was extracted from the head + prothorax, mesothorax + metathorax, and abdomen of presumed *I. luminosus* males using the RNeasy Lipid Tissue Mini Kit (Qiagen, USA), and sent on dry-ice to Beijing Genomics Institute (BGI, China). Transcriptome libraries for

RNA each sample were prepared from total RNA using the BGISEQ-500 (BGI, China) RNA sample prep protocol. Briefly, poly-A mRNA was purified using oligo (dT) primed magnetic beads and chemically fragmented into smaller pieces. Cleaved fragments were converted to double-stranded cDNA by using N6 primers. After gel purification and end-repair, an “A” base was added at the 3'-end of each strand. The Ad153-2B adapters with barcode was ligated to both ends of the end repaired/dA tailed DNA fragments, then amplification by ligation-mediated PCR. Following this, a single strand DNA was separated at a high temperature and then a Splint oligo sequence was used as bridge for DNA cyclization to obtain the final library. Then rolling circle amplification (RCA) was performed to produce DNA Nanoballs (DNBs). The qualified DNBs were loaded into the patterned nanoarrays and the libraries were sequenced as 50x50 bp (PE-50) read through on the BGISEQ-500 platform. Sequencing-derived raw image files were processed by BGISEQ-500 base-calling software with the default parameters, generating the “raw data” for each sample stored in FASTQ format. This library preparation and sequencing was provided free of charge as an evaluation of the BGISEQ-500 platform.

Table S3.6.3: *I. luminous* RNA-Seq libraries

Library name	Source	N	Sex	Tissue	Notes
Pyrophorus_luminosus_head	This report	1	M*	Prothorax and head (lantern containing)	Illumina RNA-Seq
Prothorax_A3	This report	1	M*	Prothorax and head (lantern containing)	BGISEQ-500 RNA-Seq
Thorax_A3	This report	1	M*	Mesothorax and metathorax	BGISEQ-500 RNA-Seq
Abdomen_A3	This report	1	M*	Abdomen (lantern containing)	BGISEQ-500 RNA-Seq
Prothorax_A4	This report	1	M*	Prothorax and head (lantern containing)	BGISEQ-500 RNA-Seq
Thorax_A4	This report	1	M*	Mesothorax and metathorax	BGISEQ-500 RNA-Seq
Abdomen_A4	This report	1	M*	Abdomen (lantern containing)	BGISEQ-500 RNA-Seq

* Gender inferred. See Supplementary Text 3.3 for a discussion on this inference.

3.7 Transcriptome analysis

Both *de novo* (Supplementary Text 3.7.1) and reference guided (Supplementary Text 3.7.2) transcriptome assembly approaches using Trinity and Stringtie respectively were used.

3.7.1 *De novo* transcriptome assembly and alignment

For the *de novo* transcriptome approach, all available *I. luminosus* RNA-Seq reads (head+prothorax,metathorax+mesothorax, abdomen - both Illumina and BGISEQ-500) were pooled and input into Trinity. A non strand-specific *de novo* transcriptome assembly was produced with Trinity (v2.4.0) (62) using default parameters exception the following: (--min_glue 2 --min_kmer_cov 2 --jaccard_clip --no_normalize_reads). Peptides were predicted from the *de novo* transcripts via Transdecoder (v5.0.2; default parameters). *De novo* transcripts were then aligned to the *I. luminosus* genome (Ilumi1.1) using the PASA pipeline with blat (v36x2) and gmap (v2017-09-11) (--aligners blat,gmap), parameters for alternative splice analysis and strand specificity (--ALT_SPLICE --transcribed_is_aligned_orient), and input of the previously extracted Trinity accessions (--tdn tdn.accs). Importantly, it was necessary to set (--NUM_BP_PERFECT_SPLICE_BOUNDARY=0) for the validate_alignments_in_db.dbi step, to ensure transcripts with natural variation near the splice sites were not discarded. Direct coding gene models (DCGMs) were then produced with the Transdecoder “cdna_alignment_orf_to_genome_orf.pl” utility script, with the PASA assembly GFF and transdecoder predicted peptide GFF as input. The resulting DCGM GFF3 file was manually lifted over to the Ilumi1.2 assembly. The unaligned *de novo* transcriptome assembly is dubbed “ILUMI_Trinity_unstranded”, whereas the aligned direct coding gene models are dubbed “Ilumi1.2_Trinity_unstranded-DCGM”.

3.7.2 Reference guided transcriptome alignment and assembly

A reference guided transcriptome was produced from all available *I. luminosus* RNA-seq reads (head+prothorax, mesothorax+metathorax, abdomen - both Illumina and BGISEQ-500) using HISAT2 (v2.0.5) (68) and StringTie (v1.3.3b) (69). Reads were first mapped to the *I. luminosus* draft genome with HISAT2 (parameters: -X 2000 --dta --fr). Then StringTie assemblies were performed on each separate .bam file corresponding to the original libraries using default parameters. Finally, the produced .GTF files were merged using StringTie (--merge). A transcript fasta file was produced from the StringTie GTF file with the transdecoder “gtf_genome_to_cdna.fasta.pl” utility script, and peptides were predicted for these transcripts using Transdecoder (v5.0.2) with default parameters. The Stringtie .GTF was converted to GFF format with the Transdecoder “gtf_to_alignment_gff3.pl” utility script, and direct coding gene models (DCGMs) were then produced with the Transdecoder “cdna_alignment_orf_to_genome_orf.pl” utility script, with the Stringtie-provided GFF and transdecoder predicted peptide GFF as input. The resulting DCGM GFF3 file was manually lifted over to the Ilumi1.2 assembly. The reference guided transcriptome assembled was dubbed “ILUMI_Stringtie_unstranded”, whereas the aligned direct coding gene models were dubbed “Ilumi1.2_Stringtie_unstranded-DCGM”

3.7.3 Transcript expression analysis

I. luminosus RNA-Seq reads were pseudoaligned to the ILUMI_OGS1.0 geneset mRNAs using Kallisto (v0.43.1) (70) with 100 bootstraps (-b 100), producing transcripts-per-million reads (TPM). Kallisto expression quantification analysis results are available on FigShare ([10.6084/m9.figshare.5715157](https://doi.org/10.6084/m9.figshare.5715157)).

3.8 Official coding geneset annotation (ILUMI_OGS1.0)

We annotated the coding gene structure of *I. luminosus* by integrating direct coding gene models produced from the *de novo* transcriptome (Supplementary Text 3.7.1) and reference guided transcriptome (Supplementary Text 3.7.2), with a lower weighted contribution of *ab initio* gene predictions, using the Evidence Modeler (EVM) algorithm (v1.1.1) (63). First, Augustus (v3.2.2) (74) was trained against Ilumi1.0 with BUSCO (parameters: -l endopterygota_odb9 --long --species tribolium2012). Augustus predictions of Ilumi1.0 were then produced through the MAKER pipeline, with hints derived from MAKER blastx/exonerate mediated protein alignments of peptides from *Drosophila melanogaster* (NCBI GCF_000001215.4_Release_6_plus_ISO1_MT_protein.faa), *Tribolium castaneum* (NCBI GCF_000002335.3_Tcas5.2_protein), *Photinus pyralis* (PPYR_OGS1.0; this report), *Aquatica lateralis* (AlatOGS1.0; this report), the *I. luminosus* *de novo* transcriptome translated peptides, and MAKER blastn/exonerate transcript alignments of the *I. luminosus* *de novo* transcriptome transcripts.

We then integrated the *ab initio* predictions with our *de novo* and reference guided direct coding gene models, using EVM. In the final version, eight sources of evidence were used for EVM: *de novo* transcriptome direct coding gene models (Ilumi1.2_Trinity_unstranded-DCGM; weight=8), reference guided transcriptome direct coding gene models (Ilumi1.1_Stringtie_unstranded-DCGM; weight=4), MAKER/Augustus *ab initio* predictions (Ilumi1.1_maker_augustus_ab-initio; weight=1), protein alignments (*P. pyralis*, *A. lateralis*, *D. melanogaster*, *T. castaneum*, *I. luminosus*; weight=1 each). A custom script(78) was used to convert the input MAKER GFF to an EVM compatible GFF format. Gene model errors for the *I. luminosus* luciferase homologs were manually fixed, and the results in GFF format lifted over to Ilumi1.2.

3.9 Repeat annotation

A *de novo* species-specific repeat library for *I. luminosus* was constructed using RepeatModeler (v1.0.9), yielding a final library of 4251 interspersed repeats. We used this library and RepeatMasker (v4.0.5) (134) via the MAKER pipeline (v3.0.0β) (135) to identify and mask interspersed and tandem repeats in the genome assembly.

Table S3.9.1: Annotated repetitive elements in *I. luminosus*

Repeat class	family	counts	bases	% of assembly
DNA	All	158849	71221295	8.44
	Helitrons	346	140017	0.01
LTR	All	23440	11341876	1.3
Non-LTR	All	97694	40051539	4.75
	LINE	97694	40051539	4.75
	SINE	0	0	0
Unknown interspersed		757178	159566359	18.9
Satellite		0	0	0
Simple repeat		113654	5270254	0.62
low complexity		0	0	0
rRNA		0	0	0

3.10 Mitochondrial genome assembly and annotation

The mitochondrial genome sequence of *I. lumenosus* was assembled by a targeted sub-assembly approach. First, Chromium linked-reads were mapped to the previously sequenced mitochondrial genome of the Brazilian elaterid beetle *Pyrophorus divergens* (NCBI ID: NC_009964.1) (173), using Bowtie2 (v2.3.1; parameters: --very-sensitive-local)(109). Although these reads still contain the 16bp Chromium library barcode on read 1 (R1), Bowtie2 in “local mapping mode” can accurately map these reads. Mitochondrial mapping R1 reads with a mapping read 2 (R2) pair were extracted with "samtools view -bh -F 4 -f 8", whereas mapping R2 reads with a mapping R1 pair were extracted with "samtools view -bh -F 8 -f 4". R1 & R2 singleton mapping reads were extracted with "samtools view -bh -F 12" for diagnostic purposes, but were not used further in the assembly. The R1, R2, and singleton reads in .BAM format were merged, sorted, and converted to FASTQ format with samtools and "bedtools bamtofastq" respectively. The resultant R1 and R2 FASTQ files containing only the paired mapped reads (995523 pairs, 298 Mbp) were assembled with SPAdes (174) without error correction and with the plasmidSPAdes module (175) enabled (parameters: -t 16 --plasmid -k55,127 --cov-cutoff 1000 --only-assembler). The resulting “assembly_graph.fastg” file was viewed in Bandage(176), revealing a 16,088 bp node with 1119x average coverage that circularized through two possible paths: a 246 bp node with 252x average coverage, or a 245 bp node with 1690x coverage. The lower coverage path was observed to differ only in a “T” insertion after a 10-nucleotide poly-T

stretch when compared to the higher coverage path. Given that increased levels of insertions after polynucleotide stretches are a known systematic error of Illumina sequencing, it was concluded that the lower coverage path represented technical error rather than an authentic genetic variant and was deleted. This produced a single 16,070 bp circular contig. This contig was “restarted” with seqkit(v0.7.0) (59) to place the FASTA record break in the AT-rich region, and was submitted to the MITOSv2 mitochondrial genome annotation web server. Small mis-annotations (e.g. low scoring additional predictions of already annotated mitochondrial genes) were manually inspected and removed. This annotation indicated that all expected features were present on the contig, including subunits of the NAD⁺ dehydrogenase complex (NAD1, NAD2, NAD3, NAD4, NAD4I, NAD5, NAD6), the large and small ribosomal RNAs (rrnL, rrnS), subunits of the cytochrome c oxidase complex (COX1, COX2, COX3), cytochrome b oxidase (COB), ATP synthase (atp6, atp8), and tRNAs. BLASTN of the *Ignelater luminosus* mitochondrial genome against published complete mitochondrial genomes from beetles indicated 96-89% alignment with 86-73% nucleotide identity, with poor or no sequence level alignment in the A-T rich region. Like other reported elaterid beetle genomes, the *I. luminosus* mitochondrial genome does not contain the tandem repeat unit (TRU) previously reported in Lampyridae (177).

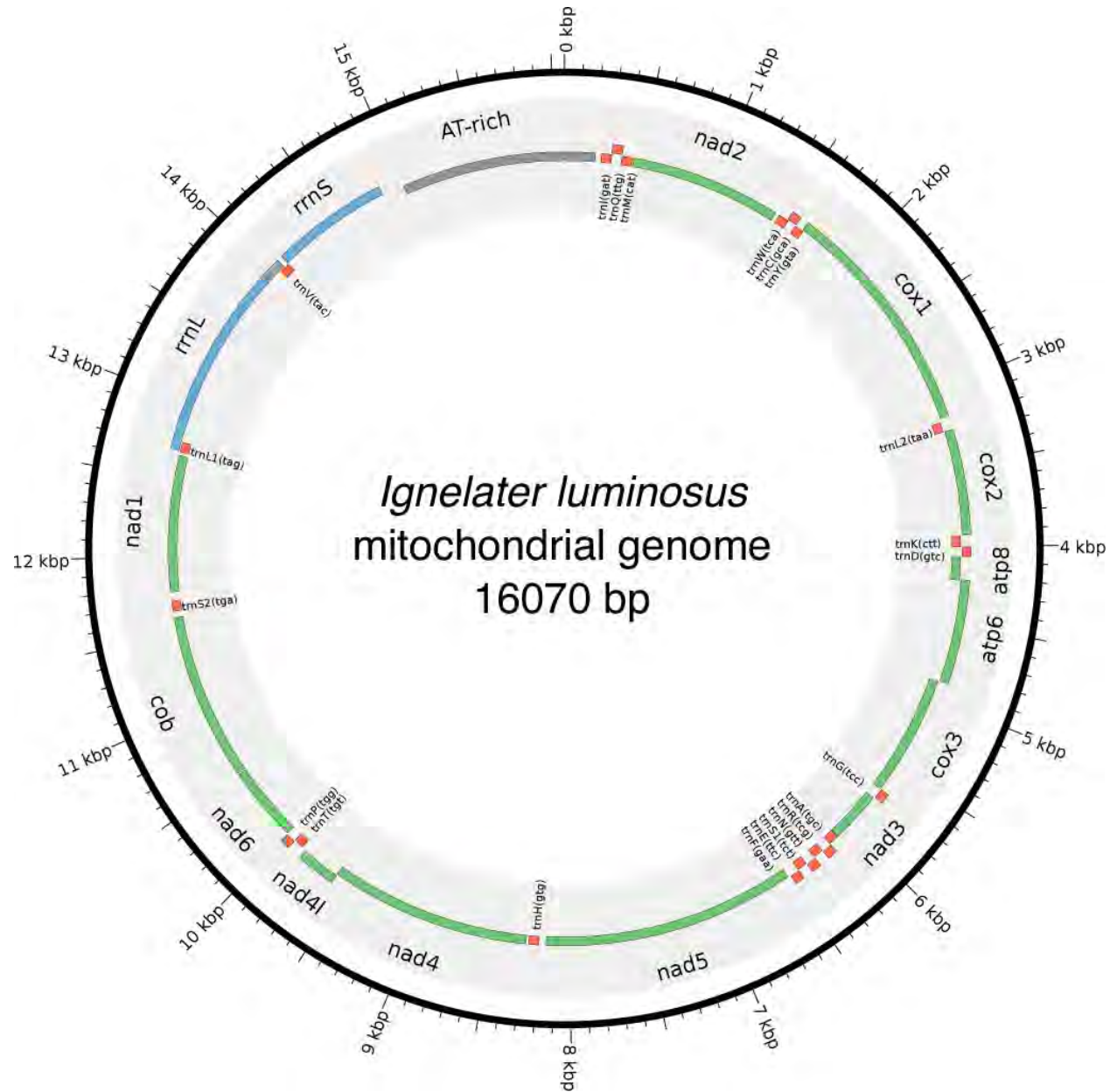


Figure S3.10.1: Mitochondrial genome of *I. luminosus*

The mitochondrial genome of *I. luminosus* was assembled and annotated as described in the Supplementary Text 3.10. Figure produced with Circos (61).

SUPPLEMENTARY TEXT 4: Comparative analyses

4.1 Assembly statistics and comparisons

The level of non-eukaryote contamination of the raw read data for each *P. pyralis* library was assessed using kraken v1.0 (178) using a dust-masked minikraken database to eliminate comparison with repetitive sequences. Overall contamination levels were low, in agreement with a low level of contamination in our final assembly. On average, contamination was 3.5% in the PacBio reads (whole body) and 1.6% in the Illumina reads (only thorax) (Table S1). There was no support for Wolbachia in any of the *P. pyralis* libraries, with the exception of a single read from a single library which had a kraken hit to Wolbachia. QUAST version 4.3 (179), was used to calculate genome quality statistics for comparison and optimization of assembly methods (Table S4.1.1). BUSCO (v3.0.2) (180) was used to estimate the percentage of expected single copy conserved orthologs captured in our assemblies and a subset of previously published beetle genome assemblies (Table S4.1.2). The endopterygota_odb9 (metamorphosing insects) BUSCO set was used. The bacteria_odb9 gene set was used to identify potential contaminants by screening contigs and scaffolds for conserved bacterial genes. For genome predictions from beetles, the parameter “--species tribolium2012” was used to improve the BUSCO internal Augustus gene predictions. For non-beetle insect genome predictions, “--species=fly” was used.

Table S4.1.1: Assembly statistics

Assembly	Libraries	Assembly scheme	Assembly*/measured** genome size (Gbp)	Scaffold/Contig (#)	Contig NG50*** (Kbp)	Scaffold NG50*** (Kbp)	BUSCO statistics
Ppyr0.1-PB	PacBio (61 SMRT cells)	Canu (no polishing)	721/422	25986/25986	86	86	C:93.8% [S:65.2%, D:28.6%], F:3.3%, M:2.9%
Pyr1.1	Short read Mate Pair PacBio	MaSuRCA + redundancy reduction	473/422	8065/8285	193.4	202	C:97.2% [S:88.8%, D:8.4%], F:1.9%, M:0.9%
Ppyr1.2	Short	Ppyr1.1 + Phase Genomics scaffolder (in-house)	473/422	2535/7823	193.4	50,607	C:97.2% [S:88.8%, D:8.4%], F:1.9%, M:0.9%
	PacBio						
	Hi-C						
Ppyr1.3	Short read Mate Pair PacBio	Ppyr1.2 + Blobtools + manual filtering	472/422	2160/7533	192.5	49,173	C:97.2% [S:88.8%, D:8.4%], F:1.9%,

							M:0.9%
Alat1.2	Short read Mate Pair	ALLPATHS-LG	920/940	7313/ 36467	38	673	C:97.4% [S:96.2%, D:1.2%], F:1.8%, M:0.8%
Alat1.3	Short read Mate Pair	Alat1.2 + Blobtools + manual filtering	909/940	5388/ 34298	38	670	C:97.4% [S:96.2%, D:1.2%], F:1.8%, M:0.8%
Ilumi1.0	Linked-read	Supernova	845/764	91560/ 105589	31.6	116.5	C:93.7% [S:92.3%, D:1.4%], F:4.3%, M:2.0%,
Ilumi1.1	Linked read	Ilumi1.0 + Blobtools + Pilon indel & gap polishing	842/764	91305/ 105262	34.5	115.8	C:94.8% [S:93.4%, D:1.4%], F:3.5%, M:1.7%

* Calculated from genome assembly file with "seqkit stat"

** Measured via flow cytometry of propidium iodide stained nuclei. See Supplementary Text 1.4, 2.4, 3.4.

*** Calculated with QUAST (v4.5) (179), parameters “-e --scaffolds --est-ref-size X --min-contig 0” and the measured genome size for “est-ref-size”

Table S4.1.2: Comparison of BUSCO conserved gene content with other insect genome assemblies

Species	Genome version (NCBI, or this report)	Note	Genome BUSCO (endopterygota_odb9)	Protein geneset BUSCO (endopterygota_odb9)
<i>Drosophila melanogaster</i>	GCA_000001215.4 Release 6	Model insect	C:99.4%[S:98.7%,D:0.7%], F:0.4%,M:0.2%,n:2442	C:99.8%[S:43.0%,D:56.8%], F:0.2%,M:0.0%,n:2442
<i>Tribolium castaneum</i>	GCF_000002335.3 Release 5.2	Model beetle	C:98.4%[S:97.9%,D:0.5%], F:1.2%,M:0.4%,n:2442	C:99.0%[S:69.2%,D:29.8%], F:0.5%,M:0.5%,n:2442
<i>Photinus pyralis</i> *	Ppyr1.3*	North American firefly	C:97.2%[S:88.8%,D:8.4%], F:1.8%,M:1.0%,n:2442	C:94.2%[S:84.0%,D:10.2%], F:1.2%,M:4.6%,n:2442
<i>Aquatica lateralis</i>	Alat1.3*	Japanese firefly	C:97.4%[S:96.2%,D:1.2%], F:1.8%,M:0.8%	C:90.0%[S:89.1%,D:0.9%], F:3.2%,M:6.8%,n:2442
<i>Nicrophorus vespilloides</i> (113)	GCF_001412225.1 Release 1.0	Burying beetle	C:96.8%[S:95.3%,D:1.5%], F:2.1%,M:1.1%,n:2442	C:98.7%[S:69.4%,D:29.3%], F:0.8%,M:0.5%,n:2442
<i>Agrius planipennis</i> (181)	GCF_000699045.1 Release 1.0	Emerald Ash Borer beetle	C:92.7%[S:91.8%,D:0.9%], F:4.6%,M:2.7%,n:2442	C:92.1%[S:64.1%,D:28.0%], F:4.5%,M:3.4%,n:2442

<i>Ignelater luminosus</i>	Ilumi1.1 / Ilumi1.2	Puerto Rican bioluminescent click beetle	C:94.8%[S:93.4%,D:1.4%], F:3.5%,M:1.7%,n:2442	C:91.8%[S:89.8%,D:2.0%], F:4.4%,M:3.8%,n:2442
----------------------------	---------------------	--	--	--

* This report

4.2 Protein sequence analyses

4.2.1 Protein orthogroup clustering

Orthologs were identified by clustering the *P. pyralis*, *A. lateralis*, and *I. luminosus* reference geneset peptides with the *D. melanogaster* (NCBI GCF_000001215.4) and *T. castaneum* (NCBI GCF_000002335.3) reference protein genesets using the Orthofinder (v2.1.2) (182) pipeline with parameters “-A mafft -T fasttree -l 1.5”. Results are available on FigShare (DOI: [10.6084/m9.figshare.5715136](https://doi.org/10.6084/m9.figshare.5715136)).

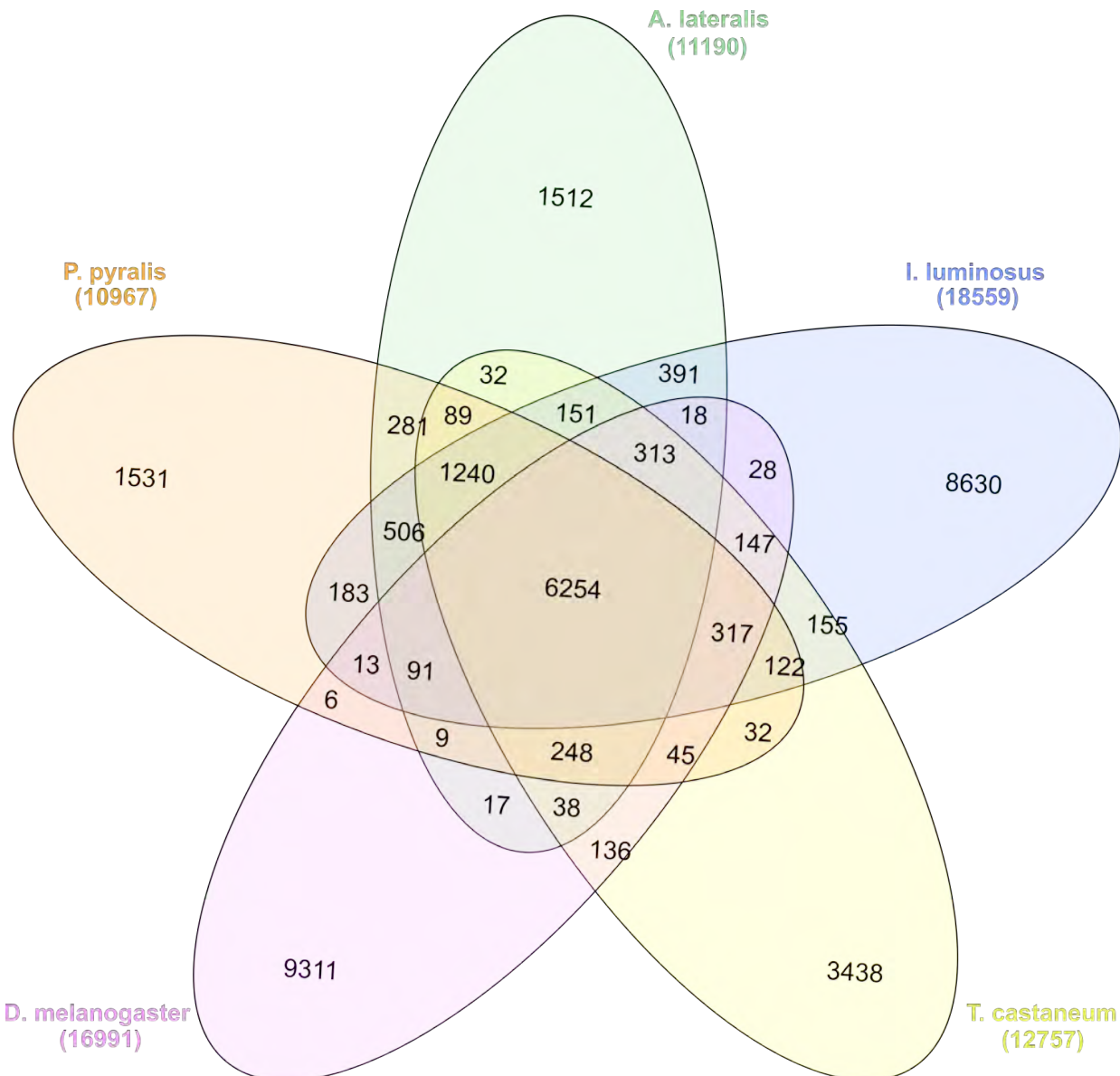


Figure S4.2.1.1: Venn diagram of *P. pyralis*, *A. lateralis*, *I. lumenosus*, *T. castaneum*, and *D. melanogaster* orthogroup relationships.

Orthogroups were calculated between the PPYR_OGS1.0, Alat_OGS1.0, ILUMI_OGS1.0, genesets, and the *T. castaneum* and *D. melanogaster* NCBI reference genesets using OrthoFinder (182). See Supplementary Text 4.2 for description of clustering method.

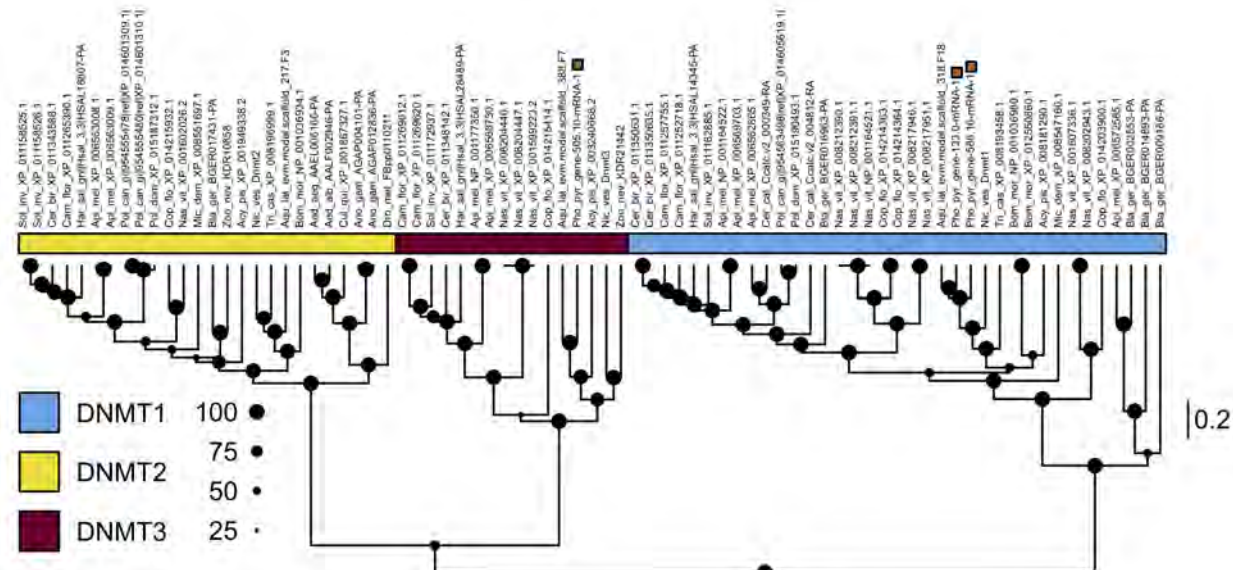


Figure S4.2.2: DNA and tRNA methyltransferase gene phylogeny

Levels and patterns of mCG in *P. pyralis* are corroborated by the presence of *de novo* and maintenance DNMTs (DNMT3 and DNMT1, respectively). Notably, *P. pyralis* possesses two copies of DNMT1, which is in contrast to a single copy of DNMT1 in the firefly *A. lateralis*. Size of circles at nodes corresponds to posterior probability support. Branch lengths are in amino acid substitutions per site.

4.2.3 CYP303 evolutionary analysis

Candidate P450s were identified using BLASTP (e-value: 1×10^{-20}) of a *P. pyralis* CYP303 family member (PPYR_OGS1.0: PPYR_14345-PA) against the *P. pyralis*, *A. lateralis*, and *I. luminosus* reference set of peptides, and the *D. melanogaster* (NCBI GCF_000001215.4) and *T. castaneum* (NCBI GCF_000002335.3) geneset peptides. Resulting hits were merged, aligned with MAFFT E-INS-i (v7.243) (183), and a preliminary neighbor-joining (NJ) tree was generated using MEGA7 (184). Genes descending from the common ancestor of the CYP303 and CYP304 genes were selected from this NJ tree, and the peptides within this subset re-aligned with MAFFT using the L-INS-i algorithm. Then the maximum likelihood evolutionary history of these genes was inferred within MEGA7 using the LG+G model (5 gamma categories (+G, parameter = 2.4805). Initial tree(s) for the heuristic search were obtained automatically by applying Neighbor-Join and BioNJ algorithms to a matrix of pairwise distances estimated using a JTT model, and then selecting the topology with the best log likelihood value. The resulting tree was rooted using *D. melanogaster* Cyp6a17 (NP_652018.1). The tree shown in Figure 4c was truncated in Dendroscope (v3.5.9) (185) to display only the CYP303 clade. The multiple sequence alignment FASTA files and newick files of the full and truncated tree are available on FigShare (DOI: [10.6084/m9.figshare.5716045](https://doi.org/10.6084/m9.figshare.5716045)).

4.3 Luciferase evolution analyses

4.3.1 Luciferase genetics overview

The gene for firefly luciferase was first isolated from the North American firefly *P. pyralis* (3, 186, 187) and then identified from the Japanese fireflies *Luciola cruciata* (188) and *A. lateralis* (189). To date, firefly luciferase genes have been isolated from more than 30 lampyrid species in the world. Two different types of luciferase genes, *Luc1* and *Luc2*, have been reported from *Photuris pennsylvanica* (190) (Photurinae), *L. cruciata* (191) (Luciolinae), *A. lateralis* (192) (Luciolinae), *Luciola parvula* (193) (Luciolinae), and *Pyrocoelia atripennis* (194) (Lampyrinae).

Luciferase genes have also been isolated from members of the other luminous beetles families: Phengodidae, Rhagophthalmidae, and Elateridae (195–198) with amino acid identities to firefly luciferases at >48% (199). The chemical structures of the substrates for these enzymes are identical to firefly luciferin. These results that the bioluminescence systems of luminous beetles are essentially the same, supports a single origin of the bioluminescence in elateroid beetles. Recent molecular analyses based on the mitochondrial genome sequences strongly support a sister relationship between the three luminous families: Lampyridae, Phengodidae, and Rhagophthalmidae (200) (201), suggesting the monophyly of Elateroidea and a single origin of the luminescence in the ancestor of these three lineages (199). However, ambiguity in the evolutionary relationships among luminous beetles, including luminous Elaterids, does not yet exclude multiple origins.

Molecular analyses have suggested that the origin of Lampyridae was dated back to late Jurassic (156) or mid-Cretaceous periods (202). Luciolinae and Lampyrinae was diverged at the basal position of the Lampyridae (203) and the fossil of the Luciolinae firefly dated at Cretaceous period was discovered in Burmese amber (204, 205). Taken together, the divergence of *Luciola* and Lampyridae is dated back at least 100 Mya.

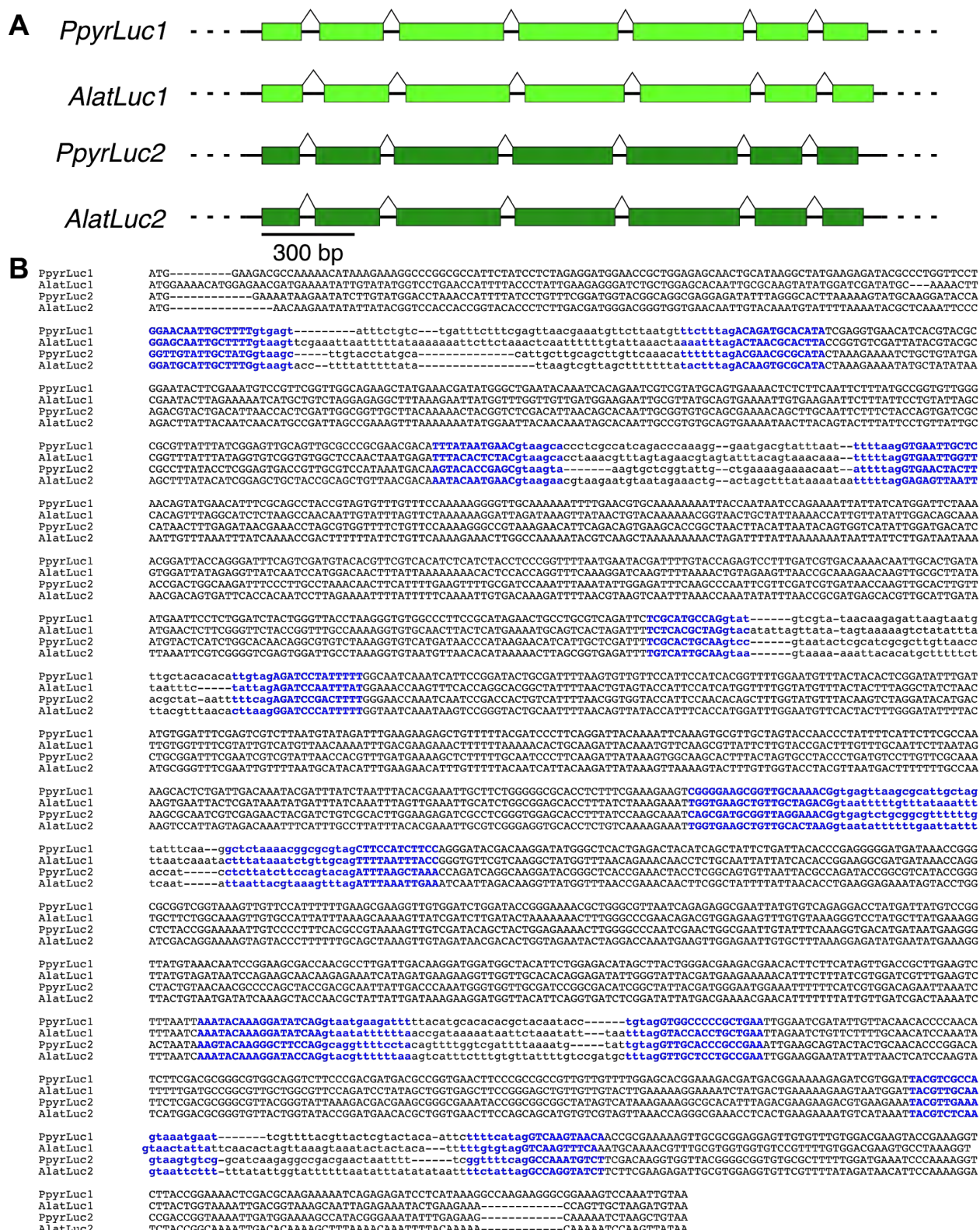


Figure S4.3.1.1: Conserved intron-exon structure of *P. pyralis* and *A. lateralis* luciferases

(A) Intron-exon structure of *P. pyralis* & *A. lateralis* *Luc1* & *Luc2* from Ppyr1.3 and Alat1.3. The structure of these genes is globally similar with 7 exons and similar intron lengths **(B)** MAFFT(95) L-INS-i multiple sequence alignment of luciferase gene nucleotide sequences from PpyrOGS1.0 and AlatOGS1.0 demonstrates the location of intron-exon junctions (bolded blue text) is completely conserved amongst the 4 luciferases. Exonic sequence is capitalized, whereas intronic sequence is lowercase.

4.3.2 Luciferase homolog gene tree

From our reference genesets, protein BLAST search detected 30 luciferase homologs ($E\text{-value} < 1 \times 10^{-60}$) to *P. pyralis* luciferase (PpyrLuc1; Genbank accession AAA29795) from *P. pyralis*, *A. lateralis*, and *I. luminosus*. We defined the luciferase co-orthology as followings: (i) shows an BLASTP E-value lower than 1.0×10^{-60} towards *DmelPACS* (CG6178), (ii) phylogenetically sister to *DmelPACS*, which is the most similar gene to firefly luciferase in *D. melanogaster*, based on the maximum likelihood (ML) phylogenetic reconstruction (Fig. S4.3.1). To examine luciferase evolution, a gene tree was constructed for *P. pyralis*, *A. lateralis*, and *I. luminosus* luciferase homologs. Candidate homologs were first identified by protein blast of *DmelPACS* (CG6178), the most similar gene to firefly luciferase in *D. melanogaster*, against the genomes and transcriptomes ($e\text{-value} < 1.0 \times 10^{-60}$). Additionally, peroxisomal targeting signal 1 (PTS1) was predicted using the regular expressions provided by the Eukaryotic Linear Motif database (206) and verified using the mendel PTS1 prediction server(207, 208). Then homologs were confirmed to be phylogenetically sister to *DmelPACS* (CG6178) and their evolution examined using a maximum likelihood (ML) gene phylogeny approach. First, amino acid sequences were aligned using (MAFFT v7.308) (183) using the BLOSUM62 matrix and filtered for spurious sequences and poorly aligned regions using trimAI (209) (parameters: $gt = 0.5$). The final alignment was 544 amino acids. Then, the best fit amino acid substitution model, LG+F Gamma, was estimated by Aminosan (v1.0.2016.11.07) (210) using the Akaike Information Criterion. Finally, a maximum likelihood gene phylogeny was estimated using RAxML (v8.2.9; 100 bootstrap replicates) (211). The tree was rooted using *DmelPACS* as an outgroup. Supporting files such as multiple sequence alignment, gene accession numbers, and other annotation and expression values are available on FigShare (DOI: [10.6084/m9.figshare.5725690](https://doi.org/10.6084/m9.figshare.5725690)).

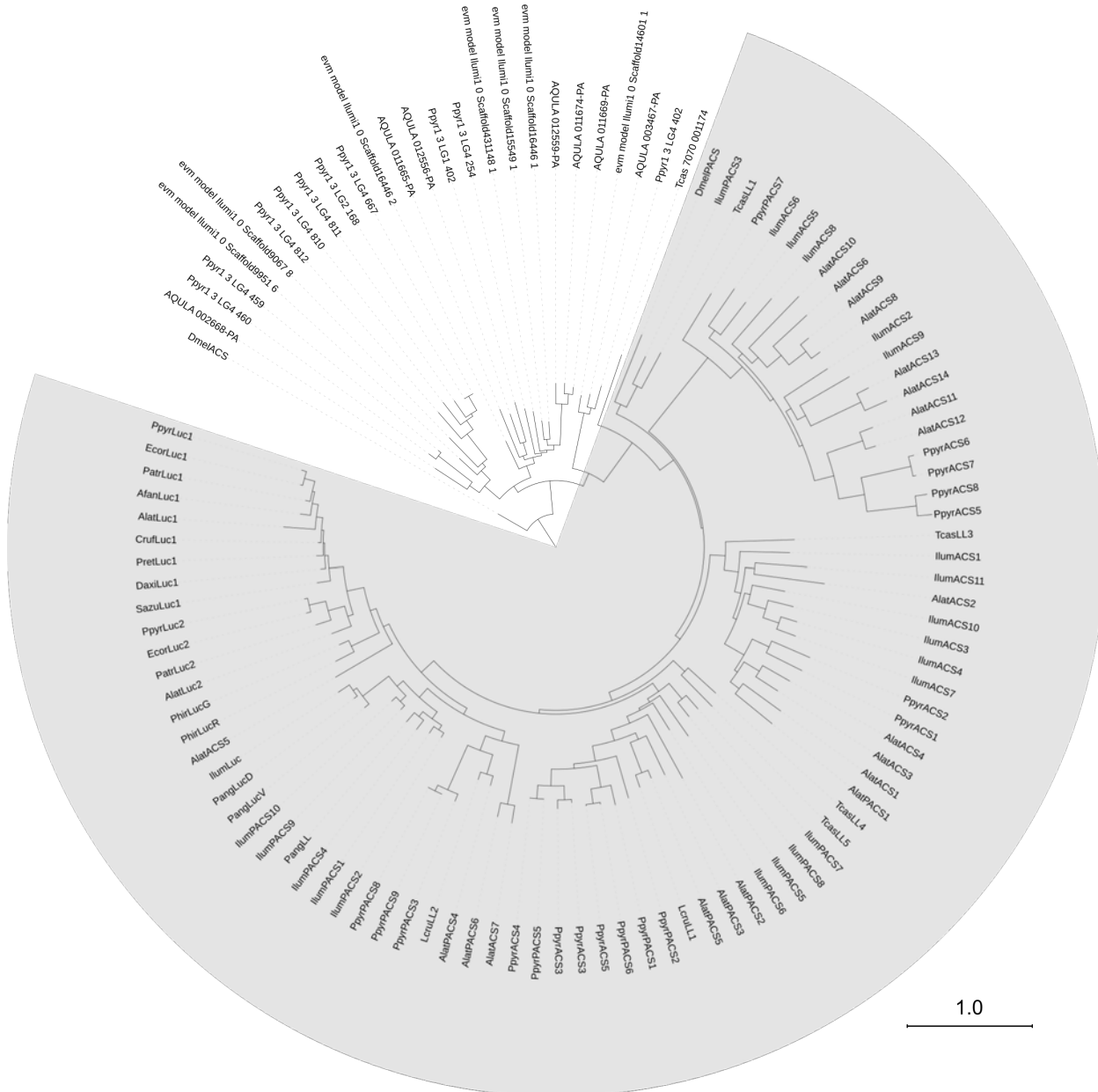


Figure S4.3.2.1: Maximum likelihood phylogeny of luciferase homologs

The maximum likelihood tree was reconstructed from a 541 amino acid multiple sequence alignment, generated via a BLASTP search using *P. pyralis* luciferase as query (e-value: 1.0 x 10⁻⁶⁰). Members of the clade that includes both known firefly luciferase and CG6178 of *D. melanogaster* are defined as luciferase co-orthologous genes (highlighted in gray). Branch length represents substitutions per site.

4.3.3 Ancestral state reconstruction of luciferase activity

We performed an ancestral character state reconstruction of luciferase activity on the luciferase homolog gene tree within Mesquite (v3.31) (212), using an unordered parsimony analysis, and maximum likelihood (ML) analyses. First, the gene tree from Fig. 3C in Newick format was filtered using Dendroscope (v3.5.9) (185) to include only the clade descending from the common ancestor of TcasPACS4 and PpyrLuc1. TcasPACS4 was set as the rooting outgroup. Luciferase activity of these extant genes was coded as a character state within Mesquite with: (0=no luciferase activity, 1=luciferase activity, ?=undetermined). A gene was given the 1-state if it had been previously characterized as having luciferase activity, or was orthologous to a gene with previously characterized luciferase activity against firefly D-luciferin. A gene was given the 0-state if it had been previously characterized as a non-luciferase, or was orthologous to a gene previously characterized to not have luciferase activity towards firefly D-luciferin. The non-luciferase activity determination for TcasPACS4 was inferred via orthology to the previously characterized non-luciferase *Tenebrio molitor* enzyme Tm-LL2 (213). The non-luciferase activity of AlatPACS4 (AQULA_005073-PA) was inferred via orthology to the non-luciferase enzyme LcruPACS2 (214). The non-luciferase activity of IlumPACS4 (ILUMI_06433-PA) was inferred via orthology to the non-luciferase *Pyrophorus angustus* enzyme PangPACS (158, 215). IlumLuc luciferase activity was inferred via orthology to the *P. angustus* dorsal and ventral luciferases(158). The luciferase activity of PpyrLuc2 (PPYR_00002-PA) was inferred via orthology to other Luc2s, e.g. *A. lateralis* Luc2 (192). The luciferase activity of the included Phengodid (196, 216, 217), Rhagophthalmid (198, 218), and firefly luciferases (219–221) were annotated from the literature. We then reconstructed the ancestral luciferase activity character state over the tree, using an unordered parsimony model, and a maximum likelihood (ML) model. ML analyses were performed under the AsymmMk model with default parameters (i.e. Root State Frequencies Same as Equilibrium).

4.3.4 Testing for ancestral selection of Elaterid ancestral luciferase

Peptide sequences for elaterid luciferase homologs descending from the putative common ancestor of firefly and elaterid luciferase as determined by a preliminary maximum likelihood molecular evolution analysis of luciferase homologs (not shown), were selected from Uniprot, whereas their respective CDS sequences were selected from the European Nucleotide Archive (ENA) or National Center for Biotechnology Information (NCBI). These sequences include: The dorsal (PangLucD; ENA ID=BAI66600.1) and ventral (PangLucV; ENA ID=BAI66601.1) luciferases, and a luciferase-like homolog without luciferase-activity (PangPACS; ENA ID=BAI66602.1) from *Pyrophorus angustus* (158), and two unpublished but database deposited luciferase homologs without luciferase-activity (data not shown) from *Cryptalaus berus* (CberPACS; ENA ID =BAQ25863.1) and *Pectocera fortunei fortunei* (PffPACS; ENA ID=BAQ25864.1). The peptide and CDS sequence of the *Pyrearinus termitilluminans* luciferase (PtermLuc) were manually transcribed from the literature (197), as these sequences were seemingly never deposited in a publically accessible sequence database. The dorsal

(PmeLucD; NCBI ID=AF545854.1) and ventral (PmeLucV; NCBI ID=AF545853.1) luciferases of *Pyrophorus mellifluus* (222). The dorsal and ventral luciferase alleles of *Pyrophorus plagiophthalmus* (222), which were most similar to that of *Pyrophorus mellifluus* in a maximum likelihood analysis (data not shown). The CDS sequence of the complete *I. luminosus* luciferase (IlumiLuc; ILUMI_00001-PA), two closely related paralogs (IlumPACS9: ILUMI_26849-PA, IlumPACS8: ILUMI_26848-PA), and 2 other paralogs (IlumPACS2: ILUMI_02534-PA; IlumPACS1: ILUMI_06433-PA), and the CDS for *Photinus pyralis* luciferase (PyrLuc1: PPYR_00001-PA) was added as an outgroup sequence.

The 20 merged CDS sequences were multiple-sequenced-aligned with MUSCLE (223) in “codon” mode within MEGA7 (184), using parameters (Gap Open = -.2.9; Gap Extend = 0; Hydrophobicity Multiplier 1.2, Clustering Method= UPGMB, Min Diag Length (lambda)=24, Genetic Code = Standard), producing a nucleotide multiple-sequence-alignment (MSA). A maximum likelihood gene tree was produced from the nucleotide MSA within MEGA7 using the General Time Reversible model (224), with 5 gamma categories (+G, parameter = 0.8692). The analysis involved 20 nucleotide sequences. Codon positions included were 1st+2nd+3rd+Noncoding. There were a total of 1659 positions in the final dataset. Initial tree(s) for the heuristic search were obtained automatically by applying Neighbor-Join and BioNJ algorithms to a matrix of pairwise distances estimated using the Maximum Composite Likelihood (MCL) approach, and then selecting the topology with the superior log likelihood value. The tree with the highest log likelihood (-16392.22) was selected. 1000 bootstrap replicates were performed to evaluate the topology, and the percentage of trees in which the associated taxa clustered together is shown next to the branches in Fig 4B.

An adaptive branch-site REL test for episodic diversification was performed on the previously mentioned gene-tree and nucleotide MSA using the adaptive branch-site REL test for episodic diversification (aBSREL) method (225) within the HyPhy program (v2.3.11) (226). The input MSA contained 20 sequences with 553 sites (codons). All 37 branches of the gene phylogeny were formally tested for diversifying selection. The aBSREL analysis found evidence of episodic diversifying selection on 3 out of 37 branches in the phylogeny. Significance was assessed using the Likelihood Ratio Test at a threshold of $p \leq 0.01$, after the Holm-Bonferroni correction for multiple hypothesis testing. The intermediate files and results of this analysis, including the nucleotide MSA, GTR based gene-tree, and aBSREL produced adaptive rate class model gene tree are available on FigShare (DOI: [10.6084/m9.figshare.5691277](https://doi.org/10.6084/m9.figshare.5691277)).

4.4 Non-enzyme highly and differentially expressed genes of the firefly lantern

PPYR_04589, a predicted fatty acid binding protein is almost certainly orthologous to the light organ fatty acid binding protein reported from *Luciola cerata* (227). This fatty acid binding protein was previously reported to bind strongly to fatty acids, and weakly to luciferin. Three G-coupled protein receptors (GPCRs) with similarity to annotated octopamine/tyramine receptors were also detected to be highly and differentially expressed in the *P. pyralis* light organ

(PPYR_11673-PA, PPYR_11364-PA, PPYR_12266-PA). Octopamine is known to be the key effector neurotransmitter of the adult and larval firefly lantern and this identified GPCR likely serves as the upstream receptor of octopamine activated adenylate cyclase, previously reported as abundant in *P. pyralis* lanterns (228).

The neurobiology of flash control, including regulation of flash pattern and intensity, is a fascinating area of behavioral research. Our data generate new hypotheses regarding the molecular players in flash control. A particularly interesting highly and differentially expressed gene in both *P. pyralis* and *A. lateralis* is the full length “octopamine binding secreted hemocyanin”(PPYR_14966; AQULA_008529; Table S4.4.1) previously identified from *P. pyralis* light organ extracts via photoaffinity labeling with an octopamine analog and partial N-terminal Edman degradation (228). This protein is intriguing as hemocyanins are typically thought to be oxygen binding. We speculate that this octopamine binding secreted hemocyanin, previous demonstrated to be abundant, octopamine binding, and secreted from the lantern (presumably into the hemolymph of the light organ), could be triggered to release oxygen upon octopamine binding, thereby providing a triggerable O₂ store within the light organ under control of neurotransmitter involved in flash control. As O₂ is believed to be limiting in the light reaction, such a release of O₂ could enhance flash intensity or accelerate flash kinetics. Further research is required to test this hypothesis.

Table S4.4.1: Highly expressed (HE), differentially expressed (DE), non-enzyme annotated (NotE), lantern genes whose closest relative in the opposite species is also HE, DE, NotE. BSN-TPM = between sample normalized TPM

P. pyralis ID (OGS1.0)	Predicted function	Ppyr BSN-TPM	Ppyr expression rank	Alat expression rank	Alat BSN-TPM	A. lateralis ID (OGS1.0)
PPYR_04589	Fatty-acid binding protein	71119	1	8	10464	AQULA_005257
PPYR_05098	Peroxisomal biogenesis factor 11 (PEX11)	4016	14	26	3294	AQULA_005466
PPYR_14966	Octopamine binding secreted hemocyanin	2095	35	21	3658	AQULA_008529
PPYR_11733	MFS transporter superfamily	1859	42	84	1335	AQULA_012209
PPYR_07633	Reticulon	1561	56	109	1123	AQULA_005090
PPYR_09394	lysosomal Cystine Transporter	1101	87	69	1494	AQULA_009474
PPYR_05852	Vacuolar ATP synthase 16kDa subunit	839	118	287	475	AQULA_001418

PPYR_ID	Domain Superfamily	Count	Count	Count	Count	Accession
PPYR_11443	RNA-binding domain superfamily	784	134	1221	108	AQULA_003174
PPYR_11300	Mitochondrial outer membrane translocase complex	511	232	402	349	AQULA_004355
PPYR_04602	Leucine-rich repeat domain superfamily	460	262	378	373	AQULA_004134
PPYR_13497	Mitochondrial substrate/solute carrier	440	285	379	372	AQULA_003680
PPYR_04424	Domain of unknown function (DUF4782)	380	332	1296	101	AQULA_013946
PPYR_08278	Protein of unknown function DUF1151	366	348	430	325	AQULA_000628
PPYR_13261	Major facilitator superfamily	310	403	158	862	AQULA_007558
PPYR_05702	Sulfate permease family	226	543	396	357	AQULA_013064
PPYR_05993	V-type ATPase, V0 complex, 116kDa subunit family	211	579	541	251	AQULA_000400
PPYR_04179	Haemolymph juvenile hormone binding protein	202	606	879	152	AQULA_011187
PPYR_08298	Peroxisomal membrane protein (Pex16)	199	623	395	358	AQULA_013536
PPYR_06294	Homeobox-like domain superfamily - Abdominal-B-like	198	627	737	186	AQULA_000483
PPYR_01677	MFS transporter superfamily	108	1234	455	302	AQULA_002485

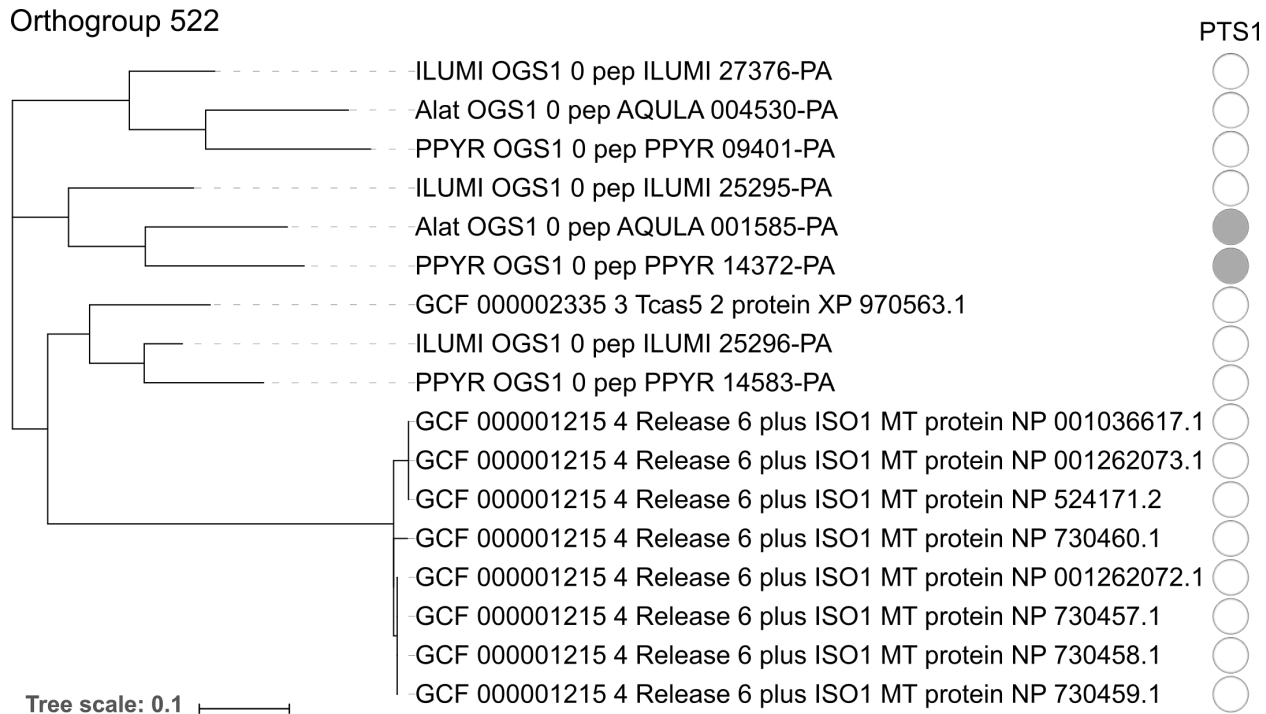


Figure S4.4.2: Maximum likelihood gene tree of the combined adenylyl-sulfate kinase & sulfate adenylyltransferase orthogroup.

Peptide sequences from *P. pyralis*, *A. lateralis*, *I. luminosus*, *T. castaneum*, and *D. melanogaster* were clustered (orthogroup # 522), multiple sequence aligned, and refactored into a species rooted maximum likelihood tree, via the OrthoFinder pipeline (Supplementary Text 4.2.1). As this is a genome-wide analysis where bootstrap replicates would be computationally prohibitive, no bootstrap replicates were performed to evaluate the support of the tree topology. PTS1 sequences were predicted from the peptide sequence using the PTS1 predictor server (208). Figure produced with iTOL (229).

4.5 Opsin analysis

Opsins are G-protein-coupled receptors that, together with a bound chromophore, form visual pigments that detect light, reviewed here (230). While opsin genes are known for their expression in photoreceptors and function in vision, they have also been found to be expressed in other tissues, suggesting non-visual functions in some cases. Insects generally use rhabdomeric opsins (r-opsins) for vision, while mammals generally use ciliary opsins (c-opsins) for vision, products of an ancient gene duplication (230, 231). Both insects and mammals may

retain the alternate opsin type, generally in a non-visual capacity. The ancestral insect is hypothesized to have 3 visual opsins - one sensitive to long-wavelengths of light (LW), one to blue-wavelengths (B), and one to ultraviolet light (UV). Previously, two opsins, one with sequence similarity to other insect LW opsins and one with similarity to other insect UV opsins, were identified as highly expressed in firefly heads (232, 233). A likely non-visual c-opsin was also detected, though not highly expressed (232, 233).

To confirm the previously documented opsin presence and expression patterns, we collected candidate opsin genes via BLASTP searches (e-value threshold: 1×10^{-20}) of the PPYR_OGS1.0, Alat_OGS1.0 and ILUMI_OGS1.0 reference genesets against UV opsin of *P. pyralis* (Genbank Accession: ALB48839.1), as well as collected non-firefly opsin sequences via literature searches, followed by maximum likelihood phylogenetic reconstruction (Fig. S4.5.1A), and expression analyses of the opsins (Fig. S4.5.1.B). The amino acid sequences of opsin were multiple aligned using MAFFT and trimmed using trimAL (parameters: -gt 0.5). The amino acid substitution model for ML analysis was estimated using Aminosan (v1.0.2016.11.07) (210). In *P. pyralis*, *A. lateralis*, and *I. luminosus*, we detected three r-opsins, including LW, UV, and an r-opsin homologous to *Drosophila Rh7* opsin, and one c-opsin. While LW and UV opsins were highly and differentially expressed in heads of both fireflies, c-opsin was lowly expressed, in *P. pyralis* head tissue only (Figure S4.5.1.B). In contrast, *Rh7* was not expressed in the *P. pyralis* light organ, but was highly and differentially expressed in the light organ of *A. lateralis* (Fig. S4.5.1 B). The detection of *Rh7* in our genomes is unusual in beetles(234), though emerging genomic resources across the order have detected it in two taxa: *Anoplophora glabripennis* (235) and *Leptinotarsa decemlineata*(236). *Rh7* has an enigmatic function - a recent study in *Drosophila melanogaster* showed that *Rh7* is expressed in the brain, functions in circadian photoentrainment, and has broad UV-to-visible spectrum sensitivity(237, 238). Extraocular opsin expression has been detected in other eukaryotes: a photosensory organ is located in the genitalia at the posterior abdominal segments in butterfly (Lepidoptera) (239). In the bioluminescent Ctenophore *Mnemiopsis leidyi*, three c-opsins are co-expressed with the luminous photoprotein in the photophores (240). In the bobtail squid, *Euprymna scolopes*, one of the c-opsin isoforms is expressed in the bacterial symbiotic light organ (241, 242). Thus, it is possible that *Rh7* has a photo sensory function in the lantern of *A. lateralis*, though this putative function is seemingly not conserved in *P. pyralis*. Future study will confirm and further explore the biological, physiological, and evolutionary significance of *Rh7* expression in the light organ across firefly taxa.

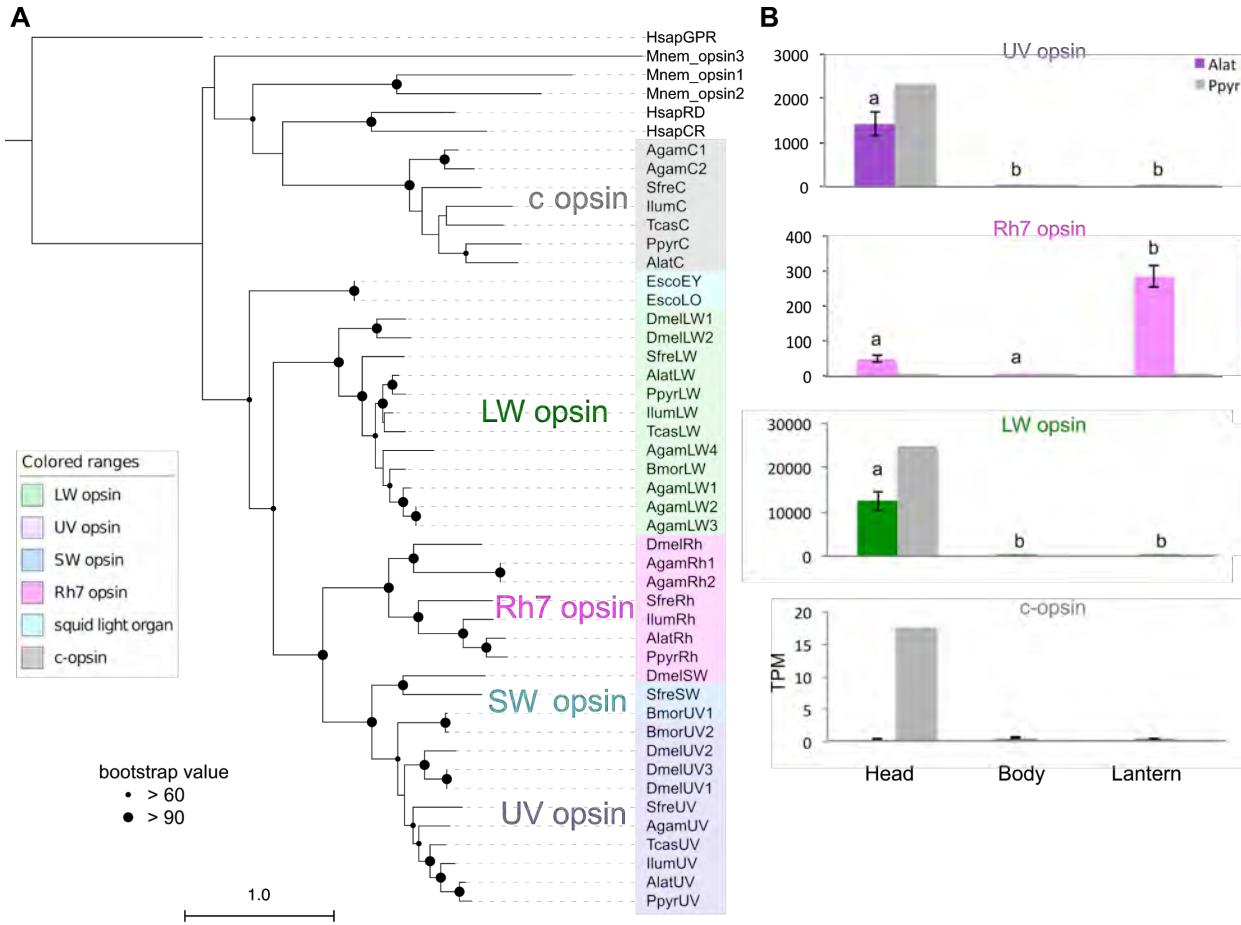


Figure S4.5.1: ML tree and gene expression levels of opsin genes.

a, Opsin Maximum likelihood (ML) tree. Collected opsin sequences were multiple sequence aligned with MAFFT L-INS-I (95) with default parameters. Gaps and ambiguous sequences were filtered with trimAL software (243) (parameter: -gt =0.5), and the ML tree reconstructed with MEGA7 (184) with LG+G (5 gamma categories (+G, parameter = 1.3856) substitution model using 362 aa of multiple amino acid alignment. 100 bootstrap replicates were performed. HsapGPR was used as the outgroup sequence. Black circles on each node indicate bootstrap values. Scale bar equals substitutions per site. Taxon abbreviation: **Hsap**: *Homo sapiens*, **Mnem**: *Mnemiopsis leidyi* **Agam**: *Anopheles gambiae*, **Sfre**: *Sympetrum frequens*, **Illum**: *Ignelater luminosus*, **Bmor**: *Bombyx mori*, **Ppyr**: *Photinus pyralis*, **Tcas**: *Tribolium castaneum*, **Dmel**: *Drosophila melanogaster*. The tree in Newick format, multiple sequence alignment files, and an excel document linking the provided gene names to the original sequence accession IDs and species name is available on FigShare (DOI: [10.6084/m9.figshare.5723005](https://doi.org/10.6084/m9.figshare.5723005)) **b**, Bar graphs indicate the gene expression levels in each body parts of averaged both male and female adult. The gene expressions in *A. lateralis* are tested with Tukey-Kramer method (three experimental replicates). UV and LW opsin are significantly highly expressed in the head ($p < 0.005$). On the other hand, Rh7 was significantly highly expressed in the lantern ($p < 0.001$). No significance was detected in c-opsin expression between all three body parts ($p > 0.5 - 0.9$) Error bar represents standard error.

4.6 LC-HRAM-MS of lucibufagin content in *P. pyralis*, *A. lateralis*, and *I. luminosus*

We assayed the hemolymph of adult *P. pyralis* and *A. lateralis*, as well as body extracts from *P. pyralis* and *A. lateralis* larvae, and *I. luminosus* adult male thorax, for lucibufagin content using liquid-chromatography high-resolution accurate-mass mass-spectrometry (LC-HRAM-MS) and MS2 spectral similarity networking approaches. We chose to analyze extracted hemolymph from both *P. pyralis*, and *A. lateralis* for lucibufagin content, as lucibufagins are known to accumulate in the adult hemolymph and hemolymph samples give less complex extracts than tissue extracts. For *P. pyralis* and *A. lateralis* larvae, and *I. luminosus* thorax, non-hemolymph was sampled as we do not have a reliable hemolymph extraction protocol for these life stages and species.

Adult male *P. pyralis* and *A. lateralis* hemolymph was extracted by the following methods: A single live adult *P. pyralis* male was placed in a 1.5 mL microcentrifuge tube with a 5 mm glass bead underneath the specimen, and centrifuged at maximum speed (~20,000xg) for 30 seconds in a benchtop centrifuge. This centrifugation crushed the specimen on top of the bead, and allowed the hemolymph to collect at the bottom of the tube. Approximately 5 µL was obtained. The extracted hemolymph was diluted with 50 µL methanol to precipitate proteins and other macromolecules. For *A. lateralis* adult hemolymph, three adult male individuals were placed in individual 1.5 mL microcentrifuge tubes with 5 mm glass beads, and spun at 5000 RPM for 1 minute in a benchtop centrifuge. The pooled extracted hemolymph (~5 µL), was diluted with 50 µL MeOH, and air dried. The *P. pyralis* extracted hemolymph was filtered through a 0.2 µm PTFE filter (Filter Vial, P/No. 15530-100, Thomson Instrument Company), whereas the *A. lateralis* hemolymph residue was redissolved in 100 µL 50% MeOH, and then filtered through the filter vial.

For extraction of *P. pyralis* larval partial body, the posterior 2 abdominal segments were first cut off from a single laboratory reared larvae (Supplementary Text 1.3.2), and the remaining partial body was placed in 180 µL 50% acetonitrile, and macerated with a pipette tip. The extract was sonicated in a water bath sonicator for ~10 minutes, not letting the temperature of the bath go above 50°C. The extract was then centrifuged (20,000xg for 10 minutes), and filtered through a 0.2 µm PTFE filter (Filter Vial, P/No. 15530-100, Thomson Instrument Company).

For extraction of *A. lateralis* larval whole body, laboratory reared *A. lateralis* larvae were flash frozen in liquid N₂, lyophilized, and the whole body (dry weight: 29.1 mg) was placed in 200 µL 50% methanol, and macerated with a pipette tip. The extract was sonicated in a water bath sonicator for 30 minutes, centrifuged (20,000xg for 10 minutes), and filtered through a 0.2 µm PTFE filter (Filter Vial, P/No. 15530-100, Thomson Instrument Company).

For extraction of *I. luminosus* adult thorax, the mesothorax through the 2 most anterior abdominal segments (ventral lantern containing segment + 1 segment) of a lyophilized *I. luminosus* adult male (Supplementary Text 3.3), was separated from the prothorax plus head and posterior 3 abdominal segments. This mesothorax + abdomen fragment was then placed in 0.5 mL 50% methanol, and macerated with a pipette tip. The extract was then sonicated in a water bath sonicator for ~10 minutes, not letting the temperature of the bath go above 50°C,

centrifuged (20,000xg for 10 minutes), and filtered through a 0.2 µm PFTE filter (Filter Vial, P/No. 15530-100, Thomson Instrument Company).

Injections of these filtered extracts (*P. pyralis* adult male hemolymph 10 µL; *A. lateralis* adult male hemolymph 5 µL; *P. pyralis* partial larval body extract 5 µL; *A. lateralis* whole larval body 5 µL; *I. lumenosus* thorax extract 20 µL) were separated and analyzed using an UltiMate 3000 liquid chromatography system (Thermo Scientific) equipped with a 150 mm C18 Column (Kinetex 2.6 µm silica core shell C18 100Å pore, P/No. 00F-4462-Y0, Phenomenex, USA) coupled to a Q-Exactive mass spectrometer (Thermo Scientific, USA). Two different instrument methods were used, a slow ~44 minute method, and an optimized ~28 minute method. Chromatographically both methods are identical up to 20 minutes.

P. pyralis hemolymph compounds were separated by the optimized method (28 minute), with separation via reversed-phase chromatography on a C18 column using a gradient of Solvent A (0.1% formic acid in H₂O) and Solvent B (0.1% formic acid in acetonitrile); 5% B for 2 min, 5-40% B until 20 min, 40-95% B until 22 minutes, 95% B for 4 min, and 5% B for 5 min; flow rate 0.8 mL/min. All other sample extracts were separated by the slow (44 minute) reversed-phase chromatography method, using a C18 column with a gradient of Solvent A (0.1% formic acid in H₂O) and Solvent B (0.1% formic acid in acetonitrile); 5% B for 2 min, 5-80% B until 40 min, 95% B for 4 min, and 5% B for 5 min; flow rate 0.8 mL/min.

The mass spectrometer was configured to perform 1 MS1 scan from *m/z* 120-1250 followed by 1-3 data-dependent MS2 scan using HCD fragmentation with a stepped collision energy of 10, 15, 25 normalized collision energy (NCE). Positive mode and negative mode MS1 and MS2 data was obtained in a single run via polarity switching for the optimized method, or in separate runs for the slow method. Data was collected as profile data. The instrument was always used within 7 days of the last mass accuracy calibration. The ion source parameters were as follows: spray voltage (+) at 3000 V, spray voltage (-) at 2000 V, capillary temperature at 275°C, sheath gas at 40 arb units, aux gas at 15 arb units, spare gas at 1 arb unit, max spray current at 100 (µA), probe heater temp at 350°C, ion source: HESI-II. The raw data in Thermo format was converted to mzML format using ProteoWizard MSConvert(244). Data analysis was performed with Xcalibur (Thermo Scientific) and MZmine2 (v2.30)(245). Raw LC-MS data are available on MetaboLights (Accession: To Be Determined).

Within MZmine2, data was from all 5 samples on positive mode was first cropped to 20 minutes in order to compare data which was obtained with the same LC gradient parameters. Profile MS1 data was then converted to centroid mode with the Mass detection module(Parameters: Mass Detector = Exact mass, Noise level = 1.0E4), whereas MS2 data was converted to centroid mode with (Noise level=1.0E1). Ions were built into chromatograms using the Chromatogram Builder module with parameters (min_time_span = 0.10,min_height = 1.0E4, *m/z* tolerance = 0.001 *m/z* or 5 ppm. Chromatograms were then deconvolved using the Chromatogram deconvolution module with parameters (Algorithm = Local Minimum Search, Chromatographic threshold = 5.0%, Search Minimum in RT range = 0.10 min, Minimum relative height = 1%, Minimum absolute height =1.0E0, Min ratio of peak top/edge = 2, Peak duration range = 0.00-10.00). Isotopic peaks were annotated to their parent features with the Isotopic

peaks grouper module with parameters (m/z tolerance = 0.001 or 5 ppm, Retention time tolerance = 0.2 min, Monotonic shape=yes, Maximum charge = 2, Representative isotope=Most intense). The five peaklists (*P. pyralis* hemolymph, *P. pyralis* larval partial body, *A. lateralis* adult hemolymph, *A. lateralis* larval whole body, *I. luminous* thorax) were then joined and retention time aligned using the RANSAC algorithm with parameters (m/z tolerance = 0.001 or 10 ppm, RT tolerance = 1.0 min, RT tolerance after correction = 0.1 min, RANSAC iterations = 100, Minimum number of points = 5%, Threshold value = 0.5). These aligned peaklists were then gap-filled. Systematic mass accuracy error was determined with the endogenous tryptophan [M+H] ion (m/z =205.09 , RT=3.5-4.5 mins), and was measured to be +0.6 ppm, +9.9 ppm, +1.6 ppm, +1.1 ppm, and +0.6ppm, for *P. pyralis* adult hemolymph, *P. pyralis* partial larval body extract, *A. lateralis* adult hemolymph, *A. lateralis* larval body extract, and *I. luminosus* thorax extract respectively.

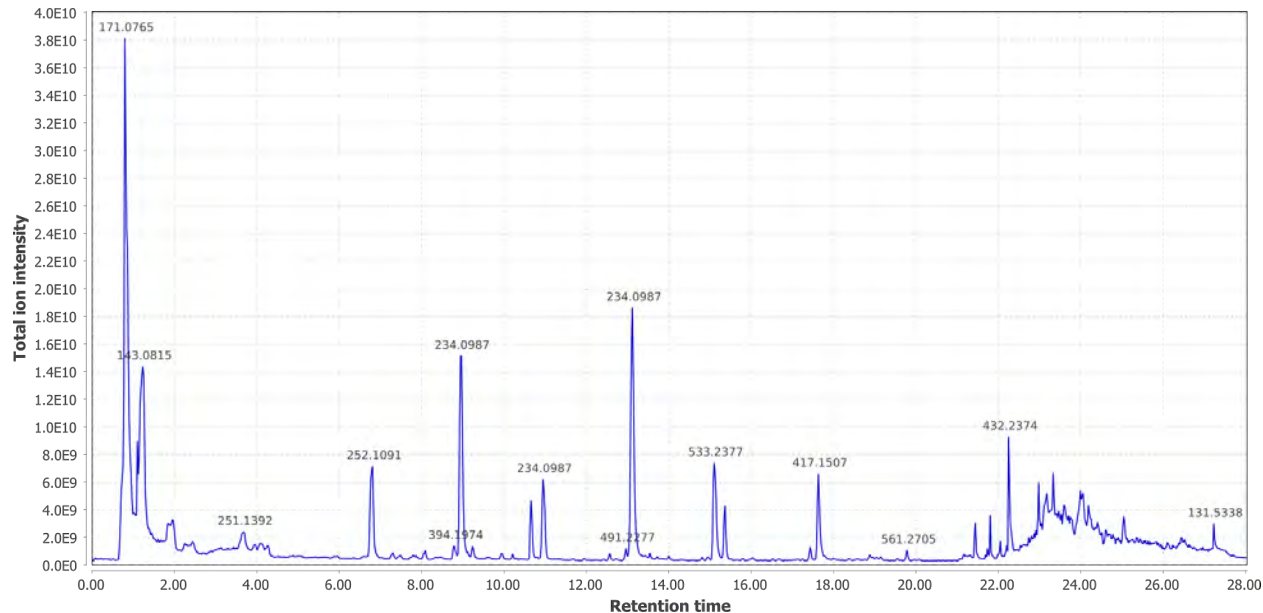


Figure S4.6.1: Positive mode MS1 total-ion-chromatogram (TIC) of *P. pyralis* adult hemolymph LC-HRAM-MS data

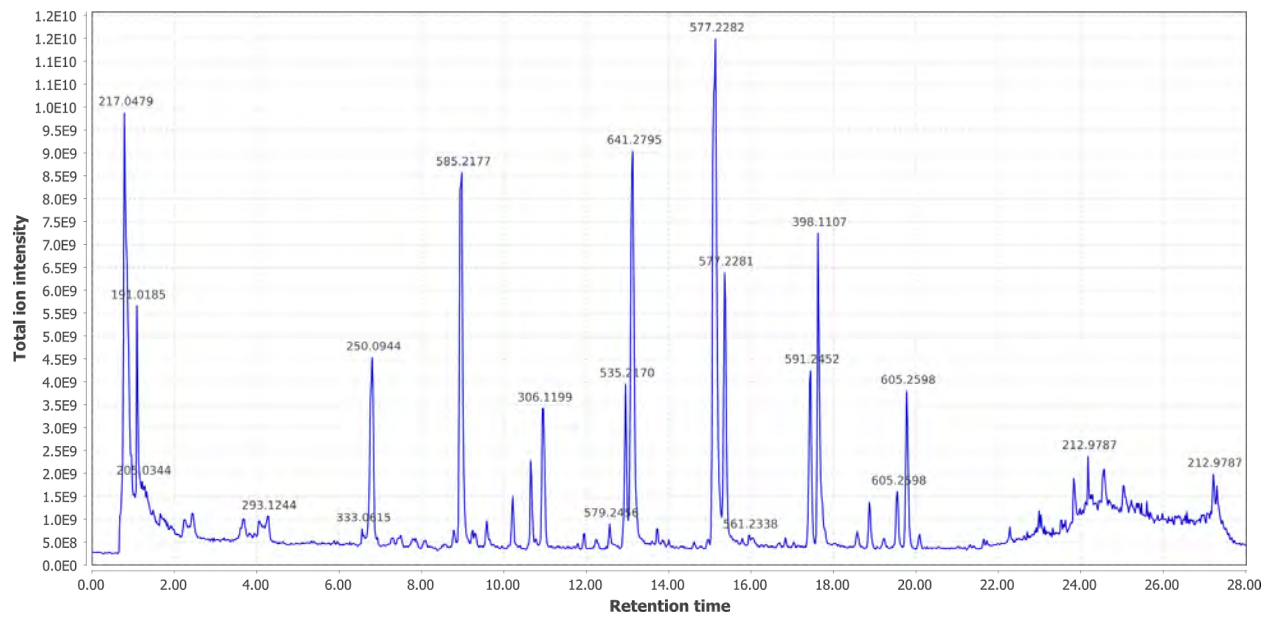


Figure S4.6.2: Negative mode MS1 total-ion-chromatogram (TIC) of *P. pyralis* adult hemolymph LC-HRAM-MS data

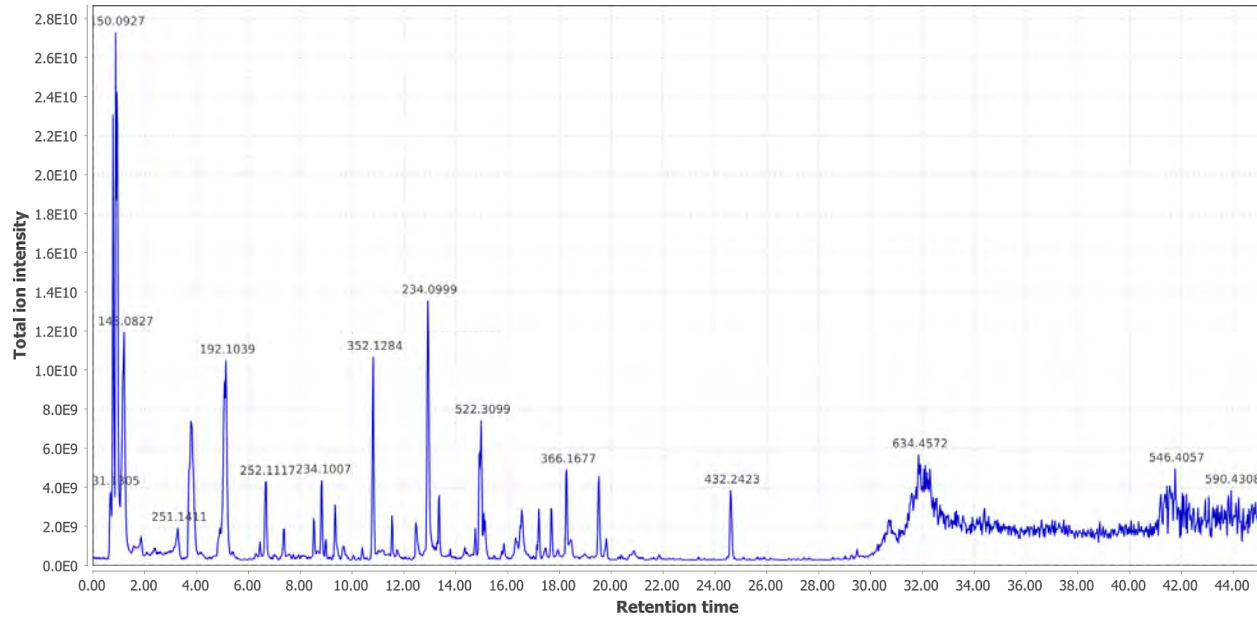


Figure S4.6.3: Positive mode MS1 total-ion-chromatogram (TIC) of *P. pyralis* larval whole body minus 2 posterior segments LC-HRAM-MS data.

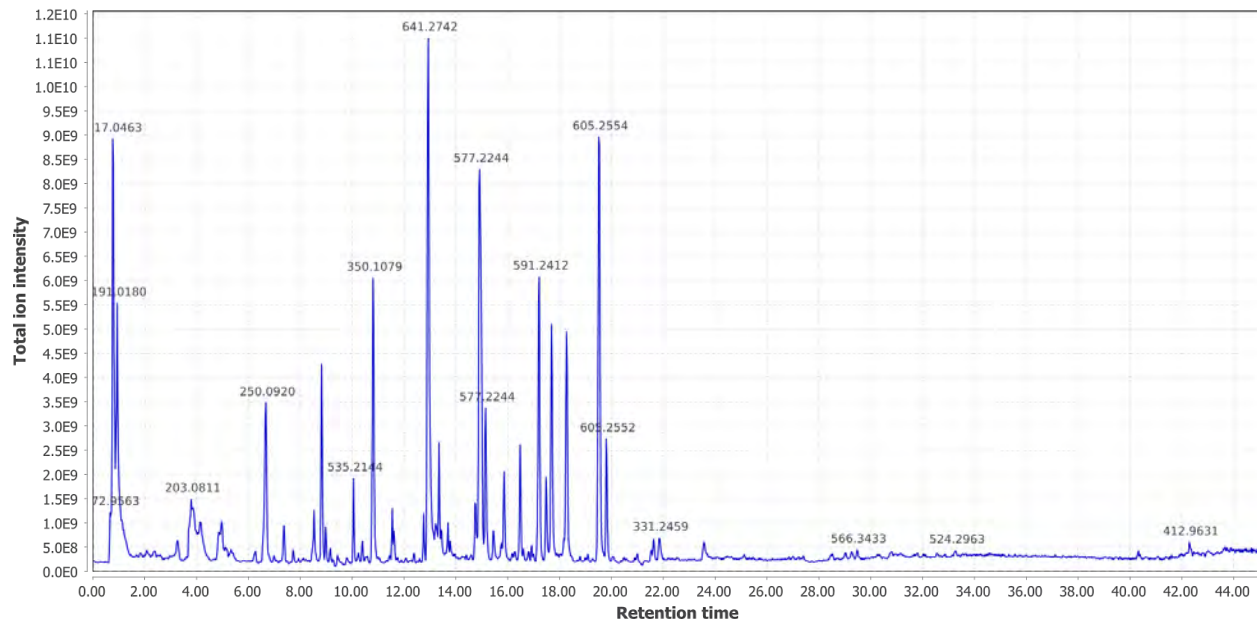


Figure S4.6.4: Positive mode MS1 total-ion-chromatogram (TIC) of *P. pyralis* larval whole body minus 2 posterior segments LC-HRAM-MS data.

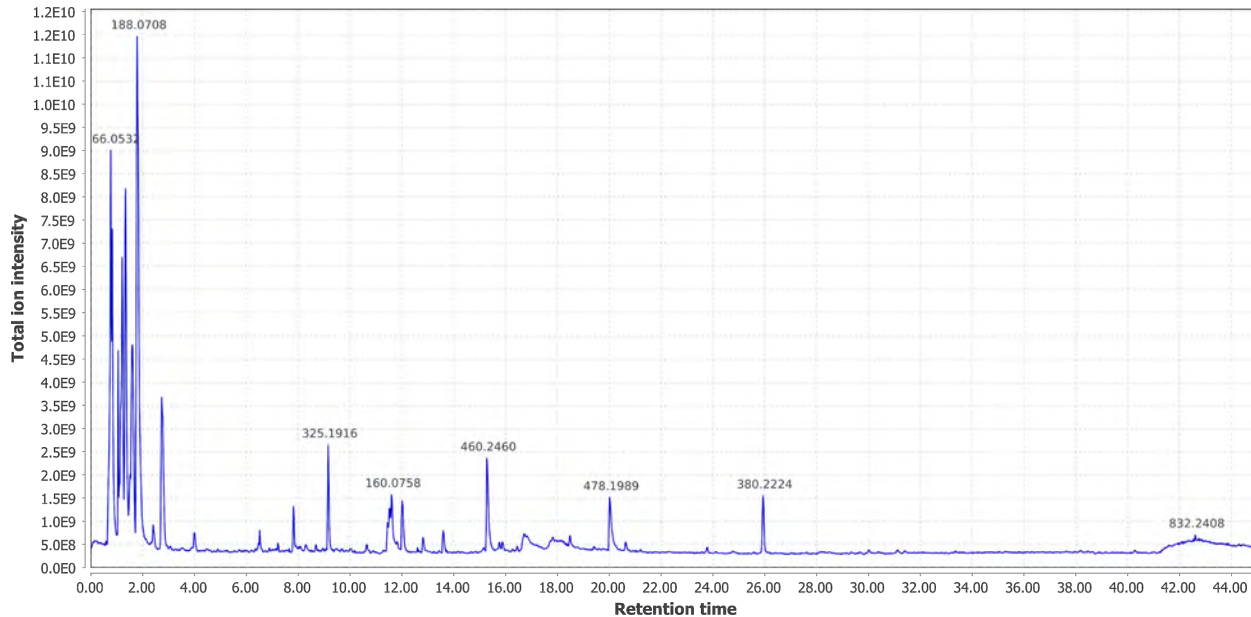


Figure S4.6.5: Positive mode MS1 total-ion-chromatogram (TIC) of *A. lateralis* adult hemolymph LC-HRAM-MS data.

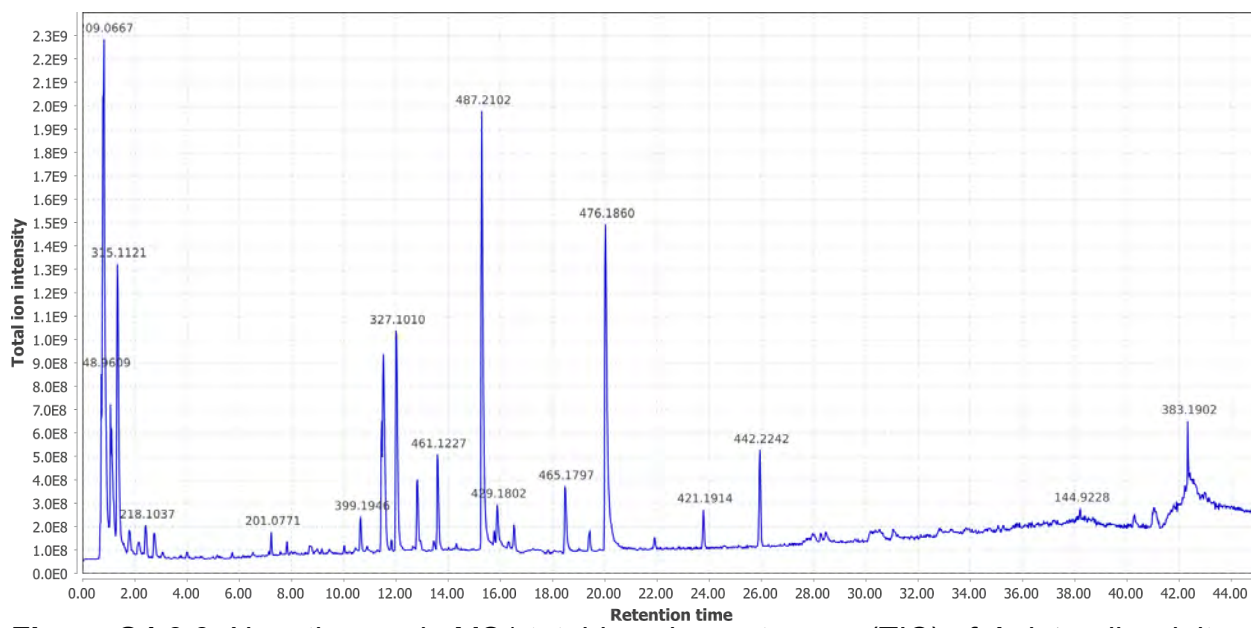


Figure S4.6.6: Negative mode MS1 total-ion-chromatogram (TIC) of *A. lateralis* adult hemolymph LC-HRAM-MS data.

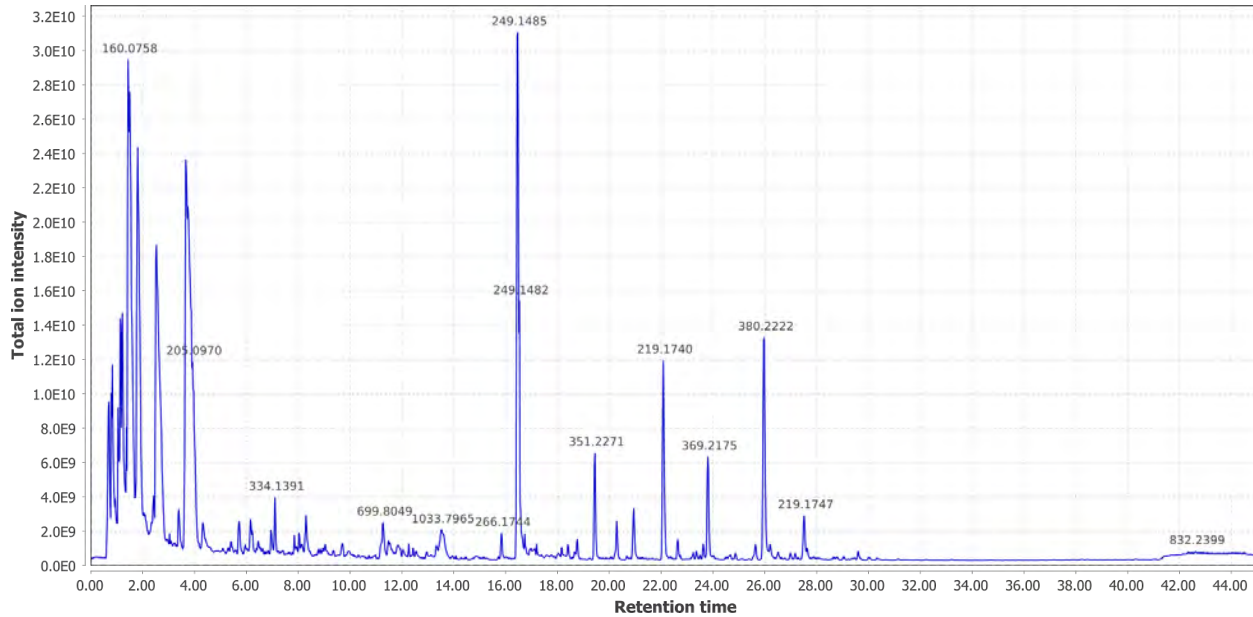


Figure S4.6.7: Positive mode MS1 total-ion-chromatogram (TIC) of *A. lateralis* larval whole body LC-HRAM-MS data

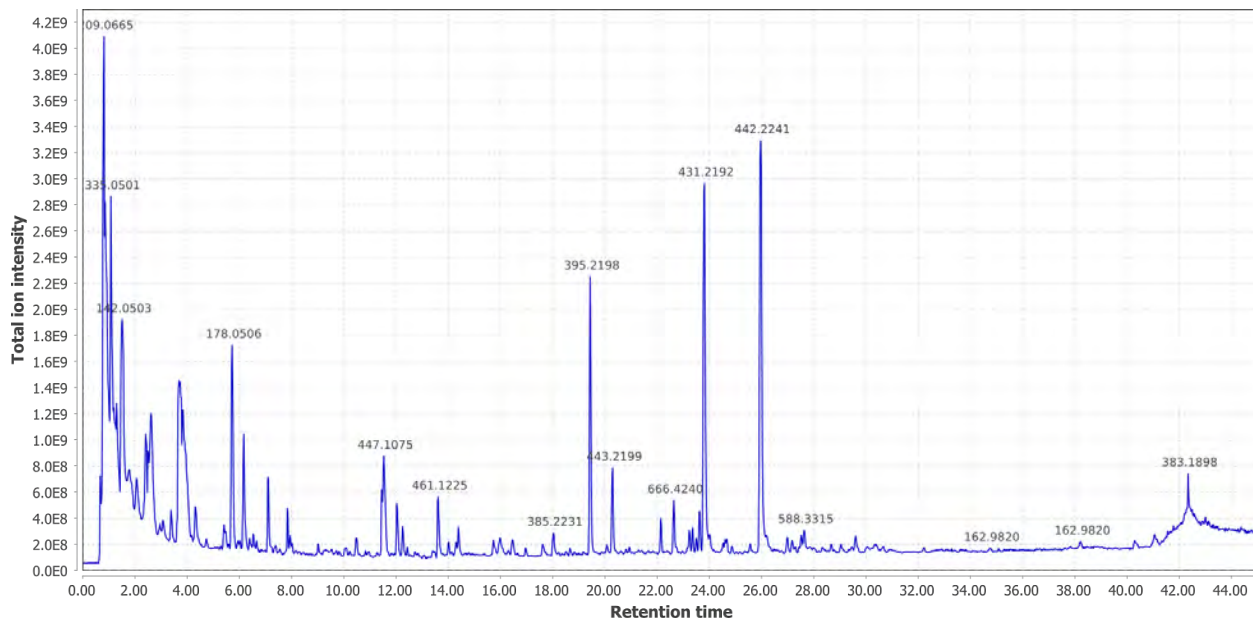


Figure S4.6.8: Negative mode MS1 total-ion-chromatogram (TIC) of *A. lateralis* larval whole body extract LC-HRAM-MS data

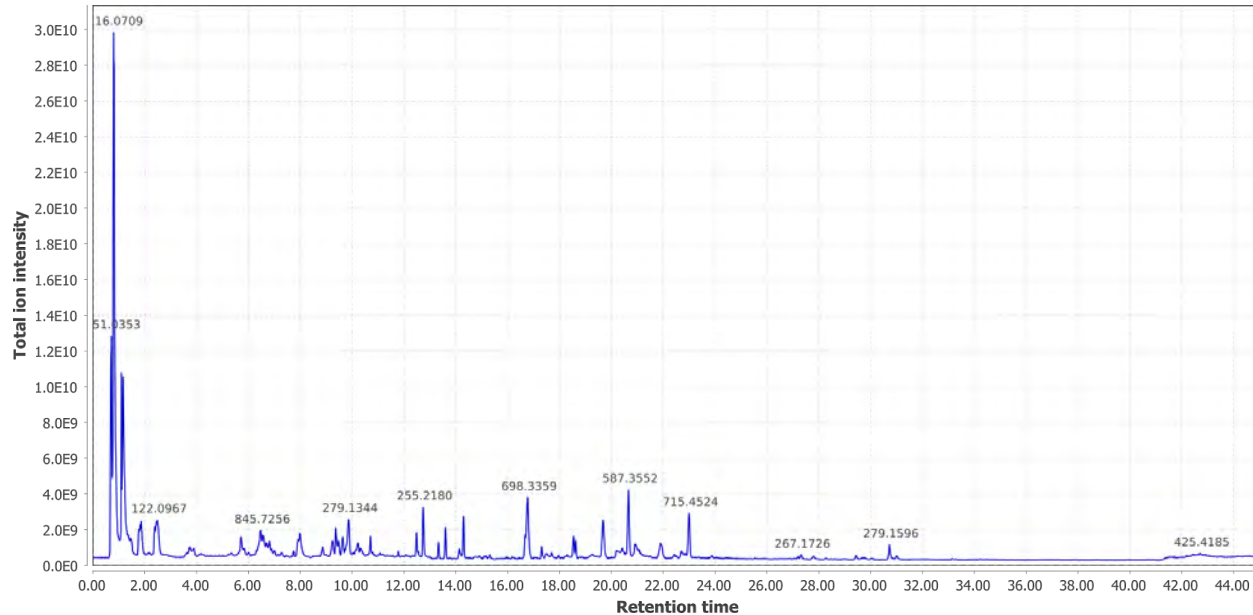


Figure S4.6.9: Positive mode MS1 total-ion-chromatogram (TIC) of *I. luminosus* abdomen extract LC-HRAM-MS data

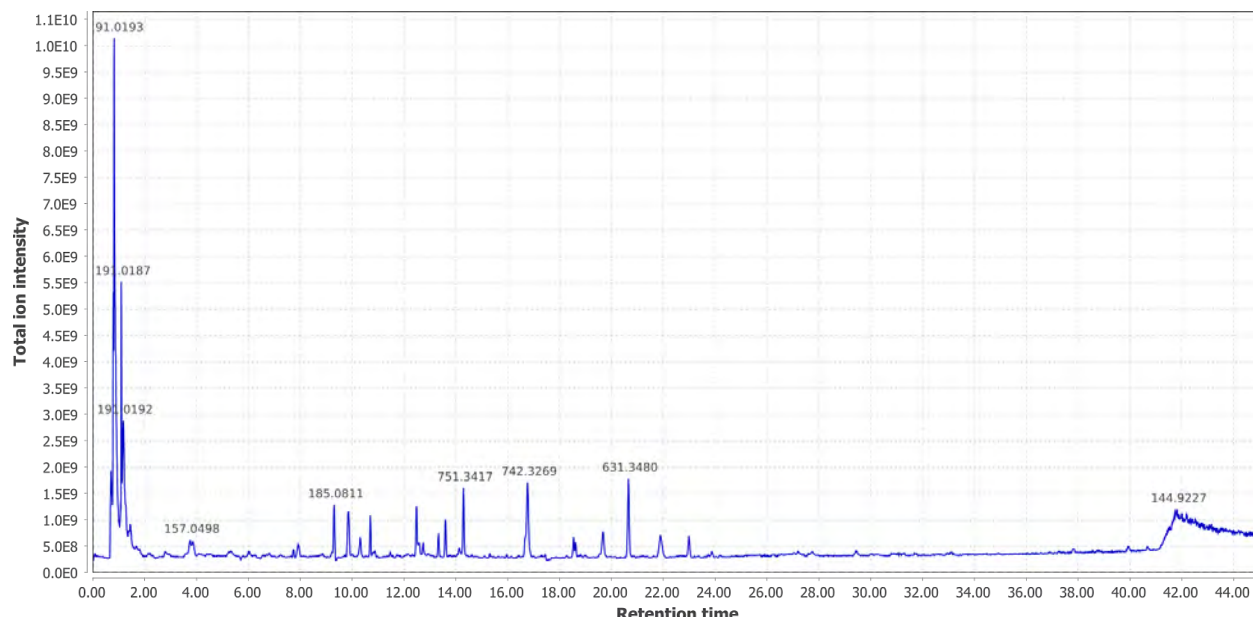


Figure S4.6.10: Negative mode MS1 total-ion-chromatogram (TIC) of *I. luminosus* abdomen extract LC-HRAM-MS data

4.6.5 MS2 similarity search for *P. pyralis* lucibufagins

We first performed a MS2 similarity search within *P. pyralis* adult hemolymph for ions that showed a similar MS2 spectra to the MS2 spectra arising from the diacetylated lucibufagin [M+H] ion from the same run ([M+H] *m/z* 533.2385, RT = 15.10 mins) (Fig. S4.6.5.1). This search was performed through the MS2 similarity search module of MZmine2 (v2.30) with parameters (*m/z* tolerance: 0.0004 *m/z* or 1 PPM; minimum # of ions to report: 3). This MS2 similarity search revealed 9 putative lucibufagin isomers with highly similar MS2 spectra (Fig. S4.6.5.2), which expanded to 17 putative lucibufagin isomers when considering features without MS2 spectra, but with identical exact masses and close retention times ($\Delta\text{RT} < 2$ min) to the previously identified 9 (Table S4.6.5.3). Chemical formula prediction was assigned to each precursor ion using the Chemical formula search module of MZmine2, whereas chemical formula predictions for product ions was performed using SIRUIS (v3.5.1) (246). The structural identity of the 9 putative lucibufagins detected via the MS2 spectra similarity search was easily interpreted in light that the different chemical formula represented the core lucibufagins that had undergone acetylation (COCH₃) or propylation (COCH₂CH₃), in different combinations. Notably the most substituted isomers, dipropylated lucibufagin ([M+H] *m/z* 561.2695, RT = 19.54 mins) were close to the edge of the cropped data (20 minutes), thus it may be possible that more highly substituted lucibufagins with a longer retention times are present, but not detected in the current analysis.

We then performed a MS2 similarity search within *P. pyralis* partial body extract for ions that showed a MS2 spectra similar to that of the dipropylated lucibufagin [M+H] ion from the same run ([M+H] *m/z* 561.2738, RT=19.53). This search was performed through the MS2 similarity search module of MZmine2 (v2.30) with parameters (*m/z* tolerance: 0.0004 *m/z* or 1 PPM; minimum # of ions to report: 5). This MS2 similarity search revealed 14 putative lucibufagin isomers with highly similar MS2 spectra (Table S4.6.5.3). Complexes, and fragments were manually removed from the analysis. Comparison of the theoretical and observed exact mass indicated that this experimental run had an unusual degree of systematic *m/z* error, of ~ +10 ppm. After manual correction *m/z*, chemical formula prediction revealed a several putative lucibufagin's of unknown structure with nitrogen in their chemical formula, suggesting that the nitrogen containing lucibufagins reported by by Gronquist and colleagues from *Lucidota atra* (247) may be present in *P. pyralis* larvae.

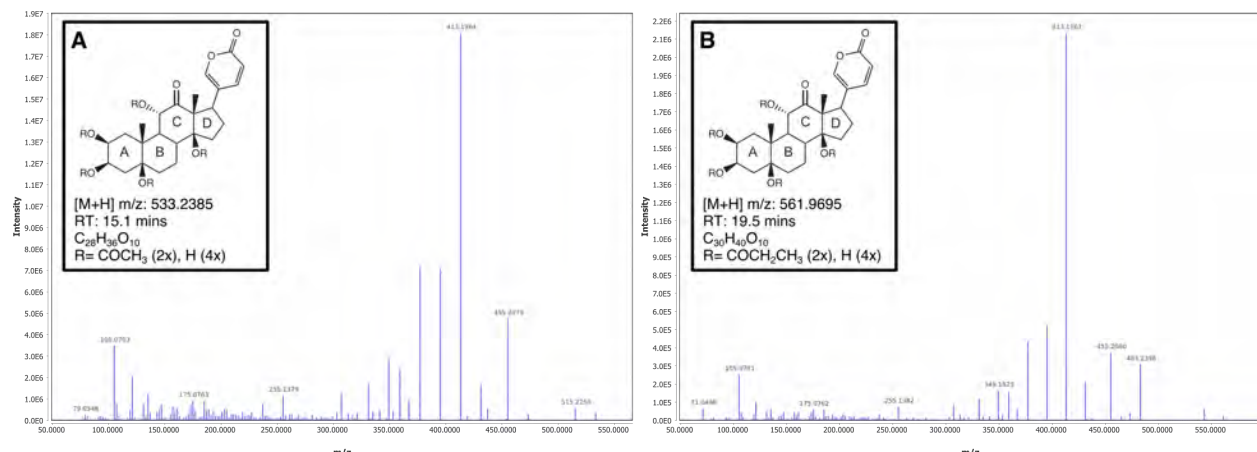


Figure S4.6.5.1: Positive mode MS2 spectra of (A) diacetylated lucibufagin and (B) dipropylated lucibufagin

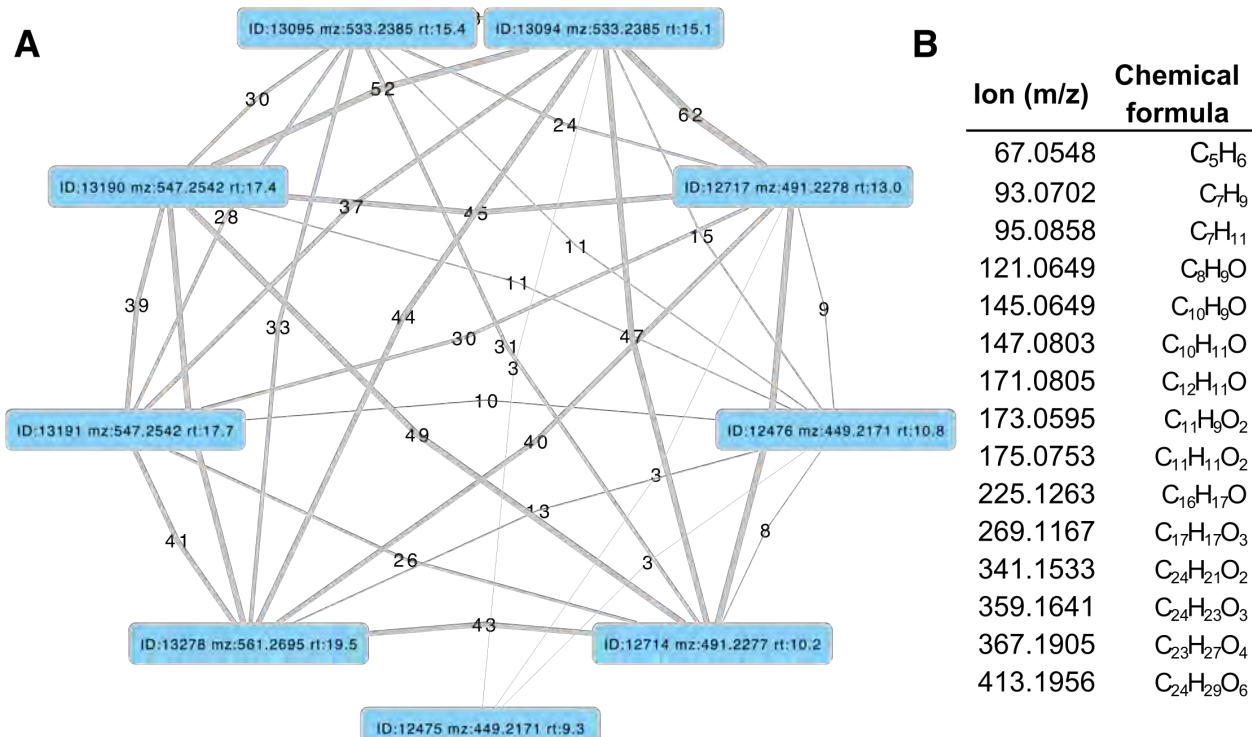


Figure S4.6.5.2: MS2 spectral similarity network for *P. pyralis* adult hemolymph lucibufagins

(A) MS2 similarity network produced with the MZmine2 MS2 similarity search module. Nodes represent MS2 spectra from the initial dataset, whereas edges represent an MS2 similarity match between two MS2 spectra. Thickness / label of the edge represents the number of ions matched between the two MS2 spectra. **(B)** Table of matched ions between diacetylated lucibufagin (m/z : 533.2385 RT:15.1), and core (unacetylated) lucibufagin (m/z : 449.2171 RT:10.8 min). MS Adducts and complexes of the presented ions were manually removed.

Table S4.6.5.3: Putative lucibufagin compounds from LC-HRAM-MS of *P. pyralis* adult hemolymph.

Retention time and m/z values are not calibrated to the other samples.

Assigned ion identity	Ion type	Chemical formula	Expected m/z	Measured m/z	m/z error (ppm)	Retention time (mins)	Feature area (arb)
Core lucibufagin isomer 1	[M+H]	C ₂₄ H ₃₃ O ₈	449.2175	449.2171	-0.89	7.9	6.7E+05
Core lucibufagin isomer 2	'''	'''	'''	'''	'''	9.3	1.1E+07
Monoacetylated lucibufagin isomer 1	'''	C ₂₆ H ₃₅ O ₉	491.2281	491.2277	-0.81	10.2	4.2E+07
Core lucibufagin isomer 3	'''	C ₂₄ H ₃₃ O ₈	449.2175	449.2171	-0.89	10.8	1.7E+07
Monoacetylated lucibufagin isomer 2	'''	C ₂₆ H ₃₅ O ₉	491.2281	491.2277	-0.81	11.4	1.1E+06
Monoacetylated lucibufagin isomer 3	'''	'''	'''	'''	'''	11.9	1.8E+07
Monoacetylated lucibufagin isomer 4	'''	'''	'''	'''	'''	13.0	2.7E+08
Monoacetylated lucibufagin isomer 5	'''	'''	'''	'''	'''	13.2	6.0E+07
Monoacetylated lucibufagin isomer 6	'''	'''	'''	'''	'''	14.5	6.2E+06
Diacetylated lucibufagin isomer 1	'''	C ₂₈ H ₃₇ O ₁₀	533.2387	533.2385	-0.37	15.1	4.0E+09
Diacetylated lucibufagin isomer 2	'''	'''	'''	'''	'''	15.4	1.9E+09
Monoacetylated, mono propylated lucibufagin isomer 1	'''	C ₂₉ H ₃₉ O ₁₀	547.2543	547.2542	-0.18	17.0	1.5E+07
Monoacetylated, mono propylated lucibufagin isomer 2	'''	'''	'''	'''	'''	17.4	2.8E+08
Monoacetylated, mono propylated lucibufagin isomer 3	'''	'''	'''	'''	'''	17.7	1.2E+08
Dipropylated lucibufagin isomer 1	'''	C ₃₀ H ₄₁ O ₁₀	561.2700	561.2695	-0.89	18.9	1.4E+08
Dipropylated lucibufagin isomer 2	'''	'''	'''	'''	'''	19.5	3.9E+07
Dipropylated lucibufagin isomer 3	'''	'''	'''	'''	'''	19.8	1.8E+08

Table S4.6.5.4: Putative lucibufagin compounds from LC-HRAM-MS of *P. pyralis* larval partial body extracts.

*= m/z error and expected m/z extrapolated from ions with similar m/z , and chemical formula predicted from resulting chemical formula. Retention time and m/z values are not calibrated to the other samples.

Assigned ion identity	Ion type	Chemical formula	Expected m/z	Measured m/z	m/z error (ppm)	Retention time (mins)	Feature area (arb)
Core lucibufagin isomer 1	[M+H]	C ₂₄ H ₃₃ O ₈	449.2175	449.2215	+8.9	9.15	8.5E+06
Monoacetylated lucibufagin isomer 1	""	C ₂₆ H ₃₅ O ₉	491.2277	491.2326	+9.9	10.04	1.2E+07
Unknown	unknown	C ₂₈ H ₃₉ O ₁₀ *	535.2543*	535.2592	+9.1*	12.40	1.6E+07
Unknown	unknown	C ₂₄ H ₃₈ NO ₆ *	436.2695*	436.2735	+9.1*	13.30	2.2E+07
Unknown	unknown	C ₂₇ H ₄₅ N ₂ O ₈ *	525.3173*	525.3221	+9.1*	13.35	1.3E+08
Unknown	unknown	C ₂₄ H ₄₀ NO ₇ *	454.2799*	454.2840	+9.1*	13.73	1.3E+07
Diacetylated lucibufagin isomer 1	[M+H]	C ₂₈ H ₃₇ O ₁₀	533.2387	533.2426	+7.3	14.93	1.7E+09
Diacetylated lucibufagin isomer 2	[M+H]	""	""	533.2426	+7.3	15.16	3.5E+08
Unknown	Unknown	C ₂₉ H ₄₆ NO ₈ *	536.3216*	536.3256	+7.3*	16.57	4.1E+07
Unknown	Unknown	Unknown	563.2854*	563.2896	+7.3*	16.80	1.3E+07
Unknown	Unknown	C ₂₆ H ₃₁ O ₇	455.2056	455.2097	+9.1*	17.22	5.8E+07
Dipropylated lucibufagin isomer 3	Unknown	C ₃₀ H ₄₁ O ₁₀	561.2700	561.2738	+6.7	19.53	2.0E+09
Dipropylated lucibufagin isomer 4	Unknown	C ₃₀ H ₄₁ O ₁₀	561.2700	561.2738	+6.7	19.82	2.2E+08

Table S4.6.5.5: Putative lucibufagin [M+H] exact masses adjusted for instrument run specific systematic m/z error (Fig. 5B)

*= Chemical formula assigned from structurally unclear putative lucibufagins

Chemical formula	Predicted exact mass	Exact mass adjusted to <i>P. pyralis</i> hemolymph data (+0.6 ppm)	Exact mass adjusted to <i>P. pyralis</i> partial larval body data (+9.9 ppm)	Exact mass adjusted to <i>A. lateralis</i> hemolymph data (+1.6 ppm)	Exact mass adjusted to <i>A. lateralis</i> larval body data (+1.1 ppm)	Exact mass adjusted to <i>I. luminosus</i> thorax data (+0.6 ppm)
C24H33O8	449.2175	449.2178	449.2219	449.2182	449.2180	449.2178
C24H38NO6*	436.2699	436.2702	436.2742	436.2706	436.2704	436.2702
C24H40NO7*	454.2804	454.2807	454.2849	454.2811	454.2809	454.2807
C26H31O7	455.2069	455.2072	455.2114	455.2076	455.2074	455.2072
C26H35O9	491.2281	491.2284	491.2330	491.2289	491.2286	491.2284
C27H45N2O8*	525.3175	525.3178	525.3227	525.3183	525.3181	525.3178
C28H37O10	533.2386	533.2389	533.2439	533.2395	533.2392	533.2389
C28H39O10*	535.2543	535.2546	535.2596	535.2552	535.2549	535.2546
C29H39O10	547.2543	547.2546	547.2597	547.2552	547.2549	547.2546
C29H46NO8*	536.3223	536.3226	536.3276	536.3232	536.3229	536.3226
C30H41O10	561.2699	561.2702	561.2755	561.2708	561.2705	561.2702

4.6.7 MS2 similarity search for *A. lateralis* lucibufagins

Although our earlier LC-HRAM-MS analysis (Fig 5B; Supplementary Text 4.6) indicated *A. lateralis* adult male hemolymph does not contain detectable quantities of the *P. pyralis* lucibufagins, this does not exclude that structurally unknown lucibufagins with chemical formula not present in *P. pyralis*, are present in *A. lateralis*. To address this, we performed a MS2 similarity search against the *A. lateralis* adult male hemolymph MS2 spectra, with the MS2 spectra of lucibufagin “C” (*m/z* 533.2385, RT=15.1) as bait, using the MZmine2 similarity search module with parameters (*m/z* tolerance= 0.001 or 10 ppm, Minimum # of matched ions=10). After filtering to those precursors that were mostly likely to be the [M+H]⁺ of a lucibufagin-like molecule (*m/z* 350-800, RT=8-20 mins), 9 MS2 spectra were matched (Table S4.6.7.1). None of

these features were detected in *P. pyralis* (Table S4.6.7.1). Chemical formula prediction was difficult due to the high m/z of the ions, but in those cases where it was successful, the additions of nitrogens and/or phosphorus to the chemical formula was confident. Notably, the most confident chemical formula predictions reported <=23 carbons, and as the core lucibufagin of *P. pyralis* contains 24 carbons, it is unlikely that these ions are derived from lucibufagins. The notable degree of MS2 similarity may be due to the *A. lateralis* compounds also being steroid derived compounds. That being said, the identity and role of the compound giving rise to ion 460.2462 is intriguing, as it is highly abundant in the *A. lateralis* adult hemolymph, is absent from the *P. pyralis* adult hemolymph, as is possibly a steroidal compound.

Table S4.6.7.1: Relative quantification of features identified by lucibufagin MS2 similarity search

Assigned identity	m/z	Chemical formula	RT (mins)	Similarity score	# of ions matched	A. lateralis Feature area (arb)	P. pyralis feature area (arb)
Unknown	460.2462	C22H38NO7P*; C25H29N7O2*	15.27	4.10E+11	34	7.04E+08	0.00E+00
""	657.2229	N.D.	12.01	9.50E+11	29	6.13E+07	""
""	414.2043	N.D.	18.07	1.20E+11	25	5.61E+06	""
""	381.2176	C23H28N2O3*	15.77	3.80E+11	18	1.22E+08	""
""	476.1839	N.D.	15.93	3.80E+11	16	9.87E+06	""
""	456.2148	N.D.	19	2.30E+11	14	5.03E+06	""
""	351.228	N.D.	19.42	2.60E+11	13	1.56E+07	""
""	479.1948	N.D.	19.83	2.20E+11	12	1.11E+07	""

* Determined with Sirius (MS2 analysis), and MZmine2 (isotope pattern analysis).

N.D., Not determined

SUPPLEMENTARY TEXT 5: Holobiont analyses

5.1 Assembly and annotation of the complete *Entomoplasma luminosum* subsp. *pyralis* genome

The complete genome of the molicute (Phylum: Tenericutes) *Entomoplasma luminosum* subsp. *pyralis* was constructed by a long-read metagenomic sequencing and assembly approach from the *P. pyralis* PacBio data. First, BUSCO v.3 with the bacterial BUSCO set was used to identify those contigs from the PacBio only Canu assembly (Ppyr0.1-PB) which contained conserved bacterial genes. A single 1.04 Mbp contig with 73 bacterial BUSCO genes was the only contig identified with more than 1 BUSCO hit. Inspection of the assembly graph with Bandage v0.8.1 (176), revealed that the contig had a circular assembly path. BLASTN alignment of the contig to the NCBI nt database indicated that this contig had a high degree of similarity to annotated Mycoplasmal genomes. Together this data suggested that this contig represented a complete Mycoplasmal genome. Polishing of the contig was performed by mapping and PacBio consensus-calling using SMRTPortal v2.3.0.140893 with the “RS_Resequencing.1” protocol with default parameters. The median coverage was ~50x. The resulting consensus sequence was restarted with seqkit(59) to place the FASTA record junction 180° across the circular chromosome, and reentered into the polishing process to enable efficient mapping across the circular junction. This mapping, consensus calling, and rotation process was repeated 3 times total, after which no additional nucleotide changes occurred. The genome was “restarted” with seqkit such that the FASTA start position began between the ribosomal RNAs, and annotation was conducted through NCBI using their prokaryotic gene annotation pipeline (PGAP). Analysis with BUSCO v.3 of the peptides produced from the aforementioned genome annotation indicated that 89.8% of expected Tenericutes single-copy conserved orthologs were captured in the annotation (C:89.8%[S:89.8%,D:0.0%], F:2.4%, M:7.8%, n:166). Comparison of the predicted 16S RNA gene sequence to the NCBI 16S RNA gene database indicated that this gene had 99% identity to the *E. luminosum* 16S sequence (ATCC 49195 - formerly *Mycoplasma luminosum*; NCBI Assembly ID ASM52685v1) (248, 249), leading to our description of this genome as the genome of *Entomoplasma luminosum* subspecies (subsp.) *pyralis*. Protein overlap comparisons using the Orthofinder pipeline (v1.1.10) (182) between our predicted protein geneset for *E. luminosum* var. *pyralis* and the protein geneset of *Entomoplasma luminosum* (ATCC 49195 - formerly *M. luminosum*; NCBI Assembly ID ASM52685v1), indicated that 94% (670/709) of the previously annotated *E. luminosum* proteins are present in our genome of *E. luminosum* subsp. *pyralis*.

5.2 Assembly and annotation of Phorid mitochondrial genome

The complete mitochondrial genome of the dipteran parasitoid *Apocephalus antennatus*, first detected as a concatemerized sequence in the Canu PacBio only assembly (Ppyr0.1-PB) was constructed in full by a long-read metagenomic sequencing and assembly

approach. First, PacBio reads were mapped to the NCBI set of mitochondrial genomes concatenated with the *P. pyralis* mitochondrial genome assembly reported in this manuscript (NCBI accession KY778696.1), using GraphMap v0.5.2 with parameters “align -C -t 4 -P”. Of the mitochondrially mapped reads (45949 reads), 98% (45267 reads) were partitioned to the *P. pyralis* mtDNA. The next most abundant category at 1.1% (531 reads), was partitioned to the mtDNA of the Phorid fly *Megaselia scalaris* (NCBI accession: KF974742.1). The next most abundant category at 0.11% (53 reads) was partitioned to the mitochondrion of the Red algae *Galdieria sulphuraria* (NCBI accession: NC_024666.1). The reads were then split into 3 partitions: *P. pyralis* mapping, *M. scalaris* mapping, and other, and input into Canu (v1.6+44) (55) for assembly. Each partitioned assembly by Canu produced a single circular contig, notably the “other” and *Megaselia* partitions produced highly similar sequences, whereas the *P. pyralis* partition produced a circular sequence that was highly similar to *P. pyralis* DNA. We inspected the *M. scalaris* partition further as it was produced with more reads. Notably, although an inspection of the contig was circular, and showed a high degree of similarity upon blastn to the *M. scalaris* mtDNA, the contig was ~2x larger than expected (29,821 bp). An analysis of contig’s self-complementarity with Gepard (v1.40) (250), indicated that this contig had 2x tandem repetitive regions, and was duplicated overall twice. Similarly, the .GFA output of Canu noted an overlap of 29,821, indicating that the assembler was unable to determine an appropriate overlap, other than the entire contig. Manual trimming of the contig to the correct size, 180° restarting with seqkit, and polishing using SMRTPortal v2.3.0.140893 with the “RS_Resequencing.1” protocol with default parameters, followed by 180° seqkit “restarting”, followed by another round of polishing, produced the final mtDNA (18,674 bp; Fig. S5.2.1). This mtDNA was taxonomically identified in a separate analysis to originate from *A. antennatus* (Supplementary Text 5.3). Coding regions, tRNAs, and rRNAs were predicted via the MITOSv2 mitochondrial genome annotation web server (60). Small mis-annotations (e.g. low scoring additional predictions of already annotated mitochondrial genes) were manually inspected and removed. Tandem repetitive regions were manually annotated. The complete *A. antennatus* genome plus assembly is available on NCBI Genbank (Accession: MG546669).

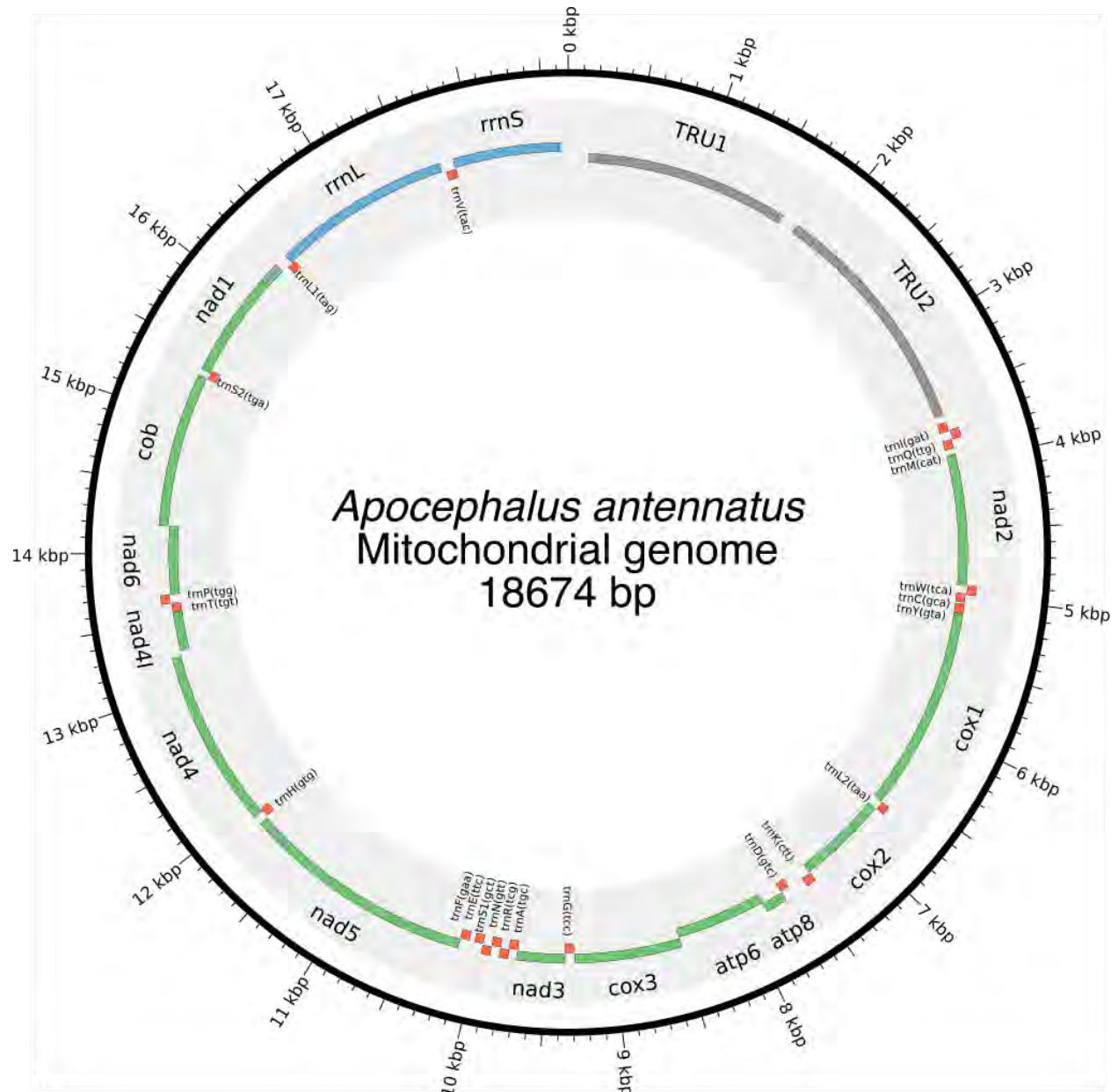


Figure S5.2.1: Mitochondrial genome of *Apocephalus antennatus*.

The mitochondrial genome of *A. antennatus* was assembled and annotated as described in the Supplementary Text 5.2, and taxonomically identified as described in Supplementary Text 5.3. Figure produced with Circo s(61)

5.3 Taxonomic identification of Phorid mitochondrial genome origin

After the successful metagenomic assembly of the mitochondrial genome of an unknown Phorid fly species from the *P. pyralis* PacBio library (Supplementary Text 5.2), we sought to characterize the species of origin for this mitochondrial genome. We planned to achieve this by collecting the Phorid flies which emerged from adult *P. pyralis*, taxonomically identifying them, and performing targeted mitochondrial PCR and sequencing experiments to correlate their

mitochondrial genome sequence to our mtDNA assembly. We successfully obtained phorid fly larvae emerging from *P. pyralis* adult males collected from MMNJ (identical field site to PacBio collection), and Rochester, NY (RCNY), in the summer of 2017. The MMNJ phorid larvae did not successfully pupate, however we obtained 5 adult specimens from successful pupations of the RCNY larvae. Two adults from this batch were identified as *A. antennatus* (Malloch), by Brian V. Brown, Entomology Curator of the Natural History Museum of Los Angeles County. DNA was extracted from one of these specimens and a COI fragment was PCR-amplified and Sanger sequenced. The forward primer was 5'-TTTGATTCTCGGCCACCCA-3', the reverse primer 5'-AGCATCGGGTAGTCTGAGT-3'. This COI fragment from had 99% identity (558/563 nt) to the COI gene of our mitochondrial assembly. This sequenced COI fragment has been submitted to GenBank (GenBank Accession: MG517481). We conclude that this is sufficient evidence to denote that our assembled Phorid mitochondrial genome is the mitochondrial genome of *A. antennatus*. Notably, *A. antennatus* was previously reported by Lloyd (251) to be a parasite of several firefly species in genera *Photuris*, *Photinus*, and *Pyractomena*, from collection sites ranging from Florida to New York. To our knowledge, this is the first report of a mitochondrial genome which was first assembled via an untargeted metagenomic approach and then later correlated to its species of origin.

5.4 *Photinus pyralis* orthomyxo-like viruses

We identified the first two viruses associated to *P. pyralis* and the *Lampyridae* family. The proposed *Photinus pyralis* orthomyxo-like virus 1 & 2 (PpyrOMLV1 & 2) present a multipartite genome conformed by five RNA segments encoding a putative nucleoprotein (NP), hemagglutinin-like glycoprotein (HA) and a heterotrimeric viral RNA polymerase (PB1, PB2 and PA). The viral genomes for *Photinus pyralis* orthomyxo-like virus 1 & 2 are available on NCBI Genbank with accessions MG972985-MG972994. Expression analyses on 24 RNA libraries of diverse individuals/developmental stages/tissues and geographic origins of *P. pyralis* indicate a dynamic presence, widespread prevalence, a pervasive tissue tropism, a low isolate variability, and a persistent life cycle through transovarial transmission of PpyrOMLV1 & 2. Genomic and phylogenetic studies suggest that the detected viruses correspond to a new lineage within the *Orthomyxoviridae* family (ssRNA(-)) (Figure S5.4.1.A-I). The concomitant occurrence in the *P. pyralis* genome of species-specific signatures of Endogenous viral-like elements (EVEs) associated to retrotransposons linked to the identified Orthomyxoviruses, suggest a past evolutionary history of host-virus interaction (Supplementary Text 5.5, Fig. S5.4.1.J). This tentative interface is correlated to low viral RNA levels, persistence and no apparent phenotypes associated with infection. We suggest that the identified viruses are potential endophytes of high prevalence as a result of potential evolutionary modulation of viral levels associated to EVEs. *Photinus pyralis* orthomyxo-like virus 1 and 2 (PpyrOMLV1 & PpyrOMLV2) share their genomic architecture and evolutionary clustering (Fig. S5.4.1.A-H, Fig. S5.4.2). They are multipartite linear ssRNA negative strand viruses, conformed by five genome segments generating a ca. 10.8 Kbp total RNA genome. Genome segments one through three (ca. 2.3-2.5 Kbp long)

encode a heterotrimeric viral polymerase constituted by subunit Polymerase Basic protein 1 - PB1 (PpyrOMLV1: 801 aa, 91 kDa; PpyrOMLV2: 802 aa, 91.2 kDa), Polymerase Basic protein 2 - PB2 (PpyrOMLV1: 804 aa, 92.6 kDa; PpyrOMLV2: 801 aa, 92.4 kDa) and Polymerase Acid protein - PA (PpyrOMLV1: 754 aa, 86.6 kDa; PpyrOMLV2: 762 aa, 87.9 kDa). PpyrOMLV1 & PpyrOMLV2 PB1 present a Flu_PB1 functional domain (Pfam: pfam00602; PpyrOMLV1: interval= 49-741, e-value= 2.93e-69; PpyrOMLV2: interval= 49-763, e-value= 1.42e-62) which is the RNA-directed RNA polymerase catalytic subunit, responsible for replication and transcription of virus RNA segments, with two nucleotide-binding GTP domains. PpyrOMLV1 & PpyrOMLV2 PB2 present a typical Flu_PB2 functional domain (Pfam: pfam00604; PpyrOMLV1: interval= 26-421, e-value= 5.10e-13; PpyrOMLV2: interval= 1-692, e-value= 1.57e-11) which is involved in 5' end cap RNA structure recognition and binding to further initiate virus transcription (Supp Table 2). PpyrOMLV1 & PpyrOMLV2 PA subunits share a characteristic Flu_PA domain (Pfam: pfam00603; PpyrOMLV1: interval= 122-727, e-value= 3.73e-07; PpyrOMLV2: interval= 117-732, e-value= 5.63e-10) involved in viral endonuclease activity, necessary for the cap-snatching process(252). Genome segment four (1.6 Kbp size) encodes a Hemagglutinin protein – HA (PpyrOMLV1: 526 aa, 59.7 kDa; PpyrOMLV2: 525 aa, 58.6 kDa) presenting a Baculo_gp64 domain (Pfam: pfam03273; PpyrOMLV1: interval= 108-462, e-value= 2.16e-15; PpyrOMLV2: interval= 42-460, e-value= 1.66e-23), associated with the gp64 glycoprotein from baculovirus as well as other viruses, such as Thogotovirus (*Orthomyxoviridae* - OMV) which was postulated to be related to the arthropod-borne nature of these specific Orthomyxoviruses. In addition, HA as expected, presents an N-terminal signal domain, a C terminal transmembrane domain, and a putative glycosylation site. Lastly, genome segment five (ca. 1.8 Kbp size) encodes a putative nucleocapsid protein – NP (PpyrOMLV1: 562 aa, 62.3 kDa; PpyrOMLV2: 528 aa, 58.5 kDa) with a Flu_NP structural domain (Pfam: pfam00506; PpyrOMLV1: interval= 145-322, e-value= 1.32e-01; PpyrOMLV2: interval= 94-459, e-value= 1.47e-04) this single-strand RNA-binding protein is associated to encapsidation of the virus genome for the purposes of RNA transcription, replication and packaging (Fig. S5.4.1.E). Despite sharing genome architecture and structural and functional domains of their predicted proteins, PpyrOMLV1 & PpyrOMLV2 pairwise identity of ortholog gene products range between 21.4 % (HA) to 49.8 % (PB1), suggesting although a common evolutionary history, a strong divergence indicating separated species, borderline to be considered even members of different virus genera (Fig. S5.4.2). The conserved 3' sequence termini of the viral genomic RNAs are (vgRNA ssRNA(-) 3'-end) 5'-GUUCUUACU-3' for PpyrOMLV1, and 5'-(G/A)U(U/G)(G/U/C)(A/C/U)UACU-3'. for PpyrOMLV2. The 5' termini of the vgRNAs are partially complementary to the 3' termini, supporting a panhandle structure and a hook like structure of the 5' end by a terminal short stem loop. PpyrOMLV1 & PpyrOMLV2 genome segments present an overall high identity in their respective RNA segments ends (Fig. S5.4.1 F). These primary and secondary sequence cues are associated to polymerase binding and promotion of both replication and transcription. In influenza viruses, and probably every OMV, the first 10 nucleotides of the 3' end form a stem-loop or 'hook' with four base-pairs (two canonical base-pairs flanked by an A-A base-pair). This compact RNA structure conforms the promoter, which activates polymerase initiation of RNA

synthesis (253). The presence of eventual orthologs of OMV additional genome segments and proteins, such as Neuraminidase (NA), Matrix (M) and Non-structural proteins (NS1, NS2) was assessed retrieving no results by TBLASTN relaxed searches, nor with *in silico* approaches involving co-expression, expression levels, or conserved terminis. Given that the presence of those additional segments varies among diverse OMV genera, and that 35 related tentative new virus species identified in TSA did not present any additional segments, we believe that these lineages of viruses are conformed by five genome segments. Further experiments based on specific virus particle purification and target sequencing could corroborate our results. Based on sequence homology to best BLASTP hits, amino acid sequence alignments, predicted proteins and domains, and phylogenetic comparisons to reported species we assigned PpyrOMLV1 & PpyrOMLV2 to the OMV virus family. These are the first viruses that have been associated with the *Lampyridae* beetle family, which includes over 2,000 species. The OMV virus members share diverse structural, functional and biological characters that define and restrict the family. OMV virions are 80–120 nm in diameter, of spherical or pleomorphic morphology. The virion envelope is derived from the host cell membrane, incorporating virus glycoproteins and eventually non-glycosylated proteins (one or two in number). Typical virion surface glycoprotein projections are 10–14 nm in length and 4–6 nm in diameter. The virus genome is multisegmented, has a helical-like symmetry, consisting of different size ribonucleoproteins (RNP), 50–150 nm in length. Influenza RNPs can perform either replication or transcription of the same template. Virions of each genus contain different numbers of linear ssRNA (-) genome segments(254). Influenza A virus (FLUAV), influenza B virus (FLUBV) and infectious salmon anemia virus (ISAV) are conformed of eight segments. Influenza C virus (FLUCV), Influenza D virus (FLUDV) and Dhori virus (DHOV) have seven segments. Thogoto virus (THOV) and Quaranfil virus (QUAV) have six segments. Johnston Atoll virus (JAV) genome is still incomplete, and only two segments have been described. Segment lengths range from 736 to 2396 nt. Genome size ranges from 10.0 to 14.6 Kbp(254). As described previously, every OMV RNA segment possess conserved and partially complementary 5'- and 3'-end sequences with promoter activity(255). OMV structural proteins are tentatively common to all genera involving the three polypeptides subunits that form the viral RdRP (PA, PB1, PB2)(256); a nucleoprotein (NP), which binds with each genome ssRNA segment to form RNPs; and the hemagglutinin protein (HA, HE or GP), which is a type I membrane integral glycoprotein involved in virus attachment, envelope fusion and neutralization. In addition, a non-glycosylated matrix protein (M) is present in most species. There are some species-specific divergence in some structural OMVs proteins. For instance, HA of FLUAV is acylated at the membrane-spanning region and has widespread N-linked glycans(257). The HA protein of FLUCV, besides its hemagglutinating and envelope fusion function, has an esterase activity that induces host receptor enzymatic destruction (254). In contrast, the HA of THOV is divergent to influenza virus HA proteins, and presents high sequence similarity to a baculovirus surface glycoprotein(258). The HA protein has been described to have an important role in determining OMV host specificity. For instance, human infecting Influenza viruses selectively bind to glycolipids that contain terminal sialyl-galactosyl residues with a 2-6 linkage, in contrast, avian influenza viruses

bind to sialyl-galactosyl residues with a 2-3 linkage(254). Furthermore, FLUAV and FLUBV share a neuraminidase protein (NA), which is an integral, type II envelope glycoprotein containing sialidase activity. Some OMVs possess additional small integral membrane proteins (M2, NB, BM2, or CM2) that may be glycosylated and have diverse functions. As an illustration, M2 and BM2 function during un-coating and fusion by equilibrating the intraluminal pH of the trans-Golgi apparatus and the cytoplasm. In addition, some viruses encode two nonstructural proteins (NS1, NS2)(254). OMV share replication properties, which have been studied mostly in Influenza viruses. It is important to note that gene reassortment has been described to occur during mixed OMV infections, involving viruses of the same genus, but not between viruses of different genera(259). This is used also as a criteria for OMV genus demarcation. Influenza virus replication and transcription occurs in the cell nucleus and comprises the production of the three types of RNA species (i) genomic RNA (vRNA) which are found in virions; (ii) cRNA molecules which are complementary RNA in sequence and identical in length to vRNA; and also (iii) virus mRNA molecules which are 5' capped by cap snatching of host RNAs and 3' polyadenylated by polymerase stuttering on U rich stretches. These remarkable dynamic multifunction characters of OMV polymerases are associated with its complex tertiary structure, of this modular heterotrimeric replicase (260). We explored in detail the putative polymerase subunits of the identified firefly viruses. The PB1 subunit catalyzes RNA synthesis in its internal active site opening, which is formed by the highly conserved polymerase motifs I-III. Motifs I and III (Fig. S5.4.1.H) present three conserved aspartates (PpyrOMLV1: Asp 346, Asp 491 and Asp 492; PpyrOMLV2: Asp 348, Asp 495 and Asp 496) which coordinate and promote nucleophilic attack of the terminal 3' OH from the growing transcript on the alpha-phosphate of the inbound NTP(256). Besides presenting, with high confidence, the putative functional domains associated with their potential replicase/transcriptase function, we assessed whether the potential spatial and functional architecture was conserved at least in part in FOML viruses. In this direction we employed the SWISS-MODEL automated protein structure homology-modelling server to generate a 3D structure of PpyrOMLV1 heterotrimeric polymerase. The SWISS server selected as best-fit template the trimeric structure of Influenza A virus polymerase, generating a structure for each polymerase subunit of PpyrOMLV1. The generated structure shared structural cues related to its multiple role of RNA nucleotide binding, endonuclease, cap binding, and nucleotidyl transferase (Fig. S5.4.1.G-H). The engendered subunit structures suggest a probable conservation of PpyrOMLV1 POL, that could allow the predicted functional enzymatic activity of this multiple gene product. The overall polymerase rendered structure presents a typical U shape with two upper protrusions corresponding to the PA endonuclease and the PB2 cap-binding domain. The PB1 subunit appears to plug into the interior of the U and has the distinctive fold of related viral RNA polymerases with fingers, palm and thumb adjacent to a tentative central active site opening where RNA synthesis may occur (253, 261). OMV Pol activity is central in the virus cycle of OMVs, which have been extensively studied. The life cycle of OMVs starts with virus entry involving the HA by receptor-mediated endocytosis. For Influenza, sialic acid bound to glycoproteins or glycolipids function as receptor determinants of endocytosis. Fusion between viral and cell membranes occurs in endosomes. The infectivity

and fusion of influenza is associated to the post-translational cleavage of the virion HA. Cleavability depends on the number of basic amino acids at the target cleavage site(254). In thogotoviruses, no requirement for HA glycoprotein cleavage have been demonstrated(258). Integral membrane proteins migrate through the Golgi apparatus to localized regions of the plasma membrane. New virions form by budding, incorporating matrix proteins and viral RNPs. Viral RNPs are transported to the cell nucleus where the virion polymerase complex synthesizes mRNA species(262). Another tentative function of the NP could be associated to the potential interference of the host immune response in the nucleus mediated by capsid proteins of some RNA virus, which could inhibit host transcription and thus liberate and direct it to viral RNA synthesis(263). mRNA synthesis is primed by capped RNA fragments 10–13 nt in length that are generated by cap snatching from host nuclear RNAs which are sequestered after cap recognition by PB2 and incorporated to vRNA by PB1 and PA proteins which present viral endonuclease activity(264). In contrast, thogotoviruses have capped viral mRNA without host-derived sequences at the 5' end. Virus mRNAs are polyadenylated at the 3' termini through iterative copying by the viral polymerase stuttering on a poly U track in the vRNA template. Some OMV mRNAs are spliced generating alternative gene products with defined functions. Protein synthesis of influenza viruses occurs in the cytoplasm. Partially complementary vRNA molecules act as templates for new viral RNA synthesis and are neither capped nor polyadenylated. These RNAs exist as RNPs in infected cells. Given the diverse hosts of OMV, biological properties of virus infection diverge between species. Influenzaviruses A infect humans and cause respiratory disease, and they have been found to infect a variety of bird species and some mammalian species. Interspecies transmission, though rare, is well documented. Influenza B virus infect humans and cause epidemics, and have been rarely found in seals. Influenzaviruses C cause limited outbreaks in humans and have been occasionally found on dogs. Influenza spreads globally in a yearly outbreak, resulting in about three to five million cases of severe illness and about 250,000 to 500,000 human deaths (265). Influenzavirus D has been recently reported and accepted and infects cows and swine (266). Natural transmission of influenzaviruses is by aerosol (human and non-aquatic hosts) or is water-borne (avians). In contrast, Thogoto and Dhori viruses which also infect humans, are transmitted by, and able to replicate in ticks. Thogoto virus was identified in *Rhipicephalus* sp. ticks collected from cattle in the Thogoto forest in Kenya, and Dhori virus was first isolated in India from *Hyalomma dromedarri*, a species of camel ticks (267, 268). Dhori virus infection in humans causes a febrile illness and encephalitis. Serological evidence suggests that cattle, camel, goats, and ducks might be also susceptible to this virus. Experimental hamster infection with THOV may be lethal. Unlike influenzaviruses, these viruses do not cause respiratory disease. The transmission of fish infecting isaviruses (ISAV) is via water, and virus infection induces the agglutination of erythrocytes of many fish species, but not avian or mammalian erythrocytes (269). Quaranfil and Johnston Atoll are transmitted by ticks and infect avian species (270).

We have limited biological data of the firefly detected viruses. Nevertheless, a significant consistency in the genomic landscape and predicted gene products of the detected viruses in

comparison with accepted OMV species sufficed to suggest for PpyrOMLV1 and PpyrOMLV2 a tentative taxonomic assignment within the OMV family. Besides relying on the OMV structural and functional signatures determined by virus genome annotation, we explored the evolutionary clustering of the detected viruses by phylogenetic insights. We generated MAFFT alignments and phylogenetic trees of the predicted viral polymerase of firefly viruses and the corresponding replicases of all 493 proposed and accepted species of ssRNA(-) virus. The generated trees consistently clustered the diverse sequences to their corresponding taxonomical niche, at the level of genera. Interestingly, PpyrOMLV1 and PpyrOMLV2 replicases were placed unequivocally within the OMV family (Fig. S5.4.1.B). When the genetic distances of firefly viruses proteins and ICTV accepted OMV species were computed, a strong similarity was evident (Fig. S5.4.1.B-D). Overall similarity levels of PpyrOMLV polymerase subunits ranged between 11.03 % to as high as 37.30 % among recognized species, while for the more divergent accepted OMV (*ISAV* - *Isavirus* genus) these levels ranged only from 8.54 % to 20.74 %, illustrating that PpyrOMLV are within the OMV by genetic standards. Phylogenetic trees based on aa alignments of structural gene products of recognized species and PpyrOMLV supported this assignment, placing ISAV and issavirus as the most distant species and genus within the family, and clustering PpyrOMLV1 and PpyrOMLV2 in a distinctive lineage within OMV, more closely related to the *Quaranjavirus* and *Thogotovirus* genera than the *Influenza A-D* or *Isavirus* genera (Fig. S5.4.2). Furthermore, it appears that virus genomic sequence data, while it has been paramount to separate species, in the case of genera, there are some contrasting data that should be taken into consideration. For instance, DHOV and THOV are both members of the *Thogotovirus* genus, sharing a 61.9 % and a 34.9 % identity at PB1 and PB2, respectively. However, FLUCV and FLUDV are assigned members of two different genus, *Influenzavirus C* and *Influenzavirus D*, while sharing a higher 72.2 % and a 52.2 % pairwise identity at PB1 and PB2, respectively (Fig. S5.4.2). In addition, FLUAV and FLUBV, assigned members of two different genus, *Influenzavirus A* and *Influenzavirus D* present a comparable identity to that of DHOV and THOV thogotoviruses, sharing a 61 % and a 37.9 % identity at PB1 and PB2, respectively. It is worth noting that similarity thresholds and phylogenetic clustering based in genomic data have been used differently to demarcate OMV genera, hence there is a need to eventually re-evaluate a series of consensus values, which in addition to biological data, would be useful to redefine the OMV family. Perhaps, these criteria discrepancies are more related to a historical evolution of the OMV taxonomy than to pure biological or genetic standards. In contrast to FLUDV, JOV and QUAU, the other virus members of OMV have been described, proposed and assigned at least 34 years ago.

The potential prevalence, tissue/organ tropism, geographic dispersion and lifestyle of PpyrOMLV1 & 2 were assessed by the generation and analyses of 29 specific RNA-Seq libraries of *P. pyralis* (refer to Specimens/libraries Table). As RNA was isolated from independent *P. pyralis* individuals of diverse origin, wild caught or lab reared, the fact that we found at least one of the PpyrOMLV present in 82 % of the libraries reflects a widespread presence and potentially a high prevalence of these viruses in *P. pyralis* (Fig. S5.4.1J, Table S5.4.5, and S5.4.6). Wild caught individuals were collected in period spanning six years, and

locations separated as much as 900 miles (New Jersey – Georgia, USA). Interestingly PpyrOMLV1 & 2 were found in individuals of both location, and the corresponding assembled isolate virus sequences presented negligible differences, with an inter-individual variability equivalent to that of isolates (0.012%). A similar result was observed for virus sequences identified in RNA libraries generated from samples collected in different years. We were not able to identify fixed mutations associated to geographical or chronological cues. Further experiments should explore the mutational landscape of PpyrOMLV1 & 2, which appears to be significantly lower than of Influenzaviruses, specifically *Influenza A virus*, which are characterized by high mutational rate (ca. 1 mutation per genome replication) associated to the absence of RNA proofreading enzymes (271). In addition we evaluated the presence of PpyrOMLV1 & 2 on diverse tissues and organs of *P. pyralis*. Overall virus RNA levels were generally low, with an average of 9.47 FPKM on positive samples. However, PpyrOMLV1 levels appear to be consistently higher than PpyrOMLV2, with an average of 20.50 FPKM for PpyrOMLV1 versus 4.22 FPKM for PpyrOMLV2 on positive samples. When the expression levels are scrutinized by genome segment, HA and NP encoding segments appear to be, for both viruses, at higher levels, which would be in agreement with other OMV such as Influenzaviruses, in which HA and NP proteins are the most expressed proteins, and thus viral mRNAs are consistently more expressed (254). Nevertheless, these preliminary findings related to expression levels should be taken cautiously, given the small sample size. Perhaps the more remarkable allusion derived from the analyses of virus presence is related to tissue and organ deduced virus tropism. Strikingly, we found virus transcripts in samples exclusively obtained from light organs, complete heads, male or female thorax, female spermatheca, female spermatophore digesting glands and bursa, abdominal fat bodies, male reproductive spiral gland, and other male reproductive accessory glands (Table S5.4.5, S5.4.6), indicating a widespread tissue/organ tropism of PpyrOMLV1 & 2. This tentatively pervasive tropism of PpyrOMLV1 & 2 emerges as a differentiation character of these viruses and accepted OMV. For instance, influenza viruses present a epithelial cell-specific tropism, restricted typically to the nose, throat, and lungs of mammals, and intestines of birds. Tropism has consequences on host restriction. Human influenza viruses mainly infect ciliated cells, because attachment of all *influenza A virus* strains to cells requires sialic acids. Differential expression of sialic acid residues in diverse tissues may prevent cross-species or zoonotic transmission events of avian influenza strains to man (272). Tropism has also influence in disease associated effects of OMV. Some *influenza A virus* strains are more present in tracheal and bronchial tissue which is associated with the primary lesion of tracheobronchitis observed in typical epidemic influenza. Other *influenza A virus* strains are more prevalent in type II pneumocytes and alveolar macrophages in the lower respiratory tract, which is correlated to diffuse alveolar damage with avian influenza (273). The presence of PpyrOMLV1 & 2 virus RNA in reproductive glands raises some potential of the involvement of sex in terms of prospective horizontal transmission. Given that most libraries corresponded to 3-6 pooled individuals samples of specific organs/tissue, direct comparisons of virus RNA levels were not always possible. However, this valuable data gives important insights into the widespread potential presence of the viruses in every analyzed

organ/tissue. Importantly, RNA levels of the putative virus segments shared co-expression levels and a systematic pattern of presence/absence, supporting the suggested multipartite nature of the viruses. We observed the presence of virus RNA of both PpyrOMLV1 & 2 in eight of the RNA-Seq libraries, thus mixed infections appear to be common. Interestingly, we did not observe in any of the 24 virus positive samples evidence of reassortment. Reassortment is a common event in OMV, a process by which influenza viruses swap gene segments. Genetic exchange is possible due to the segmented nature of the OMV viral genome and may occur during mixed infections. Reassortment generates viral diversity and has been associated to host gain of Influenzavirus (274). Reassorted Influenzavirus have been reported to occasionally cross the species barrier, into birds and some mammalian species like swine and eventually humans. These infections are usually dead ends, but sporadically, a stable lineage becomes established and may spread in an animal population (259). Besides its evolutionary role, reassortment has been used as a criterion for species/genus demarcation, thus the lack of observed gene swap in our data supports the phylogenetic and sequence similarity insights that indicates species separation of PpyrOMLV1 & 2.

In light of the presence of virus RNA in reproductive glands, we further explored the potential life style of PpyrOMLV1 & 2 related to eventual vertical transmission. Vertical transmission is extremely exceptional for OMV, and has only been conclusively described for the *Infectious salmon anemia virus (Isavirus)* (275). In this direction, we were able to generate a strand-specific RNA-Seq library of one *P. pyralis* adult female PpyrOMLV1 virus positive (parent), another library from seven eggs of this female at ~13 days post fertilization, and lastly an RNA-Seq library of four 1st instar larvae (offspring). When we analyzed the resulting RNA reads, we found as expected virus RNA transcripts of every genome segment of PpyrOMLV1 in the adult female library. Remarkably, we also found PpyrOMLV1 sequence reads of every genome segment of PpyrOMLV1 in both the eggs and larvae samples. Moreover, virus RNA levels fluctuated among the different developmental stages of the samples. The average RNA levels of the adult female were 41.10 FPKM, in contrast, the fertilized eggs sample had higher levels of virus related RNA, averaging at 61.61 FPKM and peaking at the genome segment encoding NP (104.49 FPKM). Interestingly, virus RNA levels appear to drop in 1st instar larvae, in the sequenced library average virus RNA levels were of 10.42 FPKM. Future experiments should focus on PpyrOMLV1 & 2 virus titers at extended developmental stages to complement these preliminary results. However, it is interesting to note that the tissue specific library corresponding to female spermatheca, where male sperm are stored prior to fertilization, presented relatively high levels of both PpyrOMLV1 & 2 virus RNAs, suggesting that perhaps during early reproductive process and during egg development virus RNAs tend to raise. This tentatively differential and variable virus RNA titers observed during development could be associated to an unknown mechanism of modulation of latent antiviral response that could be repressed in specific life cycle stages. Further studies may validate these results and unravel a mechanistic explanation of this phenomenon. Nevertheless, besides the preliminary developmental data, the consistent presence of PpyrOMLV1 in lab-reared, isolated offspring of

an infected *P. pyralis* female is robust evidence demonstrating mother-to-offspring vertical transmission for this newly identified OMV.

One of many questions that remains elusive here is whether PpyrOMLV1 & 2 are associated with any potential alteration of phenotype of the infected host. We failed to unveil any specific effect of the presence of PpyrOMLV1 & 2 on fireflies. It is worth noting that subtle alterations or symptoms would be difficult to pinpoint in these insects. Future studies should enquire whether PpyrOMLV1 & 2 may have any influence in biological attributes of fireflies such as fecundity, life span or life cycle. Nevertheless, we observed in our data some hints that could be indicative of a chronic state status, cryptic or latent infection of firefly individuals: (i) virus positive individuals presented in general relatively low virus RNA levels. (ii) virus RNA was found in every assessed tissue/organ. (iii) vertical transmission of the identified viruses. The first hint is hardly conclusive, it is difficult to define what a relatively low RNA level is, and high virus RNA loads are not directly associated with disease on reported OMV. The correlation of high prevalence, prolonged host infection, and vertical transmission observed in several new mosquito viruses has resulted in their classification as “commensal” microbes. A shared evolutionary history of viruses and host, based in strategies of immune evasion of the viruses and counter antiviral strategies of the host could occasionally result in a modulation of viral loads and a chronic but latent state of virus infection (276).

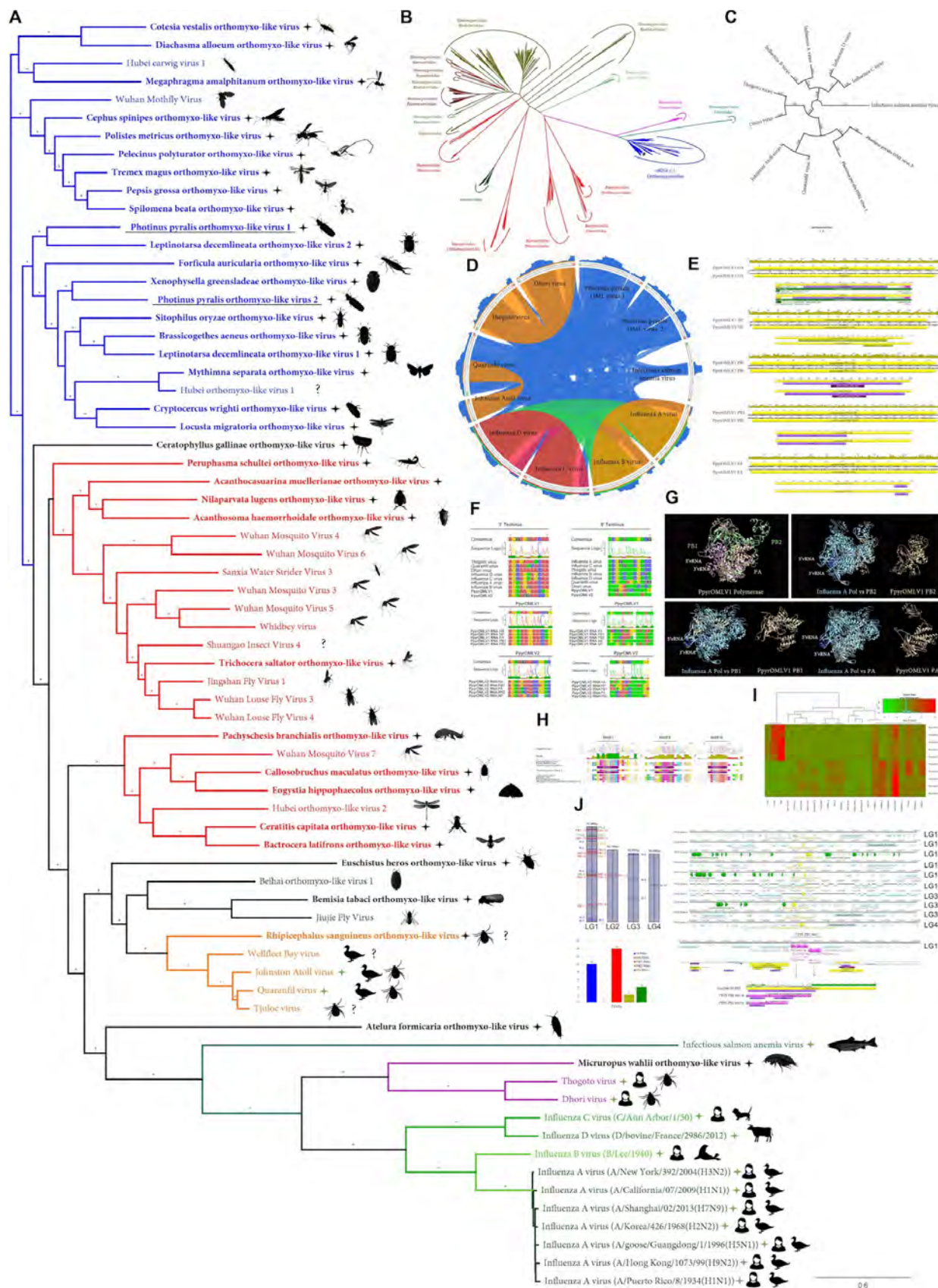
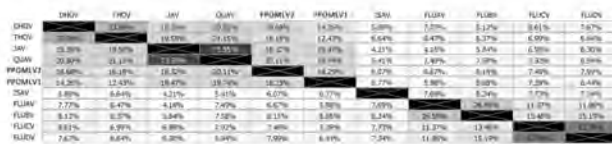
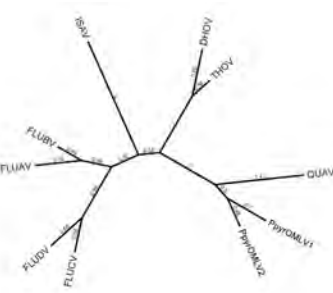


Figure S5.4.1: *Photinus pyralis* viruses and endogenous viral-like elements.

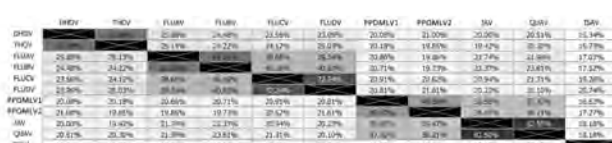
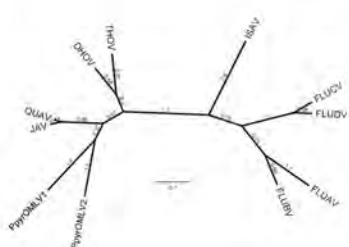
(A) Phylogenetic tree based in MAFFT alignments of predicted replicases of *Orthomyxoviridae* (OMV) ICTV accepted viruses (green stars), new *Photinus pyralis* viruses (underlined) and tentative OMV-like virus species (black stars). ICTV recognized OMV genera: *Quaranjavirus* (orange), *Thogotovirus* (purple), *Issavirus* (turquoise), *Influenzavirus A-D* (green). Silhouettes correspond to host species. Asterisk denote FastTree consensus support >0.5. Question marks depict viruses with unidentified or unconfirmed host. **(B)** Phylogenetic tree of OMV proposed and recognized species in the context of all ssRNA (-) virus species, based on MAFFT alignments of refseq replicases. *Photinus pyralis* viruses are portrayed by black stars. **(C)** Phylogenetic tree of ICTV recognized OMV species and PpyrOLMV1 & 2. Numbers indicate FastTree consensus support. **(D)** Genetic distances of concatenated gene products of OMV depicted as circoletto diagrams. Proteins are oriented clockwise in N-HA-PB1-PB2-PA order when available. Sequence similarity is expressed as ribbons ranging from blue (low) to red (high). **(E)** Genomic architecture, predicted gene products and structural and functional domains of PpyrOLMV1 & 2. **(F)** Virus genomic noncoding termini analyses of PpyrOLMV1 & 2 in the context of ICTV OMV. The 3' and 5' end, A and U rich respectively, partially complementary sequences are associated to tentative panhandle polymerase binding and replication activity, typical of OMV. **(G)** 3D renders of the heterotrimeric polymerase of PpyrOLMV1 based on Swiss-Expsy generated models using as template the Influenza A virus polymerase structure. Structure comparisons were made with the MatchAlign tool of the Chimera suite, and solved in PyMOL. **(H)** Conserved functional motifs of PpyrOLMV1 & 2 PB1 and related viruses. Motif I-III are essential for replicate activity of viral polymerase. **(I)** Dynamic and prevalent virus derived RNA levels of the corresponding PpyrOLMV1 & 2 genome segments, determined in 24 RNA libraries of diverse individuals/developmental stages/tissues and geographic origins. RNA levels are expressed as normalized TPM, heatmaps were generated by Shinyheatmap. Values range from low (green) to high (red). **(J)** Firefly EVEs (FEVEs) identified in the *P. pyralis* genome assembly mapped to the corresponding pseudo-molecules. A 15 Kbp region flanking nucleoprotein like FEVES are depicted, enriched in transposable elements. Representative products of a putative PB2 FEVE are aligned to the corresponding protein of PpyrOLMV 2.



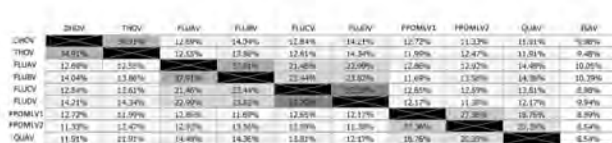
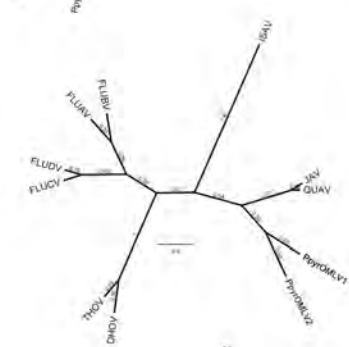
Nucleoprotein



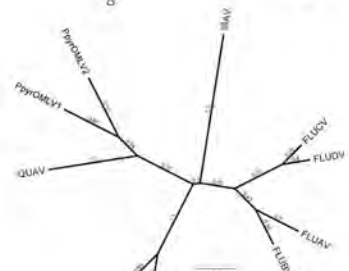
Hemagglutinin



PB1
Polymerase



PB2
Polymerase



PA
Polymerase

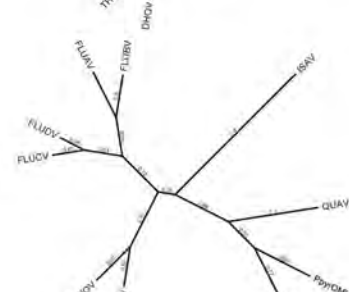


Figure S5.4.2: Pairwise identity of OMLV viral proteins amongst identified OMLV viruses.

Table S5.4.3: Best hits from BLASTP of PpyrOMLV proteins against the NCBI database

Genome Segment	Size (nt)	Gene product (aa)	Best hit	Best hit Taxonomy	Query cover	E value	Identity
PpyrOMLV1-PB1	251 0	801 PB1	Wuhan Mothfly Virus	Orthomyxoviridae	83%	0.0	51%
PpyrOMLV1-PA	234 6	754 PA	Hubei earwig virus 1	Orthomyxoviridae	98%	4.00E-137	35%
PpyrOMLV1-HA	166 7	526 HA	Tjuloc virus	Orthomyxoviridae	91%	9.00E-25	25%
PpyrOMLV1-PB2	251 7	804 PB2	Hubei earwig virus 1	Orthomyxoviridae	91%	3.00E-118	31%
PpyrOMLV1-N	183 5	562 N	Hubei earwig virus 1	Orthomyxoviridae	93%	8.00E-74	30%
PpyrOMLV2-PB1	249 5	802 PB1	Hubei orthomyxo-like virus 1	Orthomyxoviridae	93%	0.0	48%
PpyrOMLV2-PA	234 9	762 PA	Hubei earwig virus 1	Orthomyxoviridae	98%	1.00E-107	31%
PpyrOMLV2-HA	166 8	525 HA	Wellfleet Bay virus	Orthomyxoviridae	82%	3.00E-40	26%
PpyrOMLV2-PB2	250 6	801 PB2	Hubei earwig virus 1	Orthomyxoviridae	96%	3.00E-86	27%
PpyrOMLV2-N	173 8	528 N	Hubei earwig virus 1	Orthomyxoviridae	95%	6.00E-82	32%

Table S5.4.4: InterProScan domain annotation of PpyrOMLV proteins

Genome product	Annotation	Start	End	Length	Database	Id	InterPro ID	InterPro name
PpyrOMLV1-PB1	Flu_PB1	48	752	705	PFAM	PF00602	IPR001407	RNA_pol_PB1_influenza
	RDRP_SSRNA	330	529	200				
PpyrOMLV2-PB1	Flu_PB1	54	766	713	PFAM	PF00602	IPR001407	RNA_pol_PB1_influenza
	RDRP_SSRNA	337	539	203				
PpyrOMLV1-PB2	Flu_PB2	13	421	409	PFAM	PF00604	IPR001591	RNA_pol_PB2_orthomyxovir
PpyrOMLV2-PB2	Flu_PB2	13	415	403	PFAM	PF00604	IPR001591	RNA_pol_PB2_orthomyxovir
PpyrOMLV1-HA	SignalP-noTM	1	19	19	SIGNALP_EUK	SignalP-noTM	IPR004955	Unintegrated
	Baculo_gp64	108	432	325				
PpyrOMLV2-HA	SignalP-noTM	1	21	21	SIGNALP_EUK	SignalP-noTM	IPR004955	Unintegrated
	Baculo_gp64	66	426	361				
PpyrOMLV1-PA	Flu_PA	663	736	74	PFAM	PF00603	IPR001009	RNA-dir_pol_influenzavirus
PpyrOMLV2-PA	Flu_PA	667	740	74	PFAM	PF00603	IPR001009	RNA-dir_pol_influenzavirus
PpyrOMLV1-PB1	flu NP-like	94	459	366	SUPERFAMILY	SSF161003		Unintegrated
PpyrOMLV2-PB1	flu NP-like	363	483	121	SUPERFAMILY	SSF161003		Unintegrated

Table S5.4.5: Reads mapped to PpyrOMLV genome segments in available SRA and newly described *P. pyralis* RNA-Seq datasets

	SRR 3883773	SRR 3883772	SRR 3883758	SRR 3883771	SRR 3883770	SRR 3883769	SRR 3883768	SRR 3883767	SRR 3883765	SRR 3883764	SRR 3883763	SRR 3883762
Ppyr OMLV 1 HA	11	541	2	160	0	4	881	2	0	2	199	2848
Ppyr OMLV 1 NP	0	321	0	141	0	0	523	0	0	0	120	1460
Ppyr OMLV 1 PA	3	256	0	95	0	0	306	1	0	5	100	660
Ppyr OMLV 1 PB1	2	364	2	208	0	4	820	0	0	0	669	1464
Ppyr OMLV 1 PB2	5	194	0	152	2	0	319	2	0	0	106	696
Ppyr OMLV 2 HA	12	444	266	124	54	247	549	38	22	10	232	710
Ppyr OMLV 2 NP	29	526	275	144	66	299	653	24	205	57	274	1067
Ppyr OMLV 2 PA	12	88	216	72	40	204	97	18	15	8	50	838
Ppyr OMLV 2 PB1	9	115	75	72	26	78	76	8	74	57	146	493
Ppyr OMLV 2 PB2	5	50	57	67	47	131	110	22	85	72	173	728

	SRR 3883761	SRR 3883760	SRR 3883759	SRR 3883757	SRR 3883756	SRR 3883766	SRR 2103867	SRR 2103849	SRR 2103848	Ppyr_larvae	Ppyr_Female	Ppyr_eggs
Ppyr OMLV 1 HA	0	578	2	6	867	0	0	0	0	1664	7826	15586
Ppyr OMLV 1 NP	0	289	0	3	647	0	2	0	0	644	5216	6562
Ppyr OMLV 1 PA	0	124	0	2	626	0	0	0	0	1264	3692	9564
Ppyr OMLV 1 PB1	2	460	0	3	1607	2	0	0	0	2824	7144	15952

Ppyr OMLV 1 PB2	0	188	0	2	848	0	0	0	0	648	2562	10568
Ppyr OMLV 2 HA	13	236	23	546	337	286	43	190	415	0	0	0
Ppyr OMLV 2 NP	32	248	22	501	482	196	51	127	432	0	0	0
Ppyr OMLV 2 PA	14	93	6	234	222	131	75	54	97	0	0	0
Ppyr OMLV 2 PB1	29	90	4	168	180	63	22	96	190	0	0	0
Ppyr OMLV 2 PB2	49	90	6	256	230	94	22	57	96	0	0	0

Table S5.4.6: Reads mapped to PpyrOMLV genome segments in with FPKM values in available SRA and newly described *P. pyralis* RNA-Seq datasets

	SRR 3883773	SRR 3883772	SRR 3883758	SRR 3883771	SRR 3883770	SRR 3883769	SRR 3883768	SRR 3883767	SRR 3883765	SRR 3883764	SRR 3883763	SRR 3883762
Ppyr OMLV1 HA	19.10	0.32	0.05	6.46	0.00	0.11	30.69	0.05	0.00	0.08	4.07	69.54
Ppyr OMLV1 NP	10.37	0.00	0.00	5.21	0.00	0.00	16.66	0.00	0.00	0.00	2.24	32.61
Ppyr OMLV1 PA	6.46	0.06	0.00	2.74	0.00	0.00	7.62	0.02	0.00	0.13	1.46	11.52
Ppyr OMLV1 PB1	8.53	0.04	0.04	5.57	0.00	0.07	18.95	0.00	0.00	0.00	9.07	23.72
Ppyr OMLV1 PB2	4.50	0.10	0.00	4.03	0.05	0.00	7.29	0.03	0.00	0.00	1.42	11.16
Ppyr OMLV2 HA	16.13	0.36	7.41	5.15	2.31	6.80	19.68	0.90	1.05	0.39	4.88	17.84
Ppyr OMLV2 NP	17.36	0.79	6.96	5.44	2.57	7.48	21.27	0.52	8.87	2.01	5.24	24.36
Ppyr OMLV2 PA	2.21	0.25	4.17	2.07	1.19	3.89	2.41	0.30	0.49	0.21	0.73	14.58
Ppyr OMLV2 PB1	2.73	0.18	1.37	1.95	0.73	1.40	1.78	0.12	2.30	1.44	2.01	8.10

Ppyr OMLV2 PB2	SRR 3883761	SRR 3883760	SRR 3883759	SRR 3883757	SRR 3883756	SRR 3883766	SRR 2103867	SRR 2103849	SRR 2103848	Ppyr_lar vae	Ppyr_Fe male	Ppyr_eg gs
Ppyr OMLV 1 HA	0.00	18.29	0.08	0.21	23.44	0.00	0.00	0.00	0.00	15.89	74.25	104.49
Ppyr OMLV 1 NP	0.00	8.37	0.00	0.09	16.00	0.00	0.04	0.00	0.00	5.62	45.27	40.24
Ppyr OMLV 1 PA	0.00	2.81	0.00	0.05	12.10	0.00	0.00	0.00	0.00	8.63	25.05	45.85
Ppyr OMLV 1 PB1	0.04	9.66	0.00	0.07	28.83	0.04	0.00	0.00	0.00	17.89	44.97	70.96
Ppyr OMLV 1 PB2	0.00	3.91	0.00	0.05	15.05	0.00	0.00	0.00	0.00	4.06	15.96	46.51
Ppyr OMLV 2 HA	0.43	7.68	0.95	19.30	9.38	9.74	1.02	4.94	8.95	0.00	0.00	0.00
Ppyr OMLV 2 NP	0.97	7.34	0.82	16.09	12.19	6.07	1.10	3.00	8.47	0.00	0.00	0.00
Ppyr OMLV 2 PA	0.32	2.10	0.17	5.73	4.28	3.09	1.23	0.97	1.45	0.00	0.00	0.00
Ppyr OMLV 2 PB1	0.63	1.92	0.11	3.88	3.27	1.40	0.34	1.63	2.68	0.00	0.00	0.00
Ppyr OMLV 2 PB2	1.06	1.90	0.16	5.88	4.16	2.08	0.34	0.96	1.35	0.00	0.00	0.00

5.5 *P. pyralis* Endogenous virus-like Elements (EVEs)

To gain insights on the potential shared evolutionary history of *P. pyralis* and the IOMV PpyrOMLV1 & 2, we examined our assembly of *P. pyralis* for putative signatures or paleovirological traces (277–279) that would indicate ancestral integration of virus related sequences into the firefly host. Remarkably, we found Endogenous virus-like Elements (EVEs) (280), sharing significant sequence identity with most PpyrOMLV1 & 2 genome segments, spread along four *P. pyralis* linkage-groups. Virus integration into host genomes is a frequent event derived from reverse transcribing RNA viruses (*Retroviridae*). Retroviruses are the only

animal viruses that depend on integration into the genome of the host cell as an obligate step in their replication strategy (281). Viral infection of germ line cells may lead to viral gene fragments or genomes becoming integrated into host chromosomes and subsequently inherited as host genes.

Animal genomes are paved by retrovirus insertions (282). These insertions, which are eventually eliminated from the host gene pool within a few generations, and may, in some cases, increase in frequency, and ultimately reach fixation. This fixation in the host species can be mediated by drift or positive selection, depending on their selective value. On the other hand, genomic integration of non-retroviral viruses, such as PpyrOMLV1 & 2, is less common. Viruses with a life cycle characterized by no DNA stage, such as OMV, do not encode a reverse transcriptase or integrase, thus are not retro transcribed nor integrated into the host genome. However, exceptionally and recently, several non-retroviral sequences have been identified on animal genomes; these insertions have been usually associated with the transposable elements machinery of the host, which provided a means to genome integration (283, 284). Interestingly, when we screened our *P. pyralis* genome assembly Ppyr1.2 by BLASTX searches (E-value <1e⁻⁶) of PpyrOMLV1 & 2 genome segments, we identified several genome regions that could be defined as Firefly EVEs, which we termed FEVEs (Fig. S5.1 J; Table S5.5.1-5.5.5). We found 30 OMV related FEVEs, which were mostly found in linkage group one (LG1, 83 % of pinpointed FEVEs). The majority of the detected FEVEs shared sequence identity to the PB1 encoding region of genome segment one of PpyrOMLV1 & 2 (ca. 46 % of FEVEs), followed by N encoding genome segment five (ca. 33 % of detected FEVEs). In addition we identified four FEVEs related to genome segment three (PA region) and two FEVEs associated to genome segment two (PB2 encoding region). We found no evidence of FEVEs related to the hemagglutinin coding genome segment four (HA). The detected *P. pyralis* FEVEs represented truncated fragments of virus like sequences, generally presenting frameshift mutations, early termination codons, lacking start codons, and sharing diverse mutations that altered the potential translation of eventual gene products. FEVEs shared sequence similarity to the coding sequence of specific genome segments of the cognate FOLMV. We generated best/longest translation products of the corresponding FEVEs, which presented an average length of ca. 21.86 % of the corresponding PpyrOMLV genome segment encoding gene region (Table S5.5.1-5.5.5), and an average pairwise identity to the FOLMV virus protein of 55.08 %. Nevertheless, we were able to identify FEVEs that covered as high as ca. 60 % of the corresponding gene product, and in addition, although at specific short protein regions of the putative related FOLMV, similarity values were as high as 89 % pairwise identity. In addition, most of the detected FEVEs were flanked by Transposable Elements (TE) (Figure S5.4.1 J) suggesting that integration followed ectopic recombination between viral RNA and transposons. We found several conserved domains associated to reverse transcriptases and integrases adjacent to the corresponding FEVEs, which supports the hypothesis that these virus-like elements could be reminiscent of an OMV-like ancestral virus that could have been integrated into the genome by occasional sequestering of viral RNAs by the TE machinery. The finding of EVEs in the *P. pyralis* genome is not trivial, OMV EVEs are extremely rare. There has been only

one report of OMV like sequences integrated into animal host genomes, which is the case of *Ixodes scapularis*, the putative vector of *Quaranfil virus* and *Johnston Atoll virus* corresponding to genus *Quaranjavirus* (280). The fact that besides FEVEs, the only other OMV EVE corresponded to an Arthropod genome, given the ample studies of bird and mammal genomes, is suggestive that perhaps OMV EVEs are restricted to Arthropod hosts. Sequence similarity of FEVEs and firefly viruses suggest that these viral ‘molecular fossils’ could have been tightly associated to PpyrOLMV1 & 2 ancestors. Moreover, we found potential NP and PB1 EVEs in our genome of light emitting click beetle *Ignelater luminosus* (*Elateridae*), an evolutionary distant coleoptera. Sequence similarity levels of the corresponding EVEs averaging 52 %, could not be related with evolutionary distances of the hosts. We were not able to generate conclusive phylogenetic insights of the detected EVEs, given their partial, truncated and altered nature of the virus like sequences. In specific cases such as PB1-like EVEs there appears to be a trend suggesting an indirect relation between sequence identity and evolutionary status of the firefly host, but this preceding findings should be taken cautiously until more gathered data is available. The widespread presence of DNA sequences significantly similar to OMV in the explored firefly and related genomes are an interesting and intriguing result. At this stage is prudently not to venture to suggest more likely one of the two plausible explanations of the presence of these sequences in related beetles genomes: (i) Ancestral OMV like virus sequences were retrotranscribed and incorporated to an ancient beetle, followed by speciation and eventual stabilization or lost of EVEs in diverse species. (ii) Recent and recursive integration of OMV like virus sequences in fireflies and horizontal transmission between hosts. These propositions are not mutually exclusive, and may be indistinctly applied to specific cases. Future studies should enquire in this genome dark matter to better understand this interesting phenomenon. When more data is available EVE sequences may be combined with phylogenetic data of host species to expose eventual patterns of inter-class virus transmission. Either way, more studies are needed to explore these proposals, Katzourakis & Gifford (280) suggested that EVEs could reveal novel virus diversity and indicate the likely host range of virus clades.

After identification and confirmation that firefly related EVEs are present in the host DNA genome, an obvious question follows: Are these EVEs just signatures of an evolutionary vestige of stochastic past infections; or could they be associated with an intrinsic function? It has been suggested that intensity and prevalence of infection may be a determinant of EVEs integration, and that exposure to environmental viruses may not (285). Previous reports have suggested that EVEs may firstly function as restriction factors in their hosts by conferring resistance to infection by exogenous viruses, and the eventual counter-adaptation of virus populations of EVE positive hosts, could reduce the EVE restriction mechanism to a non-functional status (286). Recently, in mosquitoes, a new mechanism of antiviral immunity against RNA viruses has been proposed, relying in the production and expression of EVEs DNA (287). Alternatively, eventual EVE expression could lend to the production viral like truncated proteins that may compete in trans with virus proteins from infecting viruses and limit viral replication, transcription or virion assembly (288). In addition, integration and eventual modulation in the host genome may be associated with an interaction between viral RNA and the mosquito RNAi machinery (289). The

piRNA pathway mediates through small RNAs and Piwi-Argonaut proteins the repression of TE derived nucleic acids based on sequence complementarity, and has also been associated to regulation of arbovirus viral related RNA, suggesting a functional connection among resistance mechanisms against RNA viruses and TEs (284, 290). Furthermore, arbovirus EVEs have been linked to the production of viral derived piRNAs and virus-specific siRNA, inducing host cell immunity without limiting viral replication, supporting persistent and chronic infection (287). Perhaps an EVE dependent mechanism of modulation of virus infection could have some level of reminiscence to the paradigmatic CRISPR/Cas system which mediates bacteriophage resistance in prokaryotic hosts.

In sum, genomic studies are a great resource for the understanding of virus and host evolution. Here we glimpsed an unexpected hidden evolutionary tale of firefly viruses and related FEVEs. Animal genomes appear to reflect as a book, with many dispersed sentences, an antique history of ancestral interaction with microbes, and EVEs functioning as virus related bookmarks. The exponential growth of genomic data would help to further understand this complex and intriguing interface, in order to advance not only in the apprehension of the phylogenomic insights of the host, but also explore a multifaceted and dynamic virome that has accompanied and even might have shifted the evolution of the host.

Table S5.5.1: FEVE hits from BLASTX of PpyrOMLV PB1

Scaffold	Start	End	Strand	id with PpOMLV	E value	Coverage	FEVE
Ppyr1.2_LG1	12787323	12786796	(-)	56.30%	8.22E-50	39.10%	EVE PB1 like-1
Ppyr1.2_LG1	13016647	13016120	(-)	56.30%	8.22E-50	39.10%	EVE PB1 like-2
Ppyr1.2_LG1	34701480	34701560	(+)	37.00%	2.88E-26	26.70%	EVE PB1 like-3
Ppyr1.2_LG1	34701562	34701774	(+)	37.60%	2.88E-26	30.20%	EVE PB1 like-3
Ppyr1.2_LG1	34701801	34702214	(+)	45.30%	2.88E-26	34.00%	EVE PB1 like-3
Ppyr1.2_LG1	35094645	35095094	(+)	28.10%	2.15E-10	9.50%	EVE PB1 like-4
Ppyr1.2_LG1	35110084	35109956	(-)	53.50%	2.37E-14	4.40%	EVE PB1 like-5
Ppyr1.2_LG1	35110214	35110107	(-)	75.00%	2.37E-14	14.70%	EVE PB1 like-5

Ppyr1.2_LG1	35110347	35110213	(-)	42.60%	2.37E-14	2.90%	EVE PB1 like-5
Ppyr1.2_LG1	50031464	50031330	(-)	64.40%	1.18E-09	10.00%	EVE PB1 like-6
Ppyr1.2_LG1	50031498	50031457	(-)	71.40%	1.18E-09	11.60%	EVE PB1 like-6
Ppyr1.2_LG1	50613130	50612921	(+)	49.40%	3.71E-11	4.90%	EVE PB1 like-7
Ppyr1.2_LG1	50673211	50673621	(+)	38.50%	1.03E-12	9.70%	EVE PB1 like-8
Ppyr1.2_LG1	51208464	51207634	(-)	77.20%	0	56.40%	EVE PB1 like-9
Ppyr1.2_LG1	51209399	51208467	(-)	68.50%	0	53.60%	EVE PB1 like-9
Ppyr1.2_LG1	51209556	51209398	(-)	71.70%	0	39.20%	EVE PB1 like-9
Ppyr1.2_LG1	61871682	61872158	(+)	31.10%	2.84E-23	36.00%	EVE PB1 like-10
Ppyr1.2_LG1	61872158	61872319	(+)	46.30%	2.84E-23	28.30%	EVE PB1 like-10
Ppyr1.2_LG1	61872355	61872456	(+)	41.20%	2.84E-23	27.00%	EVE PB1 like-10
Ppyr1.2_LG1	61930528	61930205	(-)	38.00%	3.58E-27	30.90%	EVE PB1 like-11
Ppyr1.2_LG1	61930686	61930504	(-)	63.60%	3.58E-27	35.90%	EVE PB1 like-11
Ppyr1.2_LG1	68038999	68039073	(+)	60.00%	7.73E-12	6.60%	EVE PB1 like-12
Ppyr1.2_LG1	68039072	68039314	(+)	40.70%	7.73E-12	5.00%	EVE PB1 like-12
Ppyr1.2_LG1	68039289	68039330	(+)	64.30%	7.73E-12	8.00%	EVE PB1 like-12
Ppyr1.2_LG1	68128820	68129008	(+)	51.50%	1.89E-06	4.90%	EVE PB1 like-13
Ppyr1.2_LG2	34545814	34545680	(-)	58.70%	3.84E-06	7.20%	EVE PB1 like-14

Ppyr1.2_LG2 34546169 34545801 (-) 52.80% 1.16E-31 34.10% EVE PB1 like-14

Table S5.5.2: FEVE hits from BLASTX of PpyrOMLV PB2

Scaffold	Start	End	Strand	id with PpOMLV	E value	Coverage	FEVE
Ppyr1.2_LG1	50313869	50314219	(+)	82.10%	6.91E-54	48.30%	EVE PB2 like-1
Ppyr1.2_LG1	50314216	50315016	(+)	82.40%	1.92E-142	57.90%	EVE PB2 like-1
Ppyr1.2_LG1	50315772	50315002	(-)	89.10%	9.97E-145	60.60%	EVE PB2 like-1
Ppyr1.2_LG1	58707403	58706942	(-)	52.60%	6.19E-42	35.80%	EVE PB2 like-2

Table S5.5.3: FEVE hits from BLASTX of PpyrOMLV PA

Scaffold	Start	End	Strand	id with PpOMLV	E value	Coverage	FEVE
Ppyr1.2_LG1	34977392	34977231	(-)	48.10%	7.73E-07	3.50%	EVE PA like-1
Ppyr1.2_LG1	62052289	62052023	(-)	28.70%	8.92E-11	7.10%	EVE PA like-2
Ppyr1.2_LG1	62117077	62116811	(-)	28.70%	1.22E-10	7.10%	EVE PA like-3
Ppyr1.2_LG1	62117493	62117101	(-)	26.30%	1.22E-10	8.60%	EVE PA like-3
Ppyr1.2_LG1	68122348	68122440	(+)	77.40%	3.40E-06	15.70%	EVE PA like-4

Table S5.5.4: FEVE hits from BLASTX of PpyrOMLV HA
(None detected)

Table S5.5.5: FEVE hits from BLASTX of PpyrOMLV NP

Scaffold	Start	End	Strand	id with PpOML V	E value	Coverage	FEVE
Ppyr1.2_LG1	181303	181404	(+)	79.40%	7.01E-09	17.90%	EVE NP like-1
Ppyr1.2_LG1	1029425	1029568	(+)	93.80%	9.59E-21	27.40%	EVE NP like-2
Ppyr1.2_LG1	2027860	2027438	(-)	35.50%	3.00E-21	30.80%	EVE NP like-3
Ppyr1.2_LG1	36568324	36568551	(+)	42.10%	8.99E-11	7.20%	EVE NP like-4
Ppyr1.2_LG1	52877256	52877086	(-)	68.40%	3.87E-15	14.60%	EVE NP like-5
Ppyr1.2_LG1	59927414	59927271	(+)	93.80%	5.60E-20	26.40%	EVE NP like-6
Ppyr1.2_LG3	17204346	17204122	(-)	46.70%	7.60E-13	7.10%	EVE NP like-7
Ppyr1.2_LG3	31635344	31635030	(-)	35.80%	3.30E-08	10.00%	EVE NP like-8
Ppyr1.2_LG3	50175821	50175922	(+)	79.40%	7.01E-09	17.90%	EVE NP like-9
Ppyr1.2_LG4	27811681	27811758	(+)	38.50%	3.22E-13	2.50%	EVE NP like-10
Ppyr1.2_LG4	27811853	27812179	(+)	39.00%	3.22E-13	10.90%	EVE NP like-10

Table S6: Experiment.com donors

Liliana Bachrach	Doug Fambrough	Benjamin Lower	Luis Cunha	Joshua Guerriero
Atsuko Fish	Tom Alar	Noreen Huefner	David Esopi	John Skarha
Rutong Xie	Richard Hall	Zachary Michel	Jack Hynes	Keith Guerin
Nathan Shaner	Joe Doggett	Joe T. Bamberg	Michael McGurk	Pureum Kim
Sara Lewis	Mark Lewis	Lauren Solomon	Peter Berx	Milo Grika
Jing-Ke Weng	Sarah Sander	Dr. Husni Elbahesh	Matt Grommes	Daniel Zinshteyn
Peter Rodenbeck	Daniel Bear	Kathryn Larracuente	Colette Dedyn	Tom Brekke
Larry Fish	Don Salvatore	Matthew Cichocki	Florencia Schlamp	Edoardo Gianni
Amanda Larracuente	Emily Davenport	Marcel Bruchez	Marie Lower	Cindy Wu
Hunter Lower	Ted Sharpe	Robert Unckless	Michael R. McKain	Christina Tran
Allan Kleinman	David Plunkett	Arvid Ågren	Ben Pfeiffer	Eric Damon Walters
Misha Koksharov	Tim Fallon	Margaret S Butler	Kathryn Keho	Geoffrey Giller
Sarah Shekher	Edward Garrity	Yasir Ahmed-Braimah	Jenny Wayfarer	Fahd Butt
Jared Lee	Huaping Mo	Ruth Ann Grissom	Darby Thomas	Christophe Mandy
Raphael De Cock	TimG	Tomáš Pluskal	Emily Hatas	
Linds Fallon	Jan Thys	Genome Galaxy	Richard Casey	
Grace Li	Francisco Martinez Gasco	Dustin Greiner	William Nicholls	

SUPPLEMENTARY TEXT 7: Data availability

Files on FigShare:

- (1) *Photinus pyralis* sighting records (Excel spreadsheet)
- (2) Ppyr1.2 Blobtools results
- (3) Alat1.2 Blobtools results
- (4) Ilumi1.0 Blobtools results
- (5) Nucleotide multiple sequence alignment for Elaterid luciferase homolog branch selection test (Supplementary Text 4.3)
- (6) Protein multiple sequence alignment for P450 tree - Figure S1.10.1.1
- (7) Table S1 - Genomic sequencing library statistics
- (8) *Photinus pyralis* orthomyxo-like virus 1 sequence and annotation
- (9) *Photinus pyralis* orthomyxo-like virus 2 sequence and annotation
- (10) Orthofinder protein clustering analysis
- (11) PPYR_OGS1.0 Kallisto RNA-Seq expression quantification (TPM)
- (12) Alat_OGS1.0 Kallisto RNA-Seq expression quantification (TPM)
- (13) Fig 4e. PPYR_OGS1.0 Sleuth / differential expression Venn diagram analysis (BSN-TPM)
- (14) Fig 4e. Alat_OGS1.0 Sleuth / differential expression Venn diagram analysis (BSN-TPM)
- (15) ILUMI_OGS1.0 Kallisto RNA-Seq expression quantification (TPM)
- (16) Video S1: A *Photinus pyralis* courtship dialogue
- (17) Figure 4C. CYP303 maximum likelihood gene tree
- (18) Figure S4.5.1A Opsin gene tree
- (19) Figure 3C Maximum likelihood tree of luciferase homologs.

Files on www.firebaseio.org:

- (1) *P. pyralis/A. lateralis/I. luminosus* geneset GFF files
- (2) *P. pyralis/A. lateralis/I. luminosus* mRNA nucleotide FASTA files

Tracks on www.firebaseio.org JBrowse genome browser:

For each genome:

- (1) Gaps
- (2) Repeats
- (3) Direct gene-models (Stringtie)
- (4) Direct gene-models (Trinity)
- (5) Official geneset gene-models (OGS1.0)

Bibliography

1. J. E. Lloyd, Studies on the flash communication system in *Photinus* fireflies (1966) (available at <https://deepblue.lib.umich.edu/bitstream/handle/2027.42/56374/MP130.pdf?sequence=1&isAllowed=y>).
2. J. E. Lloyd, in *Encyclopedia of Entomology*, J. L. Capinera, Ed. (Springer Netherlands, Dordrecht, 2008), pp. 1429–1452.
3. J. R. de Wet, K. V. Wood, D. R. Helinski, M. DeLuca, Cloning of firefly luciferase cDNA and the expression of active luciferase in *Escherichia coli*. *Proc. Natl. Acad. Sci. U. S. A.* **82**, 7870–7873 (1985).
4. J. F. Case, Flight studies on photic communication by the firefly *Photinus pyralis*. *Integr. Comp. Biol.* **44**, 250–258 (2004).
5. E. D. van der Reijden, J. D. Monchamp, S. M. Lewis, The formation, transfer, and fate of spermatophores in *Photinus* fireflies (Coleoptera: Lampyridae). *Can. J. Zool.* **75**, 1202–1207 (1997).
6. N. Al-Wathiqui, T. R. Fallon, A. South, J.-K. Weng, S. M. Lewis, Molecular characterization of firefly nuptial gifts: a multi-omics approach sheds light on postcopulatory sexual selection. *Sci. Rep.* **6**, 38556 (2016).
7. C. K. Cratsley, J. A. Rooney, S. M. Lewis, Limits to Nuptial Gift Production by Male Fireflies, *Photinus ignitus*. *J. Insect Behav.* **16**, 361–370 (2003).
8. J. Rooney, S. M. Lewis, Fitness advantage from nuptial gifts in female fireflies. *Ecol. Entomol.* **27**, 373–377 (2002).
9. L. Faust, H. Faust, The Occurrence and Behaviors of North American Fireflies (Coleoptera: Lampyridae) on Milkweed, *Asclepias syriaca* L. *Coleopt. Bull.* **68**, 283–291 (2014).
10. W. N. Hess, Notes on the biology of some common Lampyridae. *Biol. Bull.* **38**, 39–76 (1920).
11. L. F. Faust, *Fireflies, Glow-worms, and Lightning Bugs: Identification and Natural History of the Fireflies of the Eastern and Central United States and Canada* (University of Georgia Press, 2017).
12. J. Meinwald, D. F. Wiemer, T. Eisner, Lucibufagins. 2. Esters of 12-oxo-2. β ,5. β ,11. α -trihydroxybufalin, the major defensive steroids of the firefly *Photinus pyralis* (Coleoptera: Lampyridae). *J. Am. Chem. Soc.* **101**, 3055–3060 (1979).
13. M. A. Goetz, J. Meinwald, T. Eisner, Lucibufagins, IV. New defensive steroids and a pterin from the firefly, *Photinus pyralis* (coleoptera: Lampyridae). *Experientia*. **37**, 679–680 (1981).
14. M. S. Blum, A. Sannasi, Reflex bleeding in the lampyrid *Photinus pyralis*: Defensive function. *J. Insect Physiol.* **20**, 451–460 (1974).

15. L. Faust, R. De Cock, S. Lewis, Thieves in the Night: Kleptoparasitism by Fireflies in the Genus *Photuris* Dejean (Coleoptera: Lampyridae). *Coleopt. Bull.* **66**, 1–6 (2012).
16. S. P. L. Luk, S. A. Marshall, M. A. Branham, The fireflies of Ontario (Coleoptera: Lampyridae). *Can. J. Arthropod Identif.* **16**, 1–105 (2011).
17. Common Eastern Firefly (*Photinus pyralis*). *iNaturalist*, (available at <https://www.inaturalist.org/taxa/129350-Photinus-pyralis>).
18. O. S. G. Foundation, *QGIS Geographic Information System* (2017; <http://qgis.osgeo.org>).
19. T. R. Fallon, *Ppyralis_QGIS_sighting_to_centroided_county.py*, (available at https://github.com/photocyte/2017_misc_scripts/blob/master/Ppyralis_QGIS_sighting_to_ce ntroided_county.py).
20. United States Census Bureau, Cartographic Boundary Shapefiles - Counties, (available at https://www.census.gov/geo/maps-data/data/cbf/cbf_counties.html).
21. D. M. Olson *et al.*, Terrestrial Ecoregions of the World: A New Map of Life on Earth: A new global map of terrestrial ecoregions provides an innovative tool for conserving biodiversity. *Bioscience*. **51**, 933–938 (2001).
22. W. W. Fund, Terrestrial Ecoregions of the World, (available at <https://www.worldwildlife.org/publications/terrestrial-ecoregions-of-the-world>).
23. J. W. Green, Revision of the nearctic species of *Photinus* (Coleoptera: Lampyridae). *Proc. Calif. Acad. Sci.* **28**, 561–613 (1956).
24. K. F. Stanger-Hall, J. E. Lloyd, Flash signal evolution in *Photinus* fireflies: character displacement and signal exploitation in a visual communication system. *Evolution*. **69**, 666–682 (2015).
25. J.-Z. Ho, P.-H. Chiang, C.-H. Wu, P.-S. Yang, Life cycle of the aquatic firefly *Luciola picta* (Coleoptera: Lampyridae). *J. Asia. Pac. Entomol.* **13**, 189–196 (2010).
26. J. Lloyd, Where can I find information on raising fireflies? *Fireflyer Companion*. **1** (1996), p. 20.
27. M. McLean, J. Buck, F. E. Hanson, Culture and Larval Behavior of Photurid Fireflies. *Am. Midl. Nat.* **87**, 133–145 (1972).
28. L. L. Buschman, Larval Development and Its Photoperiodic Control in the Firefly *Pyractomena lucifera* (Coleoptera: Lampyridae). *Ann. Entomol. Soc. Am.* **81**, 82–90 (1988).
29. E. N. Harvey, *Bioluminescence* (Academic Press, 1952).
30. F. X. Williams, Notes on the life-history of some North American Lampyridae. *J. N. Y. Entomol. Soc.* **25**, 11–33 (1917).
31. M. Wasserman, L. Ehrman, Firefly Chromosomes, II. (Lampyridae: Coleoptera). *Fla. Entomol.* **69**, 755–757 (1986).
32. S. S. Lower *et al.*, Genome Size in North American Fireflies: Substantial Variation Likely

- Driven by Neutral Processes. *Genome Biol. Evol.* **9**, 1499–1512 (2017).
33. C. M. Dias, M. C. Schneider, S. P. Rosa, C. Costa, D. M. Celli, The first cytogenetic report of fireflies (Coleoptera, Lampyridae) from Brazilian fauna. *Acta Zool.* **88**, 309–316 (2007).
 34. P. Biosciences, SMRT Analysis Software, (available at <http://www.pacb.com/products-and-services/analytical-software/smrt-analysis/>).
 35. E. Lieberman-Aiden *et al.*, Comprehensive mapping of long-range interactions reveals folding principles of the human genome. *Science*. **326**, 289–293 (2009).
 36. J. N. Burton *et al.*, Chromosome-scale scaffolding of de novo genome assemblies based on chromatin interactions. *Nat. Biotechnol.* **31**, 1119–1125 (2013).
 37. D. M. Bickhart *et al.*, Single-molecule sequencing and chromatin conformation capture enable de novo reference assembly of the domestic goat genome. *Nat. Genet.* **49**, 643–650 (2017).
 38. A. V. Zimin *et al.*, The MaSuRCA genome assembler. *Bioinformatics*. **29**, 2669–2677 (2013).
 39. A. V. Zimin *et al.*, Hybrid assembly of the large and highly repetitive genome of *Aegilops tauschii*, a progenitor of bread wheat, with the MaSuRCA mega-reads algorithm. *Genome Res.* **27**, 787–792 (2017).
 40. A. V. Zimin *et al.*, The MaSuRCA genome assembler. *Bioinformatics*. **29**, 2669–2677 (2013).
 41. A. V. Zimin *et al.*, Hybrid assembly of the large and highly repetitive genome of *Aegilops tauschii*, a progenitor of bread wheat, with the MaSuRCA mega-reads algorithm. *Genome Res.* **27**, 787–792 (2017).
 42. J. O'Connell *et al.*, NxTrim: optimized trimming of Illumina mate pair reads. *Bioinformatics*. **31**, 2035–2037 (2015).
 43. L. P. Prysycz, T. Gabaldón, Redundans: an assembly pipeline for highly heterozygous genomes. *Nucleic Acids Res.* **44**, e113 (2016).
 44. A. C. English *et al.*, Mind the gap: upgrading genomes with Pacific Biosciences RS long-read sequencing technology. *PLoS One*. **7**, e47768 (2012).
 45. H. Li, R. Durbin, Fast and accurate short read alignment with Burrows-Wheeler transform. *Bioinformatics*. **25**, 1754–1760 (2009).
 46. N. C. Durand *et al.*, Juicer Provides a One-Click System for Analyzing Loop-Resolution Hi-C Experiments. *Cell Syst.* **3**, 95–98 (2016).
 47. N. C. Durand *et al.*, Juicebox Provides a Visualization System for Hi-C Contact Maps with Unlimited Zoom. *Cell Syst.* **3**, 99–101 (2016).
 48. B. Langmead, S. L. Salzberg, Fast gapped-read alignment with Bowtie 2. *Nat. Methods*. **9**, 357–359 (2012).

49. K. Okonechnikov, A. Conesa, F. García-Alcalde, Qualimap 2: advanced multi-sample quality control for high-throughput sequencing data. *Bioinformatics*. **32**, 292–294 (2016).
50. C. Camacho *et al.*, BLAST+: architecture and applications. *BMC Bioinformatics*. **10**, 421 (2009).
51. G. S. C. Slater, E. Birney, Automated generation of heuristics for biological sequence comparison. *BMC Bioinformatics*. **6**, 31 (2005).
52. G. Koutsovoulos *et al.*, No evidence for extensive horizontal gene transfer in the genome of the tardigrade *Hypsibius dujardini*. *Proc. Natl. Acad. Sci. U. S. A.* **113**, 5053–5058 (2016).
53. D. R. Laetsch, M. L. Blaxter, BlobTools: Interrogation of genome assemblies. *F1000Res.* **6** (2017), doi:10.12688/f1000research.12232.1.
54. B. Buchfink, C. Xie, D. H. Huson, Fast and sensitive protein alignment using DIAMOND. *Nat. Methods*. **12**, 59–60 (2015).
55. S. Koren *et al.*, Canu: scalable and accurate long-read assembly via adaptive k-mer weighting and repeat separation. *Genome Res.* **27**, 722–736 (2017).
56. J. S. Bae, I. Kim, H. D. Sohn, B. R. Jin, The mitochondrial genome of the firefly, *Pyrocoelia rufa*: complete DNA sequence, genome organization, and phylogenetic analysis with other insects. *Mol. Phylogenet. Evol.* **32**, 978–985 (2004).
57. S. Nurk *et al.*, in *Lecture Notes in Computer Science* (2013), pp. 158–170.
58. B. J. Walker *et al.*, Pilon: an integrated tool for comprehensive microbial variant detection and genome assembly improvement. *PLoS One*. **9**, e112963 (2014).
59. W. Shen, S. Le, Y. Li, F. Hu, SeqKit: A Cross-Platform and Ultrafast Toolkit for FASTA/Q File Manipulation. *PLoS One*. **11**, e0163962 (2016).
60. M. Bernt, A. Donath, F. Jühling, F. Externbrink, C. Florentz, G. Fritzsch, J. Pütz, M. Middendorf, P. F. Stadler, MITOS2 WebServer, (available at <http://mitos2.bioinf.uni-leipzig.de>).
61. M. Krzywinski *et al.*, Circos: an information aesthetic for comparative genomics. *Genome Res.* **19**, 1639–1645 (2009).
62. M. G. Grabherr *et al.*, Full-length transcriptome assembly from RNA-Seq data without a reference genome. *Nat. Biotechnol.* **29**, 644–652 (2011).
63. B. J. Haas *et al.*, Automated eukaryotic gene structure annotation using EVidenceModeler and the Program to Assemble Spliced Alignments. *Genome Biol.* **9**, R7 (2008).
64. W. J. Kent, BLAT--the BLAST-like alignment tool. *Genome Res.* **12**, 656–664 (2002).
65. T. D. Wu, C. K. Watanabe, GMAP: a genomic mapping and alignment program for mRNA and EST sequences. *Bioinformatics*. **21**, 1859–1875 (2005).
66. T. R. Fallon, PASA_expression_filter_2017.py, (available at https://github.com/photocyte/PASA_expression_filter_2017).

67. B. J. Haas, TransDecoder, (available at <https://github.com/TransDecoder/TransDecoder/wiki>).
68. D. Kim, B. Langmead, S. L. Salzberg, HISAT: a fast spliced aligner with low memory requirements. *Nat. Methods.* **12**, 357–360 (2015).
69. M. Pertea *et al.*, StringTie enables improved reconstruction of a transcriptome from RNA-seq reads. *Nat. Biotechnol.* **33**, 290–295 (2015).
70. N. L. Bray, H. Pimentel, P. Melsted, L. Pachter, Near-optimal probabilistic RNA-seq quantification. *Nat. Biotechnol.* **34**, 525–527 (2016).
71. H. Pimentel, N. L. Bray, S. Puente, P. Melsted, L. Pachter, Differential analysis of RNA-seq incorporating quantification uncertainty. *Nat. Methods.* **14**, 687–690 (2017).
72. T. R. Fallon, interproscan_to_enzyme_go.py, (available at https://github.com/photocyte/interproscan_to_enzyme_go/tree/master).
73. H. Tang *et al.*, GOATOOLS: tools for gene ontology. *Zenodo.* (2015).
74. M. Stanke, O. Schöffmann, B. Morgenstern, S. Waack, Gene prediction in eukaryotes with a generalized hidden Markov model that uses hints from external sources. *BMC Bioinformatics.* **7**, 62 (2006).
75. C. Holt, M. Yandell, MAKER2: an annotation pipeline and genome-database management tool for second-generation genome projects. *BMC Bioinformatics.* **12**, 491 (2011).
76. I. Korf, Gene finding in novel genomes. *BMC Bioinformatics.* **5**, 59 (2004).
77. MAKER Tutorial for GMOD Online Training 2014, (available at http://weatherby.genetics.utah.edu/MAKER/wiki/index.php/MAKER_Tutorial_for_GMOD_Online_Training_2014).
78. T. R. Fallon, maker_gff_to_evm_gff_2017.py, (available at https://github.com/photocyte/maker_gff_to_evm_gff_2017).
79. W. Li, A. Godzik, Cd-hit: a fast program for clustering and comparing large sets of protein or nucleotide sequences. *Bioinformatics.* **22**, 1658–1659 (2006).
80. K. F. Rewitz, M. B. O'Connor, L. I. Gilbert, Molecular evolution of the insect Halloween family of cytochrome P450s: phylogeny, gene organization and functional conservation. *Insect Biochem. Mol. Biol.* **37**, 741–753 (2007).
81. C. Helvig, J. F. Koener, G. C. Unnithan, R. Feyereisen, CYP15A1, the cytochrome P450 that catalyzes epoxidation of methyl farnesoate to juvenile hormone III in cockroach corpora allata. *Proc. Natl. Acad. Sci. U. S. A.* **101**, 4024–4029 (2004).
82. E. Guittard *et al.*, CYP18A1, a key enzyme of *Drosophila* steroid hormone inactivation, is essential for metamorphosis. *Dev. Biol.* **349**, 35–45 (2011).
83. H. Sezutsu, G. Le Goff, R. Feyereisen, Origins of P450 diversity. *Philos. Trans. R. Soc. Lond. B Biol. Sci.* **368**, 20120428 (2013).

84. Clustal Omega, (available at <https://www.ebi.ac.uk/Tools/msa/clustalo/>).
85. M. Zuker, Mfold web server for nucleic acid folding and hybridization prediction. *Nucleic Acids Res.* **31**, 3406–3415 (2003).
86. M. A. Larkin *et al.*, Clustal W and Clustal X version 2.0. *Bioinformatics*. **23**, 2947–2948 (2007).
87. D. L. Wheeler, Database resources of the National Center for Biotechnology. *Nucleic Acids Res.* **31**, 28–33 (2003).
88. A. Marchler-Bauer *et al.*, CDD/SPARCLE: functional classification of proteins via subfamily domain architectures. *Nucleic Acids Res.* **45**, D200–D203 (2017).
89. I. Letunic, P. Bork, 20 years of the SMART protein domain annotation resource. *Nucleic Acids Res.* (2017), doi:10.1093/nar/gkx922.
90. R. D. Finn *et al.*, The Pfam protein families database: towards a more sustainable future. *Nucleic Acids Res.* **44**, D279–85 (2016).
91. C. J. A. Sigrist *et al.*, PROSITE: a documented database using patterns and profiles as motif descriptors. *Brief. Bioinform.* **3**, 265–274 (2002).
92. P. Rice, I. Longden, A. Bleasby, EMBOSS: the European Molecular Biology Open Software Suite. *Trends Genet.* **16**, 276–277 (2000).
93. T. N. Petersen, S. Brunak, G. von Heijne, H. Nielsen, SignalP 4.0: discriminating signal peptides from transmembrane regions. *Nat. Methods*. **8**, 785–786 (2011).
94. L. Käll, A. Krogh, E. L. L. Sonnhammer, A combined transmembrane topology and signal peptide prediction method. *J. Mol. Biol.* **338**, 1027–1036 (2004).
95. K. Katoh, D. M. Standley, MAFFT multiple sequence alignment software version 7: improvements in performance and usability. *Mol. Biol. Evol.* **30**, 772–780 (2013).
96. M. N. Price, P. S. Dehal, A. P. Arkin, FastTree 2 – Approximately Maximum-Likelihood Trees for Large Alignments. *PLoS One*. **5**, e9490 (2010).
97. N. Darzentas, Circoletto: visualizing sequence similarity with Circos. *Bioinformatics*. **26**, 2620–2621 (2010).
98. G. E. Crooks, G. Hon, J.-M. Chandonia, S. E. Brenner, WebLogo: a sequence logo generator. *Genome Res.* **14**, 1188–1190 (2004).
99. M. Biasini *et al.*, SWISS-MODEL: modelling protein tertiary and quaternary structure using evolutionary information. *Nucleic Acids Res.* **42**, W252–8 (2014).
100. E. F. Pettersen *et al.*, UCSF Chimera--a visualization system for exploratory research and analysis. *J. Comput. Chem.* **25**, 1605–1612 (2004).
101. B. B. Khomtchouk, J. R. Hennessy, C. Wahlestedt, shinyheatmap: Ultra fast low memory heatmap web interface for big data genomics. *PLoS One*. **12**, e0176334 (2017).

102. A. Smit, R. Hubley, *RepeatModeler* (2017; <http://www.repeatmasker.org.>).
103. Y. Han, S. R. Wessler, MITE-Hunter: a program for discovering miniature inverted-repeat transposable elements from genomic sequences. *Nucleic Acids Res.* **38**, e199 (2010).
104. Z. Bao, S. R. Eddy, Automated de novo identification of repeat sequence families in sequenced genomes. *Genome Res.* **12**, 1269–1276 (2002).
105. A. L. Price, N. C. Jones, P. A. Pevzner, De novo identification of repeat families in large genomes. *Bioinformatics*. **21 Suppl 1**, i351–8 (2005).
106. M. A. Urich, J. R. Nery, R. Lister, R. J. Schmitz, J. R. Ecker, MethylC-seq library preparation for base-resolution whole-genome bisulfite sequencing. *Nat. Protoc.* **10**, 475–483 (2015).
107. M. D. Schultz *et al.*, Human body epigenome maps reveal noncanonical DNA methylation variation. *Nature*. **523**, 212–216 (2015).
108. M. Martin, Cutadapt removes adapter sequences from high-throughput sequencing reads. *EMBnet.journal*. **17**, 10–12 (2011).
109. B. Langmead, C. Trapnell, M. Pop, S. L. Salzberg, Ultrafast and memory-efficient alignment of short DNA sequences to the human genome. *Genome Biol.* **10**, R25 (2009).
110. Picard Tools - By Broad Institute, (available at <http://broadinstitute.github.io/picard>).
111. B. R. Herb *et al.*, Reversible switching between epigenetic states in honeybee behavioral subcastes. *Nat. Neurosci.* **15**, 1371–1373 (2012).
112. H. Xiang *et al.*, Single base-resolution methylome of the silkworm reveals a sparse epigenomic map. *Nat. Biotechnol.* **28**, 516–520 (2010).
113. C. B. Cunningham *et al.*, The Genome and Methylome of a Beetle with Complex Social Behavior, *Nicrophorus vespilloides* (Coleoptera: Silphidae). *Genome Biol. Evol.* **7**, 3383–3396 (2015).
114. K. M. Glastad, K. Gokhale, J. Liebig, M. A. D. Goodisman, The caste- and sex-specific DNA methylome of the termite *Zootermopsis nevadensis*. *Sci. Rep.* **6**, 37110 (2016).
115. M. D. Schultz, R. J. Schmitz, J. R. Ecker, “Leveling” the playing field for analyses of single-base resolution DNA methylomes. *Trends Genet.* **28**, 583–585 (2012).
116. R. C. Team, Others, R: A language and environment for statistical computing (2013) (available at <http://citeseerx.ist.psu.edu/viewdoc/download?doi=10.1.1.470.5851&rep=rep1&type=pdf>).
117. A. M. Larracuente, P. M. Ferree, Simple method for fluorescence DNA in situ hybridization to squashed chromosomes. *J. Vis. Exp.*, 52288 (2015).
118. X. H. Fu, L. A. Ballantyne, C. L. Lambkin, Aquatica gen. nov. from mainland China with a description of *Aquatica wuhana* sp. nov. (Coleoptera: Lampyridae: Luciolinae). *Zootaxa*. **2530**, 1–18 (2010).

119. N. Ohba, Mystery of Fireflies. Yokosuka City Mus. Yokosuka, Japan (In Japanese) (2004).
120. M. A. Branham, J. W. Wenzel, The origin of photic behavior and the evolution of sexual communication in fireflies (Coleoptera: Lampyridae). *Cladistics*. **19**, 1–22 (2003).
121. S. Kanda, Firefly (1935).
122. N. Ohba, Studies on the communication system of Japanese fireflies. *Sci. Rept. Yokosuka City Mus.* **30**, 1–62 (1983).
123. N. Ohba, T. Hidaka, Reflex bleeding of fireflies and prey-predator relationship. *Science Report of the Yokosuka City Museum*. **49**, 1–12 (2002).
124. X. Fu *et al.*, Structure and function of the eversible glands of the aquatic firefly *Luciola leii* (Coleoptera: Lampyridae). *Chemoecology*. **17**, 117–124 (2007).
125. KAWASHIMA, I, A check-list of Japanese fireflies (Coleoptera, Lampyridae and Rhagophthalmidae). *Jpn. J. syst. Ent., Matsuyama*. **9**, 241–261 (2003).
126. H. Higuchi, Ed., in *Conservation Biology* (Univ. Tokyo Press, Tokyo, 1996), pp. 71–102.
127. J. M. of Environment, Press Release (2017), (available at http://www.env.go.jp/garden/kokyogaien/topics/post_134.html).
128. H. Ikeya, Melanic strain of *Luciola lateralis*. *Bull. Firefly Mus. Toyota Town*. **8**, 175–177 (2016).
129. M. Inoue, H. Yamamoto, Cytological studies of family Lampyridae I. Karyotypes of *Luciola lateralis* and *L. cruciata*. *La Kromosomo*. **II-45**, 1440–1443 (1987).
130. S. Gnerre *et al.*, High-quality draft assemblies of mammalian genomes from massively parallel sequence data. *Proc. Natl. Acad. Sci. U. S. A.* **108**, 1513–1518 (2011).
131. S. Andrews, A quality control tool for high throughput sequence data. *FastQC*, (available at <https://www.bioinformatics.babraham.ac.uk/projects/fastqc/>).
132. C. Trapnell, L. Pachter, S. L. Salzberg, TopHat: discovering splice junctions with RNA-Seq. *Bioinformatics*. **25**, 1105–1111 (2009).
133. C. Trapnell *et al.*, Transcript assembly and quantification by RNA-Seq reveals unannotated transcripts and isoform switching during cell differentiation. *Nat. Biotechnol.* **28**, 511–515 (2010).
134. A. Smit, R. Hubley, P. Green, RepeatMasker Open-4.0. 2013--2015. *Institute for Systems Biology*. <http://repeatmasker.org> (2015).
135. B. L. Cantarel *et al.*, MAKER: an easy-to-use annotation pipeline designed for emerging model organism genomes. *Genome Res.* **18**, 188–196 (2008).
136. Slipinski, S. A., Leschen, R. A. B. & Lawrence, J. F., in *Animal Biodiversity: An Outline of Higher-level Classification and Survey of Taxonomic Richness*, Z. –Q Zhang, Ed. (Magnolia Press, Auckland., 2011), pp. 203–208.

137. Costa, C., Lawrence, J. F. & Rosa, S. P., in *Handbook of Zoology, Vol. IV, Arthropoda: Insecta, Teilband 39, Coleoptera, Beetles. Vol. 2: Morphology and Systematics*, Leschen, R. A. B., Beutel, R. G. & Lawrence, J. F., Ed. (Walter de Gruyter, Berlin., 2010), pp. 75–103.
138. C. Costa, Systematics and evolution of the tribes Pyrophorini and Heligmini, with description of Campyloxeninae, new subfamily (Coleoptera, Elateridae). *Arq. Zool.* . **26**, 49–190 (1975).
139. E. N. Harvey, K. P. Stevens, THE BRIGHTNESS OF THE LIGHT OF THE WEST INDIAN ELATERID BEETLE, PYROPHORUS. *J. Gen. Physiol.* **12**, 269–272 (1928).
140. H. C. Levy, in *Book of Insect Records*, T. J. Walker, Ed. (Univ. Florida, Florida., 1998), pp. 72–73.
141. E. T. Arias-Bohart, Malalcahuelloocaresi gen. & sp. n. (Elateridae, Campyloxeninae). *Zookeys*, 1–13 (2015).
142. J. N. L. Stibick, Classification of the Elateridae (Coleoptera). *Relationships and classification of the subfamilies and tribes. Pacific Insects.* **20**, 145–186 (1979).
143. C. Costa, Note on the bioluminescence of Balgus schnusei (Heller, 1974)(Trixagidae, Coleoptera). *Rev. Bras. Entomol.* (1984) (available at <http://agris.fao.org/agris-search/search.do?recordID=US201302648173>).
144. H. Douglas, Phylogenetic relationships of Elateridae inferred from adult morphology, with special reference to the position of Cardiophorinae. *Zootaxa*. **2900**, 1–45 (2011).
145. Y. Oba, R. Sagegami-Oba, Phylogeny of Elateridae inferred from molecular analysis. *Nat Insects*. **42**, 30–42 (2007).
146. R. Sagegami-Oba, Y. Oba, H. Ohira, Phylogenetic relationships of click beetles (Coleoptera: Elateridae) inferred from 28S ribosomal DNA: insights into the evolution of bioluminescence in Elateridae. *Mol. Phylogenet. Evol.* **42**, 410–421 (2007).
147. R. Kundrata, L. Bocak, The phylogeny and limits of Elateridae (Insecta, Coleoptera): is there a common tendency of click beetles to soft-bodiedness and neoteny? *Zool. Scr.* **40**, 364–378 (2011).
148. J. A. Hyslop, The phylogeny of the Elateridae based on larval characters. *Ann. Entomol. Soc. Am.* **10**, 241–263 (1917).
149. H. Ôhira, Morphological and taxonomic study on the larvae of Elateridae in Japan (Coleoptera). *H. Ôhira, Okazaki City, Japan.* **61** (1962).
150. V. G. Dolin, Phylogeny of the click beetles (Coleoptera, Elateridae). *Vestn. Zool. May/June 1978*, **3** (1978) (available at <http://agris.fao.org/agris-search/search.do?recordID=US201302455464>).
151. H. Ôhira, Illustrated key to click beetles of Japan. *Jpn Soc Environ Entomol Zool, editor. An Illustrated Guide to Identify Insects. Osaka, Japan: Bunkyo Shuppan*, 227–251 (2013).
152. P. J. Johnson, 58. Elateridae Leach 1815. *American beetles*. **2**, 160–173 (2002).

153. S. P. Rosa, thesis, Universidade de São Paulo (2007).
154. N. Reyes, V. Lee, Behavioral and morphological observations of *Ignelater luminosus* in Dominica (2010).
155. H. Chang, A. G. Kirejtshuk, D. Ren, C. Shih, First Fossil Click Beetles from the Middle Jurassic of Inner Mongolia, China (Coleoptera: Elateridae). *Annal. Zool.* **59**, 7–14 (2009).
156. D. D. McKenna, B. D. Farrell, Beetles (Coleoptera). *The timetree of life*. **278**, 289 (2009).
157. D. Grimaldi, M. S. Engel, *Evolution of the Insects* (Cambridge University Press, 2005).
158. Y. Oba, M. Kumazaki, S. Inouye, Characterization of luciferases and its parologue in the Panamanian luminous click beetle *Pyrophorus angustus*: a click beetle luciferase lacks the fatty acyl-CoA synthetic activity. *Gene*. **452**, 1–6 (2010).
159. J. L. Feder, S. Velez, Intergenic exchange, geographic isolation, and the evolution of bioluminescent color for *Pyrophorus* click beetles. *Evolution*. **63**, 1203–1216 (2009).
160. C. Costa, S. A. Vanin, Coleoptera Larval Fauna Associated with Termite Nests (Isoptera) with Emphasis on the “Bioluminescent Termite Nests” from Central Brazil. *Psyche*. **2010** (2010), doi:10.1155/2010/723947.
161. E. Kretsch, Courtship Behavior of *Ignelater luminosus* (2000).
162. S. Vélez, thesis, University of Notre Dame (2006).
163. N. Virkki, M. Flores, J. Escudero, Structure, orientation, and segregation of the sex trivalent in *Pyrophorus luminosus* III. (Coleoptera, Elateridae). *Can. J. Genet. Cytol.* **26**, 326–330 (1984).
164. D. E. Perez-Gelabert, *Arthropods of Hispaniola (Dominican Republic and Haiti): A checklist and bibliography* (Magnolia Press, 2008).
165. S. P. Rosa, New species of *Ignelater* Costa (Coleoptera, Elateridae, Pyrophorini). *Pap. Avulsos Zool.* **50**, 445–449 (2010).
166. N. I. Weisenfeld, V. Kumar, P. Shah, D. M. Church, D. B. Jaffe, Direct determination of diploid genome sequences. *Genome Res.* **27**, 757–767 (2017).
167. Center for Disease Control and Prevention (CDC), Hymenolepiasis, (available at <https://www.cdc.gov/dpdx/hymenolepiasis/index.html#lifeCycle>).
168. I. M. Sheiman, M. F. Shkutin, N. B. Terenina, M. K. S. Gustafsson, A behavioral study of the beetle *Tenebrio molitor* infected with cysticercoids of the rat tapeworm *Hymenolepis diminuta*. *Naturwissenschaften*. **93**, 305–308 (2006).
169. K. Kryukov, FASTA Splitter, (available at <http://kirill-kryukov.com/study/tools/fasta-splitter/>).
170. H. Li, Minimap2: fast pairwise alignment for long nucleotide sequences. *ArXiv e-prints*. **2017** (2017) (available at <https://pdfs.semanticscholar.org/a703/88011f2995783e159dc21a62905753a6af44.pdf>).

171. R. Wick, adapter trimmer for Oxford Nanopore reads, (available at <https://github.com/rrwick/Porechop>).
172. R. L. Warren *et al.*, LINKS: Scalable, alignment-free scaffolding of draft genomes with long reads. *Gigascience*. **4**, 35 (2015).
173. F. Arnoldi, K. Ogoh, Y. Ohmiya, V. R. Viviani, Mitochondrial genome sequence of the Brazilian luminescent click beetle Pyrophorus divergens (Coleoptera: Elateridae): mitochondrial genes utility to investigate the evolutionary history of Coleoptera and its bioluminescence. *Gene*. **405**, 1–9 (2007).
174. S. Nurk *et al.*, in *Lecture Notes in Computer Science* (2013), pp. 158–170.
175. D. Antipov *et al.*, plasmidSPAdes: assembling plasmids from whole genome sequencing data. *Bioinformatics*. **32**, 3380–3387 (2016).
176. R. R. Wick, M. B. Schultz, J. Zobel, K. E. Holt, Bandage: interactive visualization of de novo genome assemblies. *Bioinformatics*. **31**, 3350–3352 (2015).
177. J. S. Bae, I. Kim, H. D. Sohn, B. R. Jin, The mitochondrial genome of the firefly, Pyrocoelia rufa: complete DNA sequence, genome organization, and phylogenetic analysis with other insects. *Mol. Phylogenet. Evol.* **32**, 978–985 (2004).
178. D. E. Wood, S. L. Salzberg, Kraken: ultrafast metagenomic sequence classification using exact alignments. *Genome Biol.* **15**, R46 (2014).
179. A. Gurevich, V. Saveliev, N. Vyahhi, G. Tesler, QUAST: quality assessment tool for genome assemblies. *Bioinformatics*. **29**, 1072–1075 (2013).
180. F. A. Simão, R. M. Waterhouse, P. Ioannidis, E. V. Kriventseva, E. M. Zdobnov, BUSCO: assessing genome assembly and annotation completeness with single-copy orthologs. *Bioinformatics*. **31**, 3210–3212 (2015).
181. M. Poelchau *et al.*, The i5k Workspace@NAL--enabling genomic data access, visualization and curation of arthropod genomes. *Nucleic Acids Res.* **43**, D714–9 (2015).
182. D. M. Emms, S. Kelly, OrthoFinder: solving fundamental biases in whole genome comparisons dramatically improves orthogroup inference accuracy. *Genome Biol.* **16**, 157 (2015).
183. K. Katoh, D. M. Standley, MAFFT multiple sequence alignment software version 7: improvements in performance and usability. *Mol. Biol. Evol.* **30**, 772–780 (2013).
184. S. Kumar, G. Stecher, K. Tamura, MEGA7: Molecular Evolutionary Genetics Analysis Version 7.0 for Bigger Datasets. *Mol. Biol. Evol.* **33**, 1870–1874 (2016).
185. D. H. Huson, C. Scornavacca, Dendroscope 3: an interactive tool for rooted phylogenetic trees and networks. *Syst. Biol.* **61**, 1061–1067 (2012).
186. K. V. Wood, J. R. de Wet, N. Dewji, M. DeLuca, Synthesis of active firefly luciferase by in vitro translation of RNA obtained from adult lanterns. *Biochem. Biophys. Res. Commun.* **124**, 592–596 (1984).

187. J. R. De Wet, K. V. Wood, M. DeLuca, D. R. Helinski, S. Subramani, Firefly luciferase gene: structure and expression in mammalian cells. *Mol. Cell. Biol.* **7**, 725–737 (1987).
188. T. Masuda, H. Tatsumi, E. Nakano, Cloning and sequence analysis of cDNA for luciferase of a Japanese firefly, *Luciola cruciata*. *Gene*. **77**, 265–270 (1989).
189. H. Tatsumi, N. Kajiyama, E. Nakano, Molecular cloning and expression in *Escherichia coli* of a cDNA clone encoding luciferase of a firefly, *Luciola lateralis*. *Biochim. Biophys. Acta*. **1131**, 161–165 (1992).
190. L. Ye, L. M. Buck, H. J. Schaeffer, F. R. Leach, Cloning and sequencing of a cDNA for firefly luciferase from *Photuris pennsylvanica*. *Biochim. Biophys. Acta*. **1339**, 39–52 (1997).
191. Y. Oba, N. Mori, M. Yoshida, S. Inouye, Identification and characterization of a luciferase isotype in the Japanese firefly, *Luciola cruciata*, involving in the dim glow of firefly eggs. *Biochemistry*. **49**, 10788–10795 (2010).
192. Y. Oba *et al.*, Bioluminescence of a firefly pupa: involvement of a luciferase isotype in the dim glow of pupae and eggs in the Japanese firefly, *Luciola lateralis*. *Photochem. Photobiol. Sci.* **12**, 854–863 (2013).
193. M. Bessho-Uehara, Y. Oba, Identification and characterization of the Luc2-type luciferase in the Japanese firefly, *Luciola parvula*, involved in a dim luminescence in immobile stages. *Luminescence*. **32**, 924–931 (2017).
194. M. Bessho-Uehara, K. Konishi, Y. Oba, Biochemical characteristics and gene expression profiles of two paralogous luciferases from the Japanese firefly *Pyrocoelia atripennis* (Coleoptera, Lampyridae, Lampyrinae): insight into the evolution of firefly luciferase genes. *Photochem. Photobiol. Sci.* **16**, 1301–1310 (2017).
195. K. V. Wood, Y. A. Lam, H. H. Seliger, W. D. McElroy, Complementary DNA coding click beetle luciferases can elicit bioluminescence of different colors. *Science*. **244**, 700–702 (1989).
196. V. R. Viviani, E. J. Bechara, Y. Ohmiya, Cloning, sequence analysis, and expression of active *Phrixothrix* railroad-worms luciferases: relationship between bioluminescence spectra and primary structures. *Biochemistry*. **38**, 8271–8279 (1999).
197. V. R. Viviani *et al.*, Cloning and molecular characterization of the cDNA for the Brazilian larval click-beetle *Pyrearinus termitilluminans* luciferase. *Photochem. Photobiol.* **70**, 254–260 (1999).
198. Y. Ohmiya, M. Sumiya, V. R. Viviani, N. Ohba, Comparative aspects of a luciferase molecule from the Japanese luminous beetle, *Rhagophthalmus ohbai*. *Sci. Rep. Yokosuka City Mus.* **47**, 31–38 (2000).
199. Y. Oba, K. H. Hoffmann, Insect Bioluminescence in the Post-Molecular Biology Era. *Insect Molecular Biology and Ecology*, 94–120 (2014).
200. M. J. T. N. Timmermans *et al.*, Why barcode? High-throughput multiplex sequencing of mitochondrial genomes for molecular systematics. *Nucleic Acids Res.* **38**, e197 (2010).
201. M. J. T. N. Timmermans, A. P. Vogler, Phylogenetically informative rearrangements in

- mitochondrial genomes of Coleoptera, and monophyly of aquatic elateriform beetles (Dryopoidea). *Mol. Phylogen. Evol.* **63**, 299–304 (2012).
202. D. D. Mckenna *et al.*, The beetle tree of life reveals that Coleoptera survived end-Permian mass extinction to diversify during the Cretaceous terrestrial revolution. *Syst. Entomol.* **40**, 835–880 (2015).
203. G. J. Martin, M. A. Branham, M. F. Whiting, S. M. Bybee, Total evidence phylogeny and the evolution of adult bioluminescence in fireflies (Coleoptera: Lampyridae). *Mol. Phylogen. Evol.* **107**, 564–575 (2017).
204. G. Shi *et al.*, Age constraint on Burmese amber based on U–Pb dating of zircons. *Cretaceous Res.* **37**, 155–163 (2012).
205. S. V. Kazantsev, (2015) (available at https://www.researchgate.net/profile/Sergey_Kazantsev2/publication/309576274_Protolucio_la_albertalleni_genn_spn_a_new_Luciolinae_firefly_Insecta_Coleoptera_Lampyridae_from_Burmite_amber/links/581840db08aecd7d89691138.pdf).
206. H. Dinkel *et al.*, ELM—the database of eukaryotic linear motifs. *Nucleic Acids Res.* **40**, D242–D251 (2012).
207. G. Neuberger, S. Maurer-Stroh, B. Eisenhaber, A. Hartig, F. Eisenhaber, Motif refinement of the peroxisomal targeting signal 1 and evaluation of taxon-specific differences. *J. Mol. Biol.* **328**, 567–579 (2003).
208. Georg Neuberger, Sebastian Maurer-Stroh, Birgit Eisenhaber, Andreas Hartig and Frank Eisenhaber, The PTS1 Predictor, (available at <http://mendel.imp.ac.at/mendeljsp/sat/pts1/PTS1predictor.jsp>).
209. S. Capella-Gutiérrez, J. M. Silla-Martínez, T. Gabaldón, trimAI: a tool for automated alignment trimming in large-scale phylogenetic analyses. *Bioinformatics*. **25**, 1972–1973 (2009).
210. A. S. Tanabe, Kakusan4 and Aminosan: two programs for comparing nonpartitioned, proportional and separate models for combined molecular phylogenetic analyses of multilocus sequence data. *Mol. Ecol. Resour.* **11**, 914–921 (2011).
211. A. Stamatakis, RAxML-VI-HPC: maximum likelihood-based phylogenetic analyses with thousands of taxa and mixed models. *Bioinformatics*. **22**, 2688–2690 (2006).
212. W. P. Maddison, D. R. Maddison, *Mesquite: a modular system for evolutionary analysis* (2017; <http://mesquiteproject.org>).
213. Y. Oba, M. Sato, S. Inouye, Cloning and characterization of the homologous genes of firefly luciferase in the mealworm beetle, *Tenebrio molitor*. *Insect Mol. Biol.* **15**, 293–299 (2006).
214. Y. Oba, M. Sato, Y. Ohta, S. Inouye, Identification of paralogous genes of firefly luciferase in the Japanese firefly, *Luciola cruciata*. *Gene*. **368**, 53–60 (2006).
215. D. M. Mofford *et al.*, Luciferase Activity of Insect Fatty Acyl-CoA Synthetases with Synthetic Luciferins. *ACS Chem. Biol.* **12**, 2946–2951 (2017).

216. F. G. C. Arnoldi, A. J. da Silva Neto, V. R. Viviani, Molecular insights on the evolution of the lateral and head lantern luciferases and bioluminescence colors in Mastinocerini railroad-worms (Coleoptera: Phengodidae). *Photochem. Photobiol. Sci.* **9**, 87–92 (2010).
217. D. T. Amaral, J. R. Silva, V. R. Viviani, Transcriptional comparison of the photogenic and non-photogenic tissues of *Phrixothrix hirtus* (Coleoptera: Phengodidae) and non-luminescent *Chauliognathus flavipes* (Coleoptera: Cantharidae) give insights on the origin of lanterns in railroad worms. *Gene Reports*. **7**, 78–86 (2017).
218. X. Li, K. Ogoh, N. Ohba, X. Liang, Y. Ohmiya, Mitochondrial genomes of two luminous beetles, *Rhagophthalmus lufengensis* and *R. ohbai* (Arthropoda, Insecta, Coleoptera). *Gene*. **392**, 196–205 (2007).
219. Y. Oba, M. Yoshida, T. Shintani, M. Furuhashi, S. Inouye, Firefly luciferase genes from the subfamilies Psilochladinae and Ototretinae (Lampyridae, Coleoptera). *Comp. Biochem. Physiol. B Biochem. Mol. Biol.* **161**, 110–116 (2012).
220. V. R. Viviani, D. Amaral, R. Prado, F. G. C. Arnoldi, A new blue-shifted luciferase from the Brazilian Amydetes fanestratus (Coleoptera: Lampyridae) firefly: molecular evolution and structural/functional properties. *Photochem. Photobiol. Sci.* **10**, 1879–1886 (2011).
221. B. R. Branchini, T. L. Southworth, L. J. Salituro, D. M. Fontaine, Y. Oba, Cloning of the Blue Ghost (*Phausis reticulata*) Luciferase Reveals a Glowing Source of Green Light. *Photochem. Photobiol.* **93**, 473–478 (2017).
222. U. Stoltz, S. Velez, K. V. Wood, M. Wood, J. L. Feder, Darwinian natural selection for orange bioluminescent color in a Jamaican click beetle. *Proc. Natl. Acad. Sci. U. S. A.* **100**, 14955–14959 (2003).
223. R. C. Edgar, MUSCLE: multiple sequence alignment with high accuracy and high throughput. *Nucleic Acids Res.* **32**, 1792–1797 (2004).
224. M. Nei, S. Kumar, *Molecular Evolution and Phylogenetics* (Oxford University Press, 2000).
225. M. D. Smith *et al.*, Less is more: an adaptive branch-site random effects model for efficient detection of episodic diversifying selection. *Mol. Biol. Evol.* **32**, 1342–1353 (2015).
226. S. L. K. Pond, S. D. W. Frost, S. V. Muse, HyPhy: hypothesis testing using phylogenies. *Bioinformatics*. **21**, 676–679 (2005).
227. K.-S. Goh, C.-W. Li, A photocytes-associated fatty acid-binding protein from the light organ of adult Taiwanese firefly, *Luciola cerata*. *PLoS One*. **6**, e29576 (2011).
228. J. A. Nathanson, L. Kantham, E. J. Hunnicutt, Isolation and N-terminal amino acid sequence of an octopamine ligand binding protein. *FEBS Lett.* **259**, 117–120 (1989).
229. I. Letunic, P. Bork, Interactive tree of life (iTOL) v3: an online tool for the display and annotation of phylogenetic and other trees. *Nucleic Acids Res.* **44**, W242–5 (2016).
230. A. D. Briscoe, L. Chittka, THEEVOLUTION OF COLORVISION ININSECTS. *Annu. Rev. Entomol.* **46**, 471–510 (2001).

231. M. L. Porter *et al.*, Shedding new light on opsin evolution. *Proc. Biol. Sci.* **279**, 3–14 (2012).
232. S. E. Sander, D. W. Hall, Variation in opsin genes correlates with signalling ecology in North American fireflies. *Mol. Ecol.* **24**, 4679–4696 (2015).
233. G. J. Martin, N. P. Lord, M. A. Branham, S. M. Bybee, Review of the firefly visual system (Coleoptera: Lampyridae) and evolution of the opsin genes underlying color vision. *Org. Divers. Evol.* **15**, 513–526 (2015).
234. R. Feuda, F. Marlétaz, M. A. Bentley, P. W. H. Holland, Conservation, Duplication, and Divergence of Five Opsin Genes in Insect Evolution. *Genome Biol. Evol.* **8**, 579–587 (2016).
235. D. D. McKenna *et al.*, Genome of the Asian longhorned beetle (Anoplophora glabripennis), a globally significant invasive species, reveals key functional and evolutionary innovations at the beetle-plant interface. *Genome Biol.* **17**, 227 (2016).
236. S. D. Schoville *et al.*, A model species for agricultural pest genomics: the genome of the Colorado potato beetle, *Leptinotarsa decemlineata* (Coleoptera: Chrysomelidae). *bioRxiv* (2017), p. 192641.
237. K. Sakai *et al.*, *Drosophila melanogaster* rhodopsin Rh7 is a UV-to-visible light sensor with an extraordinarily broad absorption spectrum. *Sci. Rep.* **7**, 7349 (2017).
238. J. D. Ni, L. S. Baik, T. C. Holmes, C. Montell, A rhodopsin in the brain functions in circadian photoentrainment in *Drosophila*. *Nature*. **545**, 340–344 (2017).
239. K. Arikawa, K. Aoki, Response characteristics and occurrence of extraocular photoreceptors on lepidopteran genitalia. *J. Comp. Physiol.* **148**, 483–489 (1982).
240. C. E. Schnitzler *et al.*, Genomic organization, evolution, and expression of photoprotein and opsin genes in *Mnemiopsis leidyi*: a new view of ctenophore photocytess. *BMC Biol.* **10**, 107 (2012).
241. D. Tong *et al.*, Evidence for light perception in a bioluminescent organ. *Proceedings of the National Academy of Sciences*. **106**, 9836–9841 (2009).
242. M. S. Pankey, V. N. Minin, G. C. Imholte, M. A. Suchard, T. H. Oakley, Predictable transcriptome evolution in the convergent and complex bioluminescent organs of squid. *Proc. Natl. Acad. Sci. U. S. A.* **111**, E4736–42 (2014).
243. S. Capella-Gutiérrez, J. M. Silla-Martínez, T. Gabaldón, trimAI: a tool for automated alignment trimming in large-scale phylogenetic analyses. *Bioinformatics*. **25**, 1972–1973 (2009).
244. M. C. Chambers *et al.*, A cross-platform toolkit for mass spectrometry and proteomics. *Nat. Biotechnol.* **30**, 918–920 (2012).
245. T. Pluskal, S. Castillo, A. Villar-Briones, M. Oresic, MZmine 2: modular framework for processing, visualizing, and analyzing mass spectrometry-based molecular profile data. *BMC Bioinformatics*. **11**, 395 (2010).

246. S. Böcker, M. C. Letzel, Z. Lipták, A. Pervukhin, SIRIUS: decomposing isotope patterns for metabolite identification. *Bioinformatics*. **25**, 218–224 (2009).
247. M. Gronquist, J. Meinwald, T. Eisner, F. C. Schroeder, Exploring uncharted terrain in nature's structure space using capillary NMR spectroscopy: 13 steroids from 50 fireflies. *J. Am. Chem. Soc.* **127**, 10810–10811 (2005).
248. N. C. Kyrpides *et al.*, Genomic Encyclopedia of Type Strains, Phase I: The one thousand microbial genomes (KMG-I) project. *Stand. Genomic Sci.* **9**, 1278–1284 (2014).
249. D. L. Williamson *et al.*, Mycoplasma somnilux sp. nov., Mycoplasma luminosum sp. nov., and Mycoplasma lucivorax sp. nov., new sterol-requiring mollicutes from firefly beetles (Coleoptera: Lampyridae). *Int. J. Syst. Bacteriol.* **40**, 160–164 (1990).
250. J. Krumsiek, R. Arnold, T. Rattei, Gepard: a rapid and sensitive tool for creating dotplots on genome scale. *Bioinformatics*. **23**, 1026–1028 (2007).
251. J. E. Lloyd, Firefly Parasites and Predators. *Coleopt. Bull.* **27**, 91–106 (1973).
252. D. Guilligay *et al.*, Comparative structural and functional analysis of orthomyxovirus polymerase cap-snatching domains. *PLoS One*. **9**, e84973 (2014).
253. S. Reich, D. Guilligay, S. Cusack, An in vitro fluorescence based study of initiation of RNA synthesis by influenza B polymerase. *Nucleic Acids Res.* **45**, 3353–3368 (2017).
254. A. M. Q. King, E. Lefkowitz, M. J. Adams, E. B. Carstens, *Virus Taxonomy: Ninth Report of the International Committee on Taxonomy of Viruses* (Elsevier, 2011).
255. M. T. Hsu, J. D. Parvin, S. Gupta, M. Krystal, P. Palese, Genomic RNAs of influenza viruses are held in a circular conformation in virions and in infected cells by a terminal panhandle. *Proc. Natl. Acad. Sci. U. S. A.* **84**, 8140–8144 (1987).
256. A. Pflug, M. Lukarska, P. Resa-Infante, S. Reich, S. Cusack, Structural insights into RNA synthesis by the influenza virus transcription-replication machine. 2017. *Virus Res.*, 30782–30781.
257. A. J. Eisfeld, G. Neumann, Y. Kawaoka, At the centre: influenza A virus ribonucleoproteins. *Nat. Rev. Microbiol.* **13**, 28–41 (2015).
258. M. B. Leahy, J. T. Dessens, F. Weber, G. Kochs, P. A. Nuttall, The fourth genus in the Orthomyxoviridae: sequence analyses of two Thogoto virus polymerase proteins and comparison with influenza viruses. *Virus Res.* **50**, 215–224 (1997).
259. J. B. Kimble, thesis, University of Maryland, College Park, Ann Arbor, United States (2013).
260. A. J. W. Te Velthuis, E. Fodor, Influenza virus RNA polymerase: insights into the mechanisms of viral RNA synthesis. *Nat. Rev. Microbiol.* **14**, 479–493 (2016).
261. N. Hengrung *et al.*, Crystal structure of the RNA-dependent RNA polymerase from influenza C virus. *Nature*. **527**, 114–117 (2015).
262. K. Hara, T. Kashiwagi, N. Hamada, H. Watanabe, Basic amino acids in the N-terminal

- half of the PB2 subunit of influenza virus RNA polymerase are involved in both transcription and replication. *J. Gen. Virol.* **98**, 900–905 (2017).
263. W. N. Wulan, D. Heydet, E. J. Walker, M. E. Gahan, R. Ghildyal, Nucleocytoplasmic transport of nucleocapsid proteins of enveloped RNA viruses. *Front. Microbiol.* **6**, 553 (2015).
264. D. Sikora, L. Rocheleau, E. G. Brown, M. Pelchat, Influenza A virus cap-snatches host RNAs based on their abundance early after infection. *Virology*. **509**, 167–177 (2017).
265. W. W. Thompson *et al.*, Estimates of US influenza-associated deaths made using four different methods. *Influenza Other Respi. Viruses*. **3**, 37–49 (2009).
266. B. M. Hause *et al.*, Isolation of a novel swine influenza virus from Oklahoma in 2011 which is distantly related to human influenza C viruses. *PLoS Pathog.* **9**, e1003176 (2013).
267. C. R. Anderson, J. Casals, Dhori virus, a new agent isolated from *Hyalomma dromedarii* in India. *Indian J. Med. Res.* **61**, 1416–1420 (1973).
268. D. A. Haig, J. P. Woodall, D. Danskin, THOGOTO VIRUS: A HITHERTO UNDERSCRIBED AGENT ISOLATED FROM TICKS IN KENYA. *J. Gen. Microbiol.* **38**, 389–394 (1965).
269. S. Mjaaland, E. Rimstad, K. Falk, B. H. Dannevig, Genomic characterization of the virus causing infectious salmon anemia in Atlantic salmon (*Salmo salar* L.): an orthomyxo-like virus in a teleost. *J. Virol.* **71**, 7681–7686 (1997).
270. R. M. Presti *et al.*, Quaranfil, Johnston Atoll, and Lake Chad viruses are novel members of the family Orthomyxoviridae. *J. Virol.* **83**, 11599–11606 (2009).
271. M. D. Pauly, M. Procario, A. S. Lauring, The mutation rates and mutational bias of influenza A virus. *bioRxiv* (2017), p. 110197.
272. H. Zeng *et al.*, Tropism and infectivity of influenza virus, including highly pathogenic avian H5N1 virus, in ferret tracheal differentiated primary epithelial cell cultures. *J. Virol.* **87**, 2597–2607 (2013).
273. K. G. Mansfield, Viral tropism and the pathogenesis of influenza in the Mammalian host. *Am. J. Pathol.* **171**, 1089 (2007).
274. J. Steel, A. C. Lowen, Influenza A virus reassortment. *Curr. Top. Microbiol. Immunol.* **385**, 377–401 (2014).
275. S. H. Marshall, R. Ramírez, A. Labra, M. Carmona, C. Muñoz, Bona fide evidence for natural vertical transmission of infectious salmon anemia virus in freshwater brood stocks of farmed Atlantic salmon (*Salmo salar*) in Southern Chile. *J. Virol.* **88**, 6012–6018 (2014).
276. R. A. Hall *et al.*, Commensal Viruses of Mosquitoes: Host Restriction, Transmission, and Interaction with Arboviral Pathogens. *Evol. Bioinform. Online*. **12**, 35–44 (2016).
277. M. J. Ballinger, J. A. Bruenn, J. Hay, D. Czechowski, D. J. Taylor, Discovery and evolution of bunyavirids in arctic phantom midges and ancient bunyavirid-like sequences in insect genomes. *J. Virol.* **88**, 8783–8794 (2014).

278. G. Metegnier *et al.*, Comparative paleovirological analysis of crustaceans identifies multiple widespread viral groups. *Mob. DNA*. **6**, 16 (2015).
279. C. Feschotte, C. Gilbert, Endogenous viruses: insights into viral evolution and impact on host biology. *Nat. Rev. Genet.* **13**, 283–296 (2012).
280. A. Katzourakis, R. J. Gifford, Endogenous viral elements in animal genomes. *PLoS Genet.* **6**, e1001191 (2010).
281. H. M. Temin, Reverse transcription in the eukaryotic genome: retroviruses, pararetroviruses, retrotransposons, and retrotranscripts. *Mol. Biol. Evol.* **2**, 455–468 (1985).
282. F. Bushman *et al.*, Genome-wide analysis of retroviral DNA integration. *Nat. Rev. Microbiol.* **3**, 848–858 (2005).
283. C. Gilbert, R. Cordaux, Viruses as vectors of horizontal transfer of genetic material in eukaryotes. *Curr. Opin. Virol.* **25**, 16–22 (2017).
284. U. Palatini *et al.*, Comparative genomics shows that viral integrations are abundant and express piRNAs in the arboviral vectors *Aedes aegypti* and *Aedes albopictus*. *BMC Genomics*. **18**, 512 (2017).
285. K. E. Olson, M. Bonizzoni, Nonretroviral integrated RNA viruses in arthropod vectors: an occasional event or something more? *Curr Opin Insect Sci.* **22**, 45–53 (2017).
286. P. Aiewsakun, A. Katzourakis, Endogenous viruses: Connecting recent and ancient viral evolution. *Virology*. **479-480**, 26–37 (2015).
287. B. Goic *et al.*, Virus-derived DNA drives mosquito vector tolerance to arboviral infection. *Nat. Commun.* **7**, 12410 (2016).
288. J. Aaskov, K. Buzacott, H. M. Thu, K. Lowry, E. C. Holmes, Long-term transmission of defective RNA viruses in humans and *Aedes* mosquitoes. *Science*. **311**, 236–238 (2006).
289. B. Goic *et al.*, RNA-mediated interference and reverse transcription control the persistence of RNA viruses in the insect model *Drosophila*. *Nat. Immunol.* **14**, 396–403 (2013).
290. P. Miesen, J. Joosten, R. P. van Rij, PIWIs Go Viral: Arbovirus-Derived piRNAs in Vector Mosquitoes. *PLoS Pathog.* **12**, e1006017 (2016).

Table S1: Genomic sequencing library statistics

ID: NCBI BioProject or Gene Expression Omnibus (GEO) ID. **N:** Number of individuals used for sequencing. **Date:** collection date for wild-caught individuals. **Locality:** GSMNP: Great Smoky Mountains National Park, TN, USA; MMNJ: Mercer Meadows, Lawrenceville, NJ, USA; IY90: laboratory strain Ikeya-Y90; MAPR: Mayagüez, Puerto Rico. **Tissue:** Thr: thorax; WB: whole-body; **Type:** SI: Illumina short insert; MP: Illumina mate pair; PB: Pacific Biosciences, RSII P6-C4; HC: Hi-C; BS: Bisulfite; CH: 10x Chromium; ONT: Oxford Nanopore MinION R9.4. Reads: PE: paired-end, CLR: continuous long read. **Number:** number of reads. **Cov:** Mode of autosomal coverage (mode of putative X chromosome, LG3a, coverage), determined from mapped reads with QualiMap (v2.2). ND: Not Determined. **Insert size:** Mode of insert size after alignment (orientation: FR: forward, RF: reverse), determined from mapped reads with QualiMap. **Contamination:** Percent contamination as estimated by kraken v1.0.

Library	ID	N	Date	Locality	Sex	Tissue	Type	Reads	Number	Cov	Insert size (Ori)	Contamination
<i>Photinus pyralis</i>												
8369 ^a	PRJNA289908	1	6/13/11	GSMNP	M	Thr	SI	101x101 PE	203,074,230	98 (49)	354 bp (FR)	0.28
8375_3K ^b	PRJNA378805	1	6/13/11	GSMNP	M	Thr	MP	101x101 PE	101,624,630	21	2155 bp (RF)	2.63
8375_6K ^b	PRJNA378805	1	6/13/11	GSMNP	M	Thr	MP	101x101 PE	23,564,456	5	4889 bp (RF)	3.36
83_3K ^b	PRJNA378805	3	6/13/11	GSMNP	M	Thr	MP	101x101 PE	121,757,858	13	2247 bp (RF)	0.79
83_6K ^b	PRJNA378805	3	6/13/11	GSMNP	M	Thr	MP	101x101 PE	17,905,700	1	4877 bp (RF)	1.38
1611_PpyrPB1	PRJNA378805	4	7/9/16	MMNJ	M	WB	PB	CLR-PB	3,558,201	38 (21)	7 Kbp ^c	3.5
1704	PRJNA378805	2	7/9/16	MMNJ	M	WB	HC	80x80 PE	93,850,923	ND	ND	ND
1705	GSE107177	1	7/9/16	MMNJ	M	WB	BS	150 SE	113,761,746	~16x ^d	ND	ND
<i>Aquatica lateralis</i>												
FFGPE_PE200	PRJDB6460	1	NA	IY90	F	WB	SI	126x126 PE	561,450,686	72	180 bp (FR)	ND
FFGPE_PE800	PRJDB6460					WB	SI	126x126 PE	218,830,950	20	476 bp (FR)	ND
FFGMP_MPFG	PRJDB6460					WB	MP	101x101 PE	358,601,808	31	2300 bp (RF)	ND
<i>Ignelater luminosus</i>												
1610_IlumiHiSeqX ^e	PRJNA418169	1		MAPR	M ^f	WB	CH	151x151 PE	408,838,927	99	339 bp (FR)	ND
1706_IlumiHiSeq2500 ^e	PRJNA418169					WB	CH	150x150 PE	145,250,480	48	334 bp (FR)	ND
18_lib1	PRJNA418169					ONT	CLR		824,248	~2x	2984 ^c	

^a: Mean of 3 sequencing lanes^b: Mean of 2 sequencing lanes^c: Mean subread (PacBio) or read (Oxford Nanopore) length after alignment^d: Estimate from quantity of mapped reads^e: Same library, different instruments^f: Inferred from specimens collected at the same time and locality